CERN–2011–003
EuCARD–Conf–2011–001
8 April 2011

ORGANISATION EUROPÉENNE POUR LA RECHERCHE NUCLÉAIRE
CERN EUROPEAN ORGANIZATION FOR NUCLEAR RESEARCH

EuCARD-AccNet-EuroLumi Workshop

The High-Energy Large Hadron Collider

Villa Bighi, Malta, 14–16 October 2010

Proceedings

Editors: E. Todesco
F. Zimmermann

GENEVA
2011

ISBN 978-92-9083-360-4
ISSN 0007-8328

This Report should be cited as: Proceedings of the Workshop "The High-Energy Large Hadron Collider", Villa Bighi, Malta, 14–16 October 2010, edited by E. Todesco and F. Zimmermann, CERN-2011-003 (CERN, Geneva, 2011)
A contribution in this Report should be cited as: [Author name(s)], in Proceedings of the Workshop "The High-Energy Large Hadron Collider", Villa Bighi, Malta, 14–16 October 2010, edited by E. Todesco and F. Zimmermann, CERN-2011-003, p. [first page]-[lastpage]

Abstract

This report contains the proceedings of the EuCARD-AccNet-EuroLumi Workshop on a High-Energy Large Hadron Collider, 'HE-LHC10[1],' which was held on Malta from 14 to 16 October 2010. This is the first workshop where the possibility of building a 33 TeV centre-of-mass energy proton–proton accelerator in the LHC tunnel is discussed. The key element of such a machine will be the 20 T magnets needed to bend the particle beams: therefore much space was given to discussions about magnet technologies for high fields. The workshop also discussed possible parameter sets, issues related to beam dynamics and synchrotron radiation handling, and the need for new injectors, possibly with 1 TeV energy. The workshop searched for synergies with other projects and studies around the world facing similar challenges or pushing related technologies, revisited past experience, and explored a possible re-use of existing superconducting magnets. Last not least, it reinforced the inter-laboratory collaborations within EuCARD, especially between CERN and its European, US, and Japanese partners.

[1]The HE-LHC10 workshop was sponsored and supported by the European Commission under the FP7 "Research Infrastructures" project EuCARD, grant agreement no. 227579.

Preface

The HE-LHC10 Workshop surveyed the development of 20 T magnets for the High-Energy Large Hadron Collider (LHC); the physics motivation for such a collider; fast cycling superconducting magnets and other options for a new injector including a re-use of the present LHC; Nb_3Sn and high-temperature superconductor (HTS) accelerator-magnet development in Europe, the US, and Japan; the consequences of increased synchrotron radiation; beam parameters and beam dynamics in the presence of strong radiation damping, beam–beam interaction and intrabeam scattering; the possible redeployment of magnets from the Tevatron or HERA; intensity limits; cryogenic system and cooling capacity available; impedance effects; machine protection; vacuum system; injection; beam dump; radioprotection issues after 20 years of LHC operation; and relevant past studies from the Very Large Hadron Collider (VLHC) and Superconducting Super Collider (SSC).

HE-LHC10 was attended by 56 participants from Europe, the Americas, and Japan, including 26 from CERN and 13 from the United States of America. The workshop scope, programme, and speakers had been defined by a programme committee comprising Oliver Brüning (CERN), Antoine Dael (CEA), Steve Gourlay (LBNL), Jean-Pierre Koutchouk (EuCARD & CERN), Steve Myers (CERN), Eric Prebys (US-LARP & FNAL), Gijs de Rijk (EuCARD & CERN), Lucio Rossi (CERN), Nicholas Sammut (MCST), Walter Scandale (EuCARD-AccNet & IN2P3), Vladimir Shiltsev (FNAL), Peter Spiller (EuCARD-AccNet & GSI), Ezio Todesco (EuCARD-AccNet & CERN), and Frank Zimmermann (EuCARD-AccNet & CERN).

The general goals of the HE-LHC10 Workshop were

- to investigate critical questions for HE-LHC and to propose solutions or follow-up,
- to document the HE-LHC concepts for future reference,
- to initiate and strengthen the collaboration within EuCARD, including CERN, GSI, US, Japanese, and Maltese partners, and
- to generate and/or to identify synergies with FAIR and to learn lessons from past VLHC and SSC studies.

Further information on the HE-LHC10 Workshop can be accessed from its home web site
http://indico.cern.ch/contributionListDisplay.py?confId=97971

The compilation of these proceedings would not have been possible without the help of the conveners and speakers, and the precious support of the Scientific Text Processing service. The hospitality and help of Nicholas Sammut, Vice Chairman and CEO of the Malta Council for Science and Technology, and the exceptional organizational support by the workshop secretary Merethe Morer-Olafsen are most gratefully acknowledged. Last not least, we would like to thank all the participants for their stimulating contributions and lively discussions. The HE-LHC10 Workshop was sponsored and supported by the European Commission under the FP7 "Research Infrastructures" project EuCARD, grant agreement no. 227579.

Geneva, 8 April 2011

S. Myers, L. Rossi, E. Todesco, F. Zimmermann

Contents

High-energy LHC injectors and infrastructure
(conveners: E. Prebys and L. Bottura)

Summing up
(conveners: S. Myers and F. Zimmermann)

[1] A paper was not submitted to the proceedings. However, the slides presented are available in electronic form at `http://indico.cern.ch/conferenceDisplay.py?confId=28832`.

[2] Talk given by V. Shiltsev

ELEMENTS OF A PHYSICS CASE FOR A HIGH-ENERGY LHC

James D. Wells, Cavendish Laboratory, University of Cambridge, United Kingdom

Abstract

I outline the elements of a physics case for a high-energy upgrade to the LHC. The motivations are centered around the perspective of "blue chip" ideas that solve the hierarchy problem: technicolor-like theories, supersymmetry, and extra dimensions. In each case there is the prospect that going to higher energies is not only desirable but needed for discoveries. Nevertheless, the results from experiment over the next few years, most especially at the LHC, will sharpen the arguments and enable a more enlightened decision between the various experimental options for the future. (Based on an October 14, 2010 presentation at the Malta HE LHC meeting.)

PRINCIPLES OF MOTIVATION

It is not possible to say with precision what physics ideas we will wish to study more than a decade from now, especially given that the LHC has just begun and we do not know what surprises it has in store for us. When discussing motivations for a collider experiment that is to begin decade(s) from now, there is the risk that everything said will be of little value in the future.

However, one thing is clear, and that is the energy frontier has been kind to us historically. We go up in energy, with appropriate luminosity gains, and we find new things. The first element of any physics case for the ramping up of energy is precisely the issue that gave us anxiety in the paragraph above: we do not know what is there, so let's go there.

One is tempted to end there. However, there is a second level of motivation needed beyond just increasing the energy. We need to ask ourselves what positive contributions could this new collider make if one of our main ideas of today is correct, and LHC does its job splendidly. Of course it is possible that none of our "ideas of today" are correct, but there are at least four good reasons for applying this approach anyway.

First, any other attitude (e.g., "who knows, let's see what happens without pre-conceived prejudices") is too speculative to support. Second, the knowledge gained through studying "theories of the day" likely will transfer to the study of the emergent theories refined by discoveries of tomorrow. Third, detectors and accelerator R&D must be guided by our best physics ideas now, with an eye toward inclusiveness to cover the possibilities. And fourth, this approach is a stable "physics case" strategy which by its formulation can change in the details and take into account further insights from theory and discoveries by experiment along the way, including those results that will come from LHC operation over the next few years.

HIERARCHY PROBLEM AS GUIDE

What ideas or "theories of today" shall we consider when discussing the case of the high-energy LHC (HE LHC)? There is subjectivity in that, and the answer will depend at least in small part on the person you are listening to. But you have me here, and I shall give my views, accompanied by a discussion somewhat centered on work I have done, yet which I believe are not out of step with the community's collective sensibilities.

There is no better place to look than in the proposed answers to the biggest question of our time because it is deep, important and ripe for answering: How did elementary particles get their masses at a scale so much lower than the Planck scale? This is the mass problem and the hierarchy problem jointly stated. The simplest idea for mass generation, the Standard Model (SM) Higgs boson, does not answer the question because it yields a weak scale that is unstable to quantum corrections.

Corrections to the Higgs mass are quadratically divergent according to $\delta m_h^2 \sim \Lambda^2$, and thus is highly unstable to the existence of a high scale that couples to the Higgs. Gravity, with its intrinsic large scale $M_{Pl} \sim 10^{19}\,\mathrm{GeV}$, couples to the Higgs boson and the problem is laid bare. Our most important theories of the day attempt to rectify this problem and give a full answer to the question above. The three main directions our efforts have taken us are

- Technicolor: disallow all scalars in the theory ("Higgs vacuum expectation value" is $\langle\psi_L\psi_R\rangle$).
- Supersymmetry: cancel quadratic divergence through symmetry ($\delta m_h^2 \sim \tilde{m}^2$).
- Extra Dimensions: disallow higher mass scales ($\Lambda \sim$ TeV).

The basic point I would like to make is that the HE LHC has the prospect of playing a decisive role in each of these three theory directions. There is no guarantee at this point that the HE LHC would be needed even if we knew that nature has chosen one of these three directions – there are too many free parameters of the theory that can be adjusted in and out of HE LHC relevance – but there is a strong plausibility argument that HE LHC could be needed, and the LHC results will likely tell us if that is indeed so.

TECHNICOLOR

Let us take first the idea of technicolor. I use the term "technicolor" very broadly here to mean any theory with

strong dynamics that induces electroweak symmetry breaking and has no inherit hierarchy problem. The quintessential example is that of a bilinear operator of technifermions condensing to break electroweak symmetry in a manner similar to ordinary quark bilinear condensation breaking chiral symmetry (and also electroweak symmetry, albeit very weakly). In the past, when the community discussed the potential need for a very high energy hadron collider, often this was the primary case it made. However, given developments of experiment over the last decade, there is an argument that today it no longer should be considered the leading motivation for a higher energy hadron collider.

First, traditional technicolor ideas suffer from some standard problems such as how to get all the fermion masses out of the theory without causing problem in flavor changing neutral currents. Another challenge is what to do about the non-discovery of pseudo-Nambu-Goldstone bosons expected in the symmetry breaking. Yet another challenge is the precision electroweak constraints, which do not suggest correct values for the S parameter. These challenges, and potential solutions, are discussed in [1].

Regarding precision electroweak, there is an additional point that steers us away from traditional technicolor theories and their cousins. Back some time ago, there was very little experimental input to the question of electroweak symmetry breaking (EWSB). For example, if we assume a simple SM Higgs boson explanation for EWSB there were not even decent range limits to what this mass could be. Thus, EWSB could be just as much of a "strong" phenomenon (i.e., Higgs boson, or equivalent dynamics, quite massive) as a "weak" phenomenon (i.e., Higgs boson mass around m_Z). Today we know it is a weak phenomenon – the best fit Higgs boson mass is around m_Z with upper limit not more than about $2m_Z$ at 95% CL. This, I believe, is telling us that whatever is accomplishing EWSB it is less likely to be a strongly coupled theory at the weak scale.

The traditional argument for a very high-energy hadron collider machine was to first state that EWSB is completely unknown, and then to suggest that if it is "strongly coupled" then unitarization of the longitudinal W scattering, for example, would manifest itself by wiggles and wobbles in the very high energy scattering of those states. Perhaps a ρ-like resonance would come in at a TeV or two to save the unitarity of the theory, and the high-energy collider would see it. Today, that motivation is less appealing for the reasons given above.

Nevertheless, there can be mild conspiracies with precision electroweak, and proponents like to suggest this direction is no worse than others when it comes to making a full theory of the weak scale. These protestations might even be fair, and so it behooves us to at least state that if nature chooses this path it will be crucial to have HE LHC. It is obvious that to find a very heavy ρ-like resonance a dramatic increase in energy and/or luminosity would be needed. But energy is more important. I do not go into it in more detail here but to highlight this fact by an extended quote from the Barklow et al. report [2], where these issues have been studied:

> There has been some discussion of upgrading the LHC in luminosity and energy after the $300\,\mathrm{fb}^{-1}$ run is complete. A possible (though unlikely) doubling of the energy has been considered along with a tenfold increase in instantaneous luminosity. Since the LHC detectors were not designed for these conditions only jet and muon information is likely to be useful. Such an upgrade could double the reach for a Z' ($m_{Z'} \simeq 10$ TeV) and compositeness ($\Lambda \simeq 80$ TeV), and significantly increase the sensitivity for excited quarks ($m_{q*} \simeq 9$ TeV) and the scale of WW scattering available ($\sqrt{\hat{s}} \simeq 1.5\,\mathrm{TeV}$, assuming that forward jet tagging is still possible). *Unfortunately, most of these gains come from the energy increase* which is less plausible than a simple luminosity upgrade. [italics are mine]

My summary: inasmuch as strong dynamics ideas are worth pursuing, higher energy may be critical for success.

SUPERSYMMETRY

The second approach to discuss is supersymmetry. Supersymmetry solves the hierarchy problem via a posited symmetry between fermions and bosons (for a review see [3]). The quadratic divergence of a top quark loop in the self energy of the Higgs boson, $y_f^2\Lambda^2/4\pi$, is exactly cancelled by a top squark loop, $-y_f^2\Lambda^2/4\pi$, in the supersymmetric limit. For softly broken supersymmetry this cancellation is not exact, but effective up to supersymmetry breaking masses $\delta m_h^2 \propto \tilde{m}_t^2$, where $\tilde{m}_t$ is the supersymmetry breaking mass contribution to the top squark. For the hierarchy problem to be solved, the masses of the superpartners of the Standard Model states need to be in the neighborhood of the weak scale.

I cannot be anything more than vague about the expectations of supersymmetry partner masses. Some people make admirable and non-frivolous attempts to quantify the finetuning of the hierarchy when supersymmetry masses get heavier than the weak scale [4], but I have a difficult time taking any precise criteria seriously. Nevertheless, I do take the hierarchy problem seriously. What to do?

In the case of supersymmetry, we can confidently say that the lighter the superpartner masses are, the larger role supersymmetry plays in stabilizing the hierarchy. Whether the maximum tolerable superpartner masses should be 1 TeV, 10 TeV, or 1000 TeV, I do not know. I am not sure our finetuning sensibilities are accurate enough to strongly discount any of these scales. Furthermore, there is some advantage to having superpartner mass scales climb to larger values. In particular, there are advantages to having all the scalar superpartner masses be very heavy [5, 6, 7]. The reason is that their large masses can squash unwanted contributions to flavor changing neutral currents and CP violating observables, such as electric dipole moment of the neutron.

On the other hand, gauge coupling unification and dark matter considerations prefer the fermion superpartner masses to be much smaller. The lightest neutralino, if a wino or a higgsino (i.e., superpartner of W boson or Higgs boson), can be an excellent dark matter candidate with mass as high as 2 TeV but not higher. Restrictions on the bino (i.e., superpartner of the hypercharge gauge boson) are even tighter. Thus, a $\sim$ TeV limit on the fermion superpartners is a reasonable assumption. In most models of supersymmetry breaking the gluino (i.e., superpartner of the gluon) is a factor of ~ 2 to 10 higher in mass than the LSP. Thus, the gluino mass gets restricted to less than about 15 TeV by these considerations.

We have already established that a liberal attitude toward the hierarchy problem enables scalar superpartner masses to be well above LHC energy reach, and even a 33 TeV HE LHC collider reach. We must focus on the fermion superpartners, which have a more restricted range of possibilities. It is well-known that at the LHC with several tens of fb^{-1} of integrated luminosity, none of the fermionic superpartners over a TeV in mass has a chance of being found directly except the gluino. The limit on the sensitivity to the gluino is around 2.5 TeV with less than $50\,\mathrm{fb}^{-1}$ of data [8] in this scenario.

Given the dark matter considerations stated above and the usual limit of $m_{\tilde{g}} < 10 m_{LSP} \simeq 15\,\mathrm{TeV}$, the LHC sensitivity is far below the range of mass that would cover the "full parameter" space of these ideas. A 33 TeV HE LHC clearly will do better, all other considerations equal, and that is the crux of the supersymmetry argument: deeper exploration into the high-mass lands. Determining precisely how much better the HE LHC can do over LHC, and over a high-luminosity LHC, when the parameters of the collider luminosity and detector performance are better understood, would contribute an important element to the case for the HE LHC. It should be noted that a high-energy e^+e^- collider may very well enable the complementary probing of the lighter electroweak superpartner fermions, in which case it could compete well with a HE LHC for discovering supersymmetry at the highest mass scales.

EXTRA DIMENSIONS

We now come to a third motivation which is extra dimensions. My discussion will be about the flat extra dimensions of Arkani-Hamed, Dimopoulos and Dvali (ADD) [9], but there are analogous and extended arguments one could make with the Randall-Sundrum case of warped extra dimensions [10]. The warped case even has some phenomenological overlap with the technicolor theories, which can be understood qualitatively through the AdS/CFT correspondence (AdS is the warped extra dimension theory, and CFT is the walking technicolor theory). Due to lack of time I will forego that interesting discussion and focus on the flat extra dimensions of ADD, where the value of higher energy is immediately transparent.

If we assume that there exists n extra spatial dimensions compactified on a torus of radius R, the relationship between the fundamental scale of gravity M_D ($\sim$ TeV scale) and the ordinary Planck scale as measured by Newton's constant for gravitational attraction of bodies separated by a distance much greater than R is $M_{Pl}^2 = R^n M_D^{n+2}$. The graviton is allowed to propagate into the extra dimensional space, and since it is a compact space, the momentum components in the extra dimensions are quantized. Momentum in extra dimensions looks like mass in our ordinary $3+1$ dimensions, and thus the graviton looks like a series of Kaluza-Klein excitations with masses $m_{\vec{n}}^2 = \vec{n} \cdot \vec{n}/R^2$.

The details of this theory can be found in many review articles (e.g., see [11]). Many observables in this game are not calculable, but only qualitatively given with ignorance parametrized. A good example of that is virtual graviton exchange. When contemplating the effects of low-scale gravity contributions to Drell-Yan scattering for example, one must sum over the infinite tower of KK states in $q\bar{q} \to G^{(\vec{n})} \to e^+e^-$ which is generally divergent. The divergence can be regularized arbitrarily and the amplitude can be represented by energy momentum tensor squared with a coupling constant of Λ_T^{-4} to get the dimensionality correct. The value of Λ_T is expected to be nearly the value of M_D but the precise numerics are unknowable.

However, there are two observables that are calculable in this framework. One is the rate of external graviton emission in the limit of $E \ll M_D$, and the other is the eikonal regime of very high energy $E \gg M_D$ elastic scattering. The HE LHC has much to offer in both of these limits.

Let's take graviton emission to begin with. The cross-section to produce one KK graviton in a production cross-section such as $q\bar{q} \to G^{(n)} g$ is $\sigma_{KK} \sim 1/M_{Pl}^2$. It would take many orders of magnitude beyond the lifetime of the universe to produce even one of these KK states with energy above a GeV. However, there are very many of these gravitons spaced closely to each other. Below the energy E there are $(ER)^n$, a truly staggering number of gravitons when one realizes how large R must be to seesaw M_{Pl} down all the way to $M_D \sim$ TeV. The probability of producing *any* one graviton then goes up to $\sigma_{any\,KK} \sim (ER)^n/M_{Pl}^2$. But with $R^n = M_{Pl}^2/M_D^{2+n}$, the total summed cross-section is

$$\sigma_{any\,KK} \sim \frac{1}{M_D^2}\left(\frac{E}{M_D}\right)^n . \qquad (1)$$

Note that in the equation above the cross-section climbs steeply with energy. This is in contrast to most other high-energy cross-sections that usually decrease with energy $\sigma \sim 1/E^2$. This is one of the core reasons why it is sometimes stated "energy is everything" for extra-dimensional theories. Large increases in luminosity pale in comparison to what can be accomplished by even moderate increases in energy of the collider. The high-power scaling of this observable with respect to energy means that as one dials energy up it can be the case that nothing is seen, until a small turn of the energy knob yields an explosion of events. The HE LHC is just such an energy knob that could possibly do

this for us.

The above scenario presupposes that the LHC finds nothing, and that as we increase the energy for HE LHC a signal develops. However, it could be the case that the LHC does find a signal already for external graviton emission. Perhaps it will not know with certainty that it is graviton emission, and perhaps it does not have other phenomenological handles to pin down more details of the theory. How could going to higher energies help?

In that case going to higher energies enables us to reach another perturbative regime of the scattering. Seeing a signal of gravition emission at the LHC means that M_D is not more than a few TeV. Scattering at 33 TeV center of mass energy at the HE LHC then would enable us to probe center of mass collisions with energy much greater than M_D. At small momentum transfer, the glancing blows of partons scattering at energies well above M_D is a computable, classical amplitude. The two-parton to two-parton eikonal approximation is used for this kind of analysis [12, 13].

The corrections to this eikonal ampitude scale as $-\hat{t}/\hat{s}$ and $(M_D^2/s)^{1+2/n}$, and thus serve as expansion parameters for the eikonal resumation perturbation theory. When the expansion parameter $-\hat{t}/\hat{s}$ is small that is correlated with the impact parameter being less than the Schwarzschild radius, thereby avoiding the risk of producing a black hole [14]. When the expansion parameter M_D^2/s is small that is correlated with the impact parameter remaining in the classical regime, with minimal quantum corrections. There may be model-dependent string corrections as well, or other new physics contributions, but we do not consider them here as we are dealing only with the well-defined gravity scattering amplitude.

To give a visual representation of the computability of two-to-two scattering in the high-energy eikonal regime, we introduce the parameter ϵ, defined to be

$$\epsilon = \left|\frac{\hat{t}}{\hat{s}}\right| + \left(\frac{M_D^2}{s}\right)^{1+2/n}, \qquad (2)$$

and then compute this ϵ and the scattering rates for LHC at 14 TeV and 33 TeV [13]. For two-to-two scattering, there is a direct correspondence between $-\hat{t}/s$ and $\Delta\eta = \eta_1 - \eta_2$, the difference in rapidities of the two jets:

$$\frac{-\hat{t}}{\hat{s}} = \frac{1}{1+e^{\Delta\eta}}. \qquad (3)$$

The larger the $\Delta\eta$ separation of jets the smaller $-\hat{t}/\hat{s}$ and thus the more accurate the eikonal computation.

In Fig. 1 we have plotted the differential two-jet cross-section $d\sigma/d\Delta\eta$ as a function of $\Delta\eta$ for three different values of the fundamental gravity scale $M_D = 1.5\,\mathrm{TeV}, 3\,\mathrm{TeV}$ and $5\,\mathrm{TeV}$ in $n = 6$ extra dimensions. The background is also shown, here calculated from the leading order $2 \to 2$ QCD scattering processes. The plot was made for the dijet invariant mass greater than $M_{jj} > 9\,\mathrm{TeV}$, which means that for all collisions $\hat{s} > M_{jj,min}^2 = (9\,\mathrm{TeV})^2$. In addition, $p_T > 100\,\mathrm{GeV}$ and $|\eta| < 5$ are required for acceptance of each jet. The signal lines have three colors, green (light solid) line meaning the most calculable region with $\epsilon < 0.15$, blue (dashed) line for $0.15 < \epsilon < 0.3$ and red (dotted) for $0.3 < \epsilon < 0.5$. We do not extend the lines any further leftward for $\epsilon > 0.5$ as there is no reliability to speak of for that region. We see that for very high $\Delta\eta$ the signal is computable but the background dominates, and for very low $\Delta\eta$ the signal computation is not reliable. Thus, an intermediate region of $2 < \Delta\eta < 6$ is ideal from the standpoint of calculable signal to background advantage. Note, the $M_D = 5\,\mathrm{TeV}$ signal line never has a green (light solid) line component since the M_D^2/s correction takes $\epsilon > 0.15$ always.

At higher center of mass energy afforded by the HE LHC, we can set the dijet invariant mass cut to be much higher while at the same time boosting the total rate for the signal. We illustrate that in Fig. 2 which is the same plot as Fig. 1 except the center of mass energy of the collider is $33\,\mathrm{TeV}$ and the dijet invariant mass has been raised to $M_{jj} > 15\,\mathrm{TeV}$. We see that not only has the event rate increased while keeping the signal to background similar, but the $M_D = 5\,\mathrm{TeV}$ line has now "turned green", meaning that we have trust in the eikonal amplitude's appropriateness for the computation, and thus the result is calculable.

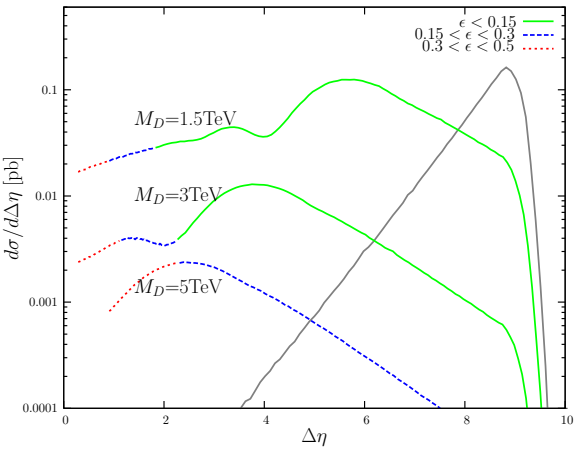

Figure 1: The differential two-jet cross-section $d\sigma/d\Delta\eta$ at 14 TeV LHC as a function of $\Delta\eta$ for three different values of the fundamental gravity scale M_D. The dijet invariant mass cut is $M_{jj} > 9\,\mathrm{TeV}$.

It is unlikely that the first discovery of physics beyond the Standard Model would come through high energy two-to-two eikonal scattering well above the Planck mass. Instead, the example here serves to illustrate just one of the many ways that building a much higher energy collider can lead to complementary information inaccessible to what came before. LHC is good for cis-Planckian and perhaps Planckian physics, and the HE LHC could then access the Planckian and trans-Planckian regions to teach us more about the underlying theory of gravity, and perhaps fill in the phase diagram of gravitational scattering [15].

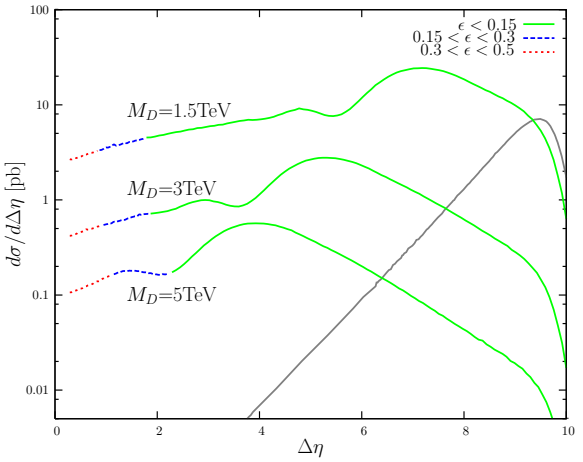

Figure 2: The differential two-jet cross-section $d\sigma/d\Delta\eta$ at 33 TeV LHC as a function of $\Delta\eta$ for three different values of the fundamental gravity scale M_D. The dijet invariant mass cut is $M_{jj} > 15$ TeV.

TOMORROW'S WORLD

What I have presented are some elements of a physics case based on what we know today. That case can be refined by more detailed statements of collider performance and would-be detector characteristics. Simulations can be done, and cost-benefit plots can be made. Comparisons can and should be made between a HE LHC option and other options that are before us as a community: ILC, CLIC, high-luminosity LHC, eLHC, muon collider, VLHC, etc.

However, it is equally obvious and important to make another point. It may be unlikely that any of the details of the justification that we can make today will be the reason why physicists will be happy to throw the on switch for HE LHC. The results of the LHC will change everything, one way or another. There will be a new "theory of the day" at each major discovery, and the arguments will sharpen in some ways and become more divergent in other ways. Yet, the need to explore the high energy frontier will remain. We will always be able to make that case, today and tomorrow.

REFERENCES

[1] K. Lane, "Two lectures on technicolor," [hep-ph/0202255].

[2] See section III.C "Super-LHC" in T. L. Barklow, R. S. Chivukula, J. Goldstein, T. Han, "Electroweak symmetry breaking by strong dynamics and the collider phenomenology," Snowmass 2001 Proceedings [hep-ph/0201243].

[3] S. P. Martin, "A Supersymmetry primer," In *Kane, G.L. (ed.): Perspectives on supersymmetry* 1-98. [hep-ph/9709356].

[4] For one of the most recent examples, see S. Cassel, D. M. Ghilencea, G. G. Ross, "Testing SUSY at the LHC: Electroweak and Dark matter fine tuning at two-loop order," Nucl. Phys. B835, 110-134 (2010). [arXiv:1001.3884 [hep-ph]].

[5] J.D. Wells, "Implications of supersymmetry breaking with a little hierarchy between gauginos and scalars," hep-ph/0306127; J. D. Wells, "PeV-scale supersymmetry," Phys. Rev. D71, 015013 (2005). [hep-ph/0411041].

[6] N. Arkani-Hamed, S. Dimopoulos, "Supersymmetric unification without low energy supersymmetry and signatures for fine-tuning at the LHC," JHEP 0506, 073 (2005). [hep-th/0405159];

[7] G. F. Giudice, A. Romanino, "Split supersymmetry," Nucl. Phys. B699, 65-89 (2004). [hep-ph/0406088].

[8] H. Baer, V. Barger, A. Lessa *et al.*, "Supersymmetry discovery potential of the LHC at s**(1/2) = 10-TeV and 14-TeV without and with missing E(T)," JHEP 0909, 063 (2009). [arXiv:0907.1922 [hep-ph]].

[9] N. Arkani-Hamed, S. Dimopoulos, G. R. Dvali, "The Hierarchy problem and new dimensions at a millimeter," Phys. Lett. B429, 263-272 (1998). [hep-ph/9803315].

[10] L. Randall, R. Sundrum, "A Large mass hierarchy from a small extra dimension," Phys. Rev. Lett. 83, 3370-3373 (1999). [hep-ph/9905221].

[11] G. D. Kribs, "TASI 2004 lectures on the phenomenology of extra dimensions," [hep-ph/0605325].

[12] G. F. Giudice, R. Rattazzi, J. D. Wells, "Transplanckian collisions at the LHC and beyond," Nucl. Phys. B630, 293-325 (2002). [hep-ph/0112161].

[13] W.J. Stirling, E. Vryonidou, J.D. Wells, in progress.

[14] S. B. Giddings, S. D. Thomas, "High-energy colliders as black hole factories: The End of short distance physics," Phys. Rev. D65, 056010 (2002). [hep-ph/0106219].

[15] S. B. Giddings, "Beyond the Planck scale," [arXiv:0910.3140 [gr-qc]].

CERN ACCELERATOR STRATEGY

S. Myers

CERN, Geneva, Switzerland

Abstract

The CERN strategy for future accelerator projects is outlined and the role of the HE-LHC inside this strategy is described.

INTRODUCTION

The EuCARD-AccNet workshop HE-LHC'10 on a higher-energy LHC (HE-LHC) had invited a presentation on motivation, status, and strategy for HE-LHC studies. The motivation for the HE-LHC should come from the users, i.e. from the particle physicists, and it was already described by the previous speaker [1]. The present HE-LHC status covering magnets, detectors, cryogenics, vacuum, beam dynamics, injectors, etc. should come from the four main workshop sessions. The accelerator strategy, indeed, should come from the CERN Directorate. It is sketched in the following.

STRATEGY

CERN has been, is, and will be the world's energy frontier laboratory. Presently, the LHC is being commissioned with beam. The LHC, with finally 7 TeV/beam, will be the highest energy collider on the planet for the foreseeable future. The higher-luminosity LHC (HL-LHC) is a proposed luminosity upgrade for installation in 2020–2021 and operation until around 2030. The HL-LHC also includes an upgrade of the LHC injector complex.

A study for an electron–proton collider based on the LHC, namely a Large Hadron electron Collider (LHeC) is supported by NuPECC and ECFA, and a Conceptual Design Report (CDR) is due to be finalized at the end of 2010 or early in 2011.

On the electron–positron front, the CLIC linear collider study will complete a CDR by 2011 and the CLIC Technical Design Report (TDR) by 2016–2020, depending on funding.

In the long-term strategic view of CERN, a Linear Collider would be constructed probably after the HL-LHC (>2030). BUT the question arises what will happen if the Linear Collider "does not fly" (e.g., for reasons of politics, finances, governance, energy and climate situation). What alternatives would exist in such a case? It seems there are two, namely HE-LHC and neutrinos. A project on the scale and innovation level of the HE-LHC has a long preparation lead time. Therefore, the HE-LHC'10 workshop appears timely. It complements the studies by a small HE-LHC working group which has been active at CERN since April 2010, and recently published its first considerations on the HE-LHC [2].

SUMMARY

The CERN accelerator strategy comprises the following ingredients:

- LHC operation at 7 TeV/beam up to design luminosity;
- HL-LHC for installation in 2020/2021;
- Linear collider TDR for 2016–2020;
- Investigation of the HE-LHC as a feasibility study;
- R&D on high power proton drivers; and
- CDR for a LHeC (with ring–ring and ring–linac options).

ACKNOWLEDGEMENTS

I thank the workshop organizers and the editors of the proceedings for their help in advancing the HE-LHC.

REFERENCES

[1] J. Wells, "Physics Case", Proc. HE-LHC'10, Malta, these proceedings.

[2] R. Assmann et al., "First Thoughts on a Higher-Energy LHC", CERN-ATS-2010-177 (2010).

HE-LHC BEAM- PARAMETERS, OPTICS AND BEAM-DYNAMICS ISSUES

O. Brüning, O. Dominguez, S. Myers, L. Rossi, E. Todesco, F. Zimmermann

CERN, Geneva, Switzerland

Abstract

The Higher-Energy LHC (HE-LHC) should collide two proton beams of 16.5-TeV energy, circulating in the LHC tunnel. We discuss the main parameter choices, as well as some optics and beam dynamics issues, in particular the time evolution of emittances, beam-beam tune shift and luminosity, with and without controlled emittance blow up, considering various constraints, and the quadrupole-magnet parameters for arcs and interaction regions.

MAIN PARAMETERS

The HE-LHC beam energy of 16.5 TeV corresponds to a dipole magnet of about 20-T field (see Table 1). These values should be compared with the LHC design parameters of 7 TeV and 8.33 T. They assume an identical geometry and the same bending-magnet filling factor. It should be noted that the 20 T operational field level is the upper limit of a 16-20 T range being considered and must be understood as design target value. Only a thorough global optimization study can indicate the most convenient, or simply the possible, field strength for the main dipoles.

The target peak luminosity at 33 TeV c.m. energy is chosen as 2×10^{34} cm^{-2} s^{-1}[1], i.e. equal to twice the LHC design luminosity. At this luminosity value the radiation effects in the interaction region (IR), e.g. for the final triplet magnets and the detectors, are similar to those for the High-Luminosity LHC (HL-LHC) at 7 TeV beam energy with a target peak luminosity of 5×10^{34} cm^{-2} s^{-1}. The IR radiation sensitivity, related to the collisions, is taken to scale with the product of beam energy and luminosity. We assume that the IR solutions found for the HL-LHC will also suit the HE-LHC IR. The HL-LHC already pushes the requirements to near - or beyond - the present state of the art.

The interaction-point (IP) beta functions are set to values between 0.4 and 1.0 m, which is comparable to the 0.55 m of the LHC design, and larger than for the HL-LHC (where proposed values range between 7 and 30 cm). Differently from LHC, the HE-LHC IP beta functions and emittances may be unequal in the two transverse planes.

The normalized transverse emittances at the start of a physics store are assumed to be in the range 1.8-3.8 μm - possibly different in the horizontal and vertical plane - and, hence, similar to those of both the nominal and the present LHC.

A total number of 1404 bunches is considered, at 50 ns spacing, at slightly more than the LHC design bunch intensity. The smaller than nominal number of bunches limits the beam-screen heat load from synchrotron radiation and image currents, keeps the stored beam energy at 480 MJ, close to the 360 MJ design value of LHC, which is important for machine protection, and has the additional benefit that the electron cloud is more benign than for a bunch spacing of 25 ns. The HE-LHC will feature additional electron-cloud mitigation measures like coatings or distributed clearing electrodes. An alternative scenario with 2808 bunches per beam, at 25 ns spacing, could operate at half the bunch charge with half the transverse emittance, with the same stored beam energy. This scenario would, however, be more challenging for machine protection and collimation, due to the increased transverse energy density, and is also likely to give rise to stronger electron-cloud effects.

The arc-dipole coil aperture is taken to be 40 mm, which is the same value as the original design value of the Superconducting Super Collider (SSC) [before it was increased and the project ultimately cancelled]. For comparison, the LHC coil diameter is 56 mm.

Taking into account margins for beam tube and beam screen, the related beam half aperture is reduced from 20 mm for the LHC to 13 mm for the HE-LHC. This represents a reduction of about 30%. The arc maximum aperture is needed at injection. A reduced aperture is acceptable since the HE-LHC injection energy will be higher than for the LHC.

Specifically, the HE-LHC injection energy is assumed to be equal to, or higher than, 1 TeV. This energy is chosen to confine the HE-LHC energy ramp to a factor of not much more than 16-20, similar to the present LHC. The beam energy of the SPS, serving as LHC injector, does not exceed 450 GeV. For the HE-LHC a new injector with beam energy above 1 TeV will be required.

With the assumed number of bunches and peak luminosity, the maximum number of events per crossing comes out to be about 4 times the nominal LHC, or 76, which is below the peak pile up considered for the HL-LHC. In this estimate, the total inelastic cross section at 33 TeV c.m. energy is assumed to be similar to the one at 14 TeV, i.e. about 60 mbarn.

The longitudinal emittance damping time from synchrotron radiation can be computed to be 1 hour, which is to be compared with 13 h for the nominal LHC. The synchrotron radiation leads to a rapid shrinkage of all three emittances, which can be controlled by noise injection in order to stabilize the beam with regard to impedance-driven instabilities or the beam-beam interaction.

Table 1: Flat and round-beam HE-LHC parameters [1].

	nominal LHC	HE-LHC	
beam energy [TeV]	7	16.5	
dipole field [T]	8.33	20	
dipole coil aperture [mm]	56	40	
beam half aperture [cm]	2.2 (x), 1.8 (y)	1.3	
injection energy [TeV]	0.45	>1.0	
#bunches	2808	1404	
bunch population [10^{11}]	1.15	1.29	1.30
initial transverse normalized emittance [μm]	3.75	3.75 (x), 1.84 (y)	2.59 (x & y)
initial longitudinal emittance [eVs]	2.5	4.0	
number of IPs contributing to tune shift	3	2	
initial total beam-beam tune shift	0.01	0.01 (x & y)	
maximum total beam-beam tune shift	0.01	0.01	
beam circulating current [A]	0.584	0.328	
RF voltage [MV]	16	32	
rms bunch length [cm]	7.55	6.5	
rms momentum spread [10^{-4}]	1.13	0.9	
IP beta function [m]	0.55	1 (x), 0.43 (y)	0.6 (x & y)
initial rms IP spot size [μm]	16.7	14.6 (x), 6.3 (y)	9.4 (x & y)
full crossing angle [μrad]	285 (9.5 $\sigma_{x,y}$)	175 (12 σ_{x0})	188.1 (12 σ_{x0})
Piwinski angle	0.65	0.39	0.65
geometric luminosity loss from crossing	0.84	0.93	0.84
stored beam energy [MJ]	362	478.5	480.7
SR power per ring [kW]	3.6	65.7	66.0
arc SR heat load dW/ds [W/m/aperture]	0.17	2.8	2.8
energy loss per turn [keV]	6.7	201.3	
critical photon energy [eV]	44	575	
photon flux [10^{17}/m/s]	1.0	1.3	
longitudinal SR emittance damping time [h]	12.9	0.98	
horizontal SR emittance damping time [h]	25.8	1.97	
initial longitudinal IBS emittance rise time [h]	61	64	~68
initial horizontal IBS emittance rise time [h]	80	~80	~60
initial vertical IBS emittance rise time [h]	~400	~400	~300
events per crossing	19	76	
initial luminosity [10^{34} $cm^{-2}s^{-1}$]	1.0	2.0	
peak luminosity [10^{34} $cm^{-2}s^{-1}$]	1.0	2.0	
beam lifetime due to p consumption [h]	46	12.6	
optimum run time t_r [h]	15.2	10.4	
integrated luminosity after t_r [fb^{-1}]	0.41	0.50	0.51
opt. av. int. luminosity per day [fb^{-1}]	0.47	0.78	0.79

The emittance shrinkage allows for a natural and easy way of leveling the luminosity or the beam-beam tune shift, simply by controlling the amount of noise injected to blow up the beam, without any changes of optics, orbit or crab-cavity voltage.

The synchrotron-radiation heat load is approximately 2.8 W/m/aperture, significantly higher than the value of 0.17 W/m/aperture for the nominal LHC, and slightly above the maximum local cooling available with the present beam-screen capillaries. The total synchrotron radiation power per beam is 66 kW, almost a factor 20 higher than the 3.6 kW for the nominal LHC, but still close to the capacity limit of the existing LHC cryogenic plants [1,2].

The 400-MHz RF voltage is taken to be 32 MV, which is twice the nominal value of 16 MV. This value had been chosen to keep the synchrotron tune approximately the same as for the present LHC (which might be important for beam and particle stability). A value of 16 MV as for the nominal LHC is also possible, however [3]. In order to maintain Landau damping the longitudinal emittance ($4\pi\sigma_z\sigma_E$) is increased with the square root of the beam energy [4], to about 4 eVs at 16.5 TeV, starting from a value of 2.5 eVs at 7 TeV. Together with the assumed RF voltage this yields an rms bunch length of 6.5 cm not much shorter than the nominal value at 7 TeV of 7.55 cm. With 16 MV RF voltage, and for the same longitudinal emittance, the rms bunch length would be 8.0 cm.

The beam lifetime due to proton consumption is about 13 h, to be compared with 46 h for the nominal LHC and about 10 h for the HL-LHC. For both energies a total cross section of 100 mbarn is considered. The optimum run time is about 10 h assuming a 5-h turnaround time. This is somewhat shorter than the 15-h run time for the nominal LHC, due to the higher luminosity. The optimum average luminosity per day is about 0.8 fb^{-1}, or some 60% larger than an optimistic value of 0.5 fb^{-1} for the nominal LHC.

The maximum total beam-beam tune shift for 2 IPs varies between 0.01 and 0.03. The maximum value can be restricted through transverse emittance control by noise injection. Without such external noise, the transverse emittance would result from the interplay of synchrotron radiation damping, intrabeam scattering, and the beam-beam interaction, which is a topic to be further investigated (see also [5]).

Both flat-beam and round-beam HE-LHC scenarios exist, as is illustrated in Table 2. The two scenarios promise similar luminosity performance.

The crossing angle for the nominal LHC corresponds to a separation of $9.5\sigma_{x,y}$ at the parasitic long-range collision points around the IP. For the HE-LHC the crossing angles chosen provide an initial separation of $12\sigma_{x0}$ at the close-by parasitic encounters and an even larger normalized separation after emittance shrinkage. Therefore, long-range beam-beam effects should not be important for the HE-LHC. Table 1 presents a more complete list of HE-LHC parameters [1].

Table 2: Flat & round-beam scenarios for the HE-LHC.

	nominal	HE-LHC	
	(round)	**Flat**	**round**
$\gamma\varepsilon$ (μm)	3.75	3.75 (x), 1.84 (y)	2.59 (x&y)
β^* (m)	0.55	1 (x), 0.43 (y)	0.6 (x&y)
σ^* [μm]	16.7	14.6 (x), 6.3 (y)	9.4 (x&y)
θ_c [μrad]	285	175	188

LUMINOSITY TIME EVOLUTION

Figure 1 shows the emittance evolution, for both flat and round beams, during a physics store with and without controlled emittance blow up. The luminosity evolution for the case with controlled blow up, in order to limit the total beam-beam tune shift to a value of 0.01, is illustrated in Fig. 2, which also demonstrates the equivalent performance of flat-beam and round-beam collisions. Figure 3 presents the time evolution of the corresponding integrated luminosities.

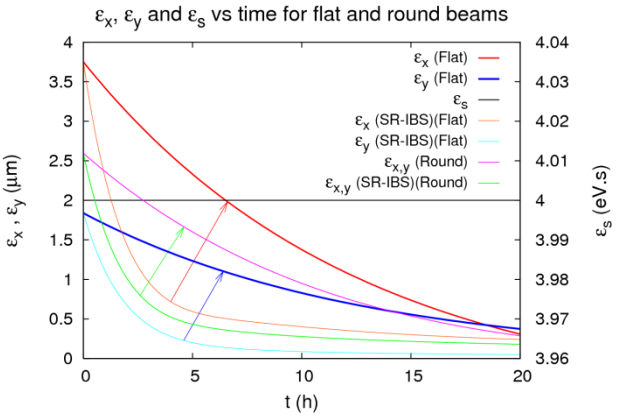

Figure 1: Evolution of the HE-LHC emittances, for flat and round beams, during a physics store with controlled blow up and constant longitudinal emittance of 4 eVs plus constant crossing angle (the thicker lines at the top), and the natural transverse emittance evolution due to radiation damping and IBS only (the thinner lines at the bottom) – still for constant longitudinal emittance and constant crossing angle, which might lead to excessive tune shifts.

What happens if we drop the constraint $\Delta Q_{tot} \leq 0.01$? This question is legitimate as the LHC has already reached a value of $\Delta Q_{tot} \sim 0.02$ (about twice the design value) without evidence for a beam-beam limit, and since LHC strong-strong beam-beam simulations by K. Ohmi, e.g. in [5], predict the LHC beam-beam limit at $\Delta Q_{tot} > 0.03$.

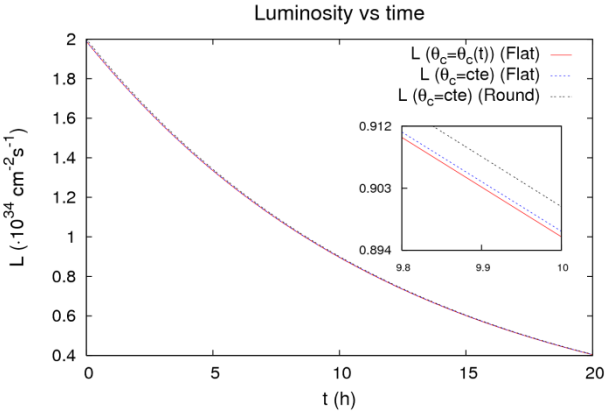

Figure 2: Time evolution of the HE-LHC luminosity, for both flat and round beams, including emittance variation with controlled blow up and proton burn off. Curves with constant or varying crossing angle lie on top of each other if the beam-beam tune shift is kept constant as assumed here.

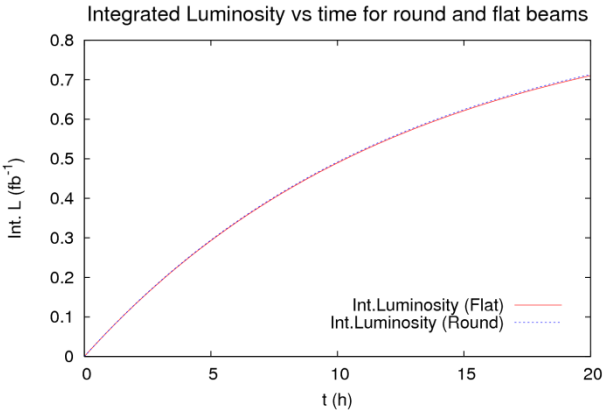

Figure 3: Time evolution of the HE-LHC integrated luminosity, for both flat and round beams, during a physics store including emittance variation with controlled blow up, keeping $\Delta Q_{tot} \leq 0.01$, and proton burn off.

Figure 4 shows the predicted tune shifts as a function of time during a physics store in the presence of synchrotron radiation damping and proton burn off, without any transverse emittance blow up, for flat and round beams, respectively. With flat beams the peak tune shift exceeds 0.03, with round beams it is about 0.02. In view of this difference, the round-beam option appears to be more conservative, with more than 30% lower beam-beam tune shift.

Figures 5 and 6 present the corresponding time evolutions of instantaneous and integrated luminosity, respectively, again with synchrotron-radiation and proton burn off, but without any controlled blow up. The gain in integrated luminosity of about 10% for the flat-beam case is much smaller than the increase in the peak beam-beam tune shift.

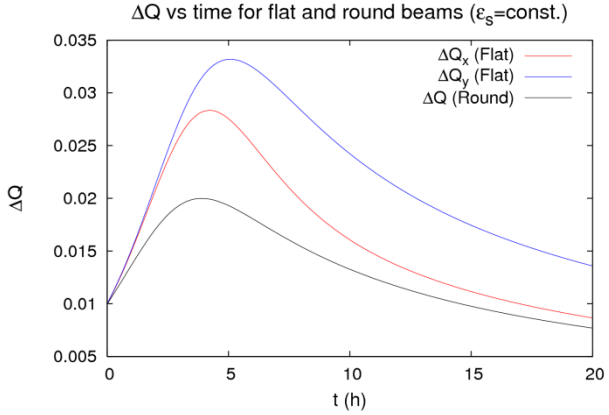

Figure 4: Time evolution of the HE-LHC tune shifts, for flat and round beams during a physics store including SR emittance shrinkage *without* controlled transverse blow up, and including proton burn off.

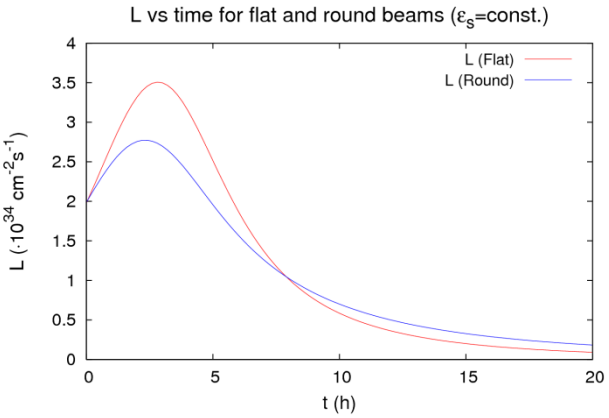

Figure 5: Time evolution of the HE-LHC instantaneous luminosity, for both flat and round beams, including SR emittance shrinkage and proton burn off, without controlled transverse blow up.

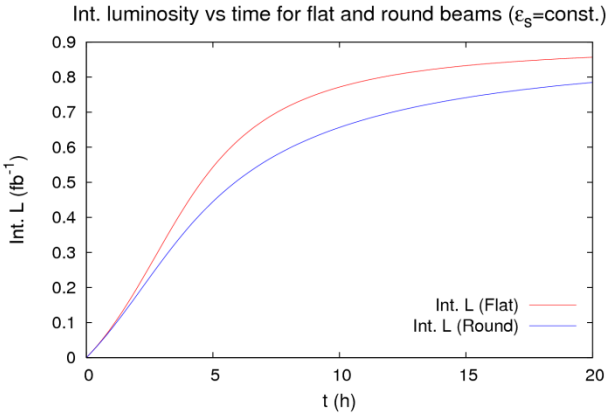

Figure 6: Time evolution of the HE-LHC integrated luminosity, for both flat and round beams, including SR emittance shrinkage and proton burn off, without controlled transverse blow up.

The sensitivity of the integrated luminosity to some of the assumptions has been investigated. For the baseline

HE-LHC we have 0.8 fb^{-1}/day as optimum average luminosity value (without any downtime and 100% availability). Without longitudinal blow up the average luminosity would be 5-20% lower, and without transverse blow up 10-20% higher. Another 25% increase of the average luminosity could be obtained, for round beams, with the ultimate bunch intensity of 1.7×10^{11} protons, along with a larger initial transverse normalized emittance of 3.6 μm, and $\beta^* \sim 0.8$ m (instead of 0.6 m).

QUADRUPOLE MAGNETS

How do the interaction-region magnets scale with energy and β*? Can one hope to get a β* of 0.5-0.6 m, similar to the nominal LHC, at 2.36 times higher beam energy? Figure 7 illustrates the interdependence of the peak beta function in the final quadrupoles, the quadrupole gradient, the magnetic field at a radius of 16.5σ plus 11 mm (margin for beam screen, orbit and alignment errors, etc), and the IP beta function for 7 TeV beam energy, considering a triplet configuration [6]. Figure 8 converts Fig. 7 to 16.5 TeV beam energy, where the gradient scales with the beam energy, and the beam size with the square root of the energy and with the square root of the normalized emittance. For example, in order to achieve β*=0.55m at 16.5 TeV, a gradient of 400 T/m results in a peak beta function of about 4 km. With a normalized emittance γε=2.64 μm, the full beam aperture needed (33 σ) is about 26 mm. This point is indicated by a blue star in the parameter plane of Fig. 8.

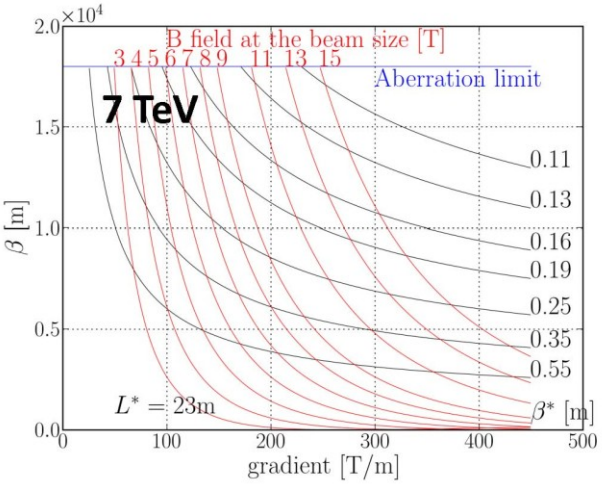

Figure 7: Peak beta function as a function of quadrupole gradient (horizontal axis), β* (red curves) and magnetic field at 16.5σ+11 mm (black curves) for 7 TeV beam energy [6].

For the arc quadrupoles we assume a full coil aperture of 40 mm as for the arc dipole magnets. If the length of the arc quadrupoles is the same as in the present LHC, their gradient must increase in proportion to the beam energy, from 223 T/m at 7 TeV to 526 T/m at 16.5 TeV. These scaled arc quadrupoles would then be more demanding the IR quadrupoles. Most probably the gradient of the arc quadrupoles needs to be lowered, or their aperture reduced. Aperture reduction is more attractive since lowering the gradient will probably lower the dipole field margin or the operating field and, in consequence, the beam energy. Clearly this point needs a thorough investigation.

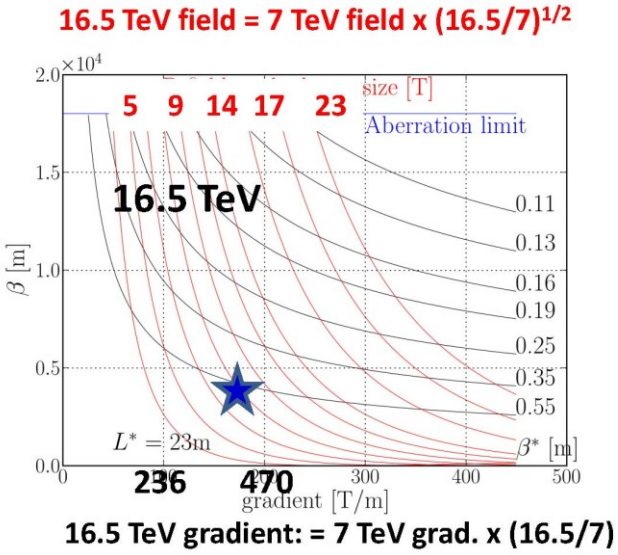

Figure 8: Peak beta function as a function of quadrupole gradient (horizontal axis), β* (red curves) and magnetic field at 16.5σ+11 mm (black curves), obtained by extrapolating Fig.8 to 16.5 TeV beam energy [the scaled values for 16.5 TeV are printed in bold face on top].

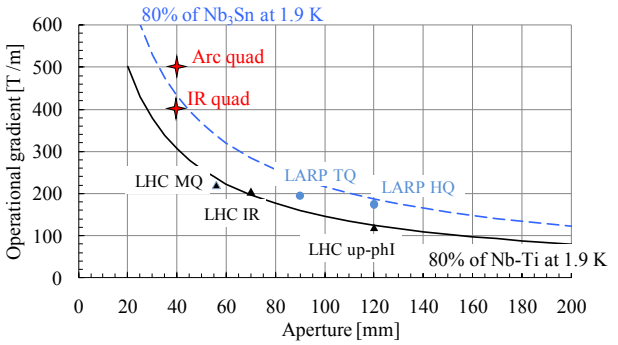

Figure 9: Operational gradient as a function of coil aperture for LHC and US-LARP quadrupoles (markers), scaling laws for limits in Nb.Ti and Nb3Sn (solid curves) [7], and expected values for HE LHC arc and IR (stars).

Figure 9 illustrates the location of the HE-LHC quadrupoles with respect to the LHC and LARP quadrupoles in the gradient-aperture plot [7]. The HE-LHC IR quadrupole still looks feasible with Nb_3Sn. However, a 40 mm aperture quadrupole for the arcs with 500 T/m is above the possibilities of Nb_3Sn. We would propose to aim for 400 T/m, which is at the limit of Nb_3Sn, and to compensate this lower gradient by a 20%

increase in arc-quadrupole length (from 3.1 to 3.6 m). The integrated quadrupole strength required in the arcs also depends on the optical cell length, which sets the values for the beta functions. One should consider the possibility of changing the cell length with respect to LHC in order to find at a better optimization between long cell length, implying less quadrupoles and more space for bending, and short cell length, yielding lower beta functions and smaller aperture in the arcs.

MISCELLANEOUS OPEN ISSUES

A larger number of points, mostly related to the higher beam energy, are outstanding and require further studies, e.g.

- the required cleaning efficiency assuming nominal quench levels;
- estimates of expected local radiation levels and implications for the dog-leg magnets in the cleaning insertions, and for the TAS and TAN designs;
- the required power converter tracking accuracy and potential implications if the HL-LHC features ca. 30-40 independent sectors (higher stored electro-magnetic energy in the magnets);
- stronger kicker elements for beam disposal (doubling the number of 15 dump kicker elements will have an impact on space and reliability), for beam diagnostics [tune measurements] and for generating large oscillation amplitudes [AC dipole, aperture kicker]), injection kickers & beam transfer with higher injection energy;
- beam diagnostics limits, e.g. for the use of beam screens and wire scanners;
- a closer inspection of the loss of longitudinal Landau damping; and the associated trade-off between bunch length and longitudinal impedance;
- persistent-current effects and field quality at injection which might, or might not, constrain the minimum injection energy required;
- the best gradient/aperture/length parameter set for the arc quadrupoles; and
- the use of crab cavities for HE-LHC: are crab cavities needed for HE-LHC? And/or could they be useful (e.g. suppose they are inherited from the HL-LHC)?

SUMMARY

The proposed key parameters for the Higher-Energy LHC have been reviewed and justified. A few beam-dynamics and optics issues have been highlighted, such as the fast radiation damping, the resulting potentially high beam-beam tune shifts, the implied need for transverse and longitudinal emittance control, and the requirements for quadrupoles in the arcs and in the IRs. The realization of the HE-LHC project will depend on the future availability and affordability of high-field dipole magnets.

ACKNOWLEDGEMENTS

We thank R. Assmann, R. Bailey, R. De Maria, G. De Rijk, B. Goddard, M. Jimenez, P. McIntyre, K. Ohmi, and L. Tavian for inspiring and helpful discussions.

The perfect workshop organization by Nicholas Sammut and Merethe Morer-Olafsen has been much appreciated.

REFERENCES

[1] R. Assmann et al., “First Thoughts on a Higher-Energy LHC,” CERN-ATS-2010-177

[2] L. Tavian, “LHC2 [HE-LHC] Cryogenics in the Arcs (First Considerations),” HE-LHC Upgrade Meeting, 17 May 2010

[3] E. Shaposhnikova, comment at HE-LHC’10 workshop, Malta, October 2010

[4] E. Shaposhnikova, “Longitudinal Beam Parameters during Acceleration in the LHC,” LHC Project Note 242 (2000).

[5] K. Ohmi, O. Dominguez, F. Zimmermann, “Beam-Beam Studies for the High-Energy LHC,” these proceedings.

[6] R. De Maria, “LHC Interaction Region Upgrade,” PhD thesis, EPFL Lausanne, CERN-Thesis-2008-079 (2008).

[7] L. Rossi and E. Todesco, “Electromagnetic Design of Superconducting Quadrupoles,” Phys. Rev. ST Accel. Beams 9, 102401 (2006).

CONCEPTUAL DESIGN OF 20 T DIPOLES FOR HIGH-ENERGY LHC

L. Rossi, E. Todesco, CERN, Geneva, Switzerland

Abstract

Availability of 20 T operational field dipole magnets would open the way for a 16.5 TeV beam energy accelerator in the LHC tunnel. Here we discuss the main issues related to the magnet design of this extremely challenging dipole: main constraints, superconductor choice, coil lay-out, iron, forces and stresses, and field quality. A tentative cost estimate is also given. The present technology, based on Nb-Ti and now near to be extended to Nb_3Sn superconductor, would allow reaching 15 T operational field. To reach 20 T, HTS conductors capable to carry 400 A/mm^2 at 15-20 T under transverse stress of 150-200 MPa are an essential element.

INTRODUCTION

The LHC main dipoles [1] are today running at 4.15 T, i.e., about 0.1 T less than Tevatron dipoles [2], which are based on the same Nb-Ti superconductor, and were built more than thirty years ago. After the consolidation of the splices in the magnet interconnects [3], the LHC main dipoles will be in conditions for reaching the design field value of 8.3 T. This will not happen before 2013. Presenting today a study for a 20 T dipole for a new machine to be installed in the LHC tunnel may seem, and actually is, a huge leap.

Indeed, the timeline of development of superconducting magnets for accelerators is long: for Nb-Ti based magnets, which is a well assessed technology for accelerators, the experience gained in the construction of several accelerators shows that five years are needed from day-zero, when aperture and field are decided, to installation and commissioning. For more performing and complex technology, like the one based on Nb_3Sn technology, the time is longer: the vigorous LARP program [4] took more than five years to successfully build a 3.4-m-long model quadrupole [5], which is a bare quadrupole with no cryostat and other integration features and, as magnet, only partly satisfies the requirements needed for installation in the LHC. Whereas for Nb_3Sn the conductor with the many – although not all – required properties is today available, in the case of high temperature superconductors (HTS), substantial improvement of the basic performance of the conductor itself is needed, both in terms of current density and strain degradation [6]. This implies even much longer times. Therefore for making credible the High Energy LHC (HE-LHC) as one of the options for CERN after the LHC, i.e., around 2030, it is necessary starting now to explore the main issues related to the magnet design, and to drive the R&D in the needed superconductors.

The maximum field reached in an accelerator-type dipole is around 14 T at 4.5 K [7], using Nb_3Sn conductor, in an aperture similar to the HE-LHC requirements (40 mm). It should be noted that in more than 10 years no dramatic improvement happened after the 13.5 T at 2 K in a 50 mm bore reached in 1997 by the D20 dipole [8]. Due to the shape of the critical surface, the maximum field attainable with Nb_3Sn accelerator magnets is around 18 T. May be 19 T could be reached with an optimized superconductor lay-out. Taking 18 T as solid figure, for the HE-LHC this gives ~15 T operating field after imposing the 20% margin, that at this stage we assume as reasonably needed for a series production of more than 1000 magnets. Of course this assumption can be challenged: however the experience of past accelerators (see Table 1) shows that a solid margin in the design is needed to compensate inevitable non-homogeneity of about 10% in performance.

Table 1: Operational dipole field, current and operational margin in high energy physics accelerators

	Operational field (T)	Operational current (kA)	Operational margin (%)
Tevatron	4.4	4.3	~26%
HERA	4.7	5.0	~31%
RHIC	3.5	5.5	~33%
SSC	*6.7*	*6.6*	*~15%*
LHC	8.3	11.8	~16%

SSC was cancelled in 1993 after 10 years of R&D and prototypes, HERA operation field was increased at 5.5 T (limiting margin reduction by lowering temperature down to 3.9 K) in 1998 [9].

Superconducting cables based on HTS are able to withstand fields larger than 15 T: they have been successfully used in high-field solenoids [6] but not in accelerator dipoles.

From the point of view of magnet design, a 20 T dipole for the LHC poses two big challenges: (i) obtain such a high field with a compact coil, and shield it with enough iron without exceeding the transverse dimensions imposed by the LHC tunnel; (ii) manage the stresses induced by electromagnetic forces to avoid degradation of the conductor.

Nb_3Sn is more than a factor five more expensive than Nb-Ti. Similarly, HTS is another factor 3-5 more expensive than Nb_3Sn. It is unlikely that the large difference in price between the three superconductors will disappear, even in the time scale of a production of the HE-LHC magnets (2025, i.e., 15 years from now). For this reason, a hybrid coil is required to minimize the cost of the conductor, which is a large fraction of the whole project. The construction of a hybrid coil poses the third difficult challenge: each material needs different heat treatments, needs different approach to stability and mechanical structure, and there is very little experience in building hybrid magnets for accelerators [10].

The proposal of an 'LHC energy upgrade' dates back to early 2000 [11] and a lay out for a 24 T (short sample, i.e., with no operational margin) hybrid magnet was proposed

in 2005 [12]. The new name HE-LHC looks more appropriate, since here we are talking about replacing at least all the LHC magnets, i.e., building practically a new machine, since many other systems will have to be upgraded or modified [13]. However, the main infrastructures of the tunnel (the 27 km of LHC machine and the 6 km of injection transfer lines with many of the technical services) would be kept or just consolidated, giving a major advantage w.r.t. other projects needing new tunnels and new infrastructure.

CONSTRAINTS AND ASSUMPTIONS

Aperture

The LHC accelerates particles from 450 GeV to 7 TeV, i.e. a factor 15.6 [14], to be compared to a factor 6 in Tevatron [2] and 25 in HERA [15]. Acceleration from 450 GeV to 16.5 TeV in the HE-LHC would imply more than a factor 30 of acceleration. Injection at 1.2 TeV brings the energy increase to a factor 14, and allows reducing the aperture of the machine, which is a critical parameter both in terms of cost and transverse size. About 1/3 of the 56 mm aperture of LHC main magnets is used for beam tubes, beam screen and clearance, while the rest are available for the beam. The beam size scales with the square root of the inverse of the energy. Increasing injection energy from 0.45 to 1.2 TeV, the aperture available for the beam can be reduced by ~40%: therefore the total aperture of the main magnets can go to ~40 mm. Certainly a study and subsequent optimization can indicate how much the aperture can be further reduced, below 40 mm. However this is a reasonable guess, especially for 15-m-long and curved dipoles. *With an injection at 1.2 TeV an aperture of 40 mm is considered.*

Magnet size and current density

The 3.8 m diameter of the LEP tunnel where the LHC is located is a strong constraint on the magnet transverse size, despite the space saving due to the twin design. In the LHC, the cold mass has a diameter of 570 mm. This size d_{cm} is given by

$$d_{cm} = d_b + 2(r + c_t + s_t + i_t + S_t)$$

where d_b = 192 mm is the beam separation, r=28 mm is the aperture radius, c_t=31 mm is the coil thickness, s_t=40 mm is the structure (collar) thickness, i_t=80 mm the iron thickness, and S_t=10 mm the shell thickness (see the sketch shown in Fig. 1).
The field in a dipole is proportional to the coil thickness and to the current density. For a 60º sector coil one has

$$B[\mathrm{T}] = 0.00069\, j_o\, [\mathrm{A/mm^2}]\, c_t\, [\mathrm{mm}]$$

An analysis of the relation coil thickness vs. operational field in accelerator magnets shows that they are not so far from the line corresponding to a overall current density of 400 A/mm^2, i.e., as in the LHC (see Fig. 2).

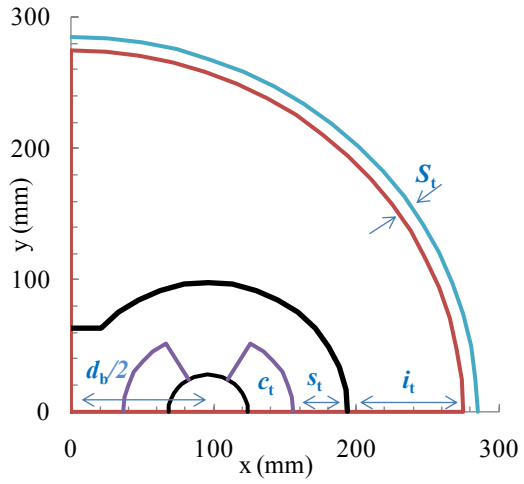

Figure 1: Schematic cross-section of the LHC dipole, one quarter shown.

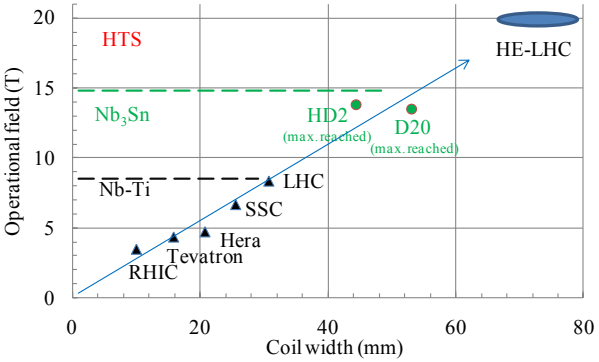

Figure 2: Operational field versus coil width in Nb-Ti accelerator magnets. For Nb_3Sn models the maximum reached field is given. The straight line fit has a slope consistent with j_0= 400 A/mm^2.

Taking for the HE-LHC dipole the same current density as in the LHC as a first guess, the coil thickness should be increased by a factor 2.5 from 30 to 75 mm, and the iron needed to shield scales with aperture and field from 80 to 130 mm. This gives a cold mass diameter ~300 mm larger than the LHC dipoles: this is close to the upper limit fixed by the requirements for installation and transport. This first estimate suggests that *the current density cannot be much lower than in the LHC coil, i.e. 350-400 A/mm^2.*

Cost

The cost of the conductor in the LHC main dipoles is approximately one third of the cost of the magnet (300 kCHF out of 1 MCHF). A coil with a thickness of 75 mm and an aperture of 40 mm has 3.2 times the surface of the LHC coil. The 8 T operational field is the upper limit of what can be reached with Nb-Ti. Nb_3Sn allows reaching operational fields in the range of ~15 T, as foreseen for the High Luminosity LHC on the 2020 horizon, but today it is at least 5 times more expensive than Nb-Ti. A coil made of Nb_3Sn would cost about 3.2×5=16 times the LHC dipole coil, i.e., about 5 MCHF

per magnet, and would not reach the 20 T. High temperature superconductors are 5 times more expensive than Nb_3Sn (with large variations): a coil made only of HTS would cost the stellar price of 3.2×5×5, i.e. 80 times an LHC coil (24 MCHF per magnet!). We assume that even in the time scale of the HE-LHC (i.e., 20 years from today) the large difference in price will not disappear. Therefore, following what is done in high field solenoids, *one has to build a hybrid coil, where cheaper superconductors are used in the lower field regions.*

Margin

We assume that the magnets will operate at 80% from the critical surface, i.e. a 20% operational margin. This may appear a rather conservative assumption: LHC magnets have a 14% operational margin (see Table 1). However, they still have to reach, in the machine, the operational field (and most probably a long training is needed [16]). With Nb_3Sn, there is not enough experience to firmly establish the needed margin, which is a rather controversial parameter, and could range between 10% and 20%: here we take a conservative estimate.

Stress

Both Nb_3Sn and HTS materials can undergo a severe degradation due to strain [17]. For this reason, the level of stress in the coil due to electromagnetic forces is a critical issue. In the LHC, the coil stress due to electromagnetic forces is of the order of 70 MPa [18]. Since the force scales with the field times the current density, going to 20 T with the same current density brings stresses to 150-200 MPa, which is the range where considerable degradation of Nb_3Sn starts (actually for certain type of Nb_3Sn serious degradation occurs even above 120 MPa). Therefore, *the stress constraints prevent from using higher current densities than what we have in the LHC dipoles.*

THE HYBRID COIL LAY-OUT

In the lower field region, the first 8 T are obtained with Nb-Ti conductor as in the LHC coils. We assume an overall current density (i.e., the current density of the coil, including voids and insulation, but not copper wedges) of 380 A/mm^2. This corresponds to a filling factor of 0.35 (i.e., 35% of the cross section of the coil is made of superconductor, and the rest is stabilizer, passive elements, void and insulation). For comparison, the LHC dipole inner cable has a 0.33 filling factor with a copper-superconductor ratio of 1.65. Using these parameters, one can reach 8 T in the Nb-Ti coils, with a 20% operational margin (see Fig. 3), similarly to the LHC case.

For Nb_3Sn we assume a rather conservative estimate for the superconductor current density of 2500 A/mm^2 at 12 T and 4.2 K, or 1250 A/mm^2 at 15 T and 4.2 K. This corresponds to 480 A/mm^2 at 16 T and 1.9 K of overall current density, with a filling factor of 0.3. These values allow reaching 13 T with a 20% operational margin (see Fig. 3). To further reduce the quantity of HTS, we suggest using a lower current density of ~200 A/mm^2 in the field region beyond 13 T. This makes the coil larger, but allows reaching 15 T (see Fig. 3, lower loadline), besides helping to reduce mechanical stresses.

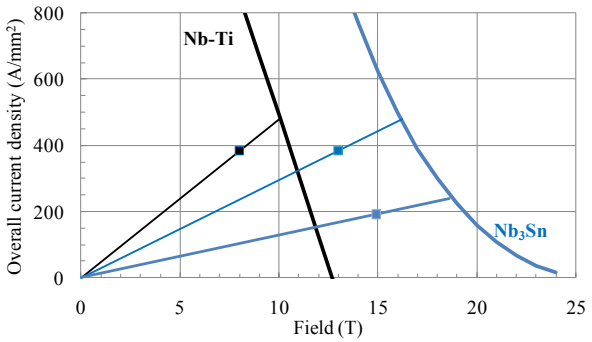

Figure 3: Overall current density in Nb-Ti and Nb_3Sn (curves), loadlines (straight lines) and operational points.

The last 5 T must be provided by HTS: a further reduction of a factor two in Nb_3Sn current density would give about 100 A/mm^2, and to gain another 2 T one would have to add 40-mm-thick coil, that would probably increase the transverse size beyond our constraints.

Among the HTS, Bi-2212 has the advantage of being available in form of round wires, but has low engineering current density and large strain degradation. The alternative is YBCO, which has a much lower degradation, higher current density but no round wire. Independently of this choice, we assume to have a cable operating with 380 A/mm^2 overall current density. This is about twice of what can be obtained today for Bi-2212, however there is consensus that with a vigorous R&D this value can be obtained in industrial scale, very much like Nb_3Sn that, by means of the US-DOE program [19] has more than doubled its current density in 10 years.

A cross-section with 11 blocks drawn according to the above guidelines is shown in Fig. 4. The two outer blocks, where the field reaches 8 T, are made with Nb-Ti. Then one has four blocks with Nb_3Sn, three blocks with Nb_3Sn at half current density, and two blocks with HTS. With this highly optimized cross-section the fraction of HTS is about 1/6, almost 1/3 is Nb-Ti, and more than half is Nb_3Sn (see Table 2). We use the cable geometry of HD2, with 28×2 0.8 mm strands, 22.2 mm width and 1.62 mm thickness, and with an insulation of 0.11 mm. A total of 150 turns are needed. Operational current for 20 T, with the iron described in next section, is 6.9 kA in the low density Nb_3Sn region and 13.8 kA elsewhere.

With respect to the pioneering work presented in [12] (see Fig. 5), where the current density was set at 800 A/mm^2, based on an optimistic guess of the progress in the Nb_3Sn and HTS development, and on the principle of stress management that removes one constraint, here we are at half of the current density. This doubles the quantity of superconductor, see Table 2. Indeed, thanks to the optimization of the grading and to the use of Nb-Ti, we manage to end up with 25% less HTS conductor w.r.t. [12]. With respect to the layout shown in Fig. 5, our proposal leaves no space for a support structure between

the blocks (see Fig. 4): this aspect should be carefully considered and could be critical. We consider a two-in-one geometry as in the LHC; the common coil option [20,21] should be also investigated.

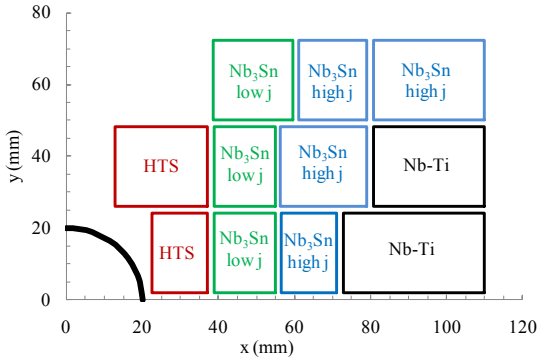

Figure 4: Block lay out of the coil (one quarter of one aperture only is shown).

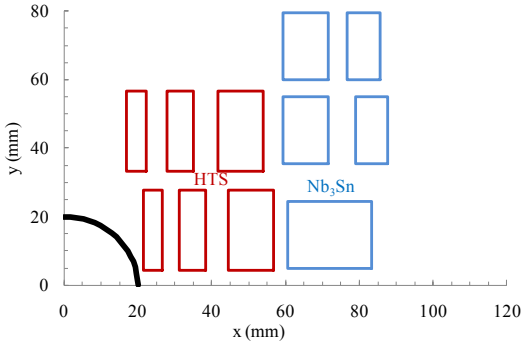

Figure 5: Block lay out of the coil proposed in [11] (one quarter of one aperture shown).

Table 2: Coil cross section (for one aperture) for layouts shown in Fig. 4 and 5.

	This work		Ref [13]	
	Surface (cm^2)	%	Surface (cm^2)	%
Nb-Ti	59	27%	-	-
Nb_3Sn	122	57%	50	52%
HTS	35	16%	46	48%
Total	216		96	

THE IRON

We use a 120 mm thick iron, placing it as close as possible to the coil. In this structure, collars are replaced by spacers, and the forces are kept by the iron-shell part. Self-supporting collars would need additional space.

The peak field in the coil blocks, in presence of iron with an external diameter of 800 mm and at operational field of 20 T in the bore, is shown in Fig. 6. The iron is placed at a larger distance in the inner part of the coil (i.e., the part towards the centre of the magnet) to reduce the influence of one aperture on the other (see Fig. 7). In fact the two-in-one structure induces higher peak field in the side of the coil which points at the centre of the magnet, and the iron can be used to partially compensate this effect. This cross-talk also requires to have some space between the coils of the two apertures, and brings the beam separation from the 192 mm of the LHC to 300 mm. Eliminating this space one could save 100 mm in the magnet size, but the margin would be largely reduced. The iron contributes to about 7% of field for a fixed current. Computations were done with ROXIE [22].

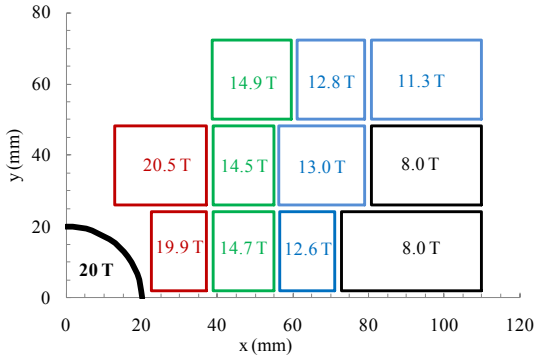

Figure 6: Peak field in the blocks at 20 T field.

Iron is largely saturated at 20 T operational field (see Fig. 7). The fringe field at 200 mm from the cold mass is 20 mT, which is within the specification for the LHC tunnel (50 mT). The iron thickness should be reduced in a more refined design, since for example we have not yet considered the thickness of the restraining cylinder. Since the 800 mm here given for the iron yoke is considered the maximum allowable diameter (and maybe even beyond!) to stay in a cryostat compatible with the LHC tunnel, this means that the 50 mT threshold should be either reached or passed. A solution may be in considering anti-coils to shield the field demagnetizing the outer iron: this solution is routinely used in MRI solenoids, but may be very difficult in dipoles. In alternative, a different lay-out of the cryostat and cryogenic system must be explored: for example reconsidering integrating the cryolines inside the magnet cryostat, like in the original LHC design [23] and in all other accelerators. This would allow larger cryostat and larger cold mass. Clearly this is a critical point to be addressed with a deep and wide investigation. A summary of the main parameters is given in Table 3. The very large stored energy (13 times the LHC dipoles) represents a big challenge for magnet protection.

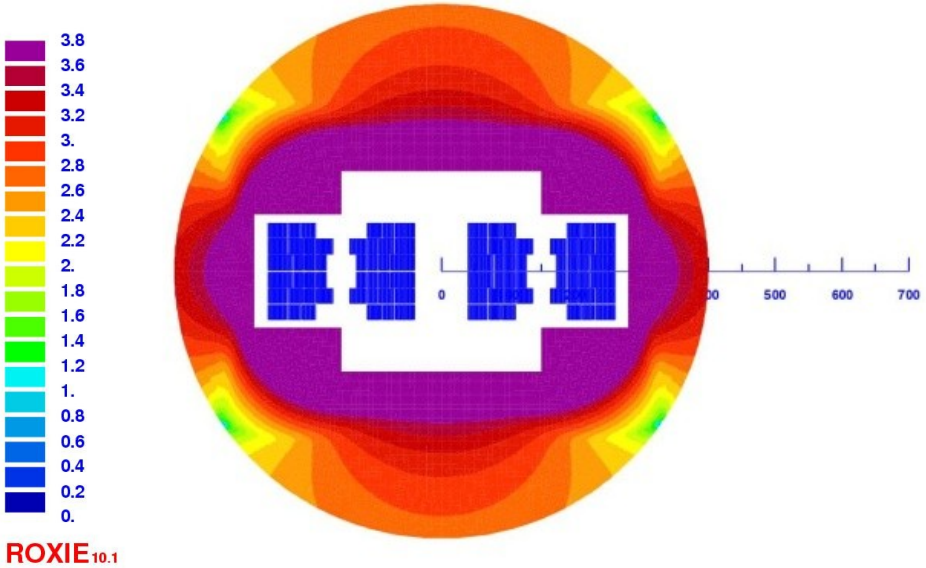

Figure 7: Cross-section of the magnet (coil, structure and yoke), showing field in the iron (color code is in tesla). The horizontal axis is in mm.

Table 3: Main parameters of the HE-LHC and LHC dipole

		HE-LHC	LHC
Operational field	(T)	20.0	8.3
Operational current	(kA)	13.8/6.9	11.8
Operational margin	(%)	20	14
Magnetic lenght	(m)	14.3	14.3
Total stored energy	(MJ)	100	7.0
Distance between beams	(mm)	300	194
Total number of turns	(adim)	150	40
Cable width (bare)	(mm)	22.2	15.1
Cable thickness (bare)	(mm)	1.62	~1.9/1.5
Insulation thickness	(mm)	0.11	0.12
Maximum coil thickness	(mm)	97.3	31
Coil height	(mm)	72.2	-
Cold mass diameter	(mm)	800	570

FIELD QUALITY

The proposed dipole layout has a ratio between the coil width and the aperture radius of ~4 (see Fig. 8). This ratio is a relevant parameter for field quality: the larger it is, the lowest are the high order multipoles, since a good part of the coil is 'far' from the beam, and therefore contributes only to the main component and not to the high order harmonics. This is why the multipole optimization is easier w.r.t. accelerator magnets which have a much lower ratio (see Fig. 8). In our case, the cross-section shown in Fig. 7 has all field harmonics within 2 units without the need of any copper wedge! The horizontal position of the three layers provides three free parameters which are enough to minimize all harmonics. The large saturation of the iron should pose no particular problems for operation, and the impact on b_2 could be corrected through quadrupoles.

On the other hand, persistent current will create large components at injection. The filaments in Nb_3Sn and HTS are at least a factor seven larger w.r.t. Nb-Ti, and since these components scale with the filament size, they will be much more relevant than in the present LHC dipoles.

This could induce a large change of b_3 during the ramp, to be corrected through spool pieces. Surprisingly Nb_3Sn has neither decay nor snapback [24]: this feature, which is not yet understood, would greatly ease operation. Cable effects needs have not yet been studied: interstrand resistance is more difficult to control than in Nb-Ti.

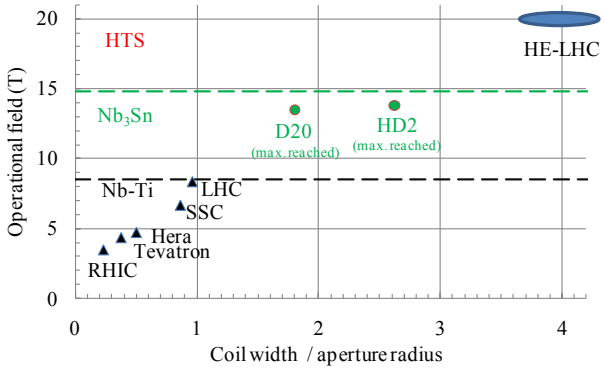

Figure 8: Operational field versus ratio coil width/aperture radius in Nb-Ti accelerator magnets. For Nb_3Sn models the maximum reached field is given.

STRESS

The use of a low current density has the drawback of giving a less compact coil, but the advantage of giving less stress. With respect to the 800 A/mm^2 used in [12], with half current density we manage to keep stresses at a

lower level. Here we give a first estimate [25] based on a coil where the block are completely glued one to the others, without structure around, and not pre-stressed (see Fig. 9). In this zero-order case one sees that the higher stresses of about 220 MPa are in the Nb-Ti region, that in Nb_3Sn stress is below 180 MPa and even lower in the HTS.

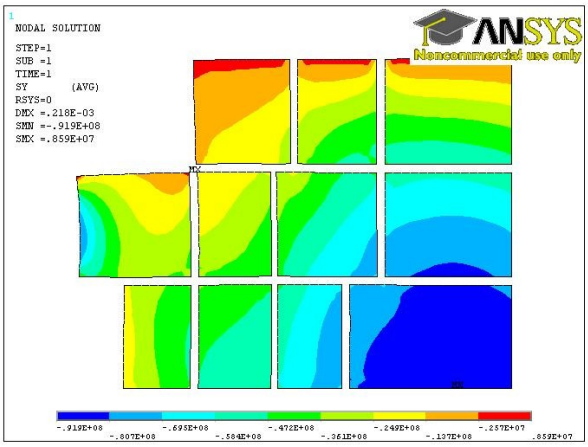

Figure 9: Estimate of horizontal stress at operational current, glued case without preloading.

Indeed, one has to take into account that the coil needs to be pre-stressed with a horizontal load which usually is 80%-100% of the maximum stress in operational conditions. Therefore, if we stay on the lower side, during assembly a uniform horizontal stress of 180 MPa should be envisaged. This is tolerable for Nb-Ti and just acceptable for Nb_3Sn. It is well beyond what Bi-2122 can withstand, but we can hope it can (or it will be) tolerated by YBCO based superconductors which are intrinsically quite robust, thanks to the steel substrate. However, compression stress limit in HTS needs to be addressed by a proper R&D program.

COST

As we are talking about prices in 2025, the cost estimate is a difficult and acrobatic exercise. Indeed, this is an essential ingredient of the story! To avoid writing something that becomes outdated or simply wrong tomorrow, one has to clearly state the hypothesis of our estimate. For the conductor, we consider 200 $/kg for Nb-Ti, that is the present cost. The Nb_3Sn price ranges today between 1000 and 1300 $/kg: we assume a price of 800 $/kg., i.e., a 20% improvement w. r. t. the cheapest price. For HTS we assume 3000 $/kg, which is the lower edge of today price, but for a material not reaching our required performances. Under these assumptions, the total cost of the conductor per magnet is 3.8 M$, half of which is for the last 5 T with HTS (see Table 4).

On the top of this, the manufacturing cost has to be added. For the LHC we had, as rough figures, 300 kCHF of components, 300 kCHF of conductor, 300 kCHF of assembly, and 100 kCHF of cryostat, testing, etc. The main difference for a 20 T magnet would be the coil manufacturing (100 kCHF out of 300 kCHF for the LHC). Doubling this component and keeping the same value for the other items, we would reach 800 kCHF of assembly, components and cryostats. This gives a final cost of 4.6 M$ per magnet (at the moment, 1$~1CHF~0.77 euro). At this level of a very preliminary budgetary estimate, choosing dollars, euros or Swiss francs (and guessing the exchange rate in 15 years …) is within the error of our estimate. Having 1200 magnets, the total cost of magnet would be around 5500 M$.

Table 4: Estimate of the cost of the conductor for a 14.3 m coil length two-in-one dipole.

	($/kg)	m^3	Kg	M$	%	Field (T)
Nb-Ti	200	0.12	960	0.19	5%	8
Nb_3Sn - h	800	0.16	1300	1.0	28%	13
Nb_3Sn - l	800	0.10	850	0.7	18%	15
HTS	3000	0.07	620	1.9	49%	20
Total		0.45	3730	3.8		

This may seem, and it is, a very high cost. Indeed, it is interesting to compare it with what could be done tomorrow with present technology: an accelerator with dipoles at 8 T, whose arcs are 2.5 longer than in the LHC. This machine would need 3000 LHC magnets for a total cost of 3000 M$. On the top of this, one should add the cost of the 65-km-long tunnel which can be estimated between 1000 and 2000 M$: this brings the total in the same range. A larger machine would then need new cryogenics, and infrastructures, whereas the HE-LHC would need an additional injector, the cost of the second being probably lower. Finally one would probably need new infrastructures for experiments.

A clear drawback shown by this preliminary analysis is that the cost of this project would be largely dominated by two components: the Nb_3Sn cable and the HTS cable, sharing each of them about one third. This is a risk for a large project, taking into account that at the moment very few producers are present on this market: for instance, the Nb_3Sn cable of the LARP, which is leading the high field magnet research, all comes from the same manufacturer.

Lowering the target from 20 T to 15 T would considerably reduce the price, possibly by 30%. Nevertheless, given the long timeline we are considering, we believe that there are considerable margins for HTS improvement, also in term of cost reduction. A recent DOE program on Bi-2212 goes in this direction. As a matter of facts, the development of HTS material has been mainly driven by applications that are far away from high energy physics, and a different strategy could lead to relevant improvements in the direction useful for the HE-LHC.

CONCLUSION

In this paper we explored the possibility of having 20 T operational field dipole magnets in the LHC tunnel. Other

important magnets, like main quadrupoles have not been studied and are shortly addressed in another paper [26].

Main constraints are (i) the transverse size of the magnet, limited by the tunnel, (ii) the stress in the coil induced by electromagnetic forces, and (iii) the cost. All these constraints call for a design based on hybrid coils that allows using cheaper conductor in the lower field regions. A hybrid layout, based on Nb-Ti, Nb_3Sn and HTS, that meets all basic requirements (including 20% field margin) is then proposed and examined. With respect to previous work [12] we reduced the overall current density from 800 A/mm^2 to 400 A/mm^2, plus a special region at 200 A/mm^2 to allow reaching 15 T with Nb_3Sn. This gives lower stresses, at the limit of what is manageable for Nb_3Sn, and allows using the HTS only in the 15 to 20 T field regions. This layout requires an HTS cable based on round wire, capable of carrying 400 A/mm^2 overall current densities at 15-25 T under 180 MPa compressive stresses, not yet available today. The main targets for future R&D should be directed toward the 13-15 T region, where Nb_3Sn good results on small coils need to be consolidated and oriented toward accelerator quality, and toward a basic improvement of HTS in term of critical current, stress tolerance and suitability to be assembled large current compact cable. The R&D on HTS is critical, also in term of time, if the goal of 20 T for 2030 has to remain credible; if in a few years new results will not be available, the HE-LHC should be reduced its target to 15 T (may be 16 T with a suitably optimized design) for the main dipole field.

ACKNOWLEDGEMENTS

We wish to thank B. Auchmann and S. Russenschuck for help building the electromagnetic model and in the energy computation, and A. Milanese for building the mechanical model and estimating the stresses.

REFERENCES

[1] L. Rossi, "Superconducting magnets for the LHC main lattice", IEEE Trans. Appl. Supercond. 14 (2004) 153.
[2] R. Hanft, et al., "Magnetic field properties of Fermilab Energy Saver Dipoles", TM-1182, 1630, 03/1983.
[3] F. Bertinelli, International Particle Accelerator Conference (2011), to be published.
[4] G. L. Sabbi, these proceedings.
[5] G. Ambrosio, et al., "Final development and test preparation of the first 3.7 m long Nb3Sn quadrupole by LARP", IEEE. Trans. Appl. Supercond. 20 (2010) 283.
[6] J. Schwartz, these proceedings.
[7] P. Ferracin, et al., "Recent test results of the high field Nb3Sn dipole magnet HD2", IEEE. Trans. Appl. Supercond. 20 (2010) 292.
[8] A. McInturff, et al., "Test results for a high field (13 T) Nb3Sn dipole", Particle Accelerator Conference (1997) 3212.
[9] B. Holzer, private communication.
[10] A. Lietzke, et al., "Test results for a Nb_3Sn dipole magnet", IEEE Trans. Appl. Supercond. 7 (1997) 739.
[11] O. Bruning, et al, "LHC luminosity and energy upgrade: a feasibility study", LHC Project Report 626 (2002).
[12] P. McIntyre, A. Sattarov, "On the feasibility of a tripler upgrade for the LHC", PAC (2005) 634.
[13] R. Assmann, et al., "First thoughts on a higher energy LHC", CERN-ATS-2010-177 (2010).
[14] O. Bruning, et al., "LHC Design report", CERN 2004-003.
[15] S. Wolff, "The superconducting magnet system for HERA", proceedings of MT19, ed. By C. Marinucci and P. Waymuth (Zurich, SIN, 1995).
[16] C. Lorin, et al., "Predicting the quench behaviour of the LHC dipoles during commissioning", IEEE Trans. Appl. Supercond. 20 (2010) 135.
[17] H. Ten Kate, et al, "Critical current degradation in Nb3Sn cables under transverse pressure", IEEE Trans. Appl. Supercond. 3 (1993) 1334.
[18] P. Fessia, D. Perini, "A novel idea for coil collar structures in accelerator superconducting magnets", IEEE Trans. Appl. Supercond. 12 (2002) 202.
[19] B. Strauss, US-DOE program in HTS, private communication.
[20] R. Gupta, "Common coil magnet system for VLHC", Particle Accelerator Conference (1999), 3239.
[21] V. Kashikin, et. al, "Development and Test of Single-Layer Common Coil Dipole Wound With Reacted Nb_3Sn Cable", IEEE Trans. Appl. Supercond. 14 (2004) 353.
[22] S. Russenschuck, "Field Computation for Accelerator Magnets" (Wiley, 2010)..
[23] The LHC study group, "Design study of the Large Hadron Collider", CERN 91-03 (1991).
[24] G. Velev, et al., "Field quality measurements and analysis of the LARP technology quadrupole models", IEEE Trans. Appl. Supercond. 18 (2008) 184.
[25] A. Milanese, CERN - Technology dept, private communication.
[26] F. Zimmermann, et al., these proceedings.

WHAT CAN THE SSC AND THE VLHC STUDIES TELL US FOR THE HE-LHC?

U. Wienands*
Stanford Linear Accelerator Center; Menlo Park, CA 94025, USA

ABSTRACT

In the SSC and the VLHC machine designs a number of accelerator physics and technology challenges were present. These challenges and the ways they were addressed are relevant also for the high-energy upgrade of the LHC that is contemplated in this workshop. In this paper I will highlight these challenges and the mitigation strategies pursued, and I will attempt to demonstrate the commonalities and lessons for the HE-LHC.

INTRODUCTION

The SSC

The Superconducting Super Collider (SSC)[1, 2] was under construction when the project was terminated by US Congress in the fall of 1993. The top-level parameters of the SSC collider are listed in Table 1.

Table 1: SSC Parameters

Parameter	Unit	Value
Energy/beam	TeV	20
Circumference	km	87
Luminosity	$\mathrm{cm}^{-2}s^{-1}$	1×10^{33}
Intensity	ppb	0.75×10^{10}
Trans. emittance	μm rad	1.0
Bunch spacing	ns	16.7
Stored Energy	GJ	0.4
Inj. energy	TeV	2
Dipole field	T	6.7

A diagram of the machine plus injectors is shown in Fig. 1.

Compared to the LHC the bunch intensity is more than a factor of 10 lower, with smaller beam emittance by a factor of three, while the bunch spacing is comparable. The stored beam energy is fairly similar, but in a machine almost four times the size of the LHC. The bending field of 6.7 T was at the time the highest field in any series-produced accelerator dipole magnets.

The VLHC

The conceptual design for the the "Very Large Hadron Collider" (VLHC)[3] was a 200+ km machine with two stages, a first stage for 20 on 20 TeV collisions and a second stage for 87.5 TeV on 87.5 TeV p-p collisions. For this paper, only the second stage is considered. This machine had a proposed bending field of close to 10 T, causing the machine parameters to be affected significantly by synchrotron radiation. Table 2 shows the top-level parameters for the VLHC collider, Fig. 2 shows a layout of the design.

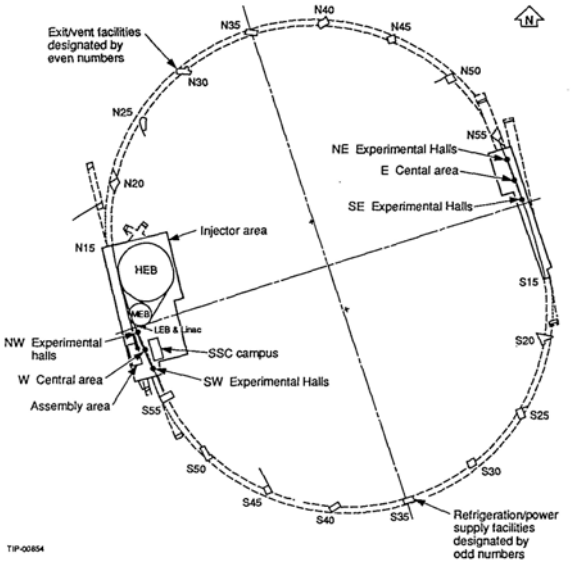

Figure 1: Diagram of the SSC Site.[2]

Table 2: VLHC Parameters

Parameter	Unit	VLHC I	VLHC II
Energy/beam	TeV	20	87.5
Circumference	km	233	233
Luminosity	$\mathrm{cm}^{-2}\mathrm{s}^{-1}$	1×10^{34}	2×10^{34}
Intensity	ppb	2.6×10^{10}	0.9×10^{10}
Trans. emittance	μm rad	1.5	0.04 [0.2]
Bunch spacing	ns	18.1	18.8
Stored Energy	GJ	3.0	3.9
Inj. energy	TeV	0.9	10
Dipole field	T	2	9.8

* Supported in part by the US DOE under the LARP framework

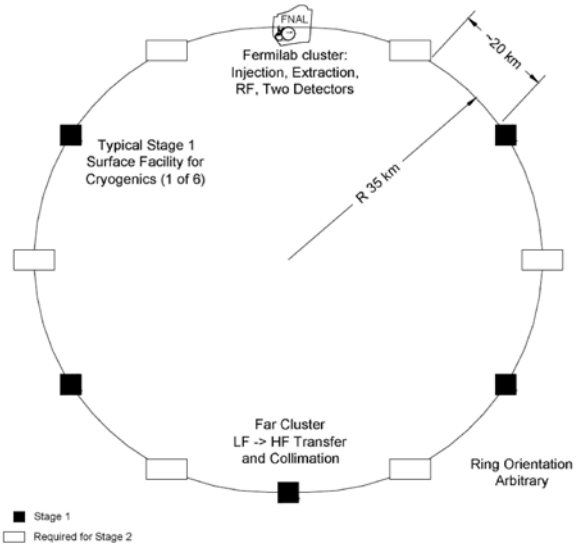

Figure 2: Diagram of the VLHC Site.[3]

DESIGN ISSUES

Magnet aperture

The aperture of the SSC was subject to several revisions, increasing the dipole aperture from 40 mm in the CDR[1] to 50 mm in the SCDR[2] and later increasing the quadrupole aperture to 50 mm as well. The arguments for this were based mostly on tracking studies, only late in the project the need to consider a liner in the vacuum system also affected the aperture discussion.

Fig. 3 shows the result of a dynamic-aperture study for the SSC with 40 mm dipoles. Machine acceptance for 10^5 turns is about 0.6 cm initial amplitude. With 50 mm this opens up significantly, see Fig 4. A different look at the

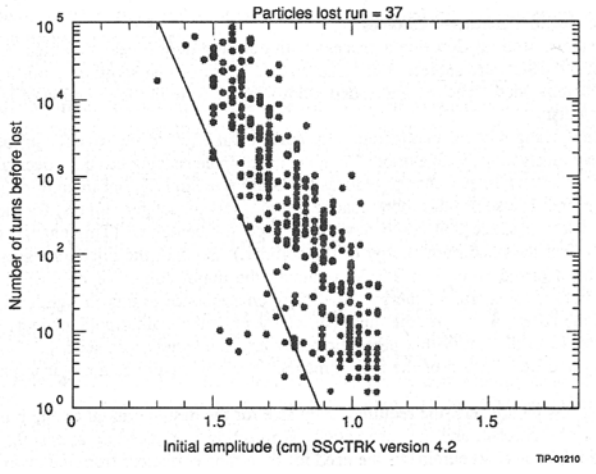

Figure 3: Survival plot for the SSC with 40 mm aperture dipole magnets.[2] Note the error on the horizontal scale (0.5 misprinted as 1.5).

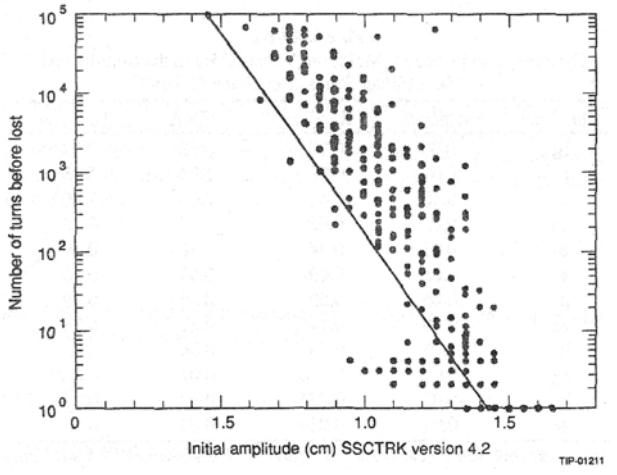

Figure 4: Survival plot for the SSC with 50 mm aperture dipole magnets.[2] Note the error on the horizontal scale (0.5 misprinted as 1.5).

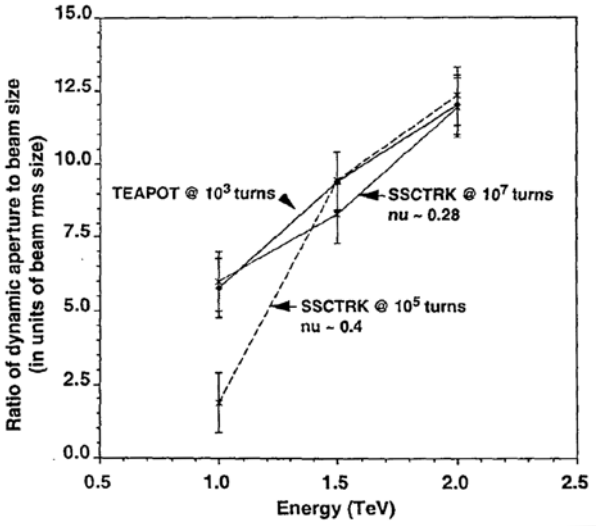

Figure 5: SSC Tracking for different injection energies. 50 mm quadrupole and dipole aperture.[4]

machine acceptance is shown in Fig. 5, with acceptance *vs* injection energy for the machine with 50 mm dipoles and quadrupoles. The 5 to 6 σ acceptance at 1 TeV was considered inadequate while the nearly 12 σ acceptance at 2 TeV was more than sufficient, leaving room to lower the HEB energy to 1.5 TeV as was considered.[4]

It is instructive to compare these with LHC tracking results. In Fig. 6 an LHC survival plot is shown, published in 1998.[5] It appears that the machine has an acceptance of about 12 σ, which would correspond to the SSC with 50 mm aperture in dipoles and quadrupoles, and which is also consistent with the rather linear behavior the LHC has exhibited in beam commissioning in 2010. In the earlier versions of the SSC lattice with smaller magnet apertures, various field-correction schemes were devised to deal with the field harmonic at injection due to the persistent cur-

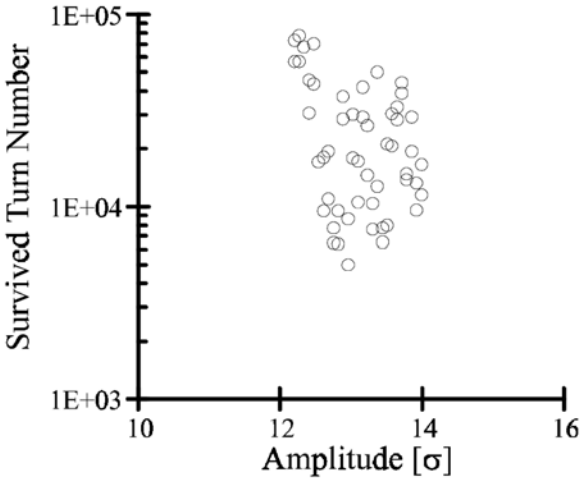

Figure 6: Survival plot for the LHC.[5]

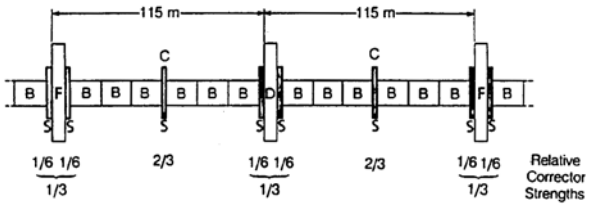

Figure 7: Mid-cell correction of dipole field errors.[6]

rents, e.g. the mid-cell corrector elements, also known as "Neuffer-Simpson" correction.[6] It consists of correctors at either end of a half-cell plus a corrector of twice the strength in the middle of the half cell, between two dipoles. This correction minimizes the introduction of extra higher-order terms arising from the correction elements, which can defeat simpler correction schemes. Sextupole and octupole correctors were foreseen. Fig. 7 shows a schematic. The 50-mm aperture design did not require these somewhat complicated mid-cell corrector packages, omitting which offset in part but not fully the increased cost of the dipoles.

The VLHC design envisaged 40 mm magnet aperture, but at a higher injection energy of 10 TeV (from the stage-1 ring in the same tunnel). At this energy the beam size is sufficiently small that the smaller magnet aperture would be sufficient (from a field-quality point of view).

Synchrotron Radiation

Synchrotron radiation will be significant in the HE-LHC. Table 3 compares the relevant parameters for the four machines considered here. The two lower-energy machines, LHC and SSC, have s.r. power density of a fraction of a W/m and damping times of 25 to 30 hours, comparable to the luminosity lifetime. VLHC and HE-LHC on the other hand have power densities of a few W/m and damping times of a couple of hours, significantly shorter than the luminosity lifetime. Therefore the radiation damping

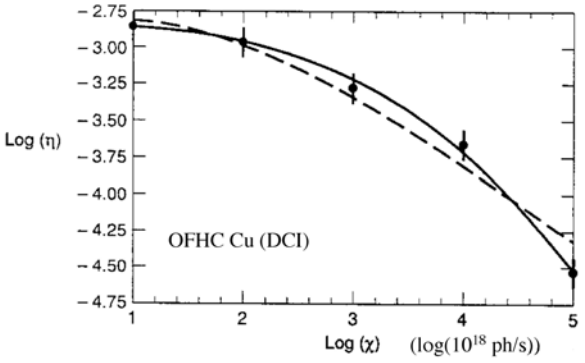

Figure 8: Photon desorption fit to data taken at DCI.[7]

dominates the beam parameters (unless specific countermeasures are taken). The power density to a certain extent is a question of effort to carry away in cooling, although reliability may suffer if the heat load on the cryo system gets too high.

In the SSC, the vacuum and cooling system were designed to absorb the power. Photon desorption became a subject of intense study as it became evident that the hydrogen frozen at the walls could cause unacceptable values of the photon-induced desorption coefficient η if allowed to form a monolayer or more. To this end, a diffusion model was created based on then-available photon-desorption data from BNL, the DCI collider at LAL, and BINP.[7] A fit is shown in Fig. 8 as an example, for oxygen-free high-conductivity copper (OFHC). The model in turn was used to predict the behavior of the SSC vacuum system. It was found that OFHC copper performed better than copper deposited onto a stainless-steel pipe—probably due to better surface smoothness. However, none of the surfaces as tested could be expected to clearly last longer than the 4000 hour required before a warm-up was necessary in order to boil off the hydrogen from the wall. The alternative solution of a liner (beam screen) was being considered; there would have been enough space in the 50-mm magnets.

For the VLHC with its potentially high gas load the pumping surface behind the liner still may not have sufficient capacity. To increase capacity, a getter behind the liner was considered.[8] The liner in turn has its own cooling carrying away the radiation energy. The temperature of the liner is chosen to avoid on one hand to much radiative power into the low-temperature beam pipe, to maximize on the other hand the cooling efficiency which favors a higher liner temperature. In the VLHC, 80 to 100k was anticipated. In this context the possibility of dedicated, warm photon stops was considered and even some engineering studies initiated[9]; however, in the HE-LHC context this approach does not work as the bending in each magnet is too large and the radiation fan hits the wall before leaving the magnet.

Table 3: Synchrotron radiation Parameters for the machines considered

Parameter	**Unit**	**LHC**	**SSC**	VLHC	HE-LHC
Energy/beam	TeV	7	20	87.5	16.5
Energy loss/turn	MeV	0.01	0.053	15.3	0.2
Radiation power/beam	kW	5.8	9	1050	255
Power density/beam	W/m	0.3	0.15	4.7	2.8
crit. Energy	keV	0.044	0.284	8.03	0.575
Transverse damping time	h	26	30	2.5	2

Table 4: VLHC IR Parameters for a flat- and a round beam

Parameter	**Unit**	**Flat beams**	Round beams
Peak Luminosity	$\mathrm{cm}^{-2}\mathrm{s}^{-1}$	2×10^{10}	2×10^{10}
Aspect ratio		0.1	1
Beam-beam parameter (x=y)		0.008	0.008
Intensity	ppb	0.75×10^{10}	0.75×10^{10}
Horizontal emittance	μm rad	0.161	0.082
Vertical emittance	μm rad	0.016	0.082
β_x^*	m	3.7	0.71
β_y^*	m	0.37	0.71
$\hat{\beta_x}$	km	7.84	14.58
$\hat{\beta_y}$	km	10.75	14.58
σ_x^*	μm	2.53	0.79
σ_y^*	μm	0.25	0.79
$\hat{\sigma_x}$	μm	116	113
$\hat{\sigma_y}$	μm	43	113
$\hat{\sigma_x'}$	μr	0.68	1.11
$\hat{\sigma_y'}$	μr	0.68	1111
Total crossing angle	μr	10	10
Separation distance	m	30	120
# parasitic crossings per IR		20	84

Electron-Cloud Effect

The threshold for electron-cloud build-up was determined for the VLHC to be about 3.5×10^{10} ppb, later revised down to 2×10^{10}.[10] These values were arrived at in light of results obtained at the SPS around 1999. While there were details to be considered, the threshold appeared safely above the bunch intensity of 0.9×10^{10}. An SEY of 1.3 (peak, at 400 eV) was assumed in these studies, a value one might expect for a well-scrubbed stainless-steel or copper surface. With its relatively low bunch population this machine design is in a different region of parameter space w.r.t. the electron-cloud effect than the HE-LHC.

Luminosity profile, beam dynamics, etc.

In the VLHC—as in the HE-LHC—the nominal damped emittance in all three planes is much smaller than the injected emittance. Thus luminosity and beam-beam parameter will increase as the beams damp. With a flat beam, the optical design of the IR can deviate from the antisymmetric triplet IR often used in round-beam hadron colliders and adopt the symmetric doublet focusing scheme used in flat-beam lepton colliders. Besides simplifying the IR design, it offers the chance for a much earlier separation with a dipole as the first magnet after the IP, without causing excessive $\hat{\beta}$. In case of the VLHC, the separation distance for a particular set of parameters (Table 4) is 30 m for the flat-beam IR *vs* 120 m for the round-beam IR. As a result the number of parasitic crossings is reduced by about a factor of 4. An optical design for a flat-beam IR is shown in Fig. 9.

Once the beam-beam limit is reached, it is necessary to stop the damping process (e.g. by injection of noise in two or all three planes) and maintain the tune shift. In the VLHC this happens in the horizontal plane first, saturating ξ_x. Once ξ_y saturates as well it was foreseen to vary the crossing angle to maintain ξ_y. Figure 10 shows the resultant luminosity profile, Fig. 11, the beam-beam parameters *vs* time. These profiles have built-in an assumption of longitudinal heating of the beam to maintain a momentum spread of about 0.5×10^{-4}. The beam is left to assume a flat shape with about a 1:10 aspect ratio.

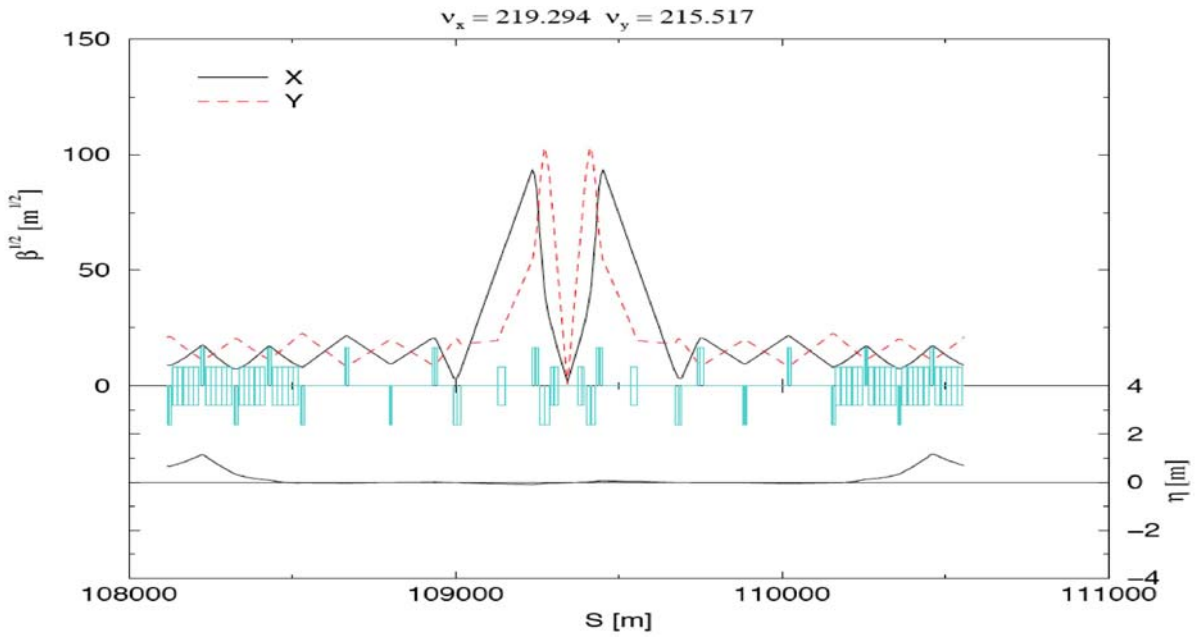

Figure 9: Optical design for a flat-beam Interaction region.[7]

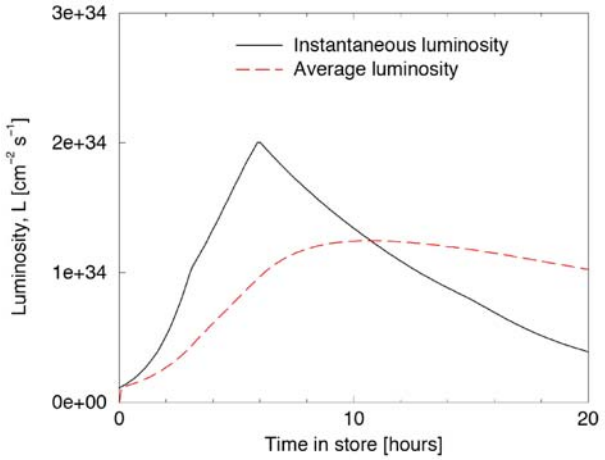

Figure 10: VLHC Luminosity *vs* time, flat beams.[7]

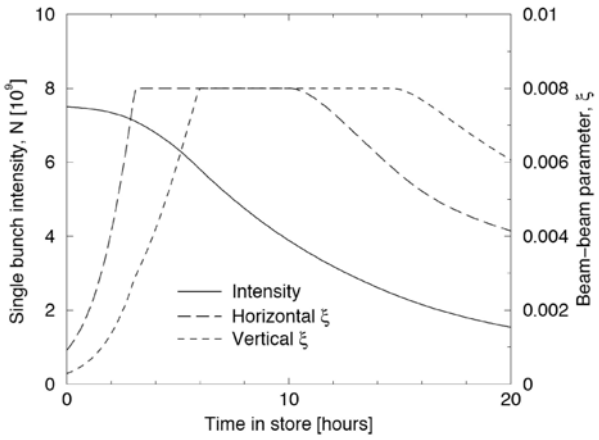

Figure 11: VLHC beam-beam parameter *vs* time, flat beams.[7]

With radiation damping times of about 2 hours, it may be argued that the beam-beam limit should be higher than for present-day hadron colliders. A comparative study of different machines was attempted for the VLHC and shown in Fig. 12. The exponent of 1/3 for the fitted equation has been found before by Assmann & Cornelis in LEP data.[11] VLHC and HE-LHC have a damping decrement of about 10^{-7}, which indicates that the gain in ξ by damping will be moderate at best, on the order of 0.0025. It does have to be noted, however, that there are newer data for the Tevatron as well as the LHC, indicating that even at negligible damping the beam-beam parameter can significantly exceed the 0.006 used in Fig. 12.

Longitudinal parameters

Table 5 gives a comparison of some of the longitudinal parameters of the machines considered here. Shorter bunch lengths can be a potential heating issue as the loss factor tends to increase with decreasing bunch length. In the VLHC II this is mitigated by the small bunch charge. In the HE-LHC, however, the combination of somewhat shorter bunches and somewhat higher bunch charge (than LHC nominal beams) may increase power loss in—or leakage through—the screen by a significant amount. Note that for VLHC and HE-LHC, a longitudinal beam-heating mechanism is assumed to keep the energy spread at a value near 0.5×10^{-4} in order to prevent bunches from becoming too short and/or beam instability.

Table 5: Longitudinal parameters.

Parameter	Unit	LHC	SSC	VLHC II	HE-LHC
Bunch length	mm	75	≈ 60	26	65
$\Delta E/E$	1	1.1×10^{-4}		0.5×10^{-4}	0.4×10^{-4}
Bunch Charge	ppb	1.1×10^{11}	0.75×10^{10}	0.9×10^{10}	1.3×10^{11}
Rf frequency	MHz	40	60	55	40

Table 6: VLHC Impedance Budget. $Z_{\perp}^{RW}$ is given for the mode with the lowest frequency

Machine	*R*(m)	*b*(mm)	$\frac{Z_{\parallel}}{n}(\Omega)$	$Z_{\perp}^{BB}(\frac{\mathrm{M}\Omega}{\mathrm{m}})$	$Z_{\perp}^{LH}(\frac{\mathrm{M}\Omega}{\mathrm{m}})$	$Z_{\perp}^{RW}(\frac{\mathrm{M}\Omega}{\mathrm{m}})$
FNAL MI	529	25.4	1.6	-	26	
LHC	4243	18	0.66	28	1.5	124
SSC	13866	16.5	0.68	54	21	4200
VLHC II	36924	10	0.6	390	90	55000

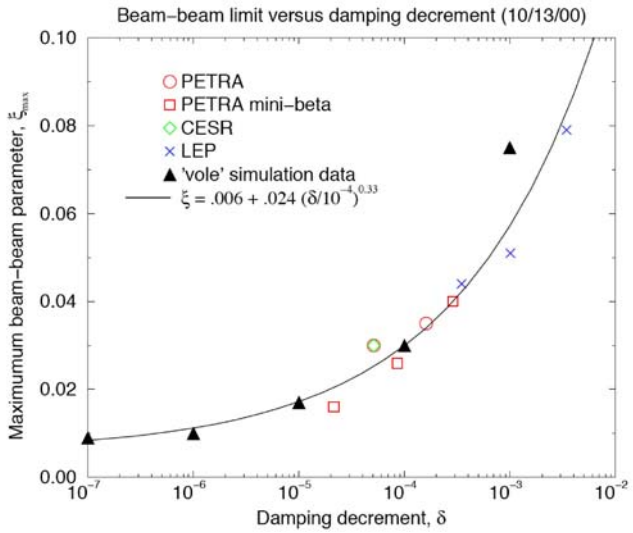

Figure 12: Fit of Beam-beam parameter *vs* damping decrement for various machines.[7]

Impedance

A rough impedance budget was drawn up for the VLHC, scaled from SSC, LHC and the FNAL Main Injector, see Table 6. The longitudinal impedance for all machines is a similar $Z_{||}/n$ near 1 Ω; while the transverse components scale up with a certain power of the length. For the HE-LHC the impedance will be comparable to that of the LHC; however, to assess the beam stability one needs to also take into account the beam parameters, in particular bunch length, energy spread, and also the slip factor of the lattice, see Table 4. It may be argued (from scaling by $\sigma_{x,y} \times \sigma_l$) that the HE-LHC (at top energy) is up-to 3 times closer to instability limits than the present LHC.

SUMMARY

The SSC studies and the VLHC studies can give useful insight in the HE-LHC context due to the similarity in energy and—in case of the VLHC—both machines being dominated by synchrotron radiation. The possibility of flat beams may be an interesting option to explore. The aperture debate of the SSC may help in setting the right aperture for the HE-LHC, and the vacuum investigations done for the SSC should, if properly updated for the newer data available now, be useful in estimating vacuum performance and the details of the liner and pumping system needed to avoid excessive photon desorption and pressure bumps.

It may be instructive to review here the main R&D issues identified in the VLHC Accelerator Physics Report[12], given here in very abbreviated form:

1. Energy deposition in the IRs.
2. Operational aperture.
3. Instabilities.
4. Diffusion as a mechanism counteracting the radiation damping.

For HE-LHC it appears that the first and last items are the most significant ones, whereas items 2 and 3 are more-or-less addressed using operational data from the present LHC. But the radiation generated in the IRs will already be a problem at the LHC, limiting the lifetime of the IR magnets. The problem of diffusion overcoming the radiation damping at some point still remains to be studied, although the LHC, once it is operating at 7 TeV beam energy, may give an indication of the strength and even nature of such processes. In addition to these, a number of areas needing further were identified in the VLHC report:

1. Diffusion, ground motion, IBS and other mechanisms of emittance growth.

2. Lattice design incl. details of the IR.
3. Simulations and particle tracking.
4. Instabilities and the need for feedback systems.
5. Energy scaling, limits of luminosity.
6. Beam experiments designed to assess possible VLHC issues.

REFERENCES

[1] J.D. Jackson, Superconducting Super Collider Conceptual Design Report, SSC-SR-2020, 1986.

[2] J.R. Sanford, D.M. Matthews, eds., *Superconducting Super Collider Site-Specific Design Report*, SSCL-SR-1056, July 1990.

[3] H.D. Glass, G.W. Foster, P.J. Limon, E.I. Malamud, P.H. Garbincius, S.G. Peggs, J.B. Strait, M. Syphers, J.C. Tompkins, A. Zlobin, eds., *Design Study for a Staged Very Large Hadron Collider*, Report SLAC-R-591, FNAL Report TM-2149, June 2001.

[4] G.F. Dugan, J.R. Sanford, eds., *The Superconducting Super Collider Retrospective Summary*, SSCL-SR-1235, April 1994.

[5] L. Evans, Proc. EPAC98, Stockholm, Sweden, p. 3, 1998.

[6] D. Neuffer, Report SSC-N-525, April 1988.

[7] G. Dugan, Report SSCL-N-863, May 1994; and Report SSCL-SR-610.

[8] S. Peggs, M. Syphers, eds., *VLHC Accelerator Physics*, Fermilab Report TM-2158, BNL C-AD/AP/49, June 2001, p. 85.

[9] P. Limon, Hadron Collider Workshop 2003, FNAL (unpublished), and P. Bauer et al., Fermilab Report TD-02-019, May 2002.

[10] S. Peggs, M. Syphers, eds., *VLHC Accelerator Physics*, Fermilab Report TM-2158, BNL C-AD/AP/49, June 2001, p. 86.

[11] R. Assmann, K. Cornelis, *The Beam-Beam Interaction in the Presence of Strong Radiation Damping*, Proc. Workshop on an e^+e^- Ring at VLHC, IIT Chicago, IL, March 2001.

[12] S. Peggs, M. Syphers, eds., *VLHC Accelerator Physics*, Fermilab Report TM-2158, BNL C-AD/AP/49, June 2001, p. 97.

A HIGH ENERGY LHC MACHINE. EXPERIMENTS 'FIRST' IMPRESSIONS

M. Nessi, CERN, Geneva, Switzerland

Abstract

These days, while the landscape of discoveries at LHC has yet to be unveiled, planning for upgrades twenty years or more in advance towards a possible experimental scenario, might sound very imaginative and ambitious. Nevertheless, as plans are being worked out for the High Luminosity LHC upgrade, it is possible to plan keeping the ATLAS and CMS detectors operational for the following High Energy phase. The natural and radiation-induced aging of some components, calorimeters especially, needs to be carefully addressed. Even planning for a very new detector might not be unreasonable.

INTRODUCTION

Trying to extrapolate a possible experimental scenario twenty years or more in advance, might sound very ambitious and imaginative, in particular today before knowing the discovery landscape of the present LHC.

At some point, while scanning through the possible rare physics signals, luminosity at LHC will not buy more statistics. Cross-sections will become simply too small and will drop by many orders of magnitude, in particular as a function of mass. Energy will buy much more, because rare physics cross-sections, and in particular if large mass objects are involved, will be boosted by the larger amount of energy available to create heavy objects. We assume that this possible changeover of strategy between high luminosity and high energy will become interesting around 2000-3000 fb^{-1} of collected integrated luminosity. At that time, probably around 2030-2032, both multi-purpose detectors, ATLAS [1] and CMS [2], will be still operational.

POSSIBLE DETECTOR REQUIREMENTS

In today's scenario, while no discoveries have been announced yet, the kind of physics we will be exploring at high energy will basically be the same we are investigating now (see Fig 1.), but with some "nuances".

- Discovery of high mass new particles (beyond what will be explored at the HL-LHC, m ~ 2.5 TeV).
- Precision measurements of known Standard Model physics (heavy flavors precision measurements and rare decays).
- Measuring in detail properties of newly discovered phenomena (masses and couplings of sparticles as an example).
- Precision measurements of LHC discoveries (Higgs spin, self- couplings, rare decays, ...).
- Searches for new phenomena, not anticipated by theory.

It is therefore hard to guess which parameters in today's detector properties might be relaxed. Today probably none. If we will still be looking for SUSY-type phenomena, with large multiplicities of leptons, jets and heavy flavor decays and missing transverse energy, then the detectors will have to count on:

- Lepton identification (in particular electrons versus jets), photon and muon identification.
- b and c quark decay tagging, via secondary vertex tagging.
- Excellent missing energy resolution, which implies detector coverage down to large pseudo-rapidity values.
- Excellent calorimeters performance in terms of resolution and energy scale.
- Excellent tracking efficiency (>98%).

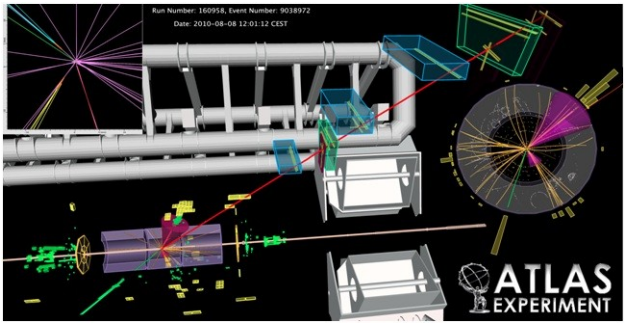

Figure 1: Example of a recently recorded top event in ATLAS, showing the various detectors components involved.

On top of this, and after a few years of enthusiasm for the high-energy regime, the community will certainly ask (because of the positive experience at HL-LHC) to run with high luminosity too. This will reopen the issue and stress even further the detector requirements.

- A high number of pile-up events with many tracks and a large risk of fake hits/tracks association (see Fig. 2).
- An important cavern background, in particular from slow neutrons captured in the detector materials.
- Unprecedented levels of radiation and track densities, in particular in the forward detectors, that will limit their effectiveness.

It is therefore impossible today to assume that some of the present detector properties or requirements will be relaxed. This means that presently we have to assume that in 20 years from now we will be able to operate and maintain the existing detectors as we do today, after an

important upgrade of the innermost components which we are planning for the HL-LHC.

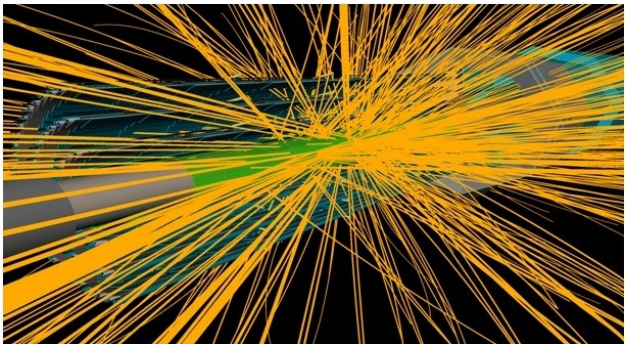

Figure 2: High tracks density in the vertex detector with just 50 pile-up events associated.

DETECTORS CONCERNS

After the HL-LHC experience, the detectors will be old in their structure and constituent materials. From the time of construction (1996-2008) about 30 years will have elapsed. Some more critical parts like rubber components, O-rings, PCBs, cables and connectors, optical fibers, cryo- and vacuum infrastructure will need a careful analysis and probably will need to be replaced.

A large part of the electronics (front-end and back-end) will be obsolete and no longer possible to keep operational. The procurement of electronics spare components will be an issue.

Some components will have been heavily irradiated. The innermost parts will be already classified as potential nuclear waste. Access will be very limited in the regions around the beam pipes (~ 2 m radius) and near to the TAS. The main issue will be the irradiation of services and electronics. In the region around the beam pipe we will probably be at the level of a few mSv/h. Today, running at a peak luminosity of 3 to 5 $\times$ 10^{31} cm^{-2} s^{-1}, we observe online an activation level around the ATLAS beam pipe well in line with the calculations obtained by simulation.

Activation and radioactive contamination, and Radio Protection (RP) issues in general will become fundamental from 2016 on, and on the very long term they will represent a real problem. We have in any case to change our culture and be more proactive in this domain.

Inner Detectors

For the HL-LHC both collaborations will have constructed a new inner detector with very high granularity and with radiation-harder sensors and front-end electronics (~2020). R&D on a new generation of Silicon- or Diamond-based sensors has already started. For example, 3D Silicon strip detectors represent a very promising technology if the industrialization process will be effective (see Fig. 3).

Having in mind to use the same layout for the HE phase, one has now to introduce in today's upgrade requirements the possibility to upgrade and exchange inner detector (ID) components continuously as a function of time. This is particularly true and valid for the innermost layers (b-layer and pixel detector in general). We have also to add to our 2020 specifications a radiation resistance up to ~6000 fb^{-1}. The alternative is to assume a new upgrade of the entire inner detectors in the early thirties, as we will have done for the HL-LHC.

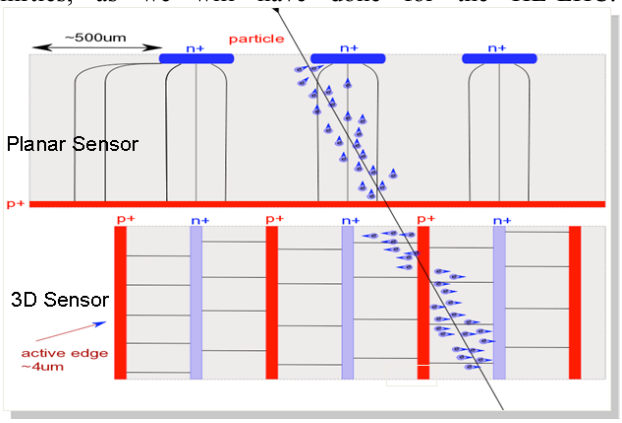

Figure 3: principle of function of planar versus 3D Silicon strip detectors. In the 3D case, the drift time, as well as the active edge dimension, are reduced considerably.

Calorimeters

Calorimeters using scintillating dopants risk being completely irradiated and therefore will have changed their transparency property regarding optimum light collection. No idea about what to do in such a case. Especially in the ATLAS case, it is practically impossible to extract and replace the calorimeters without dismounting most of the detector. This might be the critical problem we will have to face. Either one accepts a reduced light collection and a bigger constant term in the energy resolution, or one needs to start replacing components. All present light detectors (photomultipliers or diodes) will have reached the end of their life cycle and will need to be replaced.

- For example the ATLAS Tile calorimeter performance will need to be evaluated as a function of radiation. Its injection-molded 40 tons of scintillator might be fully aged in its properties and compromised by radiation. No way to dismount it without dismounting a major part of ATLAS. Maybe something can be done in the end-caps. If not, one has just to accept a reduced performance.
- Similar reasoning for the CMS calorimeters (crystals + hadronic scintillators). In particular in the end-cap regions, radiation will compromise the crystals light transmission, probably to a point where crystals need to be replaced. Differently from ATLAS, here the access is simpler and it might be easier to replace end-caps components (i.e. crystals)
- The ATLAS LAr calorimeter will be very radioactive and will be polluted with material, which one can consider as dust and might be a source of electrical shorts in the electrodes,

producing HV breakdowns. Here solutions have envisaged on how to solve the problem if one comes to a showstopper. Such an intervention will require opening the cryostats underground to gain access to the active components (probably just in the end-caps). The intervention will be very difficult, because of the radiation levels and will require at least 3 years of downtime.

Muon Spectrometers and Magnets

All experimental magnets, should still be fully operational. Over the years the operating fields may have been increased by 10-15%, increasing the resolution capability to the trackers. The controls and all peripheral services will be obsolete in their technology. An effective upgrade will be easy. Probably it will happen already in the mid twenties.

For the muon spectrometer (trigger and precision chambers) the problem lies in the natural aging of the critical components and of the base materials in general. Most of the active components have been designed for a lifetime of 15-20 years. These are gaseous detectors, therefore less robust and more subject to stresses in terms of mechanics and services (gas leaks, gas distribution infrastructure, connectors, resistive materials,…).

Already for the High Luminosity upgrades we foresee to replace the end-cap chambers in the high rapidity regions with more granular and trigger-effective components. New technologies will be adopted. In the same spirit, it is likely possible to start replacing around 2030 most or all of the muon stations during regular shutdowns. In the case of ATLAS, for some chambers a direct replacement will not be possible, access being the problem. An unconventional approach will be needed.

As for the ID, the muon spectrometer strategy should be a continuous upgrade over time, profiting from all shutdowns of the LHC machine, while keeping the technology up to date.

A NEW DETECTOR

Why not to think and plan for a very new detector in general, in parallel to ATLAS and CMS?

If we go the HE-LHC way, probably it means no Linear Collider for a while! A large detector community preparing today already for the Linear Collider is in standby, with plenty of new ideas and several new technologies to be deployed.

A new detector could be tuned from the beginning to the type of new discoveries the LHC will make and go beyond in a more effective way. It will take 16-18 years to achieve a fully functional new detector, and this means that a green light to move in this direction should be given around 2015. A new detector might imply new civil engineering work to prepare a new experimental cavern in today's LHCb or ALICE location.

CONCLUSIONS

Thinking about the ATLAS and CMS evolution in the HE-LHC scenario, the following arguments might apply:

- Most of the electronics will need to be rebuilt and upgraded. This will partially happen already for the HL-LHC, leaving therefore no reason not to do it later as well. This would solve the problem of obsolete technologies.
- Inner detectors will be upgraded after 2020, and there is no reason not to continue doing it further, maybe just in a modular way. The story is similar for the muon spectrometer. Consolidation/upgrade can be continuous.
- The calorimeters are the more critical items, needing a particular evaluation, possibly representing a serious showstopper.
- Over time, the trigger hardware and strategies will be revisited. Doing this already for the HL-LHC. Physics will guide us!

An experimental program based only on the existing detectors might be risky, also giving the fact that the investments needed for a new LHC machine with more energy will be substantial. Planning for a fully new detector might be a more rational approach. It might take more time to conceive a new detector than to upgrade the accelerator. Thus, a strategical decision might due in just a few years from now.

REFERENCES

[1] The ATLAS Experiment at the CERN Large Hadron Collider, G.Aad et al., ATLAS Collaboration, JINST 3, S08003 (2008).

[2] The CMS Experiment at the CERN Large Hadron Collider, S. Chatrchyan et al., CMS Collaboration, JINST 8, S08004 (2008).

PROGRESS IN HIGH FIELD ACCELERATOR MAGNET DEVELOPMENT BY THE US LHC ACCELERATOR RESEARCH PROGRAM*

Gian Luca Sabbi (LBNL) for the LARP collaboration

Abstract

The maximum magnetic field available to guide and focus the proton beams will be the most important factor driving the design of the High Energy LHC. The US LHC Accelerator Research Program (LARP) is a collaboration of US National Laboratories aiming at demonstrating the feasibility of Nb_3Sn magnet technology for application to future colliders. While LARP is primarily focused on the requirements of the High-Luminosity LHC (HL-LHC), it is also directly relevant to the High-Energy LHC (HE-LHC). Program results and future directions will be discussed.

INTRODUCTION

A series of upgrades to the LHC and its injectors is under study to achieve a significant increase of the luminosity with respect to the baseline design [1]. Replacing the first-generation IR quadrupoles with higher performance magnets is one of the required steps in this direction. Although designs based on NbTi conductor are being considered, the intrinsic properties of Nb_3Sn make it a strong candidate to meet the ultimate performance goals in terms of operating field, temperature margin, and radiation lifetime. Under typical upgrade scenarios, the new magnets will provide increased focusing power to double or triple the luminosity, and at the same time will be able to operate under radiation loads corresponding to a 10-fold increase in peak luminosity, and with radiation lifetime consistent with a 3000 fb^{-1} integrated luminosity goal.

Starting in 2004, the LHC Accelerator Research Program (LARP) collaboration has led the US effort to develop Nb_3Sn quadrupole magnets for the LHC luminosity upgrade [2]. The program is founded on the knowledge base and infrastructure of the DOE General Accelerator Development programs at BNL, FNAL and LBNL. With respect to these programs, it provides specific focus and resources to select the best available technologies for the luminosity upgrade and bridge the gap from proof-of-principle models to fully developed prototypes incorporating all features required for operation in the LHC accelerator. Significant progress has been made to date and the program is well positioned to complete the technology demonstration by 2014 and initiate a construction project. A successful luminosity upgrade based on Nb_3Sn will represent a significant step toward a High-Energy LHC and open the way to other applications within and outside high energy physics.

*Work supported by the US Department of Energy

HIGH FIELD MAGNET TECHNOLOGIES

Excellent mechanical and electrical properties of multi filamentary NbTi have made it the conductor of choice in all superconducting accelerators to date. However, the intrinsic properties of NbTi limit its field reach in practical accelerator applications to about 8 T. In order to surpass this threshold, superconductors with higher upper critical field are needed. Niobium-Tin (Nb_3Sn) is currently the most advanced material for practical applications. It carries current densities similar to NbTi at more than twice the field, and is available in long lengths with uniform properties. Nb_3Al offers lower strain sensitivity with respect to Nb_3Sn, but its manufacturing process is not sufficiently well developed to support magnet fabrication. The low-temperature properties of HTS materials such as Bi-2212 are far superior to both Nb_3Sn and Nb_3Al. However, many technology challenges need to be addressed before practical designs can be developed and implemented in prototypes.

All superconductors suitable for high field applications are brittle and strain sensitive, requiring new approaches to magnet design and fabrication to complement or replace those established for NbTi. In particular, because of their brittleness, high field superconductors cannot be drawn to thin filaments like NbTi, but have to be formed in the final geometry by high-temperature heat treatment. In the fully reacted state, the filaments are extremely sensitive to strain. Therefore, attempting to wind pre-reacted cables in accelerator-type coils would result in unacceptable critical current degradation at the ends. Instead, coils are wound using un-reacted cable, when components are still ductile, and the superconductor is formed by high temperature heat treatment after coil winding. This technique requires the use of insulation and coil structural components that can withstand the high reaction temperatures. In addition, new approaches to mechanical support and quench protection are required to safely handle reacted coils through magnet assembly, cool down and excitation

A significant and sustained R&D effort is required to develop technologies that can take advantage of the properties of high field superconductors while coping with the associated challenges. Early work on Nb_3Sn accelerator magnets was performed at BNL [3], CEA [4], CERN [5-6], and LBNL [7]. In the mid-90s, the dipoles MSUT (Twente University) and D20 (LBNL) reached fields of 11-13 T [8-9]. More recently, the LBNL dipoles RD3-B and HD1b achieved record field of 14.7 T and 16.1 T, respectively, using simple racetrack coil designs

[10-11]. The LARP program was established to build on this base and develop the technology to a mature state, consistent with the requirements of the High-Luminosity LHC project.

THE LARP PROGRAM

Goals and organization

LARP was established in 2004 to enable active participation of the U.S. scientific community in the accelerator research program of the LHC machine. While the program scope included accelerator commissioning and operation, special emphasis was given to the development of magnet technologies relevant to the LHC luminosity upgrade, which was recognized as one of the highest physics priorities by the US HEP advisory panel [12]. LARP is also intended to serve as a vehicle to advance collaboration among US Laboratories as well as international cooperation in large science projects.

The documents that initiated the program identified its key goals, to be achieved in close collaboration with CERN:

- Help the LHC achieve its design luminosity quickly, safely and efficiently.
- Continue to improve LHC performance by advances in understanding and the development of new instrumentation.
- Use the LHC effectively as a tool to gain a deeper knowledge of accelerator science and technology.
- Extend LHC as a frontier High Energy Physics instrument with a timely luminosity upgrade.

LARP was firmly established as an advanced R&D program, which would help the US HEP community in maintaining a leadership role in accelerator technology, and set the basis for a separately funded construction project. "Preparing to build the next generation hadron collider" was also explicitly mentioned among the key program goals in the LARP proposal (Fig.1).

The program is organized in three sections: (i) accelerator systems, (ii) magnet systems and (iii) programmatic activities. The accelerator systems section includes the development of advanced instrumentation and collimation systems, as well as accelerator physics studies. The magnet systems section is focused on the development of Nb_3Sn interaction region quadrupoles, and is described in detail in this paper. The programmatic activities section manages the long term visitor program and the Toohig post-doctoral fellowship.

Goals \ Deliverables	Hardware Commissioning	Beam Commissioning	Fundamental Accelerator Research	Instrumentation & Diagnostics	Magnet R&D
Maximize HEP at the LHC	Y	Y	Y	Y	
Improve LHC Performance			Y	Y	
Advance Accelerator Science & Technology			Y	Y	Y
Extend LHC HEP by a Timely Upgrade			Y	Y	Y
Prepare to Build the Next Generation Hadron Collider	Y	Y	Y	Y	Y

Fig. 1: LARP goals and deliverables matrix [2]

Magnet program components

The LARP magnet program was conceived as a progression of studies and technological steps, starting from simple systems designed to address specific R&D issues, and building toward more complex configurations incorporating all required features for operation in the accelerator. The program organization reflects this approach and has evolved in time to adapt to the different stages of the R&D. The main areas, corresponding to "level 2" categories in the work breakdown structure, are:

- Materials R&D, including: strand specifications, procurement and characterization; cable fabrication, insulation and qualification; coil heat treatment optimization and verification.
- Technology development with racetrack coils. This area was a key component of the program from its inception until 2008. Through the Sub-scale Quadrupole (SQ) and Long Racetrack (LR) models, it addressed fundamental issues of conductor performance, mechanical analysis, instrumentation quench protection, and most notably, scale-up of coil and structures to 4 m length, paving the way to the long quadrupole program.
- Design studies: This area was also very active in the first part of the program, to select the most promising designs for future model quadrupoles, compare different IR layouts, and perform supporting studies in areas such as radiation deposition and field quality. While the program has progressively shifted toward experimental demonstrations, renewed focus on this area is developing in connection with the HL-LHC design study [13].
- Model quadrupoles: this area oversees the detailed design, fabrication and testing of short quadrupole models, including the 90 mm aperture Technology Quadrupoles (TQC and TQS) and the 120 mm aperture High Field Quadrupoles (HQ).
- Long Quadrupoles (LQ), which covers the scale up from 1 m to 4 m length (LQ and LHQ models).

Each area is organized around tasks with specific goals and milestones. Individual task typically utilize expertise, resources and infrastructure from several laboratories,

leading to close collaboration at the level of each activity. This approach may appear less efficient with respect to a project-type organization in which responsibilities for key deliverables are distributed among laboratories, with each group working independently on its portion. However, it has proven extremely valuable in comparing and integrating the experience and methods developed by different groups, and a key element of the program success both from a technical and collaboration standpoint.

Fabrication and test database

Since its start in 2004, the LARP program has fabricated and tested a large number of models of different designs. This section summarizes the tests performed and the key issues addressed. Progress and issues in each area are summarized in the following section.

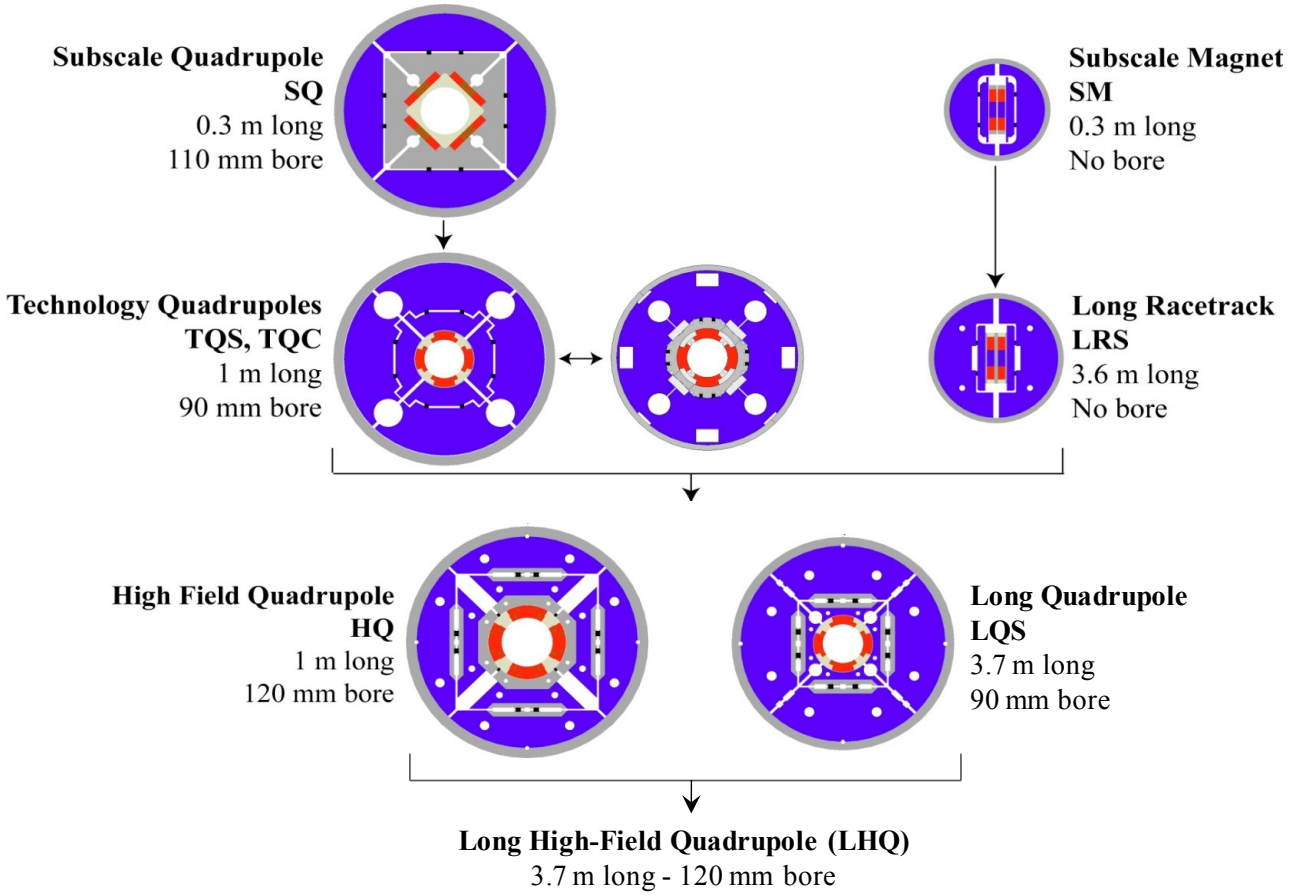

Fig. 2: LARP magnet development flow-chart

Figure 2 is a magnet development flowchart showing the LARP model magnets and their progression from technological tests toward accelerator quality designs. The main program components are:

1. Sub-scale Quadrupole - SQ (LBNL, FNAL). SQ is based on four racetrack coils of the LBNL "sub-scale" design [14]. A combination of existing and new coils was used leading to five tests at 4.5 K and two tests at 1.9 K [15-16]. Among the highlights of these tests were:
   - Demonstration of conductor performance up to the short sample limits under conditions similar to those required by the Technology Quadrupoles (field, current, stress) and using the same heat treatment.
   - Detailed 3D finite element modeling and verification of stress calculation against strain gauge measurements.
   - Studies of quench propagation and protection, including temperature and stress limits during a quench.
   - Studies of the effect of axial pre-load on the quench performance and training.

   In addition, the SQ tests indicated that block-coil quadrupoles can perform at the expected levels in practical configurations. However, cos(2θ) coils were selected for the LHC IR quad application since design studies showed that they would provide significantly better magnetic efficiency for this application.
2. Sub-scale Magnet - SM (BNL, LBNL). This magnet was used as a technology transfer tool in preparation

for the design and fabrication of the long racetrack coils at BNL. Two sub-scale coils were fabricated and assembled at BNL using design, cables, parts, mechanical structure and fabrication procedures provided by LBNL. The magnet was also tested at BNL and achieved its full conductor potential [17].

3. Long Racetrack Shell - LRS (BNL, LBNL). The main goal of LRS was to provide a first demonstration that the Nb_3Sn coils and shell based structures could be scaled to lengths significantly higher than 1 meter. The coil design was very similar to the sub-scale magnet, with a length increase of more than a factor of ten. The support structure was designed and pre-assembled at LBNL. Two coils were fabricated, assembled and tested at BNL achieving 91% of the short sample limit [17]. Based on feedback from this test, the support structure which originally utilized a one-piece shell was subdivided in four sections, leading to further performance improvements (96% of SSL) in the second test using the same coils [18].
4. Technology Quadrupole – TQ (FNAL, LBNL + CERN). The TQ models are based on the traditional cos(2θ) coil design with 90 mm aperture and 1 m length. Three generations of coils were fabricated using different wire designs. In total, more than 30 coils were fabricated using a distributed production line, with winding/curing performed at FNAL and reaction/impregnation performed at LBNL. Two support structures were compared, a collar-based structure designed by FNAL and a shell based structure designed by LBNL. About 15 models were tested in a variety of configurations at LBNL, FNAL and CERN [19-20]. Among the main studies and results obtained using the TQ models are:
   - Achieved 240 T/m in 90 mm aperture, about 20% higher than the performance target.
   - Demonstrated robust performance, in particular the capability to transport, disassemble and reassemble coils in different configurations.
   - Performed a systematic investigation of Nb_3Sn stress limits (engineering design space)
   - Completed a fatigue test involving 100 cycles from low to high current.
5. Long Quadrupole Shell – LQS (BNL, FNAL, LBNL). LQS is a scale-up of the TQS design from 1 m to 4 m. The development of long Nb_3Sn quadrupoles was recognized as a key R&D goal from the program outset. In April 2005, LARP, DOE and CERN agreed that achieving a gradient of 200 T/m in a 90 mm aperture, 4 m long quadrupole would serve as a convincing demonstration of such scale-up. The primary purpose of both TQ and LR programs was to serves as a basis for LQ. All three labs participated in the LQ design, fabrication and test activities. The 200 T/m target was achieved during the first test in December 2009 [21]. A second test with optimized preload using the same coils (LQS01b) achieved a 10% increase in performance, to 220 T/m. The next step is the assembly and test of LQS02, using four new coils, to demonstrate reproducibility. A third series of tests is also planned using the latest generation conductor (RRP 108/127).
6. High-Field Quadrupole - HQ (BNL, FNAL, LBNL + CERN). Detailed optics and layout studies of the upgraded LHC insertions indicate that increasing the quadrupole aperture leads to improved performance. Taking into account the space limitations in the tunnel, an aperture of 120 mm was selected for the development of upgraded quadrupole models based on NbTi. In order to explore the technological limits associated with larger aperture, and to provide a direct comparison between NbTi and Nb_3Sn performance, the same aperture was selected by LARP for the next series of High-Field Quadrupoles. The 120 mm aperture, two-layer coil design using a 15 mm wide cable results in a 15 T peak field and 1.2 MJ/m stored energy, about a factor of 3 higher than in TQ and LQ. For the first time in LARP, coil alignment features are included at all phases of fabrication, assembly and excitation. To date, 12 coils have been fabricated and 3 tests were performed. During the first test [22] the magnet achieved 155 T/m at 4.5 K, well above the intrinsic limit of NbTi at 1.9 K. However, high rates of insulation failures were observed, prompting a revision of the cable and coil design to decrease stress during fabrication. A scale up of the HQ design to 4 m length is planned as a final technology demonstrator.

R&D PROGRESS AND ISSUES

Strand design and fabrication

Three wire types were utilized in LARP, all produced by Oxford Superconducting Technology (OST):

- Modified Jelly Roll wire with 61 sub-elements, 54 of which contain superconducting filaments while the remaining 7 are made of copper stabilizer (MJR 54/61)
- Rod Restack Processed wire with 61 sub-elements, 54 of which contain superconducting filaments while the remaining 7 are made of copper stabilizer (RRP 54/61)
- Rod Restack Processed wire with 127 sub-elements, 108 of which contain superconducting filaments while the remaining 19 are made of copper stabilizer (RRP 108/127)

The MJR wire represents an older generation wire that was already retired from production at the beginning of the program. It was used in the first generation TQ models since it was available in sufficient quantity to allow a direct comparison of different mechanical structures.

The RRP 54/61 was used in the majority of the LARP tests to date. It delivered solid performance allowing the

LR, TQ and LQ models to reach their R&D objectives and performance goals. However, this design results in a rather large effective filament size (~70 μm) in the strand diameter of interest (0.7-0.8 mm) leading to stability thresholds which are only within a factor of 2 above the operating point. Further erosion of the stability margin may result from conductor degradation due to processing or strain. As a result, performance limitations have been observed for moderate field designs at low temperature.
The RRP 108/127 was first procured by LARP in 2007, when it was still considered an R&D wire by OST, to evaluate its performance and encourage further development and transition to the production stage. It provided solid performance in the TQS03 model with no signs of instability, leading to its adoption as a baseline LARP wire starting in 2009, However, due to the long lead times for procurement and magnet fabrication, the first models to benefit from this transition will only be tested in 2012. In addition, further improvements to the 108/127 design are required to match the average piece length and critical current densities obtained in the 54/61 design. The 5-6 year cycle from initial evaluation to full utilization in the magnet fabrication pipeline indicates that incorporating newer generations of wire (such as RRP 217 or Powder-in-Tube) before the 2015 anticipated start of IR quadrupole production will be a challenge.

Cable design and fabrication

Although the fabrication of Nb3Sn cables was already well established at the start of the program, LARP provided an opportunity for larger scale manufacturing, optimization and characterization. To date, more than 7 km of cable of three different designs were fabricated with minimal losses. The current R&D effort is focusing on transitioning from a three-step process involving a first cable fabrication pass at larger size, followed by anneal and re-roll to final size, to a one-step process using pre-annealed strand. The one-step process is expected to be more robust and efficient, and is compatible with the introduction of thin cores for control of the AC losses. Several cored cables have been fabricated for the latest generation HQ models using stainless steel and fiberglass cores. Coils have been fabricated using cored cables and will be assembled and tested in the near future.

Quench performance and training

The capability to approach the full conductor performance in model magnets is an important indicator of the maturity of the technology, and the capability to reach the design point with minimal training and no retraining is essential requirement for operation in the accelerator. On both fronts, positive results were obtained. The full conductor potential, based on critical current measurements of extracted strands, without factoring in stress degradation, has been obtained in the best SQ, LR, TQ and LQ models at 4.5 K, indicating that the design and fabrication process is well understood and optimized. The best models also showed fast training and no retraining. However, new designs tend to require several iterations in order to achieve the best results. The steady process of systematic analysis and improvement defines the success of an R&D program like LARP, but it is clear that more work is needed to achieve full control of this technology, in particular for what concerns the coil design and fabrication, and especially the reaction step.

Mechanical design and stress limits

Providing adequate mechanical support in high-field magnets based on brittle superconductors requires structures that can generate large forces while minimizing stress on the conductor at all stages of magnet fabrication and operation. Consistent with the R&D goals of the program, the application of new concepts and advanced modeling capabilities was emphasized. In particular, support structure originally developed at LBNL for high field dipoles [23] was applied to the LARP quadrupoles. This concept is based a thick aluminum shell, pre-tensioned a room temperature using water-pressurized bladders and interference keys. During cool-down, the stress in the shell increases due to differential thermal contraction relative to the iron yoke. This shell-based structure was evaluated against the more traditional collar-based structure in the TQ models, scaled-up to 4 m length in the LR and LQ models, and further optimized in the HQ models.

A series of tests were performed at CERN using TQS03 models to better understand the Nb_3Sn stress limits and its tolerance to a large number of cycles [24]. It was found that the magnet could perform satisfactorily up to 200 MPa average coil stress, which results in peak local stresses of the order of 250 MPa. This result considerably expands the engineering design space with respect to what was previously considered as the limit of 150 MPa. In addition, a cycling test involving one thousand ramps from low to high field was performed, and no degradation was found.

Alignment and Field Quality

Due to large beam sizes in the IR quadrupoles, their field quality plays a critical role on the beam dynamics during collision. Therefore, precise coil fabrication and structure alignment are required. Although early LARP magnets had limited alignment features, steady progress has been made and the last generation of HQ models incorporates full alignment at all steps of coil fabrication, magnet assembly and operation. No negative impact on mechanical support and quench performance resulting from the introduction of these features has been observed so far.

Field errors at injection are less critical, but need to be carefully analyzed since Nb_3Sn wires exhibit large magnetization due to high critical current density and

large filament size. Compensation of persistent current effects by saturation of carefully iron inserts may provide an intermediate solution. Ultimately, wires with larger number of sub-elements should be developed to decrease the effective filament size.

As previously mentioned, cored cables are being introduced in the HQ models to better control the distortions generated by eddy current during a ramp.

Coil fabrication technology

Several factors contributed to a steady improvement in coil fabrication procedures throughout the program. Different experiences and methods had to be compared and integrated in order to develop tooling and procedures that would be acceptable to all groups. Robust handling and shipping tools had to be devised to allow distributed coil production lines for the TQ, LQ and HQ models. Careful analysis was performed in relation to the scale up to 4 m length in the LR and LQ models. Nevertheless, a complete modeling framework is still not available, particularly in relation to the reaction process. The coil fabrication methods are still largely based on empirical knowledge and several iterations are typically needed to optimize new designs.

LARP RELEVANCE TO HE-LHC

As previously noted, large portions of the magnet R&D effort performed by the LARP program in support of the LHC luminosity upgrade has direct relevance to the High-Energy LHC. Although the stated goal of 20 T field is beyond reach for Nb_3Sn, it is expected that a hybrid dipole design will be used with Nb_3Sn providing a large portion of the total field. Among the key contributions of LARP to the development of technologies applicable to HE-LHC are:

- Scale up to long magnets: cable fabrication and QA, coil and structure fabrication, magnet assembly.
- Instrumentation and analysis
- Field quality, quench protection
- Accelerator integration: cooling, helium containment, alignment
- Development of radiation tolerant components
- Initial feedback on series production and operation issues:
- Infrastructure, production steps/times/cost
- Reliability, failure rates in production/operations

In addition, the capability to organize and integrate an effective R&D effort across Laboratories is a key contribution of LARP.

At the same time, it is clear that large portions of the R&D needed for HE-LHC are not covered by LARP. In particular, LARP is not involved with HTS technologies that will be required to push the field beyond 15 T. In addition, the small aperture required to limit magnet size and cost in HE-LHC will drive the magnet design in different directions with respect to those adopted for the large-aperture IR quadrupoles. Finally, an additional length scale-up of a factor of 2-3 will be required to achieve dipole lengths comparable to those used in the baseline LHC. Coupled with the small magnet aperture, this will also require incorporating a small sagitta in the magnet fabrication.

SUMMARY

Intensive magnet R&D efforts are needed to meet the requirements of future colliders at the energy frontier. The LHC luminosity upgrade provides the opportunity to refine the results obtained in proof-of-principle Nb_3Sn models and extend them to full-size production magnets suitable for operation in a challenging accelerator environment. The LARP program has made considerable progress in this direction, and is expected to complete the technology demonstration within the next several years. Successful construction and implementation in the high luminosity LHC will provide a stepping stone for the application of high field magnet technology to next generation colliders such as the High Energy LHC.

REFERENCES

[1] F. Ruggiero (editor) et al., “LHC Luminosity and Energy Upgrade: a feasibility study”, LHC Project Report 626, December 2002.

[2] R. Kephart et al., “The US LHC Accelerator Research Program – A proposal”, May 2003.

[3] W. Sampson, S. Kiss, K. Robins, A. McInturff, “Nb3Sn Dipole Magnets”, IEEE Trans. Magn., 15(1), January 1979.

[4] J. Perot, “Construction and Test of a Synchrotron Dipole Model using Nb3Sn cable”, IEEE Trans. Magn. 19(3), May 1983.

[5] A. Asner et al., “Development and Successful Testing of the First Nb3Sn Wound, in-situ Reacted, High-Field Superconducting Quadrupole of CERN”, IEEE Trans. Magn., 19(3), May 1983.

[6] A. Asner, R. Perin, S. Wenger, F. Zerobin, “First Nb3Sn, 1m long Superconducting Dipole Model Magnets for LHC break the 10 Tesla Field threshold”, MT-11, Tsukuba, Aug. 1989.

[7] C. Taylor et al., “A Nb3Sn Dipole Magnet Reacted after Winding”, IEEE Trans. Magn. 21(2), March 1985

[8] A. den Ouden et al., “Application of Nb_3Sn superconductors in accelerator magnets”, IEEE Trans. Appl. Supercond. Vol. 7, 1997.

[9] A. McInturff et al., “Test Results for a High Field (13 T) Nb3Sn Dipole”, PAC-97, Vancouver, May 1997

[10] A. Lietzke et al., “Fabrication and Test Results of a High Field, Nb3Sn Superconducting Racetrack Dipole Magnet”, PAC-2001.

[11] A. Lietzke, et al., “Test results of HD1b, an upgraded 16 T Nb3Sn dipole magnet”, IEEE Trans. Appl. Superconduct., Vol. 15, no. 2, pp. 1123-1127, June 2005.

[12] High-Energy Physics Facilities of the DOE Office of Science Twenty-Year Road Map, HEPAP report to the Director of the Office of Science, 17 March 2003.

[13] L. Rossi et al., High Luminosity Large Hadron Collider Design Study - HiLumi LHC, FP7-INFRASTRUCTURES-2011-1, November 2010.

[14] R. Hafalia et al., "An Approach for Faster High Field Magnet Technology Development", IEEE Trans. on Applied Superconductivity, Vol.13, No. 2, June 2003, pp.1258-1261.

[15] P. Ferracin et al., "Development of a large aperture Nb_3Sn racetrack quadrupole magnet", IEEE Transactions on Applied Superconductivity, vol. 15, no. 2, June 2005, pp. 1132-1135.

[16] P. Ferracin et al., "Assembly and test of SQ01b, a Nb_3Sn quadrupole magnet for the LHC Accelerator Research Program", IEEE Trans. Appl. Supercond., vol. 16, no. 2, June 2006, 382-385.

[17] P. Wanderer et al., "Construction and Test of 3.6 m Nb_3Sn Racetrack Coils for LARP", IEEE Trans. Appl. Supercond., vol. 18, no. 2, June 2008, pp. 171-174.

[18] J. Muratore et al., "Test Results of LARP 3.6 m Nb_3Sn Racetrack Coils Supported by Full-Length and Segmented Shell Structures", IEEE Trans. Appl. Supercond., vol. 19, no. 3, June 2009, 1212-1216.

[19] S. Caspi et al., "Test Results of LARP Nb3Sn Quadrupole Magnets Using a Shell-based Support Structure (TQS)" IEEE Trans. Appl. Supercond., vol. 19, no. 3, Part 2, June 2009, 1221-1225

[20] R. Bossert et al., "Fabrication and Test of LARP Technological Quadrupole Models of TQC Series", IEEE Trans. Appl. Supercond., vol. 19, no. 3, June 2009, pp. 1216-1230.

[21] G. Ambrosio et al., "Test results of the first 3.7 m long Nb3Sn quadrupole by LARP and future plans", Proceeding of the 2010 Applied Superconductivity Conference, in press.

[22] S. Caspi et al., "Test results of HQ01 - a 120 mm 15 T Nb_3Sn Quadrupole for the LHC Upgrade", Proceeding of the 2010 Applied Superconductivity Conference, in press.

[23] S. Caspi, et al., "A New Support Structure for High Field Magnets," IEEE Transactions on Applied Superconductivity, Vol. 12, No. 1, March 2002, pp. 47-50.

[24] H. Felice, S. Caspi, D. Dietderich, J. Lizarazo, A. Ghosh, P. Wanderer, G. Ambrosio, E. Barzi, R. Bossert, M. Bajko, B. Bordini, J. Feuvrior "Test results of TQS03: a LARP shell-based Nb_3Sn quadrupole using RRP 108/127 conductor" Journal of Physics: Conference Series, in press.

LBNL HIGH FIELD CORE PROGRAM*

S. Caspi Lawrence Berkeley National Laboratory, Berkeley, CA, USA

Abstract

The LBNL Superconducting Magnet Group mission is to develop and establish the technologies associated with high field superconducting magnets in order to provide cost-effective options for the next-generation high-energy physics accelerators. The research effort is part of the group core program and the development is part of the LARP program discussed elsewhere at this workshop.

INTRODUCTION

In the past twenty years the LBNL core program has made the following contributions towards high field magnet using Nb_3Sn conductor technology:

- Engineering properties of superconducting wires
- Cabling of traditional and advanced wires
- "Wind-and-React" coil fabrication technology
- Advance concepts for mechanical support
- New concepts for magnet assembly
- Modeling capabilities and diagnostic tools

The impact on the High Energy Physics community was the possible advance of a high energy/luminosity frontier of the LHC. The core program is focused on 1) conductor R&D and cable manufacturing, 2) magnet design, construction and testing and 3) new concepts and analysis.

HIGH FIELD MAGNETS

Progress in the attainable dipole fields made with Nb_3Sn conductor is plotted in Fig. 1. The type of magnets built and tested by LBNL varies from Cos-Theta (D20-13.8 T, 50 mm bore) to Common Coil (RD3-14.5 T) to Block (HD1-16 T) (Fig. 2). Other magnet were also built and tested as intermediate steps (Fig. 3)

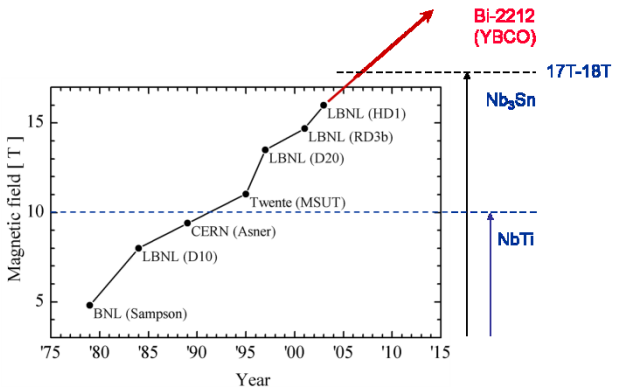

Figure.1: Progress of Nb_3Sn dipole magnets.

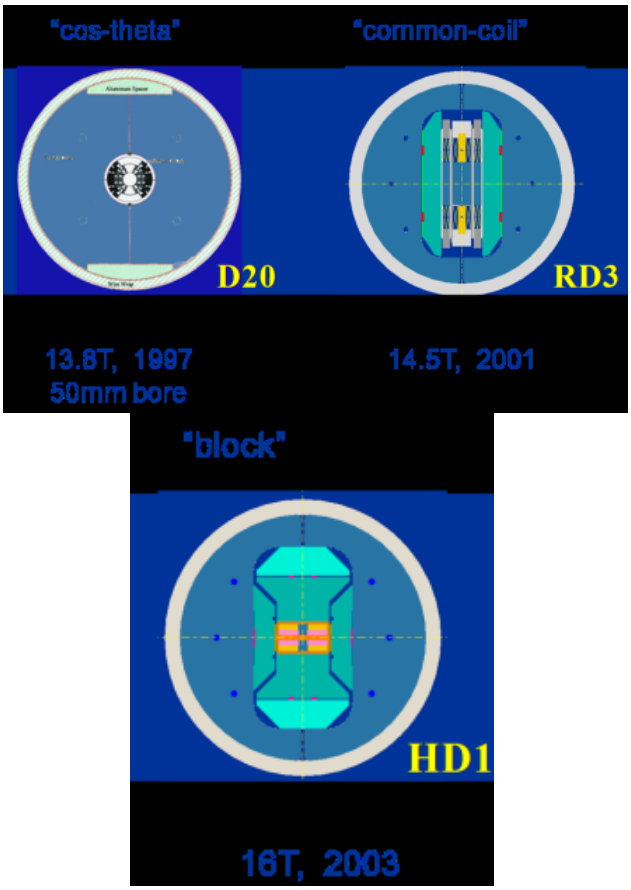

Figure 2: Three different configurations of dipole magnets constructed at LBNL

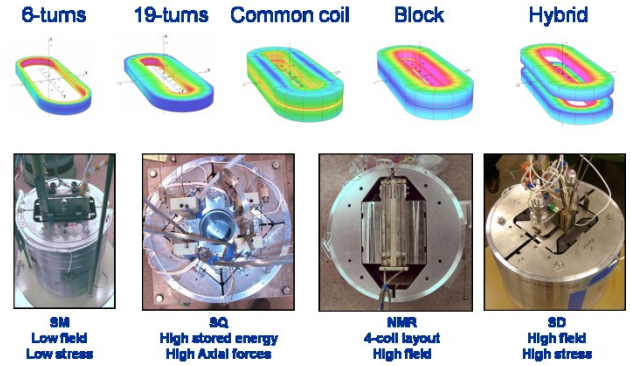

Figure 3: Left to right: SM- low field and low stress, SQ-high stored energy, high axial force, NMR-four coil layout high field, SD- high field high stress block design.

Conductor Development

The US HEP Conductor Development Program (CDP) has coordinated Nb_3Sn work between National labs, universities and industry. Over the past twenty years the

program main achievements were the doubling of Nb_3Sn current density and the improvement of wire uniformity and piece length. The program continues to work on improving the current density of Nb_3Sn as well as reducing its sub-filament size (Fig. 4). From 2007 the CDP supported the development Bi-2212 demonstrating its performance in simple configurations.

To understand the relations of the conductor state at different scales, a hierarchical model of the strain state has been developed. The model included nonlinear properties and enabled computing the strain at the filament level including stress in micro-scales due to macro loading and nonlinear deformation. The work also included cool-down effects. The work has been extended to the manufacturing and optimization of cables (Fig. 5).

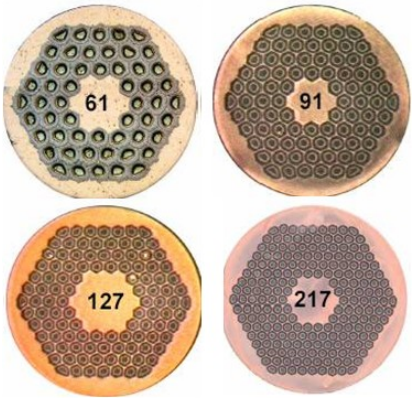

Figure 4: Nb_3Sn strands with different filament number

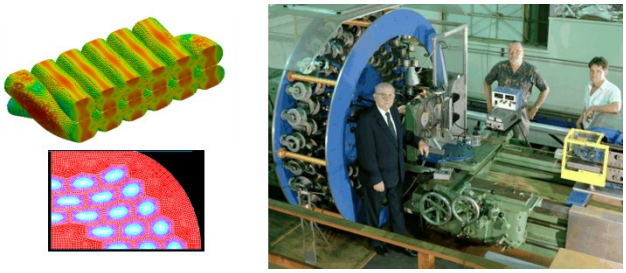

Figure 5: Manufacturing and analysis of cables

Magnet Development

The manufacturing of magnets with Nb_3Sn coils requires the integration between CAD, analysis and manufacturing (Fig. 6). The process of winding and curing coils using metallic parts (Fig. 7) reaction at 650°C, instrumentation and impregnation has been made into a continuous integrated process that closely interacts with analysis. Magnetic and structural analysis follows the magnet design from its room temperature assembly and pre-stress through cool-down and excitation to "short-sample". The magnet assembly uses "key and bladder" technology and the final pre-stress is reached during cool-down mainly due to the thermal expansion difference between iron and aluminium (Fig. 8-9).

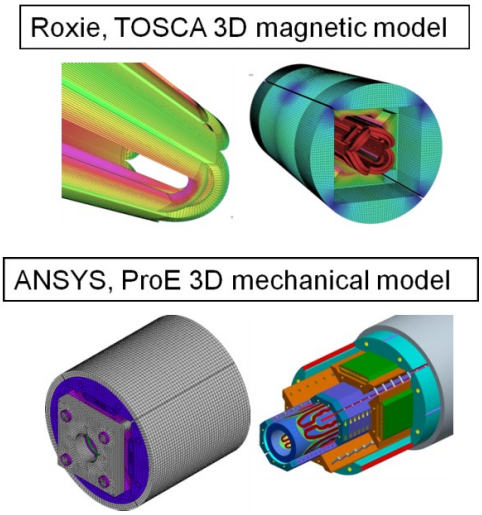

Figure 6: Integrated design between CAD, magnetic and structural analysis

Figure 7: View of magnet "end" at different stages.

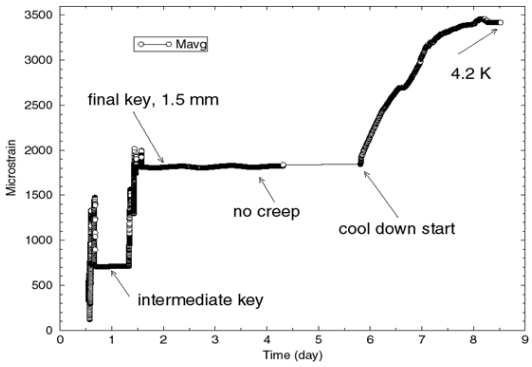

Figure 8: Typical increase of shell tension during assembly and cool-down

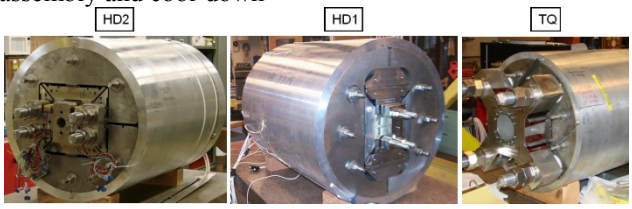

Figure 9: Aluminium shells used to pre-stress coils

As part of the development of Nb_3Sn high field magnets for the next generation of HEP colliders [1] the LBNL Superconducting Magnet Program is fabricating and testing a series of Nb_3Sn dipoles magnet HD2/3 (see Fig. 10-11). References on the conceptual design, the coil and structure mechanical analysis, the fabrication and assembly procedure and the field quality expectations are in [2-4]. Results of several tests,

carried out at the LBNL test facility, are shown in Figure 12 indicating low and incomplete training curves. Most quench origins were located at the end of the straight section just prior to the start up of the bend. A subsequent autopsy at that location showed an unintended step in the upper block (Fig. 13) created by the cable hard-way bend. In HD3 coils, under construction, the radius of the bend was increased to ease the bend and a supporting "membrane" was added between layers. Other test results including strain gauges measurements, training performance, quench locations, and ramp-rate studies are reported in [5]. Other improvements now include curing of coils (using a binder) to better position them prior to reaction. By reducing the reaction temperature of HD3 coils, a more conservative approach was taken by a corresponding reduction of the current density from 3300 A/mm^2 (12 T, 4.2 K) in HD2 to 3000 A/mm^2 in HD3. The impact of all such changes reduced the short-sample bore field from 15.6 T in HD2 to 14.9 T in HD3.

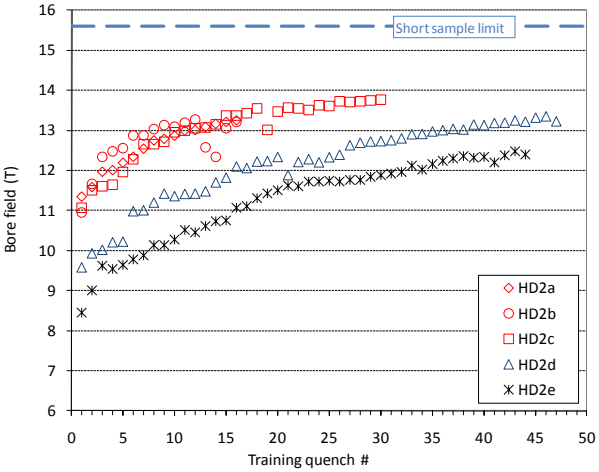

Figure 12: Bore field (T) as a function of training quenches. The short sample limit of 15.6 T bore field corresponds to a coil peak field of 16.5 T.

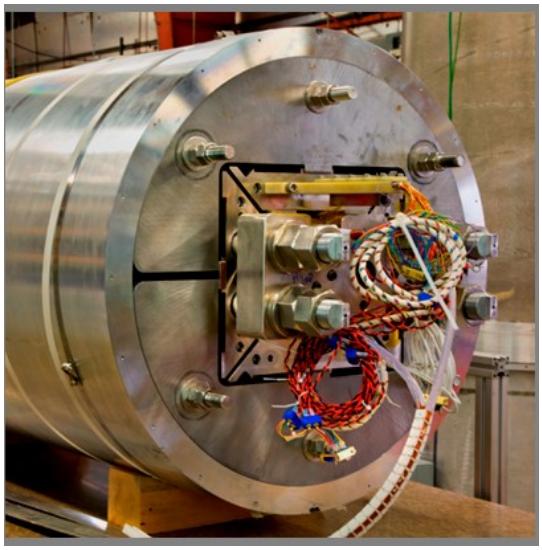

Figure 10: Magnet HD2

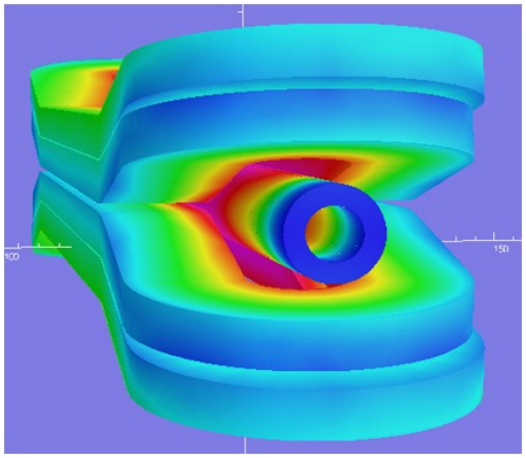

Figure 11: Computed field magnitude of HD2

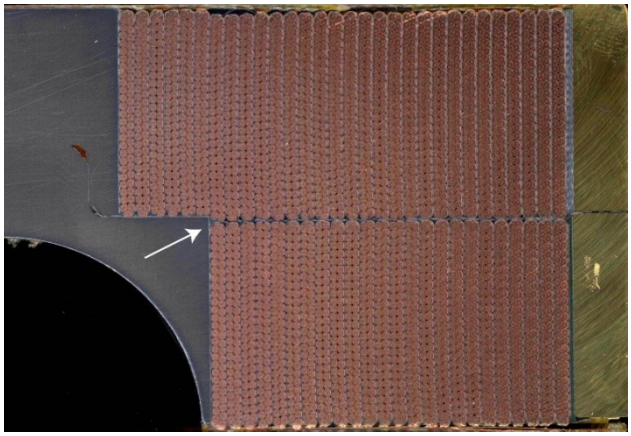

Figure 13: Cross-section cuts of HD2 coil #1 close to the beginning of the hard-way.

Analysis

LBNL has been developing 3D finite element models to predict the behaviour of high field Nb_3Sn superconducting magnets [6]. The models track the coil response during assembly, cool-down and excitation with particular interest on displacements when frictional forces arise. As Lorentz forces can be cycled and irreversible displacements can be computed and compared with strain gauge measurements. Analysis on the release of local frictional energy during magnet excitation results in a temperature increase that can be calculated. Magnet quenching and training is then correlated to that level [7]. Figures 14-15 show the results of the analysis using the programs TOSCA and ANSYS.

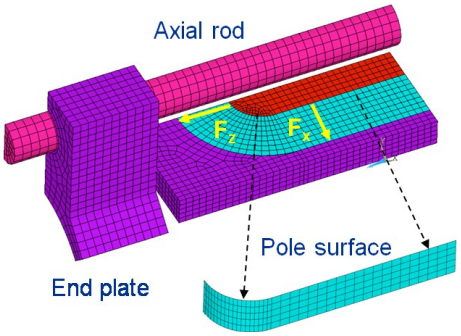

Figure 14: View of coil, island, end plate, axial support rod and contact surface between coil and island.

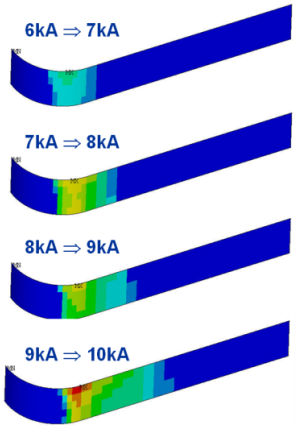

Figure 15: Surface between coil and island showing a potential increase in energy release at higher currents a leading cause of training.

ACKNOWLEDGEMENT

The Superconducting Group Team:

D. Arbelaez, B. Bingham, S. Caspi, D. Cheng, B. Collins, D. Dietderich, H. Felice, A. Godeke, R. Hafalia, J. Joseph, J. Krishnan, J. Lizarazo, M. Marchevsky, S. Prestemon, G. Sabbi, C. Vu, X. Wang. P. Bish, H. Higley, D. Horler, S. King, C. Kozy, N. Liggins, J. Swanson, P. Wong D. Pickett, J. Smithwick, G. Thomas, K. Miho

REFERENCES

[1] A. F. Lietzke, et al., "Test results for HD1, a 16 Tesla Nb_3Sn dipole magnet", IEEE Trans. Appl. Supercond., vol. 14, no. 2, pp. 345-348, (June 2004).

[2] G. Sabbi, et al., "Design of HD2: a 15 T Nb_3Sn dipole with a 35 mm bore", IEEE Trans. Appl. Supercond., vol. 15, no. 2, pp. 1128-1131, (June 2005).

[3] P. Ferracin, et al.,"Mechanical design of HD2, a 15 T Nb_3Sn dipole magnet with a 35 mm bore", IEEE Trans. Appl. Supercond., vol. 16, no. 2, pp. 378-381, (June 2006).

[4] P. Ferracin, et al., "Development of the 15 T Nb_3Sn Dipole HD2", IEEE Trans. Appl. Supercond., vol. 18, no. 2, pp. 277-280, (June 2008).

[5] P. Ferracin, et al., "Assembly and Test of HD2, a 36 mm Bore High Field Nb_3Sn Dipole Magnet", IEEE Trans. Appl. Supercond., vol. 19, no. 3, pp. 1240-1243, (June 2009).

[6] S. Caspi, et al., "Towards integrated design and modeling of high field accelerator magnets", IEEE Trans. Appl. Supercond., vol. 16, no. 2, pp. 1298-1303, (June 2006).

[7] P. Ferracin, S. Caspi, and A.F. Lietzke, "Towards Computing Ratcheting and Training in Superconducting Magnets", IEEE Trans. Appl. Supercond., vol. 17, no. 2, pp. 2373-2376, (June 2007)

KEK EFFORT FOR HIGH FIELD MAGNETS

T. Nakamoto, KEK, Tsukuba, Japan.

Abstract

KEK has emphasized efforts to develop the RHQ-Nb_3Al superconductor and a sub-scale magnet reaching 13 T towards the HL-LHC upgrade in last years. In addition, relevant R&D regarding radiation resistance has been carried out. For higher field magnets beyond 15 T, HTS in combination with A15 superconductors should be one of baseline materials. However, all these superconductors are very sensitive to stress and strain and thorough understanding of behaviour is truly desired for realization of high field magnets. KEK has launched a new research subject on stress/strain sensitivity of HTS and A15 superconductors in collaboration with the neutron diffraction facility at J-PARC and High Field Laboratory in Tohoku University. Present activity for high field magnets at KEK is reported.

INTRODUCTION

Recently, future upgrade of the LHC has been lively discussed. The high luminosity LHC upgrade (HL-LHC), which would provide 5 times higher beam luminosity than the present LHC, has been discussed as the most possible upgrade plan in near future. Present beam insertion systems for ATLAS and CMS will be replaced by new superconducting magnets to attain smaller β* with a larger beam aperture. A15 type superconductors such as Nb_3Sn and Nb_3Al can generate higher field up to 15 T and are considered to be promising materials for the HL-LHC.

Beyond the HL-LHC, the high energy LHC (HE-LHC) might be realized in 2030 or later. In the HE-LHC, the beam energy is expected to be double at least and nominal field of new main dipole magnets in the LHC tunnel should reach 20 T or more. This means that utilization of HTS (high temperature superconductors) in combination with A15 type superconductors needs to be considered. However, it is very well known that these superconductors are brittle and superconducting performance such as critical current density J_c is significantly influenced by mechanical stress and strain. Comprehension of these effects is definitely necessary to realize high field superconducting magnet for future accelerator.

KEK has been engaged to develop the Nb_3Al superconductors and the high field magnet technology towards the future accelerator. Recently, we have also launched new research subject regarding the stress and strain sensitivity of the superconductors. In this paper, present R&D status and future plan at KEK towards the high field magnet are reported.

PRESENT R&D STATUS

Under the framework of the CERN-KEK collaboration, KEK has developed the Nb_3Al superconductor for the high field accelerator magnet application. This R&D work is complementary to other R&D efforts in CERN and US-LARP with the Nb_3Sn superconductors.

A tentative target application is set to the HL-LHC where the magnets below 15 T would be utilized. In parallel with the superconductor development, KEK has been developing a sub-scale magnet to demonstrate feasibility of Nb_3Al cable. KEK has been also performing R&D on the relevant magnet technologies such as insulations, radiation resistance study.

Nb3Al Superconductor Development

For the accelerator magnet application beyond 10 T, Nb_3Sn superconductor is in the most advanced state of development. However, J_c can be degraded by excessive stress and strain. In contrary, Nb_3Al has a much better stress and strain tolerance. For instance, the previous study demonstrated that an Nb_3Al strand in an epoxy-impregnated cable sustained under transversal stress beyond 200 MPa [1].

In order to utilize the better strain tolerance, studies on the development of Nb_3Al wires have been conducted in Japan for many years. Thanks to a Rapid Heating/Quenching and transformation (RHQ) process [2] developed by NIMS (National Institute for Materials Science), J_c has been significantly improved at high field region. However, the wire temperature instantaneously reaches around 2000 °C to form supersaturated solid solution of Nb(Al)ss in the RHQ process and an ordinary copper matrix cannot be utilized because it melts. Therefore, main development items of RHQ-Nb_3Al wires for accelerator application are not only to increase of J_c but also adoption of adequate matrix and stabilizer.

KEK and NIMS have been jointly developing RHQ-Nb_3Al wires for the accelerator application. Figure 1 shows a cross section of the recent RHQ-Nb_3Al wire and the specification is listed in Table 1.

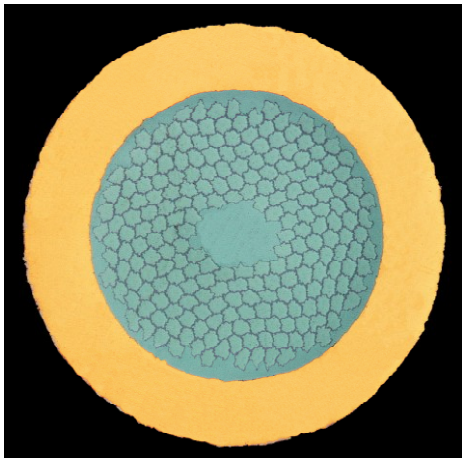

Figure 1: Cross section of the RHQ-Nb_3Al superconducting wire

Table 1: Specification of the RHQ-Nb_3Al Wires

Wire Diameter	1.0 mm
Non-Copper Diameter	0.7 – 0.73 mm
Area Reduction	~70 %
Filament Diameter	35 μm
Barrier Thickness	4 - 6 μm
Twist Pitch	45 mm
Piece Length	~ 1 km

Firstly, an ordinary Nb-matrix that has better mechanical affinity to other composite elements was incorporated. The RHQ-Nb_3Al wire with Nb-matrix showed the highest non-copper J_c of 1030 A/mm^2 at 15 T. Furthermore, wire breaking rate during cold drawing was rather small. However, it turned out that Nb-matrix wires exhibited large magnetic instability in a low-field region at 4.2 K where niobium is in the superconducting state. It was concluded that utilization of Nb-matrix was not appropriate for the accelerator application.

Accordingly, new Ta-matrix wires that are stable in a low field have been developed. Figure 2 shows magnetization curves of RHQ-Nb_3Al wires with Nb- and Ta-matrix. In comparison with Nb-matrix wire (F1), magnetization curves of Ta-matrix wires (K1 and K2) are very small and no flux jump can be seen. In terms of suppression of low field instability, adoption on Ta-matrix was very successful. Figure 3 shows non-copper Jc of Ta-matrix wires (K1-K4). Although each wire has design parameters in the cross section, behaviours of non-copper Jc are very similar. However, an average non-copper Jc at 15 T is still around 800 A/mm^2 and this value is about half of Nb_3Sn (OST-RRP).

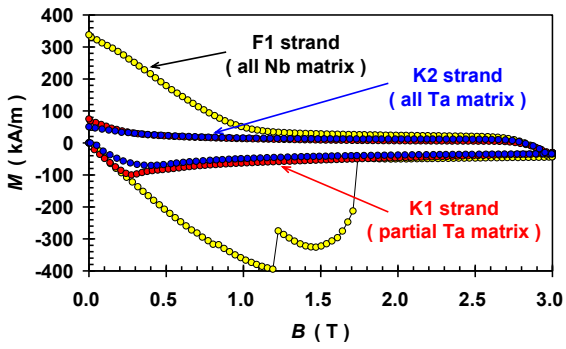

Figure 2: Magnetization curves of RHQ-Nb_3Al wires at 4.2 K. [3]

Regarding manufacturing of the Ta-matrix wires, we have suffered wire breakings during cold drawing so far because tantalum is rather stiff. Microscopic observation indicated that the breaking was initiated at very narrow tantalum matrix in the cross section. In order to reduce the breaking rate towards 10 km class long wire production, importance of quality improvement and control for tantalum sheets was recognized. Production trials of 100 m long wire using different tantalum ingredients were started in 2010. The study is still underway and the successful results would be adopted for the 1 km long wire production as a demonstration in 2011.

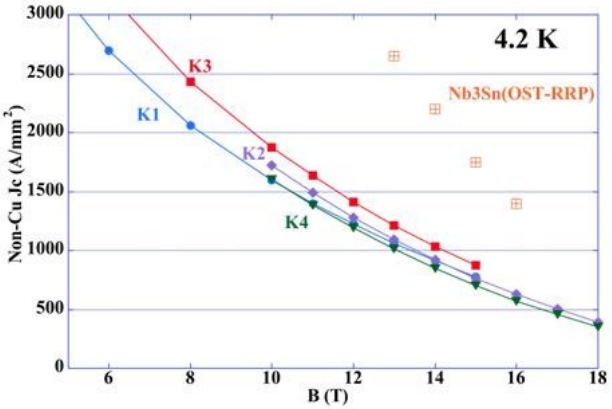

Figure 3: Non-copper J_c of RHQ-Nb_3Al wires with Ta-matrix. As a reference, non-copper J_c of Nb_3Sn-RRP is also plotted.

Nb_3Al Sub-Scale Magnet Development

In parallel with the superconductor development, KEK has made progress on the development of a 300 mm long Nb_3Al superconducting sub-scale magnet with a simple mechanical structure that is considered to be a fundamental R&D to demonstrate feasibility of high field magnets with Nb_3Al cable [4]. So far, four types of Nb_3Al Rutherford cables for the sub-scale magnet have been successfully fabricated in collaboration with Fermilab. The cable with 28 RHQ-Nb_3Al strands is 14 mm wide and 1.8 mm thick and a piece length is over 20 m.

Figure 4 shows a schematic drawing of the sub-scale magnet. The design concept is incorporated from the original development by LBNL with Nb_3Sn technology. The magnet consists of three Nb_3Al coils combined with two Nb_3Sn coils [5]. The magnet has the "common-coil" structure with a very narrow gap along the vertical median plane such that the peak field in the central Nb_3Al coil can be maximized to reach 13.2 T at 12 kA. Two additional Nb_3Sn sub-scale coils developed by LBNL with a higher current density contribute to boost up the peak field effectively. A rather thick aluminium shell is required to apply adequate pre-stress at magnet assembly and its large thermal shrinkage can increase the pre-stress even during cool-down.

Following two dummy coil fabrication with NbTi cables to evaluate the fabrication process including heat reaction in the vacuum furnace at 800 °C and the epoxy resin vacuum impregnation, the first real coil winding with Nb_3Al cable was carried out. Another two coils will be fabricated in 2011.

Relevant Magnet Technology R&D

In superconducting magnets for the HL-LHC with Nb_3Al superconductor, the coil insulation system plays very important role. The insulation system needs to fulfil the following specification: endurance at higher reaction

temperature than Nb_3Sn, mechanical reinforcement by resin impregnation under very severe radiation environment, and keeping engineering current density as high as possible.

Since heat reaction temperature of 800 °C for the Nb_3Al coil is higher than Nb_3Sn, an ordinary glass tape in the Nb_3Sn system are not applicable. Two types of alumina tape of 0.125 mm thick from different suppliers (CTD and NITIVY) have been used for the cable insulation. Recently, NITIVY has succeeded to manufacture thinner alumina tape of 0.08 mm thick aiming higher engineering current density. This insulation will be utilized for the coil winding in near future.

In terms of radiation resistance, an ordinary epoxy resin that is commonly used for the Nb_3Sn coil impregnation is only applicable up to several MGy. Cyanate ester is known to have much better radiation resistance than epoxy. However, higher curing temperature beyond 180 °C and extension of pot life with low viscosity are practical issues for the coil impregnation. KEK and other three institutes (JAEA, University of Hyogo and Mitsubushi Gas Chemical) have formed a collaboration framework and have newly developed the special cyanate ester base resin mixed with epoxy for the accelerator coil application: lower curing temperature at 150 °C and long pot life of 24 hours at 60 °C. Demonstration of the dummy coil impregnation with the cyanate ester base resin was successfully carried out and the picture of the impregnated coil is shown in Fig. 5.

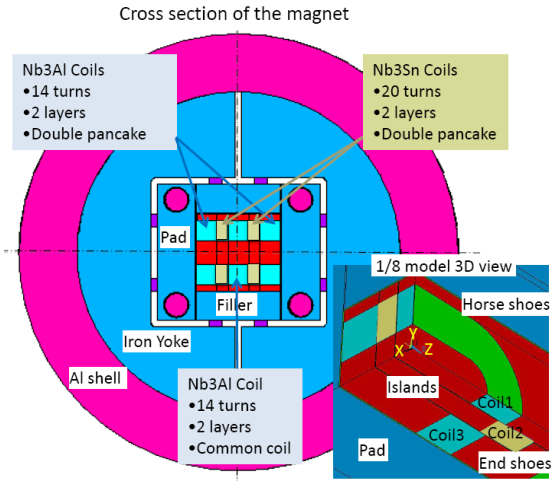

Figure 4: A schematic drawing of the Nb_3Al and Nb_3Sn hybrid sub-scale magnet.

Figure 5: Picture of a dummy sub-scale coil impregnated with the new cyanate ester base resin.

Evaluation of radiation resistance of magnet materials is crucial. We have carried out gamma ray irradiation tests on organic materials since 2003 at JAEA-Takasaki. The new cyanate ester resin is planned to be evaluated soon. In addition, a series of neutron irradiation tests at cryogenic temperature below 20 K have been launched in 2010 at KUR (Kyoto University Research Reactor). Main scope is to survey electric resistivity increase of stabilizers due to neutron irradiation: resistivity of pure metal is known to be degraded even at fast neutron fluence of 10^{21} n/m^2 or less, but the data for industrial stabilizers such as aluminium and copper with RRR up to several 100 does not exist. The quench protection scheme of the magnet system is concerned to be compromised when the resistivity of the stabilizer unexpectedly increases due to the neutron irradiation during the beam operation. The first irradiation test with aluminium samples from the superconducting cable for solenoid magnets have been made and rapid increase of resistivity has been observed even at neutron fluence of 10^{20} n/m^2. The next irradiation test for copper stabilizers for the accelerator magnets is planned in 2011.

NEW RESEARCH ON STRESS/STRAIN DEPENDENCE OF SUPERCONDCUTORS

For high field accelerator magnets beyond 15 T in future, utilization of HTS and A15 type superconductors is considered as baseline materials in the meantime. As mentioned above, however, it should be reminded that their performance like J_c depends on stress and strain of superconductors. The engineering design for such high field magnets must need thorough understanding of stress/strain dependence of the superconductor performance.

Since industrial superconducting wires/tapes are composites comprised of superconductors surrounded by other materials and stabilizers with different thermal contractions, residual strains can be naturally induced by a temperature variation of around 1000 K from the heat reaction temperature to the cold for the operation. In addition, since the shape of the Rutherford-type cable is complicated and the impregnated coil windings for the accelerator magnets are applied the complicated stress in various directions during the assembly, the cool-down and the excitation, it is very difficult to predict the actual strain of the superconductor. To design and develop the high field superconducting accelerator magnets successfully, it is very important to understand the strain behaviors of the superconductor by neutron diffraction measurements. The neutron diffraction measurement facility using pulsed neutrons at the BL-19 (TAKUMI) of J-PARC MLF, shown in Fig. 6, is the most appropriate tool to experimentally study the strain behaviors of the HTS and the A15 superconductor in the accelerator coil. The following is the main reasons;

Figure 6: Neutron diffraction measurement facility at the BL-19 (TAKUMI) of J-PARC MLF.

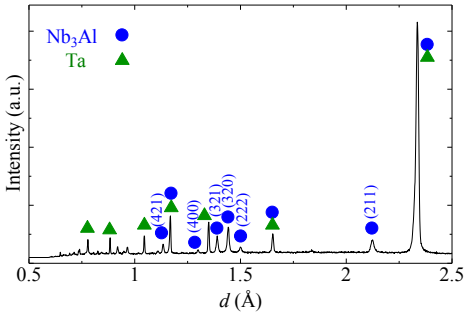

Figure 7: Diffraction peaks of RHQ-Nb_3Al with Ta-matrix measured at TAKUMI, J-PARC MLF.

Figure 8: Cryogenic load frame up to 50 kN from 6 K to 300 K.

- Three-dimensional strains of the superconducting wire can be simultaneously determined by using a pair of 90° detector banks.
- Strains of each ingredient can be determined by using several diffraction peaks measured simultaneously.
- Even small strains can be measured with its high resolution.
- Thanks to high penetration depth of neutrons into the sample, strain distribution inside the massive coil sample can be obtained.

In collaboration with NIMS, JAEA and Tohoku University, a series of neutron diffraction measurement for the stress/strain study has been started with a long-term viewpoint. Preliminary measurement of the RHQ-Nb_3Al wires with different matrixes at room temperature was made in 2010. Figure 7 shows diffraction peaks of the Ta-matrix wire as a typical case. It was observed that residual strains of Nb_3Al crystal were varied according to matrix materials.

For the neutron diffraction measurement at cryogenic temperature under loading, KEK in collaboration with JAEA has newly developed a cryogenic load frame that can apply the tensile load up to 50 kN in the temperature range from 6 K to 300 K, shown in Fig. 8. This cryogenic load frame can provide different conditions to the samples with changing the load and the temperature. Not only sole superconducting wires or tapes, but also bulk samples like epoxy-impregnated Rutherford cable stacks simulating the coil can be measured with this cryogenic load frame.

In parallel, experimental study on J_c behaviors under different stress/strain has been also started at High Field Laboratory in Tohoku University. Both experimental results of neutron diffraction measurement and Jc measurement under stress/strain will be inseparably analyzed. Knowledge and understanding from this study will improve the mechanical design of high field superconducting accelerator magnets and help to precisely predict its performance limit.

SUMMARY

KEK has promoted the R&D towards high field accelerator magnet. Development of RHQ-Nb_3Al superconductors aiming to be applied for the HL-LHC has been emphasized. The latest Ta-matrix wire showed better low field instability even though non-copper Jc is smaller than that of Nb_3Sn-RRP. Magnet technology for RHQ-Nb_3Al cable under very severe radiation environment is underway. Especially, development of the cyanate ester resin for the accelerator application is highlighted. For the long-term R&D, experimental study on stress/strain sensitivity has been launched.

REFERENCES

[1] A. Kikuchi et al., IEEE Trans. Appl. Supercond. 18 (2008) 1026.
[2] T. Takeuchi, Cryogenics 48 (2008) 371.
[3] A. Kikuchi et al., IEEE Trans. Appl. Supercond. 20 (2010) 1428.
[4] Q. Xu et al., IEEE Trans. Appl. Supercond. 20 (2010) 176.
[5] R. R. Hafalia et al., IEEE Trans. Appl. Supercond. 13 (2003) 1258.

EUCARD MAGNET DEVELOPMENT

Gijs de Rijk, CERN, Geneva, Switzerland.

Abstract

The FP7-EuCARD work package 7 (WP7), "HFM: Superconducting High Field Magnets for higher luminosities and energies" is a collaboration between 12 European institutes and firms with the objective of developing high field magnet technology. WP7 foresees to construct a 13 T dipole with a 100 mm aperture, a $\Delta B = 6$ T high temperature superconductor (HTS) dipole insert, a superconducting HTS link and a superconducting helical undulator.

EUCARD WP7 HIGH FIELD MAGNETS

The High Field Magnet work package is a collaboration between 10 institutes and 2 firms:

- CEA-Irfu Saclay, France (CEA)
- CERN, Genève, Switzerland (CERN)
- CNRS-Grenoble, France (CNRS)
- COLUMBUS, Genova, Italy (COLUMBUS)
- BHTS-Bruker, Hanau, Germany (BHTS)
- Karlsruhe Institute of Technology, Germany (KIT)
- INFN-LASA, Milano, Italy (INFN)
- Wroclaw Technical University, Poland (PWR)
- Southampton University, UK (SOTON)
- STFC-Daresbury, UK (STFC)
- Tampere Technical University, Finland (TUT)
- Université de Genève, Switzerland (UNIGE)

Besides a management task, the work package consists of 5 R&D tasks :

2. Support studies
3. High field model: 13 T, 100 mm bore (Nb_3Sn)
4. Very high field dipole insert (in HTS, up to $\Delta B = 6$ T)
5. High Tc superconducting link (powering links for the LHC)
6. Short period helical superconducting undulator (ILC e^+ source)

The duration is from April 2009 until April 2013. The total budget is 6.4 M€ from which 2.0 M€ is the EC contribution.

HIGH FIELD MODEL

Several of the technologies used for Nb_3Sn magnets (superconducting cable, insulation, coil design, support structures) were partly developed during the FP6-CARE-NED project. They are to be brought together and tested in a model dipole magnet. The aim of task 3 "High field model" is to design, build and test a 1.5 m long, 100 mm aperture dipole model with a design field of 13 T using Nb_3Sn high current Rutherford cables.

The key component in a superconducting magnet is the conductor. In order to develop high field magnets it is essential to have a facility to tests the cables (not 'just' the strands) up to the maximum field and therefore this model will afterwards be used to upgrade the superconducting cable test facility FRESCA at CERN from 10 T to 13 T.

In Fig. 1 an overview is given of existing dipole magnets. In this figure, both magnets employed in accelerators and R&D models built to prospect high fields can be found. All the existing accelerators, which operate below 10 T, employ cosΘ geometries with Nb-Ti conductors. Above 10 T both cosΘ (D20 and MSUT) and block coil (HD1 and HD2) geometries were employed on models using Nb_3Sn conductors. The proposed magnet (EuCARD-Fresca2) is at the top range of both field and aperture of all preceding projects. The design and construction of such a 13 T magnet with a 100 mm bore is thus an important challenge. To embark on such a project it is important to learn from existing HFM projects.

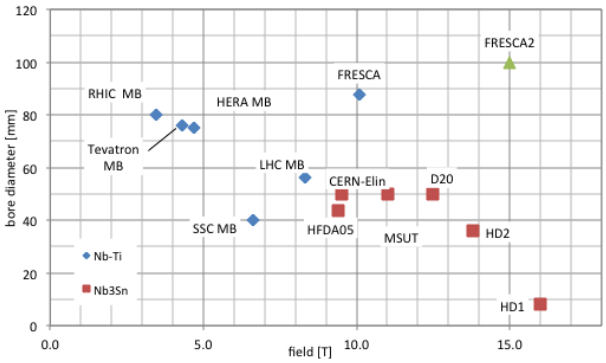

Figure 1: Field and bore diameter for a selection of superconducting magnets. For the magnets used in accelerators the fields are the real operational values. For model and prototype magnets these are the quench plateau values obtained during the tests.

During the first year of the project a study was made to compare potential coil geometries and a literature study was done on existing Nb_3Sn magnets. In June 2010 the collaboration selected the block coil geometry for the EuCARD-Fresca2 magnet. This choice was backed by winding tests on the feasibility of the "flared-ends" which are needed for this type of coils (Fig. 2).

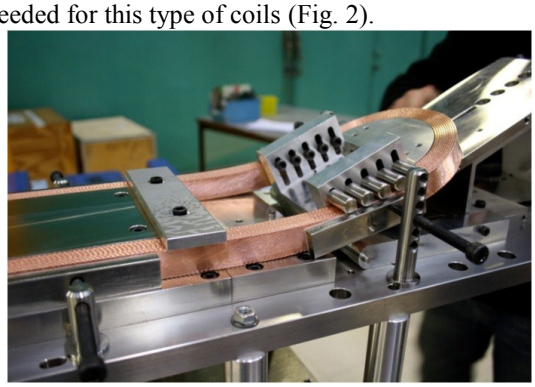

Figure 2: Winding tests at CEA for the block coil with flared ends

In Fig. 3 the choice and further development of the coil geometries in the design phase of this project can be seen.

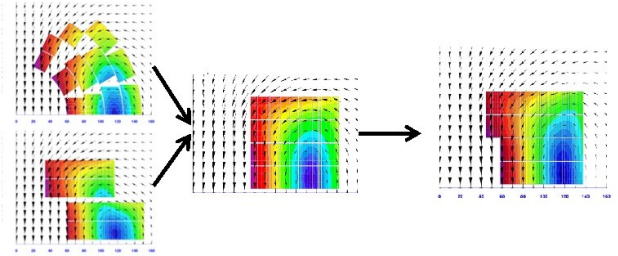

Figure 3: Development of the coil geometries during the design phase (one quarter shown).

For this magnet the conductor was selected taking into account previous developments in the CARE-NED program [1],[2] and by the LARP collaboration [3]. The cable has 40 strands of 1 mm diameter. Procurement of the strand has started and first prototype lengths have been delivered for tests.

The present layout consists of a coil with 2 double pancakes, the one close to the mid-plane has 36 + 36 turns and the outer one has 42 + 42 turns (see Fig 3 right hand picture). The picture of the magnet can be found in Fig. 4. The structure employs the shell-bladder and key system previously developed by LBNL [4]. At 13 T the magnet will operate at 82.5% of the load line at 4.2 K at a current of 10.6 kA given a degraded conductor performance of 1250 A/mm^2 at 15 T (this is 76.1% of the load line at 1.9 K). At this field the horizontal EM force is 16 MN/m and the stored energy is 3.6 MJ/m.

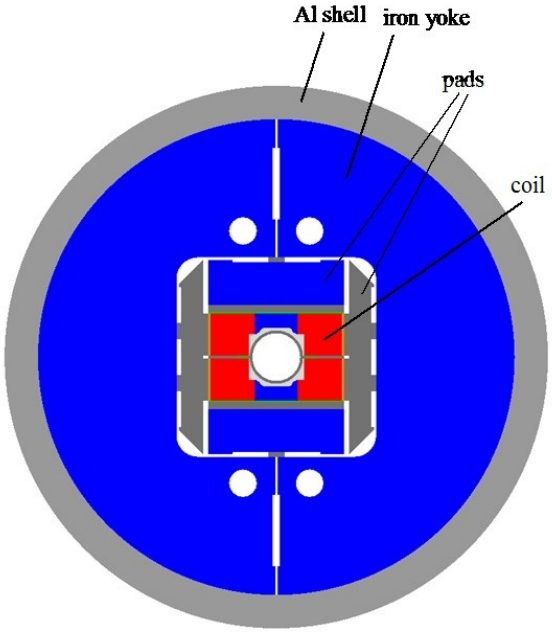

Figure 4: Schematic layout of the magnet

The main issues to be addressed for the 13 T dipole are:

- the conductor performance, quality and availability,
- the maximum field on coil,
- forces and stresses on the coil,
- the stored energy in the magnet,
- quench protection,
- the "makebility" of the coil and structure.

The structure applies nearly half of the pre-stress on the coil due to the differential shrinking between the shell and the yoke, the other half is applied at room temperature by inserting keys. The stress in the coil during the magnet lifecycle in one of the preliminary mechanical studies can be found in Fig. 5.

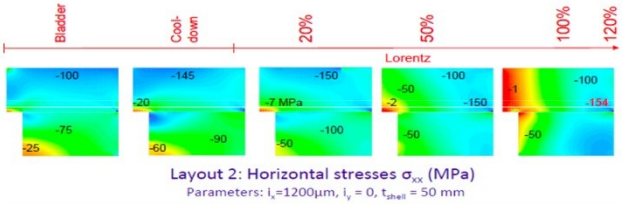

Figure 5: Coil stress during the magnet life-cycle

The flared ends of the coil imply that the cable is to be bend 'the hard way'; due to the natural elasticity of the cable the chosen bending radius of 700 mm is easy to execute. For comparison: in the HD2 magnet from LBNL the hard-way bending radius in the flared ends is 350 mm. In Fig. 6 a CAD picture of the coils in one pole can be found. In Fig. 7 a pre-design image of the ends of the magnet can be seen. Special attention will have to be paid to the design of the reaction tooling due to the combination of the thermal and reaction expansion of the conductor combined with the flared ends of the coils.

Figure 6: The coil of one pole, CAD image.

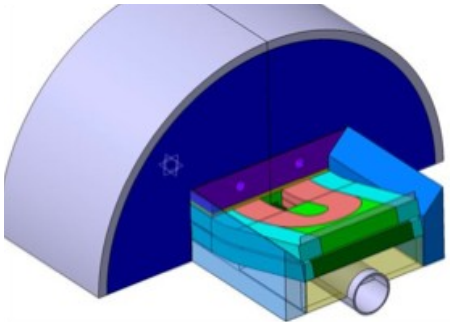

Figure 7: Pre-design image from the magnet ends.

The detailed design of the magnet was done in 2010 and a design review will be held on 20-21 January. The structure should be completed by the end of April 2011 and the mechanical behaviour in liquid nitrogen with dummy coils will be tested in the May-June 2011.

Component and tooling design will start end of 2010 and should be completed by April 2011. The critical path of the project is the conductor deliveries that are planned at regular intervals up to November 2011. The first double pancake coil with superconductor cable is planned to be ready by March 2012. Assembly of the magnet with a complete coils set will be started by end February 2013 followed by the magnet test in April 2013.

VERY HIGH FIELD DIPOLE INSERT

Recent progress on High Temperature Superconductors like YBCO and BSCCO-2212 has shown good performance on the intrinsic current transport properties (Je > 400 A/mm^2 at 4 K, B < 25 T). This should open the road to higher magnetic fields in the B = 20 T range interesting for HE-LHC. The aim this task is to design and fabricate an HTS very high field dipole insert (6-7 T), which can be installed inside the 13 T Nb_3Sn dipole of task 3 that will serve the role of the outer layer magnet. This is a very first attempt to approach 20 T in a dipole geometry. The development takes place in three steps. The first studies deal with the specification of several HTS conductors. This is to be completed by modelling work focused on stability and quench. The quench of HTS coils with very often occurring degradation is an identified issue. Due to the difficulty of making in one go a dipole insert coil of HTS conductor, several HTS solenoid insert coils will be made and tested in existing high field solenoid magnets. The experience that will be gained will be used to construct a dipole insert coil.

The main issues to be addressed for the dipole insert are:

- Jc of the HTS conductor: to reach 6 T we need an averaged Jc of ~ 300 A/mm^2;
- HTS coil fabrication;
- Electromagnetic forces in the range of 1000 t/m;
- Fixing into dipole;
- Coupling between dipole and insert, quenching either or both magnets.

The two candidate conductor types pose different strong and weak points:

1. BSCCO-2212 round strand:
- Good: cabling possibilities to reach high total currents.
- Poor: Critical heat treatment and weak mechanical performance.
2. YBCO tape:
- Good: Performance in Jc and stress (Fig. 8).
- Poor: cabling possibilities and difficult winding of coil ends.

Recent quench studies indicate that a quench of the 13 T magnet will quench the whole insert and thus a protection mechanism is inherently there for this case. Further quench studies are needed to cover all possible cases.

A first small solenoid made from YBCO has highlighted the issues to be solved: splice connections between the tapes need to be further developed and the fabrication process has to be optimized so as to avoid conductor degradation.

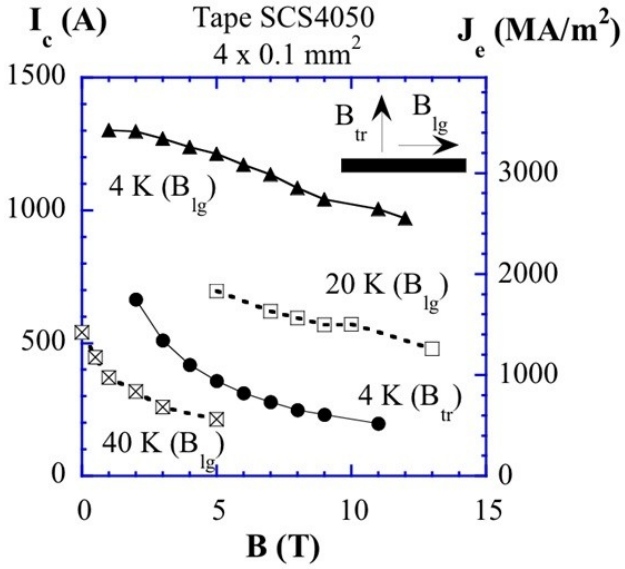

Figure 8: Measured critical current performance for a YBCO tape conductor sample tested in 2010

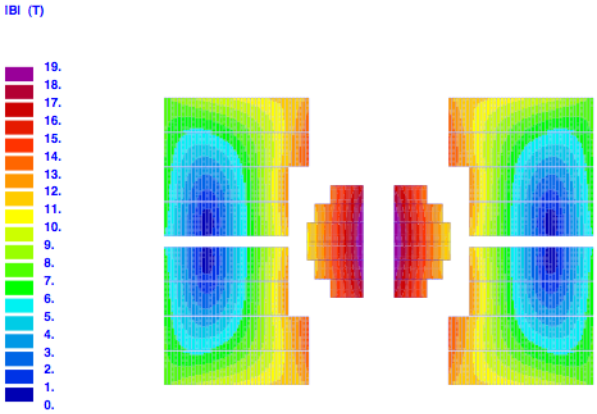

Figure 9: Field in the coils of the combined HTS insert and Nb_3Sn magnet

For the dipole insert a design was made using 12 mm wide YBCO coated conductor tape in a 'paired cable' geometry (see Fig. 9). The internal aperture is 20 mm in diameter. The current in a 12 mm tape is 610 A. The HTS dipole is located inside a 4 mm thick steel tube to contain the Lorentz forces (14 MN/m -16 MN/m) (in B=13 T from the outer dipole).

HIGH TC SUPERCONDUCTING LINK

The interest of buses linking superconducting magnets made of HTS material was recognized already before the LHC startup. In one of the cleaning insertions this will be needed to replace a Nb-Ti superconducting link which will be at a thermal limit due radiation heating. Recently an additional problem has been identified with the radiation sensitivity of electronics, which renders the power convertors vulnerable. For running at high intensity and luminosity these problems are also felt in

caverns close to the beam. To avoid the limitations imposed by these effects power convertors for the low beta insertion will have to be relocated in caverns far from the main tunnel or on the surface (see Fig. 10). For these type of solutions superconducting HTS links are needed to make efficient connections to the superconducting magnets using a minimum of space. The use of HTS enables operation at higher temperatures and offers a convenient gain in temperature margin during operation. In cases where space is limited and the radiation environment is harsh, it also provides more flexibility in the location of the cryostats supporting the current leads. HTS links of the type required for the accelerator technology did not exist, and significant work is being done to develop a long-length multi-conductor operating in helium gas at about 20 K.

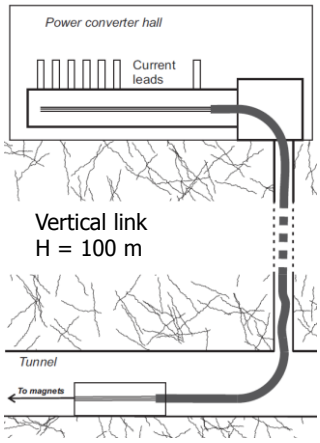

Figure 10: Schematic layout option at the LHC with the power convertors at the surface

Considerable R&D is at present being done on HTS cables for electrical utilities, and it might be a consideration that one could directly apply these technologies. However, at present this work is focused on using single or 3-phase AC conductors with high voltage insulation and liquid nitrogen cooling, and it should be noted that this is still development work yet to be concluded. Particle accelerators require high quasi- DC current carrying links with many cables (up to about 50) in parallel and cooled with liquid or gaseous helium. In the LHC there are over 50000 connecting cables with a total length of 1360 km. Thus the need specific to accelerator applications, is for a new type of link with multiple circuits, electrically isolated at around 1 kV -2 kV, carrying quasi-DC currents. The design study has to cover the options with YBCO, BSCCO and MgB_2 at a temperature of 20 K as well as the electrical connections between HTS and LTS.

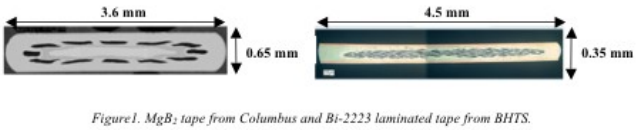

Figure1. MgB_2 tape from Columbus and Bi-2223 laminated tape from BHTS.

Figure 11: Two tape conductor candidates for a SC link

The task is studying the various conductors available on the market to find suitable candidates (Fig. 11) and lengths of up to 1 km of several tapes have been procured for this. Prototype cables are being tested at several partner of the collaboration. Studies and tests of the electrical joints between tapes (splices) are being done.

For the LHC applications several link types are being designed and one design case can be seen in Fig. 12. The task will conclude with the construction and test at CERN of prototype link segments.

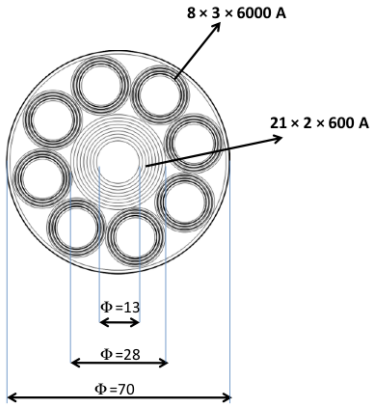

Figure 12: Example of a link layout with multiple conductors in a concentric geometry

SHORT PERIOD HELICAL SUPERCONDUCTING UNDULATOR

The aim is to increase the achievable magnetic field level in short period undulator magnets through the use of advanced materials (Nb_3Sn conductors) and innovative designs (helical coils). For example, single pass free electron lasers (e.g. X-FEL, FERMI@ELETTRA) could cover a wider wavelength range through field enhancement, or alternatively, operate at significantly lower electron energy. Additionally, short period undulator magnets could be used in the production of positrons for any future lepton collider and increased magnetic field levels will increase the positron yield and also allow for savings.

Previously an Nb-Ti helical undulator achieved an on-axis field of 0.86 T with a peak coil field of 2.74 T at 4.2 K. The aim is to reach B = 1.5 T on-axis with a peak field on the coil of 4.4 T and a period of 11.5 mm on a winding bore of 6.35 mm. Nb_3Sn will be tried to get the higher current densities at the 4 T - 5 T range combined with temperature margins of several Kelvin needed in the synchrotron light environments in the accelerator.

Known challenges are a sufficiently thin Nb_3Sn insulation system compatible with the heat treatment, the hoop stress in the wire and a controlled winding system for single (insulated) wires in a helical groove. First winding tests with a 0.5 mm thick wire (0.65 mm with insulation) have given encouraging results (Fig. 13). The task will design, construct and test a short (500 mm) undulator model and compare the results with the NB-Ti model previously tested.

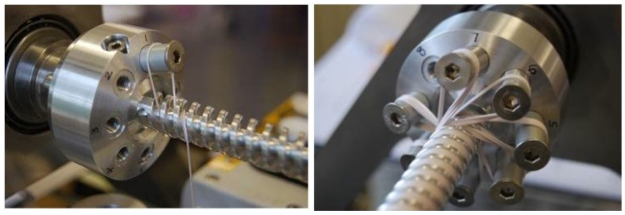

Figure 13: Winding trails for the helical undulator

SUPPORT STUDIES

The aim of the support studies is to study radiation effects on and thermal behaviour of Nb3Sn magnets to prepare for accelerator application of these magnets. For the EuCARD-Fresca2 magnet of task2 solutions for the insulation and the thermal design are to be proposed possibly compatible with accelerator applications.

Magnets in accelerators like the upgraded LHC and are subjected to very high radiation doses. In the low beta insertion quadrupole the integrated peak dose on the coil can attain 50 MGy over the lifetime of the HL-LHC. The electrical insulation employed on the coils need to be resistant to this radiation. A certification program for the radiation resistance is needed in parallel to the modelling efforts for such magnets. The same radiation is also depositing heat in the coils. The heat removal from the coils needs to be modelled. These models have to be supported with measurements. A thermal design of the dipole model coil can then be made.

Four potential impregnation materials will be tested (RAL mix 71, Epoxy TGPAP-DDS(2002), LARP CTD101K with filler ceramic and 3 Cyanite Ester mixes) to assess their suitability for high radiation environments. For this mechanical, electrical and thermal conductivity measurements will be done on samples irradiated with and electron beam up to 50 MGy. The irradiation will be done at IJP Swierk (Po) in 2011.

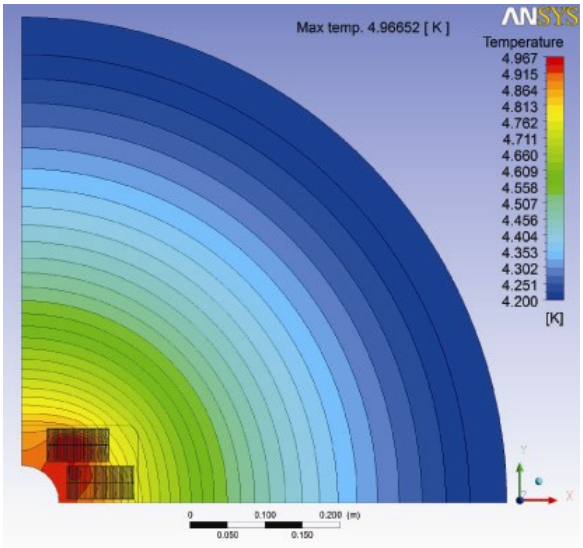

Figure 14: Calculated temperature distribution in the magnet at a total heat load of 0.167 W/m during ramping (start temperature 4.2 K)

Thermal models of Nb_3Sn magnets are being used to study cool-down scenarios and steady state heat load (at 4.2 K and 1.9 K) on the coils. In Fig 14 a thermal map from a preliminary steady state heat load study can be found.

FUTURE R&D

At present ESGARD has launched preparations for a successor project for EuCARD (EuCARD2), which is to start by the beginning of 2012. Four institutes (CERN, CEA, LBNL and KEK) envisage taking the lead in starting a larger collaboration to develop high field magnets for HE-LHC. Following the development of the 13 T wide aperture magnet in EuCARD and the HTS insert and under the condition that these developments are successful, the logical successor project is to prepare for a high field magnet for a HE-LHC type collider application.

The project could consist of the following R&D items:

1) Make a design study for a 20 T magnet for HE-LHC.

2) Construct a technology demonstrator model dipole magnet in the 15 T - 18 T range.

3) Conductor development for the 20 T field range.

For the LHC it took 22 years from the start of the magnet development to the switch-on of the machine. One has to start now with the development of 20 T magnets in order to be ready for HE-LHC in the 20+ year time scale. Experience from the LHC and presently from LARP, with the development of the low beta insertion quadrupoles for HL-LHC, indicates that this has to be done in a large international collaboration.

ACKNOWLEDGMENT

I would like to thank the colleagues of the FP7-EuCARD-HFM collaboration for their contributions to this paper.

REFERENCES

[1] T. Boutboul, L. Oberli, A. den Ouden, D. Pedrini, B. Seeber, G. Volpini, “Heat Treatment Optimization Studies on PIT Nb3Sn Strand for the NED Project”, IEEE Trans. Appl. Supercond. 19 (2009) 2564-2567.

[2] T. Boutboul, A. Devred, P. Fabbricatore, M. Greco, D. Leroy, L. Oberli, A. den Ouden, D. Pedrini, G. Volpini, “Nb3Sn conductor development and characterization for NED”, J. Phys.: Conf. Ser. 97 (2008).

[3] http://www.uslarp.org/

[4] P. Ferracin, B. Bingham, S. Caspi, D.W. Cheng, D.R. Dietderich, H. Felice, A.R. Hafalia, C.R. Hannaford, J. Joseph, A.F. Lietzke, J. Lizarazo, G. Sabbi, and X. Wang, “Recent test results of the high field Nb3Sn dipole magnet HD2”, IEEE Trans. Appl. Supercond. 20 (2010) 292.

STATUS OF Nb_3Sn ACCELERATOR MAGNET R&D AT FERMILAB*

A.V. Zlobin†, FERMILAB, Batavia, IL 60510, U.S.A.

Abstract

New accelerator magnet technology based on Nb_3Sn superconductor is being developed at Fermilab since late 90's. Six short dipole models, seven short quadrupole models and numerous individual dipole and quadrupole coils have been built and tested, demonstrating magnet performance parameters and their reproducibility. The technology scale up program has built and tested several dipole and quadrupole coils up to 4-m long. The results of this work are summarized in the paper.

INTRODUCTION

Dipole magnets for the LHC energy upgrade scenario with operating field of ~20 T would require using high-field high-temperature superconductors such as BSCCO or YBCO, which have highest upper critical magnetic field B_{c2}. However, due to the substantially higher cost and lower critical current density in magnetic fields below 15 T, a hybrid approach with Nb_3Sn superconductor in fields below 15 T is a quite attractive option even though the Nb_3Sn and HTS materials require different coil fabrication techniques.

During the past decade, Fermilab has been developing new Nb_3Sn accelerator magnet technologies in the framework of the High Field Magnet (HFM) program. Nb_3Sn accelerator magnets can provide operating fields up to 15 T and significantly increase the coil temperature margin. Such magnets are being developed for the LHC IR upgrade, Muon Collider Storage Ring, and present and future high-energy hadron colliders. The program began in 1998 with the development of the small-aperture arc dipoles for the Very Large Hadron Collider (VLHC) [1]. Since 2003, the emphasis of the program was shifted toward large-aperture Nb_3Sn quadrupoles for an LHC IR upgrade [2].

The High Field Magnet R&D program started with the development of basic technologies and studies of main magnet parameters (maximum field, quench performance, field quality) and their reproducibility using a series of short models, and then proceeded with the demonstration of technology scale up using relatively long coils. Along the way, the HFM program has made several breakthroughs in Nb_3Sn accelerator magnet technologies. The most important of them include the development and demonstration of high-performance Nb_3Sn strands and cables, reliable and reproducible coil fabrication technology, and a variety of accelerator quality mechanical structures and coil pre-load techniques. The status and the main results of the Nb_3Sn accelerator magnet R&D at Fermilab are summarized in this paper.

* Work supported by Fermi Research Alliance, LLC, under contract No. DE-AC02-07CH11359 with the U.S. Department of Energy.

†zlobin@fnal.gov

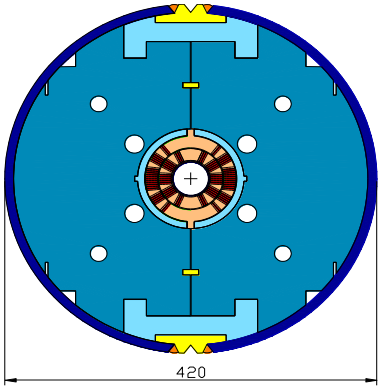

Figure 1: HFDA dipole cross-section.

MAGNET DESIGNS AND PARAMETERS

Dipole and quadrupole models

The design and main parameters of Fermilab's dipole models of the HFDA series are described in [3]. These magnets have been developed as baseline dipoles for the VLHC which was extensively studied in the U.S. around 2000 [4]. The cross-section of the dipole cold mass is shown in Fig. 1. This magnet was designed to provide a nominal field of 10-11 T (B_{max}~12 T) in a 43.5 mm aperture at an operating temperature of 4.5 K. The main R&D goal of this model magnet series was to develop robust Nb_3Sn coil technology and an inexpensive mechanical structure suitable for industrialization. This goal dictated the philosophy of magnet design and technology. The magnet design is based on a two-layer shell-type coil and a cold iron yoke. To reduce the magnet cost, a compact collarless mechanical structure with Al clamps, a 400 mm iron yoke and a 10 mm stainless steel skin was used.

The design and parameters of Fermilab's quadrupole models of TQC series are described in [5]. These magnets were proposed and used as a technological model of a new generation of large-aperture IR quadrupoles being developed by the US-LARP collaboration [6] for the planned LHC luminosity upgrade. The TQC cross-section is shown in Fig. 2.

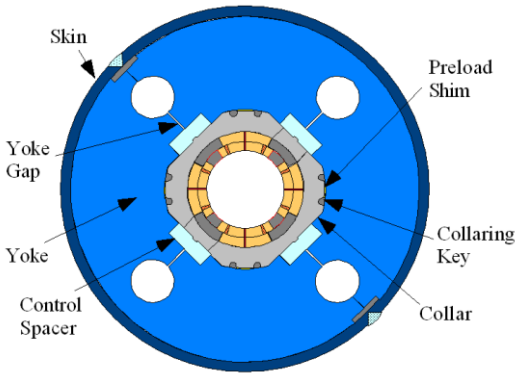

Figure 2: TQC quadrupole cross-section.

This model magnet series was designed to provide the same nominal field gradient of 200 T/m (G_{max}~250 T/m) in 90-mm aperture at the same operating temperature of 1.9 K as the present 70-mm NbTi IR quadrupoles (MQXB). The quadrupole design consists of a two-layer shell-type coil and a cold iron yoke. The design and technology of quadrupole coils used in TQC models largely rested on the results of the dipole program described above. The TQC quadrupole mechanical structure is based on the slightly modified mechanical structure of the present LHC IR quadrupoles (MQXB). It includes a 25-mm-thick round stainless-steel collar, a 400 mm iron yoke and a 12 mm thick stainless steel skin.

The dipole and quadrupole coils were wound using keystoned Nb_3Sn Rutherford cables with 27 (28 in first dipole models) strands 0.7 mm (TQC) and 1.0 mm (HFDA) in diameter. The cable used in the first two dipole models HFDA02-03 had 0.025 mm thick stainless steel core to control the strand crossover resistance while the cables used in HFDA04-07 dipoles and in all the TQC quadrupole models were without a core. The dipole and quadrupole cable parameters are summarized in Table 1.

Table 1: Cable parameters.

Parameter	Unit	HFDA	TQC
Number of strands		27(28)	27
Strand diameter	mm	1.00	0.70
Cable mean thickness	mm	1.80	1.26
Cable width	mm	14.24	10.05
Cable keystone angle	deg	0.9	1.0
Cable insulation thickness	mm	0.25	0.125

The design quench parameters at the corresponding nominal operating temperatures for the dipoles and quadrupoles, calculated for the strand critical current density J_c(12 T, 4.2 K)=2 kA/mm^2, are summarized in Table 2. Both magnets are designed for practically the same level of maximum field in the coil B_{max}~12 T at the corresponding nominal operating temperatures.

Table 2: Magnet quench parameters at 4.5 and 1.9 K.

Parameter	Operating temperature	HFDA	TQC
B_{max}, T		12.05	
Quench current, kA	4.5 K	21.66	
Coil peak field, T		12.6	
G_{max},, T/m			233
Quench current, kA	1.9 K		14.07
Coil peak field, T			12.1

Nb_3Sn strands

Three types of Nb_3Sn strand were used in the dipole and quadrupole model magnets.

The strand for the first three dipole models, HFDA02-04, was produced using the Modified Jelly Roll (MJR) process and had 54 Nb_3Sn sub-elements in cross-section. The MJR strand had a critical current density J_c(12 T, 4.2 K)~2.0-2.2 kA/mm^2 and a quite large filament size d_{eff}~100 μm in 1-mm strand [7].

The strand for the last three dipole models, HFDA05-07, was made using the Powder-in-Tube (PIT) process and had 192 Nb_3Sn filaments. The PIT strand had lower J_c(12 T, 4.2 K)~1.6-1.8 kA/mm^2 and smaller d_{eff}~50 μm at 1-mm strand diameter [7].

Then a new improved strand based on the Restack Rod Process (RRP) was developed [8]. This strand was initially produced with a 54/61 cross-section design and a high J_c(12 T, 4.2 K) up to 3 kA/mm^2. However, the quadrupole models TQC01 (a and b) and TQC02b were made using the MJR strand with lower J_c(12 T, 4.2 K)~2 kA/mm^2 and 54 sub-elements (d_{eff}~70 μm in 0.7-mm strand). The second generation of quadrupole models TQC02a, TQC02E (a and b) used the RRP strand with J_c(12 T, 4.2 K)~2.8 kA/mm^2 and 54 sub-elements.

Taking into account the importance of the strand and cable designs and parameters for accelerator magnet performance, an extensive Nb_3Sn strand and cable R&D study was conducted by Fermilab in parallel with the model magnet R&D program focusing on the improvement of strand stability, reduction of strand magnetization, minimization of strand degradation during cabling, etc. RRP strands with various cross-section designs were produced and studied in collaboration with OST [9]. Based on the results of these studies, the RRP-108/127 strand with increased sub-element spacing and reduced sub-element size was developed as a baseline conductor for the Nb_3Sn accelerator magnet R&D. This strand was used in several dipole and quadrupole coils.

The cross-sections of some Nb_3Sn strands used in the dipole and quadrupole models are shown in Fig. 3.

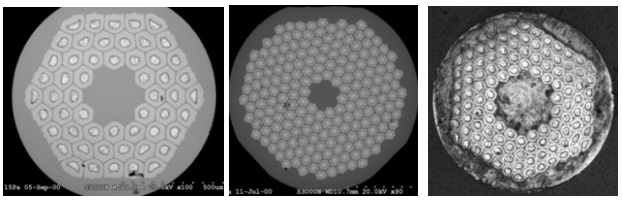

Figure 3: Nb_3Sn strand cross-sections: a) MJR-54/61, b) PIT-192 and c) RRP-108/127.

Cable insulation

Several types of cable insulation based on ceramic, S2-glass and E-glass fiber were studied [10] and used in the Nb_3Sn dipoles and quadrupoles. The insulation types, dimensions and their costs are shown in Fig. 4.

The most important differences between these materials include mechanical and electrical strength after reaction, thicknesses, and cost. Ceramic insulation has demonstrated the best electrical strength and mechanical properties during coil processing. However, its thickness is relatively large and it is much more expensive than either the S2-glass or E-glass systems. The E-glass tape is the least expensive and most readily available in a variety of thicknesses, and based on tests is acceptable for use in Nb_3Sn magnets (at least during an R&D phase).

All the dipole models were made using cables insulated with two-layers of the ceramic tape. The quadrupole

models were made using cables insulated with the S2-glass sleeve. Some dipole and quadrupole coils were made using S2- or E-glass tapes or their combinations.

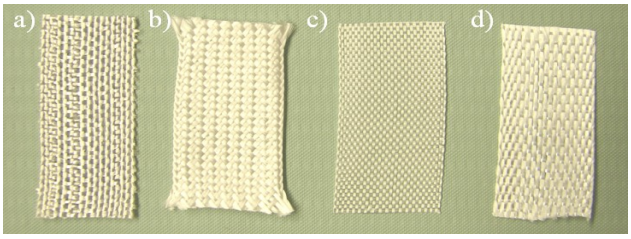

Figure 4: Insulation types and cost: a) 0.125 × 13 mm^2 ceramic tape (~20 $/m), b) 0.125 mm S2-glass sleeve (~10 $/m), c) 0.075 × 13 mm^2 E-glass tape (~0.2 $/m), and d) 0.125 × 13 mm^2 S2/E-glass combination tape (~6 $/m).

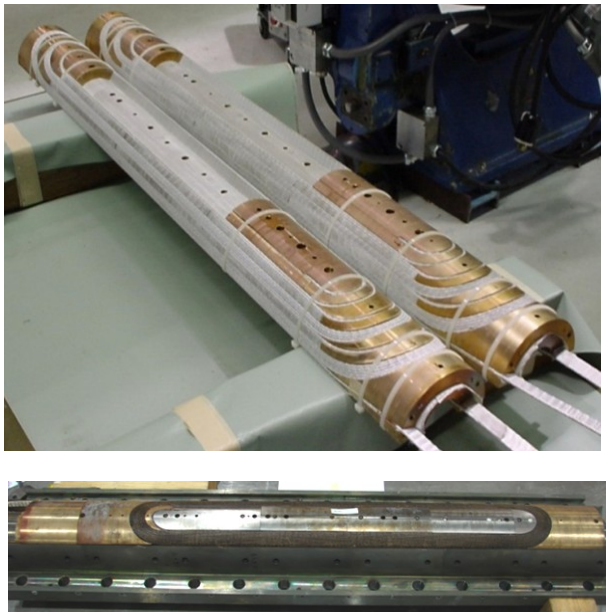

Figure 5: Nb_3Sn dipole coils impregnated with ceramic binder after winding and curing (top) and a quadrupole coil cured with ceramic binder after reaction (bottom).

Coil technology

Coils used in accelerator magnets have relatively small bending radii and thus favor the Wind&React method. The superconducting Nb_3Sn phase in this case is formed after coil winding during high-temperature heat treatment. This technique requires that coil components (wedges, pole blocks, end parts, etc.) be capable of withstanding high-temperature heat treatment under compression. An optimization method for metallic end part design was developed and used at Fermilab [11]. Implementing the rapid prototyping technique enhanced the quality and reduced the time and the cost of end part development.

A critical innovation implemented at Fermilab to the coil fabrication process was using a liquid ceramic binder [12]. The ceramic binder improves the mechanical strength of cable insulation during coil winding and glues all the coil components after coil curing, thus simplifying coil handling, forming and measuring its cross-section before reaction. During the final coil heat treatment, the binder turns into small ceramic particles. These hard dielectric particles are excellent filler during coil impregnation with epoxy increasing the coil turn-to-turn electrical strength and its mechanical properties. These improvements simplified the coil fabrication process, increased its robustness, and reduced coil fabrication cost and time. Pictures of coils impregnated with ceramic binder after winding and curing and after reaction are shown in Fig. 5. The details of the baseline dipole and quadrupole coil technology are reported in [3], [5].

All the dipole and quadrupole coils were impregnated with CTD 101K epoxy to improve their mechanical and electrical properties. The radiation strength of the regular epoxy resin is quite low and that limits the lifetime of accelerator magnets operating in hard radiation environments. Fermilab is investigating some commercially available polyimide solutions [13] and new epoxy compounds to replace traditional epoxy as an impregnation material for Nb_3Sn coils.

Mechanical structure and coil pre-load

Two quite different mechanical structures, one based on a thick stainless steel shell and the other one based on a stainless steel collar supported by stainless steel skin, were used in dipole and quadrupole models.

In the dipole structure the initial coil pre-stress of ~20 MPa and the magnet geometry control at room temperature is provided by two Al clamps. The final coil prestress of ~100-120 MPa at operating temperature, applied to reduce the radial and azimuthal turn motion under Lorentz forces, is created by the iron yoke, two clamps and a stainless steel skin.

The quadrupole mechanics involves coil initial pre-stress to ~30-50 MPa during collaring and then the final coil pre-stress to ~110-150 MPa by the stainless steel skin during assembly and cooling down to operating temperature. Control spacers prevent coil over-compression during yoking and skinning and increase the radial rigidity of the structure.

Axial coil pre-load and support in both dipole and quadrupole models is provided by thick end plates connected to the skin.

Nb_3Sn accelerator magnets with collar-based mechanical structures need a reliable collaring procedure for brittle Nb_3Sn coils [14]. The quadrupole coils collared with traditional quadrupole-style collars are usually compressed incrementally in the longitudinal direction. In order to limit the azimuthal stress gradient between adjacent sections, several passes are required to achieve the target coil prestress. The duration of the collaring procedure for this approach is proportional to the coil length and typically takes about one week per meter of coil. The maximum magnet length is also limited by the vertical space in a magnet assembly facility.

An alternative collaring method is based on a dipole-style collar. With this collar, the coils (dipole or quadrupole) are compressed simultaneously along their entire length, eliminating local stress gradients. This

method lowers the risk of damage of brittle Nb_3Sn coils as well as significantly reduces the collaring time and makes it independent of coil length.

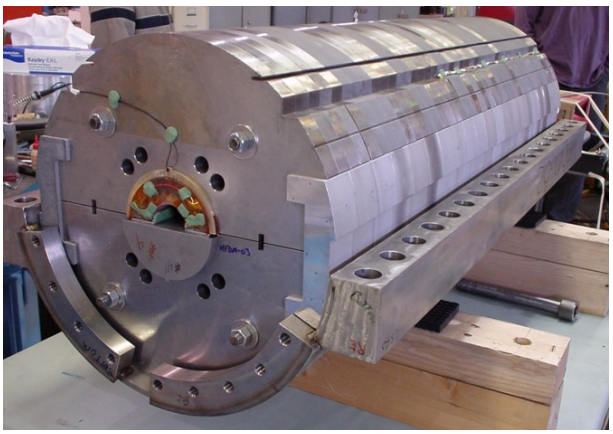

Figure 6: Dipole CTS (dipole mirror).

Coil test structures

Individual dipole and quadrupole coils were tested using special coil test structures (CTS) under operating conditions similar to those of real magnets, thus reducing the turnaround time of coil fabrication and evaluation, as well as material and labor costs. The dipole and quadrupole CTS use the same mechanical structures and assembly procedures as the corresponding complete magnets, and allow advanced instrumentation to be used.

The dipole CTS [15] is shown in Fig. 6. This structure is similar to the dipole structure of the HFDA series except that the iron yoke is split horizontally and one of the two coils is replaced with half-cylinder iron blocks. The coil inside the yoke is surrounded by bronze spacers. The transverse coil pre-stress and support is provided the same way as in the dipoles by a combination of the aluminum yoke clamps and the bolted stainless steel skin.

The quadrupole CTS [16] is shown in Fig. 7. It uses the iron yoke and skin of 90-mm quadrupoles of the TQC series. Three coils, collars and preload control spacers are replaced by iron blocks and spacers. This sub-assembly is installed in the standard TQC iron yoke and pre-compressed by a bolted stainless steel skin.

Axial coil pre-load and support in both dipole and quadrupole coil test structures is provided by two bolts in each thick end plate bolted to the skin.

SHORT MODEL TEST RESULTS

Six short dipoles of the HFDA series and six dipole CTS of the HFDM series were built and tested during 2002-2006. This was the first series of nearly identical Nb_3Sn magnets which provided the first data on magnet quench performance and field quality and their reproducibility. In 2007-2010 seven quadrupole models of the TQC series and six quadrupole CTS of the TQM series were fabricated and tested, expanding and enriching the previous results and experience. In the course of the model magnet R&D phase the production time of short dipole and quadrupole models was reduced to 5-6 months per model, which is comparable with the production time of traditional NbTi dipole and quadrupole models.

The dipole models were tested in liquid helium normally at 4.5 K and some at lower temperatures. The quadrupole models were tested at 4.5 K, 1.9 K and intermediate temperatures.

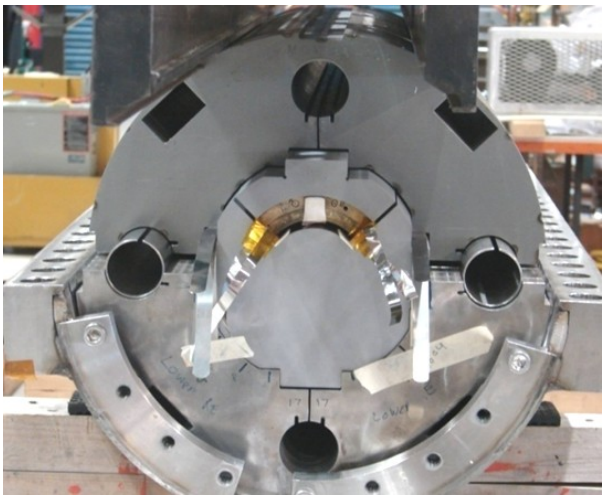

Figure 7: Quadrupole CTS (quadrupole mirror).

Quench performance

The first three dipole models, HFDA02-04, made of the MJR strand, were limited by flux jumps in the superconductor and reached 5-6 T or only 50-60% of their design field [17]. The last three dipole models HFDA05-07, made of the more stable 1-mm PIT-192 strand, reached B_{max}=9.4 T at 4.5 K and 10.2 T after cooling down to 2.2 K which corresponds to 100% of magnet short sample limit (SSL) at both temperatures. Fig. 8 shows the quench performance of the dipole models made of PIT strand. The maximum field reached by these models was ~10 T and was limited by the relatively low critical current density of the PIT strand. Nevertheless, these models clearly demonstrated that the developed Nb_3Sn coil technology and magnet mechanical structure are adequate for 10 T accelerator magnets.

A dipole coil made of high-J_c RRP-108/127 strand and tested later in 2006 using the dipole test structure HFDM06 reached B_{max}= 11.4 T at 4.5 K (97% of SSL) confirming robustness of the developed dipole coil technology and mechanical structure (see next section).

The first quadrupole models TQC01a and TQC01b, made of the low-J_c MJR strand, reached the nominal design field gradient of 200 T/m at 1.9 K [18].

Fig. 9 summarizes the quench performance of the quadrupole models TQC02Ea and TQC02Eb made of high-J_c RRP-54/61 strand at 4.5 K. TQC02Ea was collared using traditional quadrupole collars and the multi-pass partial compression technique, whereas TQC02Eb was collared using the dipole-style collars. For comparison, magnet training data of TQS02a and TQS02c models utilizing the same set of coils and based on the alternative mechanical structure [19] are also presented. It

can be seen that the quench performance of all the quadrupole models at 4.5 K was quite similar.

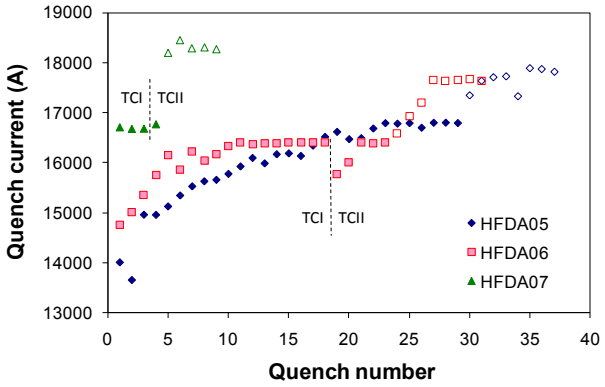

Figure 8: Dipole training quenches at 4.5 (solid markers) and 2.2 K (open markers) in thermal cycles TCI/TCII.

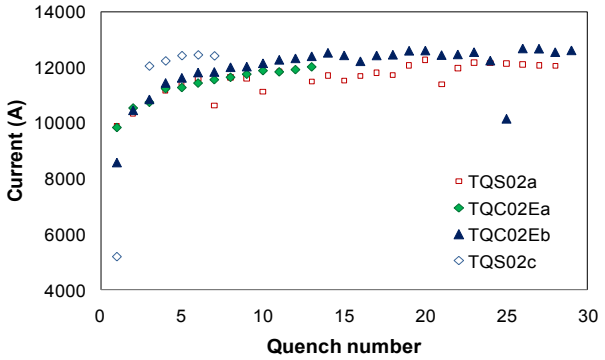

Figure 9: Quadrupole model training quenches at 4.5 K.

The maximum field gradient reached at 4.5 K in TQC models based on high-J_c RRP-54/61 strand was 211 T/m or ~90% of magnet SSL. At 3 K it increased to 217 T/m and then at lower temperatures it reduced to ~ 200 T/m due to flux jumps in superconducting strands.

A TQC quadrupole model with coils made of RRP-108/127 strand is being assembled and will be tested with the goal of achieving the design field gradient of ~230 T/m at the nominal operation temperature of 1.9 K.

Both dipole and quadrupole short models demonstrated similar training performance including the relative level of the first quench, training duration and training memory after thermal cycling in spite of the significant difference in their structures and assembly techniques.

Field quality

The average values of geometrical harmonics in dipoles at 1.8 T and in quadrupoles at 45 T/m at the reference radius R_{ref} corresponding to a half of the coil aperture are shown in Table 3. The values of the low order harmonics in both HFDA and TQC models are small, except for b_3 in HFDA and a_4 in TQC which are above one unit.

The standard deviations of normal and skew harmonics for HFDA dipole and TQC quadrupole models are shown in Fig. 10. The variation of skew harmonics in Nb_3Sn dipole and quadrupole models is quite close and still larger than in comparable dipole and quadrupole models based on traditional NbTi technology [20], [21]. The variation of normal harmonics is larger since it includes not only the coil component errors but also the adjustments of coil pre-stress shims. The reproducibility of both normal and skew harmonics in Nb_3Sn certainly can be improved by rising the tolerances of coil components, providing better coil alignment and reducing prestress variations.

Table 3: The average geometrical field harmonics for six dipole and five quadrupole models, 10^{-4}.

n	HFDA, R_{ref}=10 mm		TQC, R_{ref}=22.5 mm	
	a_n	b_n	a_n	b_n
2	-0.37	-0.15	-0.25	-0.09
3	0.55	2.06	-0.45	-0.97
4	-0.73	-0.06	-1.46	0.28
5	0.17	0.60	-0.25	0.97
6	-0.04	0.00	0.06	-0.02
7	0.01	0.20	-0.08	0.10
9	-0.02	-0.05	0.04	0.04

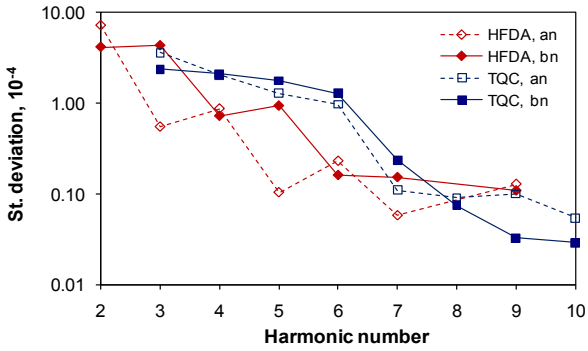

Figure 10: Normal b_n and skew a_n random field errors in Nb_3Sn dipole (HFDA) and quadrupole (TQC) models.

The coil magnetization, related to persistent currents in superconducting filaments and eddy currents in strands and cables, reduces the main field component (B in dipole and G in quadrupole) and affects the first allowed field harmonics - b_3 in dipoles and b_6 in quadrupoles.

The persistent current component is most important in the case of magnet operation with low ramp rates. It was large but reproducible in dipole and quadrupole models made of the same strand type [22], [23]. The higher strand J_c or larger d_{eff} proportionally changed the persistent current component of the magnet main field and the first allowed harmonics. In some dipole models with large flux jump activities in the coil, substantial erratic variations of sextupole field component at low fields were observed [24]. The superconductor magnetization theory and magnet experimental data suggest that the large persistent current effect and its variations observed in present Nb_3Sn accelerator magnets can be reduced by using strands with smaller sub-element size. A substantial fraction of the persistent current component can also be compensated using a passive correction based on thin iron strips [25].

The eddy current components depend on the current ramp rate, strand and cable twist pitches, transverse resistivity of the strand matrix, and interstrand resistance in the cable. The first three dipole models demonstrated a very small and reproducible eddy current effect due to large crossover resistances in the cable with the stainless steel core and the high resistivity (low RRR) of the strand matrix. The last three dipole models and all quadrupole models, all without stainless steel core in the cable and low matrix resistivity (high RRR), had large and non-reproducible eddy current components. This behavior was caused by the eddy currents in the cable due to large uncontrollable variations of cable interstrand resistance in coils. The above results suggest that the eddy current magnetization effect can be suppressed and well controlled by using cored cables and well-twisted strands.

Surprisingly, the decay and snapback effect, typical and quite strong in NbTi accelerator magnets, was not observed in either Nb_3Sn dipole [26] or quadrupole [23] magnets. Studies of this effect will continue.

Table 4. Coil design features.

CTS	Coil type	Strand type	J_c(12T, 4.2K), A/mm^2	Filament d_{eff}, μm	Cable core	Cable insulation	Pole material
HFDM01	DA05	MJR-54/61	2200	100	w/o core	Ceramic tape	Bronze
HFDM03	DA12	PIT-192	1600	50	-"-	-"-	-"-
HFDM06	DA19	RRP-108/127	2100	70	-"-	-"-	-"-
TQM01	TQ19	RRP-54/61	2800	70	w/o core	S2-glass sleeve	Bronze
TQM02	TQ17	-"-	-"-	-"-	-"-	-"-	-"-
TQM03	TQ34	RRP-108/127	2500	50	-"-	E-glass tape	Titanium
TQM04	TQ35	-"-	2300	-"-	25 μm tape	S2-glass sleeve	-"-

NB_3SN COIL STUDIES

Several issues were identified during the model magnet R&D which required experimental studies including the effect of conductor stability, cable core and insulation, coil pole materials, coil pre-stress. These and some other questions were studied and addressed by fabricating and testing series of dipole and quadrupole coils. The details of these studies are reported in [15]-[17], [27]. Coil design and fabrication features are summarized in Table 4.

Quench performance data of the dipole and quadrupole coils tested using the corresponding Coil Test Structures are plotted in Figs. 11 and 12.

The dipole coils made of different types of strand showed quite different training behavior. The coil made of the MJR strand with the largest value of $J_c \cdot d_{eff}$ and a relatively low RRR demonstrated erratic quench performance and large degradation of magnet quench current at 4.5 K. The PIT coil demonstrated stable training performance and reached its SSL at 4.5 K. At lower temperatures, it demonstrated the expected increase of the quench current.

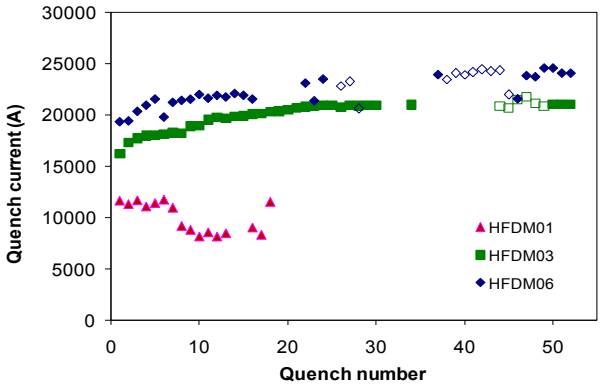

Figure 11: Dipole coil training quenches at 4.5 K (solid markers) and 2.2 K (open markers).

Table 5. Maximum pre-stress in the inner-layer pole turns.

CTS	Coil pre-stress, MPa	
	300 K	4.5 K
TQM03a	95	80
TQM03b	105	130
TQM03c	135	185

The RRP coil with reduced sub-element size reached the highest quench current, ~97% of its SSL limit, at 4.5 K. Noticeable variations of quench current on the current plateau pointed to mechanical or magnetic instabilities in the coil at high currents.

The quadrupole coils showed standard training behavior at 4.5 K with some variations of the first quench current, the number of training quenches and the maximum quench current. The training and ramp rate behaviors indicated that coils reached their SSL at 4.5 K. At 1.9 K the TQ coils (TQ17 and TQ19) made of RRP-54/61 strand with d_{eff}~70 μm showed some reduction of quench current and an erratic quench behavior which was observed also in the ramp rate measurements at the low current ramp rates. Meanwhile, coils TQ34 and TQ35, made of RRP-108/127 strand with d_{eff}~50 μm, showed the expected increase of quench current and regular ramp rate dependence at 1.9 K. After a few training quenches, these coils reached their SSL at 1.9 K.

To study the effect of pre-stress on the coil quench performance, coil TQ34 was assembled with three different warm and cold pre-stress values and tested three times using quadrupole CTS TQM03a/b/c. The values of maximum pre-stress in the inner-layer pole turns at room temperature and after cooling down are reported in Table 5. The TQM03a training data are shown in Fig. 12.

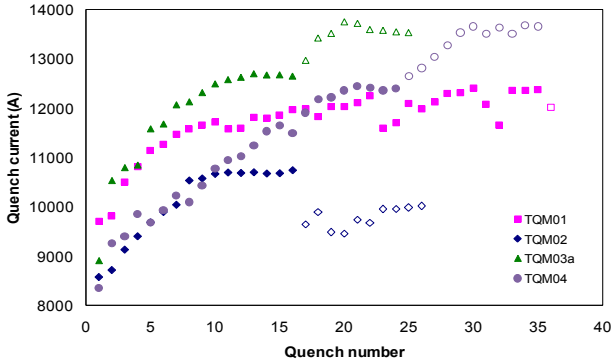

Figure 12: Quadrupole coil training quenches at 4.5 K (solid markers) and 1.9 K (open markers).

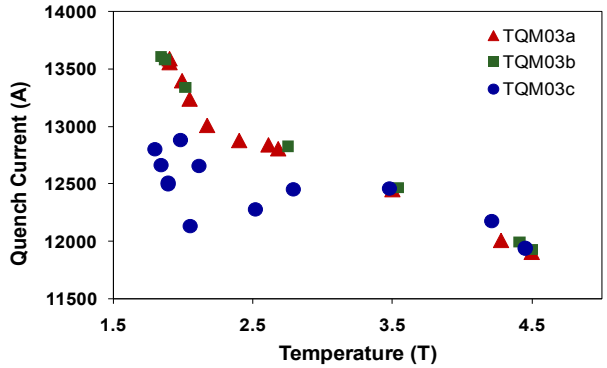

Figure 13: Coil TQ34 temperature dependence.

After re-assembly with higher pre-stress, TQM03b did not show any training and reached the same maximum quench currents both at 4.5 K and 1.9 K. TQM03c with the highest coil pre-stress also demonstrated good training memory at 4.5 K but unexpectedly low quench current increase and erratic quench behavior at 1.9 K.

The dependence of coil quench current on temperature for TQM03a/b/c is presented in Fig. 13. TQM03a and TQM03b showed stable and reproducible quenches over the entire temperature range from 1.9 to 4.5 K whereas TQM03c showed the same performance only above 3.5 K with most quenches below 3.5 K in the outer-layer blocks.

Analysis of the quench performance of the Nb_3Sn dipole and quadrupole coils as well as the dipole and quadrupole models leads to the following practical conclusions:

a) The thin stainless steel core inside the cable does not degrade the coil training and maximum quench current but significantly reduces the sensitivity of the magnet quench current to the current ramp rate. It makes this approach an efficient means of suppressing eddy currents in the cable, which cause deterioration of field quality in Nb_3Sn accelerator magnets during magnet ramping and unexpected magnet quenching during energy extraction.

b) The dipole and quadrupole coils with bronze and titanium pole parts and different cable insulation systems demonstrated similar quench performance. It confirms their compatibility with Nb_3Sn coil technology for accelerator magnets.

c) The warm coil pre-stress up to 150 MPa and cold pre-stress up to 190 MPa do not cause any degradation of the coil critical current at 4.5 K. However, substantial flux jump instabilities at temperatures below 3 K were observed due to the possible local strand damage during coil fabrication and assembly, which led to a non-uniform transport current redistribution in strand cross-sections.

d) Flux jump instabilities in high-J_c Nb_3Sn strands with large d_{eff} cause significant degradations of magnet quench performance. To suppress this effect in Nb_3Sn accelerator magnets based on high-J_c strand with B_{nom} above10 T, the value of d_{eff} has to be less than 50 μm. To meet more strict field quality requirements at injection and provide conductor stability margin in the case of high coil pre-stress, the d_{eff} should be even smaller, less than 20 μm.

Figure 14: 4-m long Nb_3Sn dipole coil (left) and LM02 cold mass (right).

TECHNOLOGY SCALE UP

The technology scale up phase addresses the issues related to winding, curing, reaction, impregnation, and handling of long Nb_3Sn coils, and long magnet assembly and performance due to the brittle nature of Nb_3Sn superconductor. The scale-up was performed in several steps starting in 2007 with fabricating and testing a 2-m long dipole coil made of PIT Nb_3Sn strand, which demonstrated stable and reproducible quench performance [22]. In 2008, the first 4-m long cos-theta dipole coil made of RRP-108/127 Nb_3Sn strand was fabricated and tested [29]. The 4-m long Nb_3Sn dipole coil and the 4-m long dipole CTS LM02 are shown in Fig. 14.

Training quenches of the 2-m long PIT coil (LM01) and the 4-m long RRP coil (LM02) at 4.5 K are shown in Fig. 15. The 2-m PIT coil after short training at 4.5 K reached its short sample limit and a field level of 10 T similar to the corresponding 1-m long PIT coil tested in dipole CTS HFDM03. The 4-m long dipole coil made of the high-J_c RRP-108/127 strand, unlike its short version, was limited at 4.5 K by strong flux jump instabilities in the coil outer layer (perhaps caused by conductor damage during coil fabrication or CTS assembly). However, after suppressing them by heating the coil outer layer using quench heaters, it reached ~90% of its short sample limit at 4.5 K. The coil maximum quench current was limited by quenches in the inner-layer mid-plane turns caused by heaters. The described results are complemented by the results of Nb_3Sn technology scale up performed by US-LARP by testing 4-m long racetrack coils [30] and recently the first 3.6-m long 90-mm quadrupole LQS01

[31]. The positive results of the Nb_3Sn technology scale up phase strengthen the high expectations for practical use of this technology in particle accelerators.

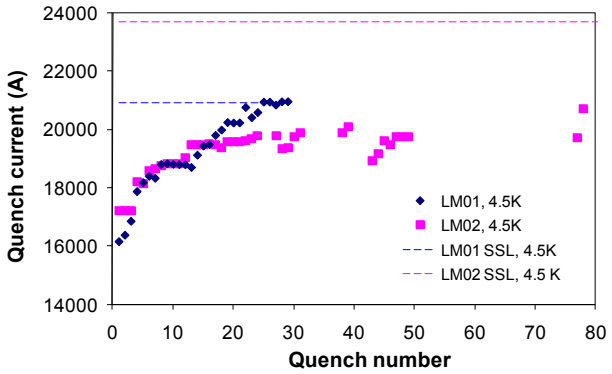

Figure 15: LM01 and LM02 training quenches at 4.5 K (markers) and short sample limits (dotted lines).

CONCLUSIONS

Fermilab has been developing Nb_3Sn accelerator magnets over the past decade. The Nb_3Sn coil design and production experience includes ~20 dipole and ~35 quadrupole 1-m long coils as well as 2-m and 4-m long dipole coils, and 14 4-m long quadrupole coils fabricated completely at Fermilab or in collaboration with BNL and LBNL. The coil technology developed at Fermilab allowed reaching good reproducibility of the major coil parameters and short fabrication time. Two mechanical structures, one based on a thick stainless steel shell and the other based on a stainless steel collar supported by stainless steel skin, were developed and successfully tested. Two collaring techniques for brittle Nb_3Sn coils were also developed and experimentally demonstrated.

The robustness of the developed technologies was confirmed by handling and transportation of the short and long Nb_3Sn coils across the country, multiple coil re-assemblies in different mechanical structures and magnet tests without performance degradation.

The accelerator quality performance, including quench behavior and field quality, was reached in series of dipole and quadrupole models. The obtained results are not final, and there is room for their further improvement.

The advances in Nb_3Sn accelerator magnet technology during the past decade make it possible for the first time to consider Nb_3Sn magnets with nominal fields up to 12 T (B_{max} up to 15 T) in present and future machines. To expand magnet operating fields up to 15 T, additional R&D effort will be required.

All the available experimental data show that superconductor properties are critical for magnet quench performance, field quality, protection, etc. Collaboration with materials groups in universities and industry on Nb_3Sn strand optimization is critical for the practical implementation of Nb_3Sn magnets in accelerators. The work on Nb_3Sn strand improvement with the goal of developing Nb_3Sn strands, which meet accelerator magnet specifications, has to be continued.

ACKNOWLEDGMENTS

The author thanks the staff of Fermilab's Technical Division and colleagues at BNL, LBNL and CERN for their contributions to this effort.

REFERENCES

[1] G. Ambrosio et al., "Conceptual Design of the Fermilab Nb_3Sn High Field Dipole Model", PAC1999, New York, 1999, p. 174.

[2] A.V. Zlobin et al., "Conceptual Design Study of Nb_3Sn Low-beta Quadrupoles for 2nd Generation LHC IRs", IEEE Trans. on Appl. Supercond., v. 13, Issue 2, June 2003, p.1266.

[3] G. Ambrosio et al., "Magnetic Design of the Fermilab 11 T Nb_3Sn Short Dipole Model", IEEE Trans. on Appl. Supercond., v.10, Issue 1, March 2000, p.322.

[4] "Design study for a staged Very Large Hadron Collider", Fermilab-TM-2149, June 4, 2001.

[5] R.C. Bossert et al., "Development of TQC01, a 90mm Nb_3Sn Model Quadrupole for LHC Upgrade based on SS Collar", IEEE Trans. on Appl. Supercond., v. 16, Issue 2, June 2006, p.370.

[6] S. A. Gourlay et al., "Magnet R&D for the US LHC Accelerator Research Program (LARP)", IEEE Trans. on Appl. Supercond., v. 16, Issue 2, June 2006, p. 324.

[7] E. Barzi et al., "Study of Nb_3Sn Strands for Fermilab's High Field Dipole Models", IEEE Trans. on Appl. Supercond., v.11, Issue 1, March 2001, p.3595.

[8] J.A. Parrell et al., "Advances in Nb_3Sn strand for fusion and particle accelerator applications", IEEE Trans. on Appl. Supercond., v. 15, Issue 2, June 2005, p. 1200.

[9] E. Barzi et al., "Development and study of Nb_3Sn strands and cables for high-field accelerator magnets", CEC/ICMC'2009, Tucson, AZ, 2009

[10] R. Bossert et al., "Tests of insulation systems for Nb_3Sn Wind and React coils", CEC/ICMC'2007, Chattanooga, TN, 2007.

[11] S. Yadav et al., "Coil Design Issues for the High Field Dipole at Fermilab," IEEE Trans. on Appl. Supercond., v. 11, Issue 1, June 2001, p. 2284.

[12] D.R. Chichili et al., "Fabrication of Nb_3Sn Shell-Type Coils with Pre-Preg Ceramic Insulation," CEC/ICMC2003, Alaska, 2003.

[13] D.R. Chichili et al., "Investigation of Alternative Materials for Impregnation of Nb_3Sn Magnets," IEEE Trans. on Appl. Supercond., v. 13, Issue 2, June 2003, p.1792.

[14] R. Bossert et al., "Development and Test of Collaring Methods for Nb_3Sn Quadrupole Magnets", CEC/ICMC'2009, Tucson, AZ, 2009.

[15] D.R. Chichili et al., "Design, Fabrication and Testing of Nb_3Sn Shell Type Coils in Mirror Magnet Configuration", CEC/ICMC'2003, Alaska, 2003.

[16] A.V. Zlobin et al., "Testing of Nb_3Sn quadrupole coils using magnetic mirror structure," CEC/ICMC'2009, Tucson, AZ, 2009.
[17] A.V. Zlobin et al., "R&D of Nb_3Sn Accelerator Magnets at Fermilab", IEEE Trans. on Appl. Supercond., v.15, Issue 2, June 2005, p.1113.
[18] R. C. Bossert, et al., "Development and Test of LARP Technological Quadrupole Models of TQC Series," IEEE Trans. on Appl. Supercond., v. 18, Issue 2, June 2008, p. 175.
[19] S. Caspi et al., "Test Results of LARP Nb_3Sn Quadrupole Magnets Using a Shell-based Support Structure (TQS)", IEEE Trans. on Appl. Supercond., v. 19, Issue 3, June 2009, p.1221.
[20] "Conceptual Design of the Superconducting Super Collider", SSC-SR-2020, March 1986, p. 127.
[21] N. Andreev et al., "Field Quality of Model Quadrupole Magnets for the LHC Interaction Regions at Fermilab", IEEE Trans. on Appl. Supercond., v. 10, Issue. 1, March 2000, p.107.
[22] A.V. Zlobin et al., "Development of Nb_3Sn accelerator magnet technology at Fermilab", PAC2007, Albuquerque, NM, 2007.
[23] G.V. Velev *et al*., "Field Quality Measurements and Analysis of the LARP Technology Quadrupole Models", IEEE Trans. On Appl. Supercond., v. 18, Issue 2, June 2008, p. 184.
[24] A.V. Zlobin et al., "Effect of Magnetic Instabilities in Superconductor on Nb_3Sn Accelerator Magnet Performance", IEEE Trans. on Appl. Supercond., v. 16, Issue 2, June 2006, p. 1308.
[25] V.V. Kashikhin et al., "Passive Correction of the Persistent Current Effect in Nb_3Sn Accelerator Magnets", IEEE Trans. on Appl. Supercond., v. 13, Issue 2, June 2003, p.1270.
[26] V.V. Kashikhin et al., "Field Quality Study in High-field Nb_3Sn Accelerator Magnets", PAC2005, Knoxville, TN, 2005, p. 366.
[27] G. Chlachidze et al., "The study of single Nb_3Sn quadrupole coils using a magnetic mirror structure," *presented at ASC'2010*, Washington, DC, 2010.
[28] H. Felice et al., "Test results of TQS03: A LARP shell-based Nb3Sn quadrupole using 108/127 conductor", *J.Phys.Conf.Ser.* v. 234, 2010.
[29] G. Chlachidze et al., "Quench performance of a 4-m long Nb_3Sn shell-type dipole coil", IEEE Trans. on Appl. Supercond., v. 19, Issue 3, June 2009, p.1217.
[30] P. Wanderer, et al., "Construction and Test of 3.6 m Nb_3Sn Racetrack Coils for LARP", IEEE Trans. on App. Supercond., v. 18, Issue 2, June 2008, p. 171.
[31] G. Ambrosio et al., "Test results of the first 3.7 m long Nb_3Sn quadrupole by LARP and future plans", *presented at ASC'2010*, Washington, DC, 2010.

STATUS OF HIGH TEMPERATURE SUPERCONDUCTOR BASED MAGNETS AND THE CONDUCTORS THEY DEPEND UPON*

J. Schwartz#, F. Hunte, W.K. Chan, X.F. Gou, X.T. Liu, M. Phillips, Q.V. Le, G. Naderi, M. Turenne, L. Ye, Department of Materials Science and Engineering, North Carolina State University, Raleigh, NC 27695, U.S.A

Abstract

This paper reviews the status of high temperature superconductors for high field magnets for future devices such as a high energy LHC or a muon collider. Some of the primary challenges faced for the implementation of systems are discussed. Two conductor technologies, $Bi_2Sr_2CaCu_2O_{8+x}$ and $YBa_2Cu_3O_{7-\delta}$, have emerged as high field conductor options, but their relative advantages and disadvantages for high field magnets are quite different. These are reviewed from an engineering perspective, including coil manufacturing, electromechanical behaviour and quench behaviour. Lastly, the important roles of "system pull" upon conductor and magnet technology development, and of interactions between the materials and magnet communities for accelerating development, are discussed.

INTRODUCTION

High temperature superconductors (HTS) have continued to advance technologically such that there are now at least six demonstrations of the generation of magnetic field greater than 25 T, and at least two that have surpassed 30 T [1, 2]. With the successful operation of the LHC, it is timely to consider the technological prospects for the development of the large, high field superconducting magnets needed for the next generation of colliders, such as a high-energy upgrade to the LHC or a muon collider [3, 4]. As HTS conductors evolve into commercial products, it is also important to assess the technological limitations and challenges that need to be addressed for large systems to ultimately come to fruition. Furthermore, with the high cost associated with development of future magnet technologies, an assessment of decision-points is also appropriate.

CONDUCTOR OPTIONS

As discussed at length in [5], the use of HTS conductors for high field magnets is necessitated by the fundamental limit to the high field behaviour of Nb_3Sn. Thus, although Nb_3Sn currently has significant advantages over HTS conductors in terms of cost, availability, experience-base and fundamental understanding, it is limited to magnets generating about 21 T for solenoids, and perhaps 18 T for dipoles. It is only the ability to carry high critical current density (J_c) at very high magnetic field (at least 45 T) that results in the consideration of HTS options. Thus, HTS conductors are viewed not as a replacement technology, but as an enabling technology for future high field magnet systems. Figure 1 plots the engineering critical current density versus magnetic field for LTS, HTS and MgB_2 conductors [6]. This data represents the highest published values for each of the emerging conductor options. Note that the high field performance of MgB_2 is poor, so it is not considered a high field conductor option.

Emerging Conductor: $REBa_2Cu_3O_{7-\delta}$

$REBa_2Cu_3O_{7-\delta}$, (REBCO), where RE refers to rare earth elements, is an HTS conductor that has been developed via thin film oxide technologies. While there are variations from manufacturer to manufacturer, in general REBCO conductors are based upon the deposition of thin oxide buffer layers atop a high strength Ni-alloy (e.g., Hastelloy or Ni-W) substrate. The REBCO layer is then deposited upon the oxide buffer layers, which provide a template for bi-axially-textured growth and a chemical barrier against Ni contamination. The bi-axial texture is known to be essential for obtaining high J_c. The REBCO layer is then covered by a thin Ag "cap layer" that provides environmental protection. Lastly, the entire conductor is encased by stabilizer, typically Cu. The resulting "coated conductor" carries the highest high-field J_c of any known superconducting material. The REBCO fill factor is only ~1-2%, however, which greatly reduces the engineering critical current density, J_e. Extensive literature exists regarding the processing of REBCO conductors, and various approaches used to enhance flux pinning, mechanical strength, REBCO layer thickness, etc. [7-14]

One of the primary limitations of REBCO coated conductors is that excellent electromagnetic performance is only obtained in a highly aspected, wide, thin tape geometry with highly anisotropic electromagnetic behaviour. The anisotropy limitations can be overcome to a significant extent in solenoids by using the REBCO only in the highest field section of the magnet system, and using NbTi and Nb_3Sn outserts to generate the lower magnetic fields. By properly designing the relative heights of the outserts and the REBCO insert, the magnetic field perpendicular to the REBCO tape (the "bad" direction) can be minimized and overall magnet performance optimized [15]. This is not so readily accomplished for dipoles or quadrupoles magnets.

Another challenge for REBCO is that the wide, thin tape geometry does not readily lend itself to traditional cabling, and Rutherford cables are not an option at

*Work partially supported by the U.S. Department of Energy through the Very High Field Superconducting Magnet Collaboration, the SBIR program and the STTR program, in collaboration with Supercon Inc. and Muons Inc.

#justin_schwartz@ncsu.edu

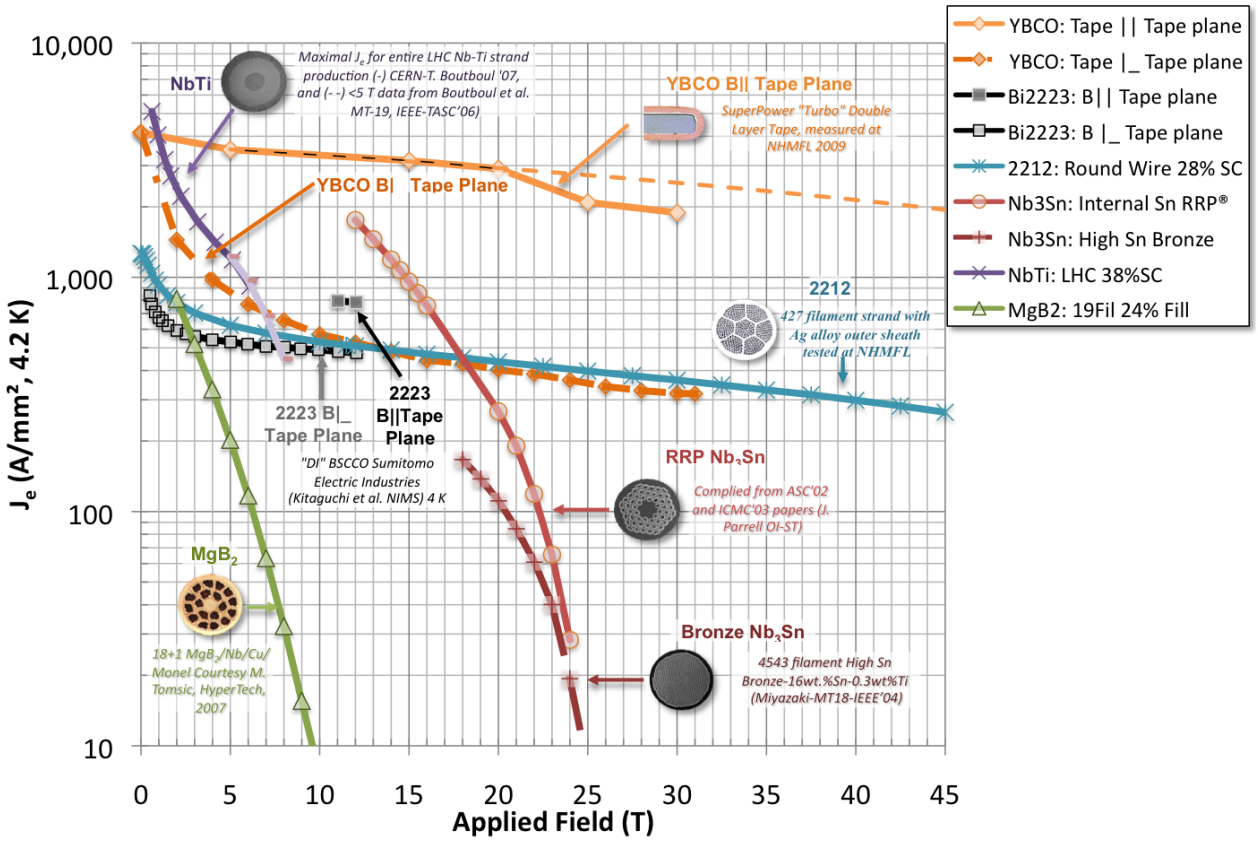

Figure 1: Engineering critical current density versus magnetic field for low temperature superconductor wires, high temperature superconductor wires and tapes and MgB_2 wires.

present. The only cabling option currently available is the Roebel cable approach, which is intrinsically more expensive as it wastes a significant percentage of the REBCO conductor in its manufacture. Although Roebel cables are clearly a low AC loss option, they are unproven for high field magnet systems, and in particular their mechanical and quench behaviours are unknown [16-19].

REBCO coated conductors can be viewed as a commercial product, although production lengths remain limited and at present the cost is high. Industrial manufacturers are currently focusing significant attention on scale-up issues in anticipation of meeting demand for a number of potentially growing markets, particularly within the energy sector. As the expectation is that the high volume market will ultimately be for energy systems operating at temperatures approaching 77 K and at relatively low magnetic field, optimizing conductors for low temperature, high field operation is not a research and development (R&D) priority. Thus, while the anticipation of market pull is driving development and scale-up, the impact on high field magnets is not as great as if there was a dedicated focus specifically upon the development of high field conductors. The potential for a large commercial market, coupled with the relatively low raw materials costs, imply that as commercialization increases and the REBCO market grows, the conductor unit price will decrease significantly. In the short term, REBCO applications will be attractive when REBCO is the enabling technology, because it is not cost competitive with LTS materials, but if sufficient demand is established such that the unit price is reduced significantly, then that price reduction is likely to fuel additional demand and a growing market.

Emerging Conductor: $Bi_2Sr_2CaCu_2O_{8+x}$

Unlike REBCO, $Bi_2Sr_2CaCu_2O_{8+x}$ (Bi2212) conductors are based on powder-in-tube technology and multifilamentary wire deformation processes developed for NbTi and Nb_3Sn. Both single and double restack architectures are manufactured industrially, but in most cases the first billet uses a high purity Ag tube, and the subsequent tubes are a Ag-alloy, typically Ag-Mg. The starting powder is typically high phase purity Bi2212. After deformation, the multifilamentary wire requires a heat treatment that first goes above the peritectic melt temperature and then resolidifies the Bi2212 phase. The partial-melt process is necessary to establish connectivity between the Bi2212 grains. During peritectic melting, however, phase segregation occurs so after resolidification the oxide is not phase-pure Bi2212, but instead contains a number of parasitic phases that reduce wire performance. Furthermore, the powder-in-tube process does not result in 100% dense filaments, so after heat treatment there is also significant porosity within the

filaments. Recent studies have shown that the heat treatment results in interfilamentary bridging which plays an important role in transport as well. Extensive literature exists regarding the processing of Bi2212 conductors [20-32].

Despite these issues, Bi2212 round wire remains a strong candidate for high field magnets. Bi2212 wires are electromagnetically isotropic and readily formed into Rutherford cables [27, 33, 34]. Industrial wire production is primarily limited by demand; the manufacturers are capable of producing significant volumes upon order. The key supply-chain concern, however, is the Bi2212 powder itself, but this is also a demand-based issue. If significant volumes of Bi2212 are required, capable powder manufacturing exists. The lack of significant demand for Bi2212 is primarily a result of the lack of a market other than high field magnets. The in-field electrical performance of Bi2212 declines rapidly for temperatures above about 20 K, so they are not competitive with REBCO for applications within the energy sector. Thus, while Bi2212 R&D is focused on high field magnets, there is no other strong driving force for scale-up. Unlike REBCO coated conductors, the unit costs of Bi2212 are not dominated by the manufacturing costs but instead by the unit cost of Ag. Thus, the price of Ag represents the "floor" below which the price of Bi2212 wire cannot drop, and the only potential for decreasing the conductor cost for Bi2212 magnets is to significantly increase J_e such that less conductor is required.

Conductor Comparison

Although REBCO and Bi2212 are both HTS conductors, technologically their similarities are few and their R&D challenges for high field magnets are quite different. This is summarized in Table 1, which compares the two conductors in terms of magnet-related issues.

ELECTROMECHANICAL BEHAVIOUR

High field magnets are intrinsically high force magnets due to the Lorentz forces present. Thus, strain tolerance and strain management grow in importance as the magnetic field increases. While low current density is one approach to lower Lorentz forces, low current density also results in very large, expensive magnets. Thus, an ideal high-field conductor not only has high $J_c(B)$, but also either strain tolerance or compatibility with approaches to reduce the conductor strain in magnets.

Electromechanical behaviour of REBCO

REBCO is manufactured on strong Ni-alloy substrates that provide significant mechanical advantages. With one of the approaches to REBCO, Hastelloy is used as the substrate and the Cu-stabilizer is attached to the conductor via electroplating. These approaches result in a particularly robust conductor and mechanical limitations are not a primary concern. The only uncertainty is in regards to tensile loads normal to the wide face of the conductor. The alternative approach to REBCO conductors is a Ni-W substrate with stabilizers attached via solder fillets. While Ni-W is stronger than most other high-field conductor options, it is not as strong as Hastelloy, and the solder fillets do not provide high strength for tensile loads normal to the wide face of the conductor or in shear. Thus, of the two conductor technologies, the former is preferred for high field magnets [35-42].

Table 1: HTS Conductor Comparison
(Note that bold text indicates a significant advantage whereas italics indicates a particularly challenging issue)

Bi2212	REBCO
Round wire	*Wide, thin tape*
~30% fill factor	*~1-2% fill factor*
Isotropic electromagnetic behaviour	*Anisotropic electromagnetic behaviour*
Rutherford cables	*Roebel cable only*
Weak Ag-alloy matrix	**Strong Ni-alloy substrate**
Poorly understood microstructure-property relationships; properties very sensitive to heat treatment details	Highly engineered microstructures
Readily scalable conductor manufacturing	*Conductor manufacturing scale-up challenges*
Wind&react magnets; magnet processing challenges	**React&wind magnets**
High field magnet applications are sole market	High temperature, low-field applications driving R&D
High price of Ag	*Expensive processing*
Active high field magnet projects on-going	**Active high field magnet projects on-going**

REBCO magnets are limited to react-and-wind magnet manufacturing which can add a non-zero bending strain to the total strain. The conductor can be designed, however, such that the REBCO layer is situated on the neutral axis or even in compression, so the bending strain contribution to the total strain is not a dominant concern [43]. Furthermore, REBCO electromechanical behaviour is reversible, so cycling within the fatigue limits does not generally result in significant degradation before failure [44, 45].

Electromechanical behaviour of Bi2212

Unlike REBCO, Bi2212 is encased within a relatively weak Ag/Ag-alloy sheath that provides significant ductility for wire drawing but does not provide high strength. Typically, the Ag-alloy is oxide dispersion strengthened (ODS) Ag-Mg, which sacrifices some ductility for increased strength and stiffness after heat treatment, but Bi2212 wire electromechanical behaviour remains a serious drawback. Primarily due to the poor

electromechanical behaviour, Bi2212 is limited to wind-and-react magnet construction, which eliminates bending strain but results in other limitations discussed below [46-48].

While the primary source of the poor electromechanical behaviour of Bi2212 is the lack of strength in the Ag/AgX matrix, the post-heat treatment Bi2212 microstructure is also a significantly contributing factor. Reacted Bi2212 multifilamentary wire microstructures are comprised of discontinuous filaments, interfilamentary bridges, non-superconducting oxide phases and porosity. As a result, the microstructure is defect-intensive with a ready supply of potential crack initiation sites that can lead to poor strain tolerance. This has recently been confirmed by statistical analysis that shows significant variance (i.e., inhomogeneity) in performance [49, 50]. This is illustrated in Figure 2, which shows Weibull reliability distribution for Bi2212 round wires tested at three different strain values (zero strain, 0.25% and 0.40%). While the high current "tail" in the 0.40% strain data indicates a high-strength electrical network within Bi2212, the reduction in reliability of the 0.25% strain relative to the zero-strain is indicative of some degree of irreversibility. The same analysis on REBCO coated conductors did not show similar inhomogeneous behaviour. Furthermore, there is evidence that the Bi2212 filaments show fractal characteristics, and subsequent fractal analysis highlights the role of these defects in the electromechanical performance.

There are significant R&D efforts currently aimed at improving Bi2212 performance. One research direction is aimed at improving the mechanical properties of the AgX sheath. By increasing the sheath stiffness, the strain on the superconductor is reduced for a constant load. Another research direction is aimed at improving Jc through improved processing and heat treatment approaches that result in an improved microstructure. If the inhomogeneous Bi2212 microstructure is a limiting factor in both Jc and the electromechanical behaviour, then it is anticipated that as Jc increases, the strain tolerance will also improve. There is recent evidence that Bi2223 (and thus perhaps Bi2212) has an underlying reversible component to its electromechanical behaviour, which may indicate the potential for significant improvements [51].

COIL MANUFACTURING

As indicated in Table 1, REBCO magnets are wound using the react-and-wind approach, simplifying the selection of insulation and instrumentation materials. Although some of the allowed strain may need to be allocated to bending strain, this has minimal impact on magnet design because the Ni-alloy substrate has high strength, and because the REBCO layer is on or near the conductor neutral axis. If the REBCO layer becomes substantially thicker, if double-sided coating of the Ni-alloy substrate becomes a standard technique for increasing J_e, or if a multilayer approach is developed, then the bending strain could become significant. At present, however, magnet manufacturing is not one of the primary challenges to high field REBCO magnets.

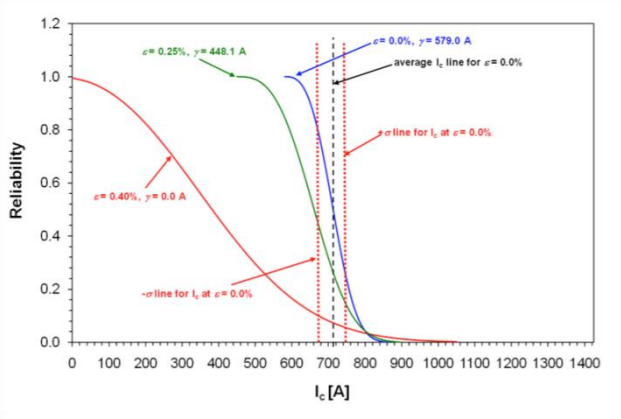

Figure 2: Weibull reliability distribution functions for Bi2212 round wire. The red curve is for 0.40% strain, the green is for 0.25% strain and the blue is for zero strain. For more details, see [49, 50].

Primarily due to their strain sensitivity, Bi2212 magnets are limited to wind-and-react (W&R) manufacturing or variations thereof [22, 23, 52, 53]. W&R manufacturing is not intrinsically problematic, as there is a large experience base to draw upon from Nb_3Sn magnets and a large number of very large magnet systems have been manufactured in this manner. W&R manufacturing of Bi2212, however, is significantly more challenging than Nb_3Sn for two unavoidable reasons: the presence of oxygen, which limits the options for insulation and instrumentation materials, and the high degree of sensitivity of the electrical performance of Bi2212 to the details of the heat treatment. In particular, due to the peritectic melting/resolidificaiton process required for high J_c Bi2212, J_c is very sensitive to a narrow temperature window (2-3 ^oC) for the peak heat treatment temperature and the amount of time spent above the peritectic melt temperature. The latter challenge is exacerbated as the size of coils increases. It is necessary to ensure that the portion of the magnet that is slowest to reach the peak temperature experiences the peritectic melting; but while waiting for the thermal diffusion, the portion of the magnet that is first to experience melting remains above the melt temperature for too long.

As a result of these challenges, insulated short samples often show a reduced I_c relative to bare wires (about 10% lower), and even relatively small Bi2212 magnets consistently show about 30% lower I_c than bare short samples (see Figure 3). Some of this decrease is likely due to the presence of insulation that can enhance the depletion of Cu from the conductor (without insulation, some Cu diffuses from the filaments into the Ag-alloy; reactions with the insulation provide an additional sink for Cu that diffuses to the edge of the wire).

Solutions to these challenges are currently under development within the Bi2212 community. Alternative

heat treatment processes that reduce the sensitivity upon the heat treatment peak temperature are being investigated, as are alternatives that attempt to minimize the presence of porosity and parasitic oxide phases. Alternative sheath alloys that deter Cu diffusion from the oxide cores, and alternative insulation materials that are not Cu-getters and are significantly thinner than presently available options, are being developed. Lastly, new heat treatment monitors that provide a continuous temperature-time map within the magnet during heat treatment offer the prospect of knowing real-time when the coldest portion of the magnet reaches the peritectic melt, facilitating dynamic control of the magnet heat treatment process such that the time above the resolidification temperature can be actively engineered [54, 55].

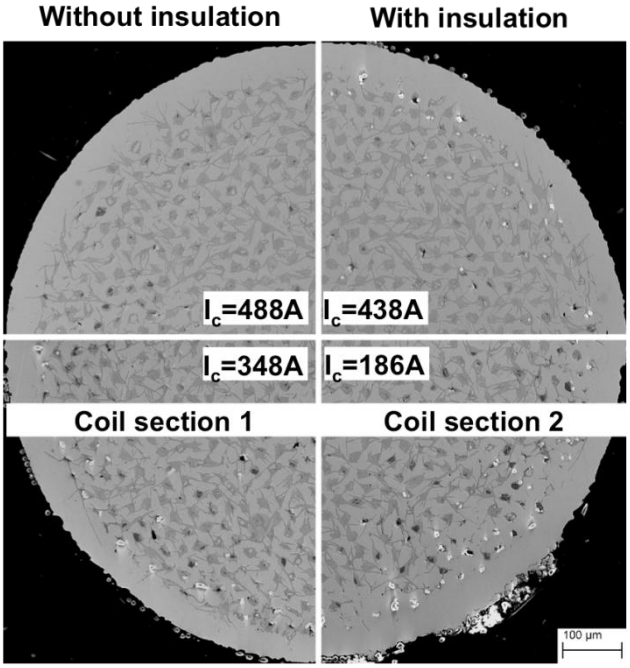

Figure 3: SEM images of heat treated Bi2212 round wire sections. The upper two images are from short samples (without and with insulation) and the lower two are from sections of an insulated Bi2212 coil. The corresponding critical currents are also shown. All samples were heat treated together during the same furnace run.

QUENCH BEHAVIOUR

An important issue for any large, high-energy superconducting magnet system is quench protection. For low-temperature superconductor (LTS) based magnets, quench protection is well understood and protection techniques are well established. For HTS-based magnets, the underlying science is qualitatively similar to that of LTS magnets, but the behaviour is quantitatively very different and thus new approaches may be required.

Typically, quench protection involves (1) quench detection: identifying that the magnet is going to quench while rejecting false signals and disturbances from which the magnet can recover, and (2) a protective response that must be implemented on a time scale fast enough to prevent the magnet from being damaged. Thus, to design a quench protection system, the magnet designer must needs to consider the time-evolution of the voltages and temperatures within the magnet during a quench so effective quench detection schemes can be designed, and the voltage-driven and temperature-driven degradation limits so that the protective response can prevent damage to the magnet. Note also that as the magnet stored energy increases, so does the risk of degradation during a quench. As the stored energy is proportional to B^2, the importance of quench protection increases with magnetic field and with magnet cost.

One of the most important differences between LTS and HTS magnets is the quench propagation velocity (QPV), which is a key parameter for quench detection. It has been consistently shown that the QPV in HTS (Bi2212 and REBCO) is significantly slower, as much as two orders of magnitude slower, than in Nb_3Sn magnets (see Figure 4) [56-69]. While slow quench propagation may also be correlated with a slower local temperature rise within the magnet, the key question is related to the rate of *localized* temperature rise as compared to the rate of voltage rise over monitored segments of the magnet. Voltage is, by definition, the integral of the electric field over the monitored length of conductor. It does not consider the spatial profile of the electric field (which is directly related to the spatial profile of the temperature in the conductor). Thus, since slow propagation results in a highly peaked temperature profile, for the same voltage, the peak temperature in an HTS magnet is likely to be much higher than in an LTS magnet. As a result, one of the key challenges for large, high field, HTS magnets is quench detection.

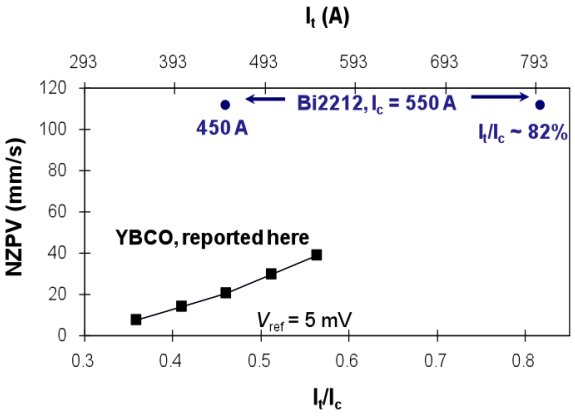

Figure 4: Experimentally measured normal zone propagation velocities of Bi2212 and YBCO coated conductors (from [60]).

A number of approaches are under development to address the HTS quench detection challenge. One approach is the development of quench detection sensors that are not voltage-based. The leading option in this regard is the implementation of optical fibers [54, 55, 70-

77]. Optical fiber sensors are in-service in a number of environments today, but as of yet have not been optimized for low temperatures. Optical fibers are small, thin fibers that can be directly incorporated into an HTS winding. Compatibility with the Bi2212 heat treatment has been demonstrated from the perspective of not causing any degradation to the Bi2212 wire. There are a number of approaches that use optical fibers as sensors, including fiber Bragg gratings, Brouillion scattering, and Rayleigh scattering. Fiber Bragg gratings are the most commonplace and the most developed of the optical fiber sensor technologies, however they are point sensors. While one fiber can be used to make measurements at a large number of points along its length, the locations must be predetermined so that gratings can be written into the fiber. Furthermore, while optical fibers in general survive the Bi2212 heat treatment, there are problems with survival of the grating itself. Rayleigh scattering is similar to fiber Bragg grating based scattering, but rather than using an engineered grating, it relies upon the natural inhomogeneities within an individual fiber to provide the necessary light scattering. Thus, in principle, the limit to the spatial resolution in Rayleigh scattering is the wavelength of the light source used. As a result, the practical resolution limits (spatial and temporal) are related to the data acquisition and data analysis. Quench detection requires obtaining a series of scattering profiles from the length of fiber and comparing them to determine if there are significant changes occurring. To effectively implement such a system, the required spatial and temporal resolutions must be understood and the data acquisition and analysis developed to meet those requirements.

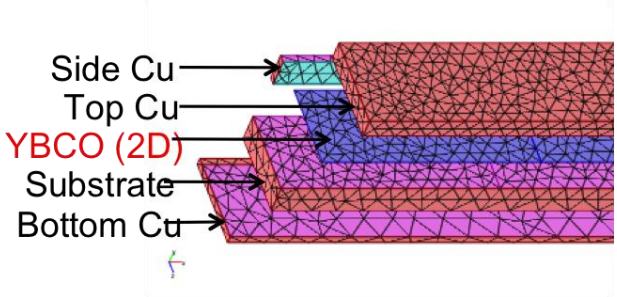

Figure 5: Meshing of a YBCO coated conductor.

In order to better understand the spatial and temporal resolution requirements for quench detection, and the microscopic behaviours during a quench (localized temperatures, voltages, current distribution, stresses and strains), and the likely failure modes during a quench, and thus to assist magnet designers in developing effective quench protection schemes, a high fidelity, experimentally validated, multiscale model of REBCO coated conductor quench behaviour has been developed. A typical meshing of a REBCO conductor is shown in Figure 5, and a resulting plot of the temperature versus location during a quench is shown in Figure 6. This important tool, which is already providing insight into the engineering of REBCO architectures for improved quench performance, is also capable of predicting both macroscopic, three-dimensional quench propagation within a magnet while simultaneously monitoring the localized behaviour within the microscopic layers of a REBCO conductor. A mesh of a coil section, with an embedded microscopic mesh of a section of conductor, is shown in Figure 6 [59, 61].

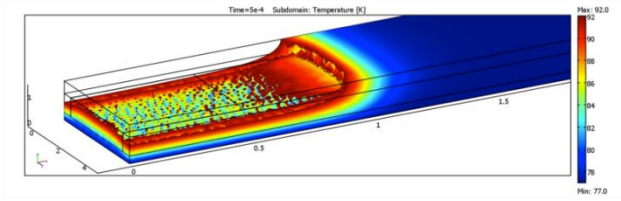

Figure 6: Temperature versus location during a quenching YBCO conductor.

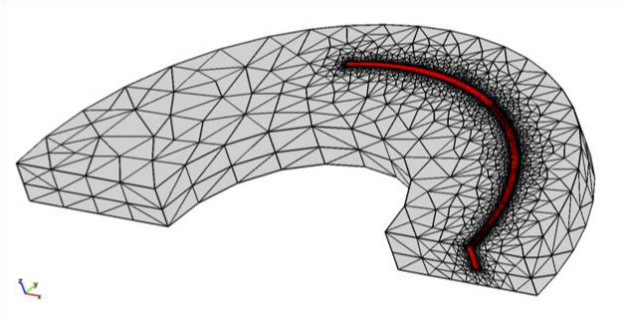

Figure 7: Multiscale model showing a course mesh for a section of a coil with a finer-scale mesh (micron-scale) for a section of YBCO conductor within the coil.

One of the key results from the three-dimensional modeling is that three-dimensional quench propagation within a magnet can significantly reduce the peak temperature for a fixed voltage within a coil. This may be obtained via the development of thermally-conducting electrical insulators to serve as turn-to-turn insulation. While it is found that the one-dimensional propagation velocity (along the conductor length) is decreased, the peak temperature in the magnet is also significantly reduced. This is illustrated in Figure 8, which shows the peak temperature (fixed voltaged) for three different insulation options. The blue (highest peak temperature) is for kapton, the black (intermediate temperature) is for alumina, and the red (lowest temperature) is for a high thermal conductivity alternative [78].

The other key question for quench protection is understanding the failure limits. For REBCO conductors, the primary concern is delamination. For conductors manufactured with solder fillets, the melting temperature of the solder is the primary concern. For electroplated conductors, two degradation mechanisms have been identified. The first is related to pre-existing defects in the conductor. These are thus a manufacturing issue that can be alleviated with improved processing, quality analysis and quality control. The second is related to delamination at the REBCO/Ag interface and has been observed during

quenching [79]. Ultimately this is likely to be the fundamental limit. If this limitation can be addressed, then the most fundamental limit becomes deoxygenation of the REBCO itself. For Bi2212, the quench limits are directly related to the electromechanical limits; i.e., the local stress and strain within the conductor [64]. As with the electromechanical behaviour, there is anticipation that with with improved Bi2212 microstructure and stiffer AgX sheaths, improved resistance to quench-induced degradation will also result.

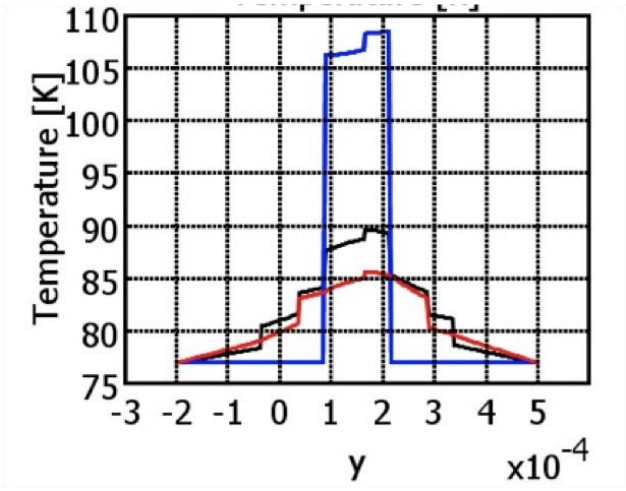

Figure 8: Impact of thermal conductivity of electrical insulator on the peak temperature within a YBCO coil during a quench.

OTHER CONSIDERATIONS

Although conductor options, electromechanical behaviour, coil manufacturing and quench behaviour are the primary issues for developing future high-field HTS magnets, other issues can also play important roles in the development and implementation of new conductor technology for accelerator magnets. For example, large magnets will require long lengths of conductor, as well as connections to current leads. Thus, joining technologies are important. These have not been effectively developed for either Bi2212 or REBCO conductors. Furthermore, the effects of irradiation on Bi2212 and REBCO magnets are not yet known. From a quench perspective, HTS magnets tend to be very stable with large minimum quench energies, so they may be ideally suited for regions of the system with large irradiation heat loads. But this is predicated upon resistance to irradiation damage, both for the conductor and any other materials (e.g. insulation) within the magnet system. Furthermore, for magnets to be used in high irradiation areas (e.g., an interaction region), HTS magnets, and in particular REBCO magnets, may offer the option of having the operating temperature as a design variable. In general, at low temperature the energy margin increases with temperature, so there may be situations where a higher operating temperature is preferred because it results in a larger temperature margin, even at the expense of some critical current density.

Another important consideration in the development of high field magnets is the impact of "magnet pull". Progress in the development of HTS technologies specifically aimed at the low temperature, high field regime is likely to be directly correlated with demand for such technologies by the magnet communities. In the over 20 years of HTS conductor development, most of the progress has been via "conductor push", with progress in the materials science of HTS conductors coming without consistent guidance regarding the specific demands of real magnet applications. In recent years, however, magnet pull has become an increasing presence in the development of HTS technology, and such pull is likely to continue to have significant impact on progress.

Lastly, it is important to consider potential "game changers" that could transform high field magnet technology. For example, if REBCO could be manufactured as an *isotropic round wire* with the same electrical and electromechanical performance as present-day REBCO coated conductors, Bi2212 would probably be eliminated from consideration and the primary R&D focus would concentrate REBCO scale-up, quench detection, joining, etc. Similarly, if Bi2212 could be manufactured with 100% dense, continuous, phase-pure filaments in a high strength, high stiffness sheath, then Bi2212 would likely leapfrog ahead of REBCO conductors and a new high field magnet technology would emerge.

SUMMARY AND CONCLUSIONS

Future devices for high-energy physics are likely to require magnetic fields greater than that which Nb_3Sn technology is capable of generating. As a result, new magnet technologies based upon HTS materials, primarily REBCO and Bi2212, are likely to be needed. These conductors are progressing and demonstrations of magnetic field generation greater than 25 T have been achieved repeatedly. Both conductor technologies, however, have significant remaining hurdles that must be overcome before the next generation of devices can be constructed. Although in many ways Bi2212 and REBCO are similar, each has distinctly different strengths and weaknesses, and thus the R&D programs required for each are quite different. For Bi2212, the primary challenges are the electromechanical behavior and large magnet manufacturing and heat treatment. For REBCO, the primary conductor challenges are the very low fill factor, electromagnetic and geometric anisotropy, and scale-up. Furthermore, both conductors show quench behaviour that is quantitatively quite different from that of LTS magnets.

Despite these challenges, Bi2212 and REBCO have made significant progress in recent years due to the presence of "magnet pull". Low temperature, high field magnets are needed for future nuclear magnetic resonance devices, future high energy physics devices, and recently even future energy storage devices. The interest from

these communities is having an important effect on the development of conductor and magnet technologies focused on the low temperature, high field regime.

REFERENCES

[1] H. W. Weijers, *et al.*, "The generation of 25.05 T using a 5.11 T $Bi_2Sr_2CaCu_2O_x$ superconducting insert magnet," *Superconductor Science & Technology,* vol. 17, pp. 636-644, Apr 2004.

[2] H. W. Weijers, *et al.*, "Tests of HTS Insert Coils above 30 T," presented at the International Symposium on Superconductivity (ISS-2008), Tsukuba, Japan, 2008.

[3] S. Kahn, "High Field Solenoid Magnets for Muon Cooling," in *2006 European Particle Accelerator Conference*, 2006, p. 2634.

[4] S. A. Kahn, "A High Field HTS Solenoid for Muon Cooling," in *2007 Particle Accelerator Conference*, 2007, p. 447.

[5] J. Schwartz, *et al.*, "High field superconducting solenoids via high temperature superconductors," *IEEE Transactions on Applied Superconductivity,* vol. 18, pp. 70-81, 2008.

[6] P. J. Lee. http://www.magnet.fsu.edu/magnettechnology/research/asc/plots.html.

[7] V. Selvamanickam, *et al.*, "High performance 2G wires : from R&D to pilotscale manufacturing," *IEEE Transactions on Applied Superconductivity,* vol. 19, 2009.

[8] C. V. Varanasi, *et al.*, "Thick YBa2Cu3O7-x+BaSnO3 films with enhanced critical current density at high magnetic fields," *Applied Physics Letters,* vol. 93, p. 3, Sep 2008.

[9] V. Selvamanickam, *et al.*, "Progress in second-generation HTS wire development and manufacturing," *Physica C,* vol. 468, pp. 1504-1509, 2008.

[10] T. Aytug, *et al.*, "Enhanced flux pinning and critical currents in YBa2Cu3O7-delta films by nanoparticle surface decoration: Extension to coated conductor templates," *Journal of Applied Physics,* vol. 104, p. 6, Aug 2008.

[11] S. H. Wee, *et al.*, "The incorporation of nanoscale columnar defects comprised of self-assembled BaZrO3 nanodots to improve the flux pinning and critical current density of NdBa2Cu3O7-delta films grown on RABiTS," *Superconductor Science & Technology,* vol. 20, pp. 789-793, Aug 2007.

[12] S. H. Wee, *et al.*, "Strong enhancement of flux pinning in thick $NdBa_2Cu_3O_{7-\delta}$ films grown on ion-beam assisted deposition-MgO templates via three-dimensional self-assembled stacks of $BaZrO_3$ nanodots," *Journal of Applied Physics,* vol. 102, Sep 2007.

[13] S. I. Kim, *et al.*, "On the through-thickness critical current density of an YBa2Cu3O7-x film containing a high density of insulating, vortex-pinning nanoprecipitates," *Applied Physics Letters,* vol. 90, Jun 2007.

[14] Z. J. Chen, *et al.*, "Top-down and bottom-up through-thickness current anisotropy in a bilayer $YBa_2Cu_3O_{7-x}$ film," *Applied Physics Letters,* vol. 91, p. 3, Jul 2007.

[15] H. W. Weijers, *et al.*, "Effects of conductor anisotropy on the design of Bi-Sr-Ca-Cu-O sections of 25 T solenoids," *Superconductor Science & Technology,* vol. 16, pp. 672-681, Jun 2003.

[16] L. S. Lakshmi, *et al.*, "Magnetic AC Loss Characteristics of 2G Roebel Cable," *IEEE Transactions on Applied Superconductivity,* vol. 19, pp. 3361-3364, Jun 2009.

[17] W. Goldacker, *et al.*, "Status of high transport current ROEBEL assembled coated conductor cables," *Superconductor Science & Technology,* vol. 22, Mar 2009.

[18] W. Goldacker, *et al.*, "Improvement of Superconducting Properties in ROEBEL Assembled Coated Conductors (RACC)," *IEEE Transactions on Applied Superconductivity,* vol. 19, pp. 3098-3101, Jun 2009.

[19] R. A. Badcock, *et al.*, "Progress in the Manufacture of Long Length YBCO Roebel Cables," *IEEE Transactions on Applied Superconductivity,* vol. 19, pp. 3244-3247, Jun 2009.

[20] T. Shen, *et al.*, "Filament to filament bridging and its influence on developing high critical current density in multifilamentary Bi2Sr2CaCu2Ox round wires," *Superconductor Science & Technology,* vol. 23, p. 025009, Feb 2010.

[21] T. Shen, *et al.*, "Development of high critical current density in multifilamentary round-wire Bi2Sr2CaCu2O8+delta by strong overdoping," *Applied Physics Letters,* vol. 95, Oct 2009.

[22] T. M. Shen, *et al.*, "Electromechanical behavior of $Bi_2Sr_2CaCu_2O_x$ conductor using a split melt process for react-wind-sinter magnet fabrication," *IEEE Transactions on Applied Superconductivity,* vol. 18, pp. 520-524, 2008.

[23] X. T. Liu, *et al.*, "React-wind-sinter processing of high superconductor fraction $Bi_2Sr_2CaCu_2O_x$/AgMg round wire," *IEEE Transactions on Applied Superconductivity,* vol. 18, pp. 1179-1183, 2008.

[24] W. T. Nachtrab, *et al.*, "Development of high superconductor fraction $Bi_2Sr_2CaCu_2O_x$/Ag wire for MRI," *IEEE Transactions on Applied Superconductivity,* vol. 18, pp. 1184-1187, 2008.

[25] W. T. Nachtrab, *et al.*, "The effect of filament diameter on Je in high filament count Bi2212/Ag

round wire," *IEEE Transactions on Applied Superconductivity,* vol. 19, pp. 3061-3066, 2009.

[26] H. Miao*, et al.*, "High field insert coils from Bi-2212/Ag round wires," *IEEE Transactions on Applied Superconductivity,* vol. 17, pp. 2262-2265, Jun 2007.

[27] A. Godeke*, et al.*, "Progress in Wind-and-React Bi-2212 Accelerator Magnet Technology," *IEEE Transactions on Applied Superconductivity,* vol. 19, pp. 2228-2231, Jun 2009.

[28] S. C. Kim*, et al.*, "Effect of filament configuration on critical current density of Bi2212/Ag wires with low Ag ratio," *IEEE Transactions on Applied Superconductivity,* vol. 18, pp. 1188-1191, June 2008.

[29] A. Villaume*, et al.*, "Misalignment angles' reduction in Bi2212 multifilaments melted by dynamic heat treatment under a magnetic field," *Superconductor Science & Technology,* vol. 20, pp. 691-696, Jul 2007.

[30] K. R. Marken*, et al.*, "Progress in Bi-2212 wires for high magnetic field applications," *IEEE Transactions on Applied Superconductivity,* vol. 16, pp. 992-995, Jun 2006.

[31] H. Miao*, et al.*, "Development of round multifilament Bi-2212/Ag wires for high field magnet applications," *IEEE Transactions on Applied Superconductivity,* vol. 15, pp. 2554-2557, Jun 2005.

[32] E. Flahaut*, et al.*, "In situ high temperature neutron study of the Bi2212 phase formation in Ag-sheathed tapes," *Physica B,* vol. 350, pp. e339-e341, 2004.

[33] E. Barzi*, et al.*, "BSCCO-2212 Wire and Cable Studies," *IEEE Transactions on Applied Superconductivity,* vol. in press, 2011.

[34] E. Barzi*, et al.*, "Study of Effects of Transverse Deformation in BSCCO-2212 Wires," *IEEE Transactions on Applied Superconductivity,* vol. in press, 2011.

[35] D. C. van der Laan and J. W. Ekin, "Dependence of the critical current of YBa2Cu3O7-delta coated conductors on in-plane bending," *Superconductor Science & Technology,* vol. 21, p. 6, Nov 2008.

[36] D. C. van der Laan and J. W. Ekin, "Large intrinsic effect of axial strain on the critical current of high-temperature superconductors for electric power applications," *Applied Physics Letters,* vol. 90, p. 3, Jan 2007.

[37] T. Takao*, et al.*, "Characteristics of Compressive strain and superconducting property in YBCO coated conductor," *IEEE Transactions on Applied Superconductivity,* vol. 17, pp. 3517-3519, 2007.

[38] T. Takao*, et al.*, "Influence of bending and torsion strains on critical currents in YBCO coated conductors," *IEEE Transactions on Applied Superconductivity,* vol. 17, pp. 3513-3516, 2007.

[39] C. C. Clickner*, et al.*, "Mechanical properties of pure Ni and Ni-alloy substrate materials for Y-Ba-Cu-O coated superconductors," *Cryogenics,* vol. 46, pp. 432-438, Jun 2006.

[40] N. Cheggour*, et al.*, "Enhancement of the irreversible axial-strain limit of Y-Ba-Cu-O-coated conductors with the addition of a Cu layer," *Applied Physics Letters,* vol. 87, p. 212505, Nov 2005.

[41] N. Cheggour*, et al.*, "Reversible axial-strain effect in Y-Ba-Cu-O coated conductors," *Superconductor Science & Technology,* vol. 18, pp. S319-S324, Dec 2005.

[42] N. Cheggour*, et al.*, "Magnetic-field dependence of the reversible axial-strain effect in Y-Ba-Cu-O coated conductors," *IEEE Transactions on Applied Superconductivity,* vol. 15, pp. 3577-3580, Jun 2005.

[43] D. Verebelyi*, et al.*, "Practical neutral-axis conductor geometries for coated conductor composite wire," *Superconductor Science & Technology,* vol. 16, pp. 1158-1161, Oct 2003.

[44] N. Cheggour*, et al.*, "Effect of fatigue under transverse compressive stress on slit Y-Ba-Cu-O coated conductors," *IEEE Transactions on Applied Superconductivity,* vol. 17, pp. 3063-3066, Jun 2007.

[45] A. L. Mbaruku and J. Schwartz, "Fatigue Behavior of Y-Ba-Cu-O/Hastelloy-C Coated Conductor at 77 K," *IEEE Transactions on Applied Superconductivity,* vol. 18, pp. 1743-1752, 2008.

[46] A. L. Mbaruku*, et al.*, "Effect of processing defects on stress-stralin-I-c for AgMg sheathed Bi-2212 tapes," *IEEE Transactions on Applied Superconductivity,* vol. 13, pp. 3522-3525, Jun 2003.

[47] J. K. Shin*, et al.*, "Estimation of Young's modulus, residual strain and intrinsic fracture strain of Bi2212 filaments in Bi2212/Ag/Ag alloy composite wire," 2008, pp. 1792-1795.

[48] D. C. van der Laan*, et al.*, "Strain effects in high temperature superconductors investigated with magneto-optical imaging," *IEEE Transactions on Applied Superconductivity,* vol. 13, pp. 3534-3539, Jun 2003.

[49] A. L. Mbaruku and J. Schwartz, "Statistical analysis of the electromechanical behavior of AgMg sheathed Bi2Sr2CaCu2O8+x superconducting tapes using Weibull distributions," *Journal of Applied Physics,* vol. 101, p. 073913, Apr 2007.

[50] A. L. Mbaruku*, et al.*, "Weibull analysis of the electromechanical behavior of AgMg sheathed Bi2Sr2CaCu2O8+x round wires and YBa2Cu3O7-delta coated conductors,"

Superconductor Science & Technology, vol. 23, Nov 2010.

[51] D. C. van der Laan, *et al.*, "Evidence that the reversible strain effect on critical current density and flux pinning in Bi2Sr2Ca2Cu3Ox tapes is caused entirely by the pressure dependence of the critical temperature," *Superconductor Science & Technology,* vol. **24**, p. 5, 2011.

[52] J. Schwartz and G. A. Merritt, "Proof-of-principle experiments for react-wind-sinter manufacturing of $Bi_2Sr_2CaCu_2O_x$ magnets," *Superconductor Science & Technology,* vol. 20, pp. L59-L62, Oct 2007.

[53] S. Boutemy, *et al.*, "React-wind-and-sinter technique for Bi2Sr2Ca1Cu2O8 high Tc coils," *IEEE Transactions on Applied Superconductivity,* vol. 7, pp. 1552-1555, Jun 1997.

[54] M. Turenne, *et al.*, "Multi-Purpose Fiber Optic Sensors for High Temperature Superconductor Magnets," presented at the 2009 Particle Accelerator Conference, Vancouver, Canada, 2009.

[55] J. Schwartz, *et al.*, "Multi-purpose fiber optic sensors for HTS magnets," presented at the 11th European Particle Accelerator Conference, Genoa, Italy, 2008.

[56] W. S. Kim, *et al.*, "Normal zone propagation in 2-dimensional YBCO winding pack models," *IEEE Transactions on Applied Superconductivity,* vol. 18, pp. 1249-1252, June 2008.

[57] D. Bocian, *et al.*, "Modeling of quench limit for steady state heat deposits in LHC magnets," *IEEE Transactions on Applied Superconductivity,* vol. 18, pp. 112-115, Jun 2008.

[58] A. A. Armenio, *et al.*, "Stability measurements on YBCO coated conductors," *IEEE Transactions on Applied Superconductivity,* vol. 18, pp. 1293-1296, 2008.

[59] W. K. Chan, *et al.*, "Three-dimensional micrometer-scale modeling of quenching in high aspect ratio YBa2Cu3O7-δ coated conductor tapes. Part I: Model development and validation," *IEEE Transactions on Applied Superconductivity,* vol. **20**, pp. 2370-2380, 2010.

[60] H. H. Song and J. Schwartz, "Stability and Quench Behavior of YBa2Cu3O7-x Coated Conductor at 4.2 K, Self-Field," *IEEE Transactions on Applied Superconductivity,* vol. 19, pp. 3735-3743, Oct 2009.

[61] W. K. Chan, *et al.*, "Influence of inter-layer contact resistances on quench propagation in YBa2Cu3Ox coated conductors," *IEEE Transactions on Applied Superconductivity,* vol. 19, p. 2490—2495, 2009.

[62] X. R. Wang, *et al.*, "Self-field quench behavior of multifilamentary MgB_2 wires in liquid helium," *Cryogenics,* vol. 48, p. 469—477, 2008.

[63] U. P. Trociewitz, *et al.*, "Quench studies on a layer-wound $Bi_2Sr_2CaCu_2Ox$/AgX coil at 4.2 K," *Superconductor Science & Technology,* vol. 21, Feb 2008.

[64] T. Effio, *et al.*, "Quench induced degradation in $Bi_2Sr_2CaCu_2O_{8+x}$ tape conductors at 4.2 K," *Superconductor Science & Technology,* vol. 21, Apr 2008.

[65] X. Wang, *et al.*, "Near-adiabatic quench experiments on short $YBa_2Cu_3O_{7-\delta}$ coated conductors," *Journal of Applied Physics,* vol. 101, p. 053904, Mar 2007.

[66] H. Song, *et al.*, "Quench behavior of conduction-cooled $YBa_2Cu_3O_{7-\delta}$ coated-conductor pancake coils stabilized with brass and copper," *Superconductor Science & Technology,* vol. 23, p. 10, 2010.

[67] G. A. Levin, *et al.*, "Stability and Normal Zone Propagation Speed in YBCO Coated Conductors With Increased Interfacial Resistance," *IEEE Transactions on Applied Superconductivity,* vol. 19, pp. 2504-2507, Jun 2009.

[68] F. Trillaud, *et al.*, "Quench behavior, quench protection of a YBCO test coil assembly," *IEEE Transactions on Applied Superconductivity,* vol. 18, pp. 1329-1332, June 2008.

[69] V. Sokolovsky and V. Meerovich, "Normal zone propagation along superconducting films deposited on wide substrates," *Cryogenics,* vol. 48, pp. 397-405, Sep-Oct 2008.

[70] F. Hunte, *et al.*, "Fiber Bragg Optical Sensors for YBCO Applications," presented at the 2009 Particle Accelerator Conference, Vancouver, Canada, 2009.

[71] R. Rajini-Kumar, *et al.*, "Performance evaluation of metal-coated fiber Bragg grating sensors for sensing cryogenic temperature," *Cryogenics,* vol. 48, pp. 142-147, Mar-Apr 2008.

[72] S. B. Mahar, "Spontaneous Brillouin Scattering Quench Diagnostics for Large Superconducting Magnets," PhD., Department of Nuclear Science & Engineering, Massachusetts Institute of Technology, Cambridge, 2008.

[73] C. Lupi, *et al.*, "Improving FBG sensor sensitivity at cryogenic temperature by metal coating," *IEEE Sensors Journal,* vol. 8, pp. 1299-1304, Jul-Aug 2008.

[74] R. RajiniKumar, *et al.*, "Fiber Bragg gratings for sensing temperature and stress in superconducting coils," 2006, pp. 1737-1740.

[75] J. H. Schultz and S. Smith, "Feasibilty of the TPX fiber optic temperature-sensor quench detection system," Massachusetts Institute of Technology, Plasma Fusion Center, PSFC/RR-9-4 1997.

[76] J. M. van Oort and R. M. Scanlan, "A fiber-optic strain measurement and quench localization system for use in superconducting accelerator dipole magnets," *IEEE Transactions on Applied Superconductivity,* vol. 5, pp. 882-885, 1995.

[77] J. M. van Oort and H. H. J. ten Kate, "A fiber-optic sensor for strain and stress measurement in superconducting accelerator magnets," *IEEE Transactions on Magnetics,* vol. 30, pp. 2600-2603, 1994.

[78] M. Phillips, "Influence of turn-to-turn insulation on quench propagation in YBCO coated conductors," Masters of Science, Department of Mechanical Engineering, Florida A&M University, Tallahassee, 2009.

[79] H. Song, "Microscopic observations of quenching and the underlying causes of degradation in YBa2Cu3O7-δ Coated Conductor," Ph.D., Electrical and Computer Engineering, Florida State University, Tallahassee, 2010.

20 T DIPOLES AND BI-2212: THE PATH TO LHC ENERGY UPGRADE*

P.M. McIntyre, K. Damborsky, E.F. Holik, F. Lu, A.D. McInturff, N. Pogue, A. Sattarov, E. Sooby
Texas A&M University, College Station, TX 60439, U.S.A.

Abstract

Increasing the energy of the LHC would require a ring of ~20 T magnets using the superconductors Nb_3Sn and Bi-2212/Ag. The technology for Bi-2212/Ag wire, cable, and coil has advanced significantly but is still far short of the performance needed for such magnets. New technology for both wire and cable is under development, which if successful would yield the needed performance.

INTRODUCTION

The possibility of tripling the energy of the Large Hadron Collider was proposed in 2004 [1]. That proposal for the Tripler was motivated by its potential for new physics and by recent advances in technology that offered a path to its feasibility. An LHC Tripler would access the entire range of masses predicted for the particles of supersymmetry. The pacing technology for the Tripler was a ~24 T arc dipole. Developments at that time were encouraging: model dipoles using the low-temperature superconductor Nb_3Sn [2] attained near-short-sample performance to >16 T; wire [3] and cable [4,5] using Bi-2212/Ag appeared to offer promise that 20 T might be attainable.

Today LHC is operating to produce hadron collisions at 7 TeV collision energy and is moving forward with a program to increase collision energy and luminosity to its design parameters. It is an appropriate time to revisit the potential for an LHC energy upgrade.

BI-2212 WIRE: STALLED AT 200 A/mm^2

Figure 1 shows the present-day performance of conductors using NbTi, Nb_3Sn, Bi-2212, and YBCO, and Bi-2223. The high-temperature superconductor Bi-2212 is the only round-wire superconductor that can operate at magnetic fields beyond 18 T for dipoles. Since round wire is generally considered to be essential for a transposed high-current cable, only Bi-2212 would seem to offer the possible basis for the inner coils of a >20 T dipole. Shown are in red on Figure 1 are the working lines for the LHC dipole (using NbTi), the working line for HD1 (using Nb_3Sn) [2], and a working line that would be required for an LHC Tripler dipole using Bi-2212/Ag inner windings. We need an engineering current density (averaged over wire cross section) of j_e~600 /mm^2 at 24 T, 4.2 K.

In 2004 Miao [3] presented encouraging results in the development of Bi-2212/Ag round wire: j_e = 400 A/mm^2 for 1 m long sample coils in 24 T, 4.2 K. The intrinsic performance in Bi-2212/Ag can be estimated from thin film studies, in which a layer current density of 7 × 10^4A/mm^2 was attained [6], so there is ample room for improvement in a practical wire.

Yet six years later the state-of-art short-sample performance of Bi-2212/Ag wire is j_e~320 A/mm^2 [7], and

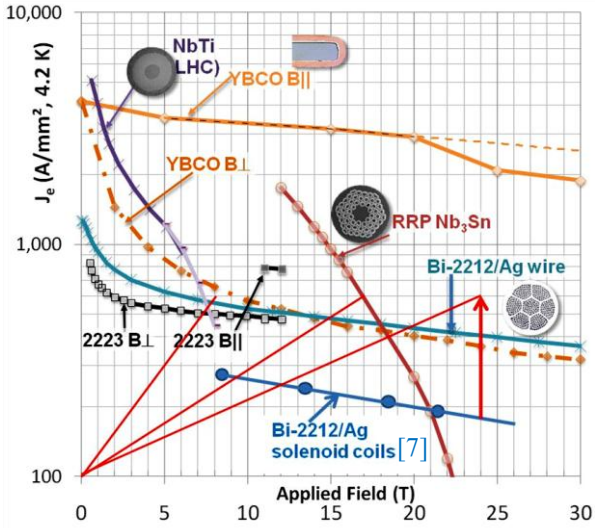

Figure 1: Recent performance of superconductors: only Bi-2212 has the potential for 20 T inner windings [8].

the state-of-art performance of this same wire in coils is j_e~200 A/mm^2 in both solenoids [7] and dipoles [9]. It might seem that we are going in the wrong direction!

The earlier wire results were obtained before serious efforts had been made to make long cables and long coils from wire. Coil fabrication must be done using a wind-and-react technique, in which a high-temperature heat treatment is required to melt and re-crystallize Bi-2212 grains in the final-form coil. It was found that the earlier wire had a tendency to leak its core material during the melt phase of heat treatment so that the stoichiometry was altered and the density of the core material was depleted. These problems were helped by adding additional Ag to the wire cross-section, but this reduced the average current density accordingly. To date it has not been possible to recover the earlier j_e performance. This remains a key challenge if an LHC energy upgrade is to be feasible.

UNDERSTANDING THE LIMITS TO J_E

Current transport in the cores of a multi-filament Bi-2212/Ag wire is hindered by porosity and poor connectivity, both of which are largely inherent to the oxide-power-in-tube (OPIT) process used in its fabrication. In this process a fine powder of Bi-2212 is loaded and sealed into an Ag tube; the tube is drawn, restacked, and redrawn to form the multi-filament composite shown in Figure 2. Hellstrom and co-workers [10] have studied the development of the microstructure in the cores of this wire during the heat treatment process, and from their studies a new understanding of the limitations to current transport is arising.

The wire starts life with significant porosity from the void space between randomly oriented powder particles.

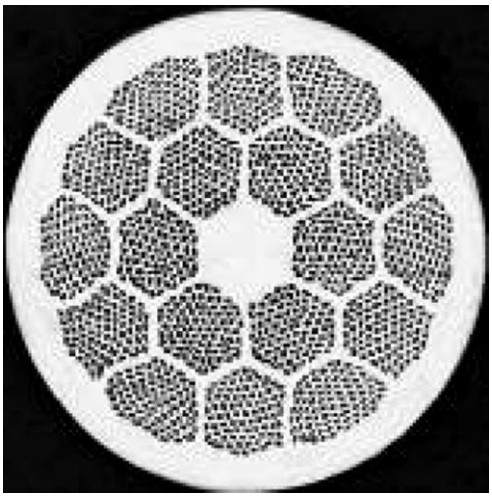

Figure 2: Cross section of OPIT Bi-2212/Ag strand [7].

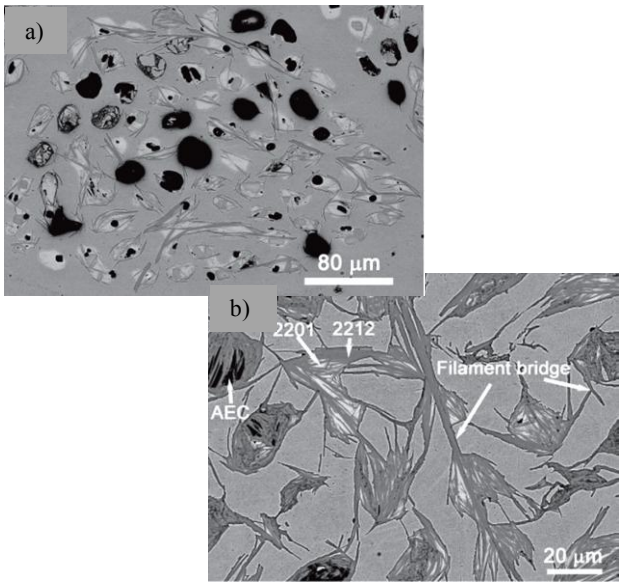

Figure 3: Scanning electron micrograph (SEM) images of core cross sections in OPIT Bi-2212/Ag wire, quenched during heat treatment: a) bubbles in melt before solidification; b) bridging, voids, and parasitic phases after annealing is complete [10].

When the powder is melted that void space becomes bubbles in the melt. The bubbles coalesce under surface tension to form large voids that span the cross section of each core. Figure 3a shows the coalesced bubbles and also the etching at Ag grain boundaries by the corrosive liquid melt. Figure 3b shows the Bi-2212 grains that have re-grown during the final anneal of the wire. Grain growth orients along the Ag interface, and the growth is fastest in the ab plane (which is the plane in which maximum current can be transported in the superconducting state). Many re-grown Bi-2212 grains now bridge between cores, and there are many high-angle grain boundaries that are problematic for supercurrent transfer from grain to grain. And so it is that the transport current density attained in OPIT wires [7] is only ~5% of that seen in thin films [6].

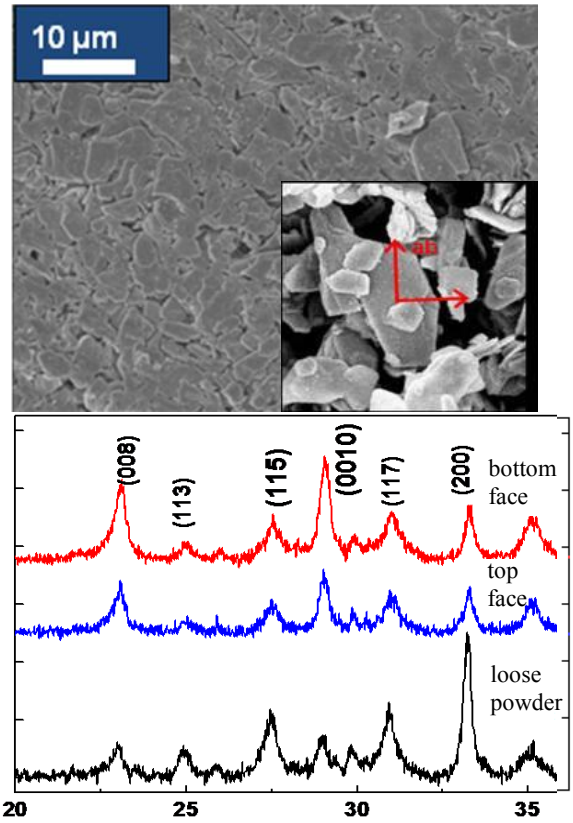

Figure 4: Study of pressed tablets of Bi-2212 fine powder: a) SEM micrograph of textured powder; b) detail showing micaceous particle morphology in loose powder; c) XRD analysis of texturing in fine powder and in pressed tablets.

TEXTURED POWDER JELLY ROLL: HOPE FOR NEW PERFORMANCE?

The above properties of OPIT-process Bi-2212/Ag wire led us to explore an alternative process for wire fabrication that directly addresses the issues of porosity and connectivity. It begins by preparing a cold-sintered flat ribbon of Bi-2212 fine powder in which most of the grains are oriented so that their ab plane is parallel to the ribbon face. This *texturing* of the powder has two important benefits: it minimizes the porosity in the final cores of a wire, and it may eliminate the necessity to fully melt the powder during processing.

The easiest way to texture Bi-2212 powder is to press a tablet using a hydraulic press [11]. The mechanical agitation among the powder particles during compression is remarkably effective in re-arranging them into a planar texture. Figure 4a shows an SEM micrograph of the pressed powder in such a tablet. Figure 4b shows a detail of the flake-like (micaceous) Bi-2212 particles. Figure 4c shows the XRD spectra for the loose powder and for tablets pressed with 70 MPa compression. A texture parameter τ (fraction of particles aligned with ab planes parallel to tablet face) has been extracted from the XRD spectra of loose powder, the powder cores in green-state OPIT wire, and tablets pressed with various degrees of compression. The data are presented in Figure 5.

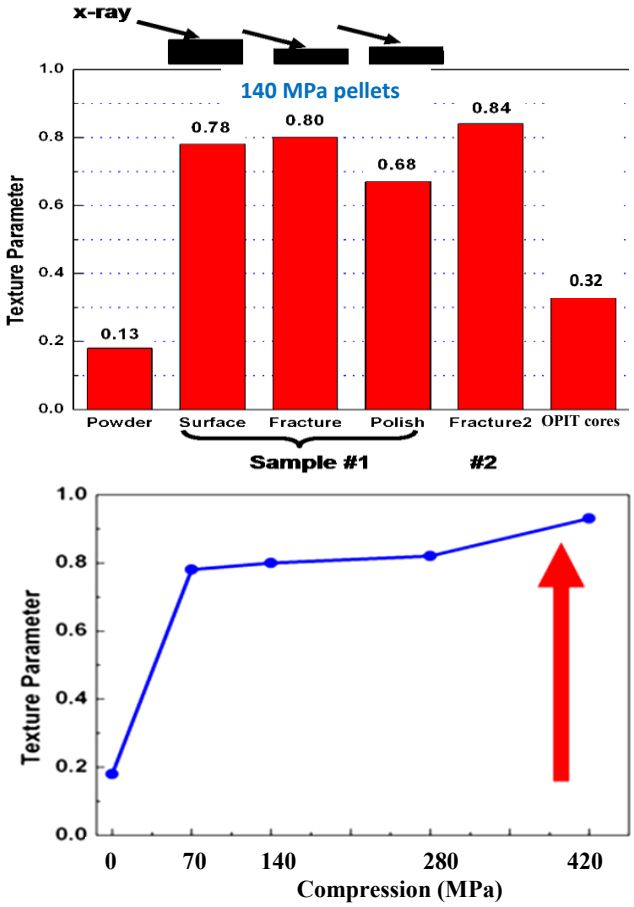

Figure 5: Texture parameter τ measured for fine-powder Bi-2212: a) loose powder, OPIT cores, and pressed tablets; b) dependence of τ on the amount of compression.

In a pellet 80% of the Bi-2212 particles are aligned with the tape face; the texture is the same in the interior of the pellet (fractured through its thickness) as on the surface; and it is largely independent of the compression (beyond 70 MPa) used to form the pellet. By contrast τ=13% for loose powder and τ=32% for the powder cores within conventional OPIT wire before heat treatment.

This development led us to conceive of an alternative method for wire fabrication in which Bi-2212 fine powder is roll-compacted to form a continuous ribbon, and the ribbon is compounded into a textured-powder 'jelly-roll' (TPJR) wire. The process begins by passing the powder though a roll-compaction system such as the Chilsonator [12], as shown in Figure 6a. The ribbons of cold-sintered Bi-2212 powder are assembled side-by-side on a ribbed Ag foil and a cover Ag foil is welded on to make a wide hermetic tape (Figure 6b). The tape is then rolled transversely, sleeved into a Cu tube, and drawn to final wire size (Figure 6c). Then the Cu is etched off to expose the final wire.

The textured micaceous powder within the laminar cores facilitates drawing of the wire. As the billet is drawn the particles in the textured powder should slide upon one another on their parallel faces and re-arrange to accommodate the area reduction.

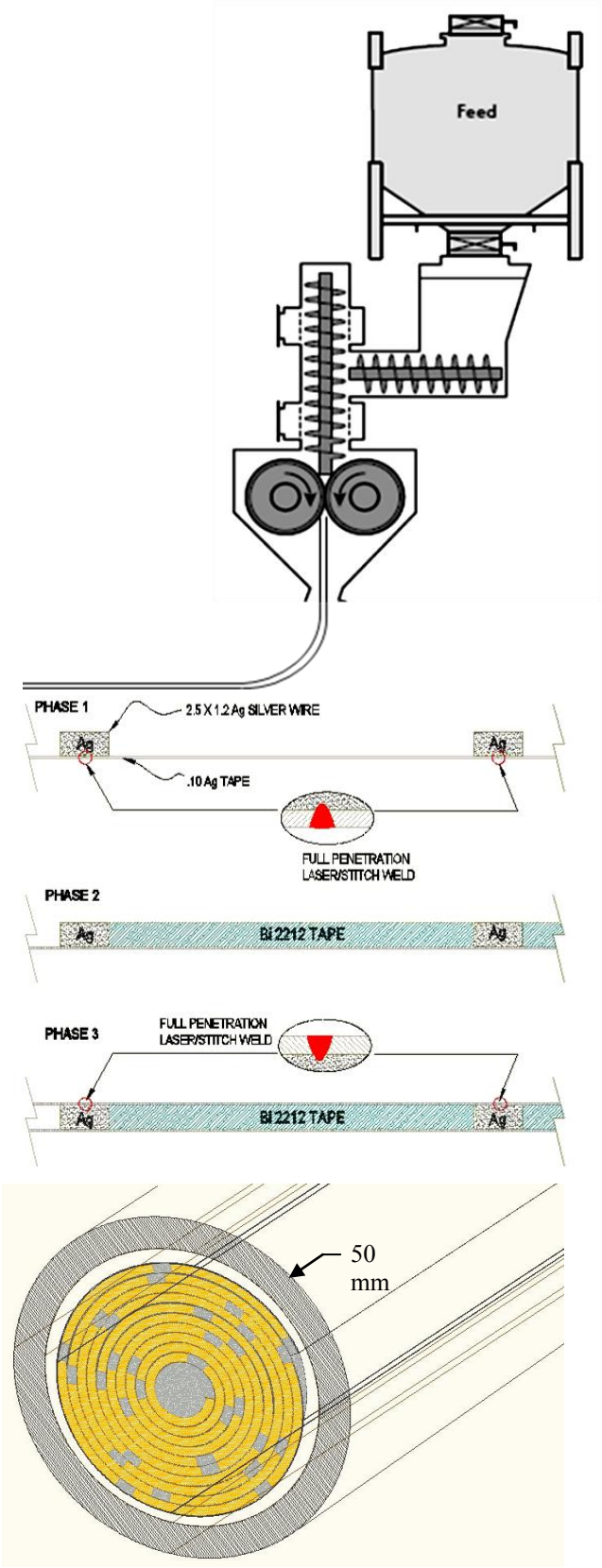

Figure 6: a) Chilsonator apparatus used to roll-compact Bi-2212 fine powder into continuous ribbons; b) incorporation of powder tape into Bi-2212/Ag tape; c) final jelly-roll round wire formed by rolling and drawing the tape.

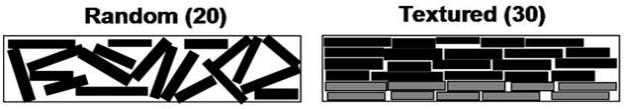

Figure 7. Illustration of the effect of texturing upon porosity in a core channel: the same channel holds 20 flakes of untextured powder, 30 flakes of textured powder.

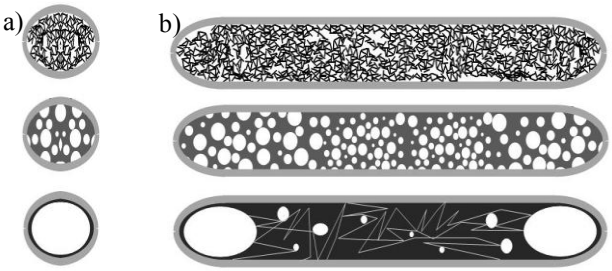

Figure 8: Illustration of bubble coalescence during full-melt heat treatment: a) full-diameter bubble forms and occludes round channel; bubbles form on the flanking edges of flat channel, leaving center free for grain growth.

We plan to evaluate possible heat treatment strategies for the TPJR wire: diffusion bonding of grains without melting, partial-melt processing, and full-melt processing. The first two methods would avoid the full-melt that is required for the OPIT process to develop texture and connectivity in its initially untextured cores. Avoiding melt would greatly reduce the issues of core leakage, cation migration, subelement bridging, and bubble coalescence that cause problems for the OPIT process. It is reasonable to hope that such non-melt treatment work well since the particles should be in face contact under compression, an ideal basis for bonding and connectivity by diffusion or partial melt.

If we find that full melt is nevertheless required, the TPJR process retains two important benefits compared with OPIT. The first benefit is improved packing. Figure 7 illustrates that there is less porosity when the flake-like particles are aligned.

The second benefit concerns the coalescence of bubbles. Figure 8a illustrates how the minimum-energy configuration of bubbles in a round channel is a large bubble that locally occludes the whole channel. Figure 8b shows the minimum-energy configuration for a highly aspected channel in the TPJR strand: bubbles coalesce on the two flanking edges of the channel, but leave the center of the channel clear for growth of textured grains of Bi-2212.

We will soon receive delivery of the roll-forming apparatus and begin development of the flat tape and jelly-roll wire. Much work is ahead to find optimum parameters for ribbon compression, tape fabrication, jelly-roll processing, and final heat treatment. The above analysis shows why we are hopeful that this approach may make possible higher j_e current transport in TPJR wire.

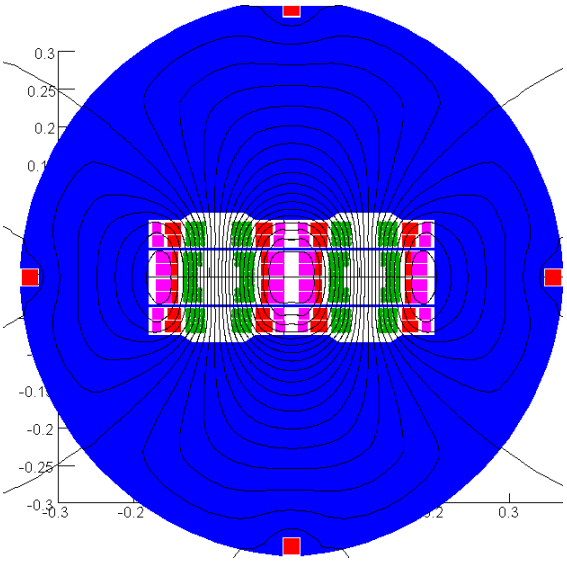

Figure 9: Cross section of dual dipole for LHC energy upgrade.

Table 1: Main Parameters of the Dual Dipole of Figure .

bore field (short sample)	21	T
coil current	15	kA
aperture	50	mm
stored energy/bore	3.3	MJ/m
max. stress in Nb_3Sn windings	170	MPa
strand cross-section/bore in coil:	52	cm^2
Nb_3Sn	55	cm^2
Bi-2212		

STRUCTURED CABLE AND 20 T DIPOLE

Figure 9 shows a conceptual design for a dual dipole that would have sufficient aperture (50 mm) for an LHC energy upgrade. The design assumes the use of Bi-2212 windings (green) in the coil region where the field strength exceeds ~16 T. It assumes that a strand performance j_e~800 A/mm^2 (20 T, 4.2 K) can be achieved in the windings, and j_c=2500 A/mm^2 (non-Cu, 12 T, 4.2K) in Nb_3Sn windings The Nb_3Sn windings are graded in wire diameter for the same $j_e(B)$ (magenta inner, red outer).

Even with the necessary current density in long-length wire and cable, it will still be necessary to protect the Bi-2212/Ag winding from strain degradation of the wires under the immense Lorentz stress produced on the windings in a 20 T dipole [13]. For this purpose we developed a structured cable [14] in which coil stress is by-passed around the fragile round wires so that no strain degradation should result. The cable is shown in Figure 10.

The Bi-2212/Ag inner winding in the coil of the dipole in Fig. 9 is a rectangular-cross-section (Fig. 11a) wound using a 16-strand structured cable (Fig. 11b) Table 1 gives the main parameters of the dual dipole. With the above assumptions of short-sample wire performance, the short-sample limit of the dipole is 21 T.

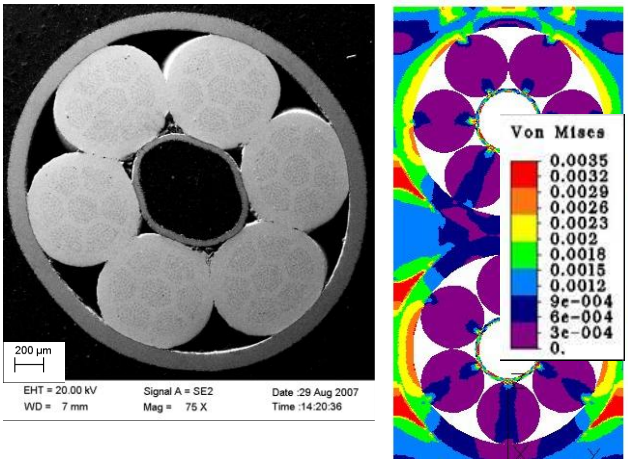

Figure 10: Structured cable of Bi-2212 round strands: a) micrograph of cross section; b) von Mises strain in structured cable when 100 MPa external load is applied [5].

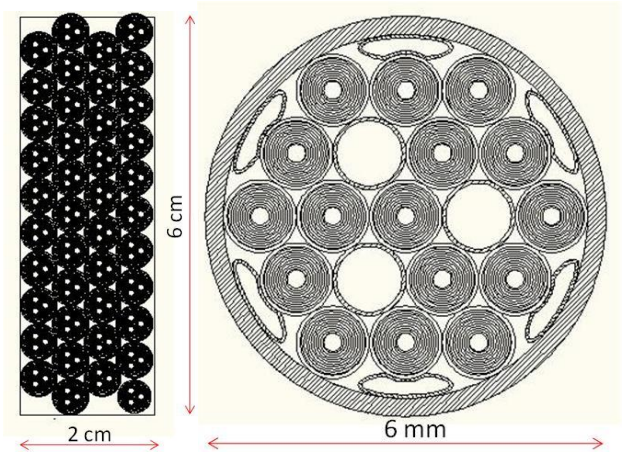

Figure 11: Cross-section of Bi-2212 inner winding, wound with 16-strand structured cable using TPJR round strands.

CONCLUSIONS

In the examination of the many challenging elements of an LHC energy upgrade that were presented at this EuCARD workshop, the high-field arc dipoles appear to present the biggest challenge at present. The critical technology for these dipoles is the current density in Bi-2212/Ag round wire and the degradation of that wire when made into thick windings and loaded with high Lorentz stress.

An alternative method for Bi-2212/Ag wire fabrication is described, which holds the potential for enabling a further improvement in current density. A design for structured cable is presented that manages stress within the coils of the Bi-2212/Ag inner windings so that it cannot accumulate to levels that would degrade performance.

The viability of an LHC energy upgrade will depend upon the success of these developments and similar ones by other authors. It is to be hoped that a successful outcome can be matured in time for consideration of an energy upgrade of LHC after its first decade of high-luminosity physics running.

This work is supported in part by the US Dept. of Energy, grant DE-FG03-95ER40924, and by an endowment from the Cynthia and George Mitchell Family Foundation.

REFERENCES

[1] P. McIntyre and A. Sattarov, 'Tripling the LHC: the path from technology to discovery', Proc. Int'l. Conf. on Dark Matter (DARK2004), College Station, TX, Oct. 3-9, 2004, eds. H.V. Klapdor-Kleingrothaus and R. Arnowitt, Springer, Heidelberg, p. 348 (2005).

[2] A. Lietzke *et al.*, 'Test Results for HD1, a 16 T Nb_3Sn dipole magnet', IEEE Trans. Appl. Supercond. **14**, 2, p. 345 (2004).

[3] H. Miao *et al.*, 'Development of Bi-2212 conductors for magnet applications', Adv. in Cryo. Eng.: Trans. Int'l Cryo. Mat. Conf. – ICMC **50**, p. 603 (2004).

[4] T. Hasegawa *et al.,* '12 kA HTS Rutherford cable', IEEE Trans. Appl. Supercond. **14**, 2, p. 1066 (2004).

[5] N. Diaczenko *et al.*, 'Strain-tolerant cable using Bi-2212 superconductor', Physica **C341**, 4, 2551 (2000).

[6] N.T. Mua *et al.*, 'High critical current density in Ag-doped Bi-2212 thin films', Supercond. Sci Tech. **21**, p. 105002 (2008).

[7] C. Friend *et al.*, 'Development of high field magnets utilizing Bi-2212 wind & react insert coils', IEEE Trans. Appl. Supercond. **20**, 3, p. 583 (2010).

[8] P. Lee, Compilation of current j_e data, http://www.magnet.fsu.edu/magnettechnology/research/asc/plots.html.

[9] A. Godeke *et al.,* 'Wind-and-react Bi-2212 coil development for accelerator magnets', Supercond. Sci. Tech. **23**, p. 034022 (2010).

[10] T. Shen *et al.*, 'Development of high critical current density in multifilamentary round-wire Bi-2212 by strong overdoping', Appl. Phys. Lett. **95**, 152516 (2009).

T. Shen *et al.,* 'Filament-to-filament bridging and its influence on developing high critical current density in multifilamentary $Bi_2Sr_2CaCu_2O_x$ round wires', Supercond. Sci. Technol. **23**, p. 025009 (2010).

[11] K. Damborsky *et al.*, 'Texturing of micaceous superconductor powder and fabrication of wire to preserve the texture', Proc. Appl. Supercond. Conf., Washington, Aug. 1-6, 2010.

[12] Fitzpatrick Co., http://www.fitzmill.com/

[13] N. Cheggour *et al.*, 'Critical-current measurements on an ITER Nb_3Sn strand: effect of axial tensile strain', **17**, 2, p. 1366 (2007).

[14] P. McIntyre, A. Sattarov, and R. Soika, 'Armored spring-core superconducting cable and method of construction', U.S. Patent 6,448,501 (2002).

HEAT LOADS AND CRYOGENICS FOR HE-LHC

D. Delikaris, L. Tavian, CERN, Geneva, Switzerland

Abstract

We report preliminary considerations on cryogenics for a higher-energy LHC ("HE-LHC") with about 16.5 TeV beam energy and 20-T dipole magnets. In particular we sketch the heat loads scaled on the proposed principal beam parameters and size the cryogenic plants for different operating temperature of the beam screens.

INTRODUCTION

Similar to the LHC, the heat deposited in the HE-LHC will reach 3 different temperature levels:

- the thermal shield temperature level (TS) between 50 and 75 K,
- the 5-K heat intercept (HI) and beam screen temperature level (BS) between 4.6 and 20 K (40-60 K or 85-100 K as an alternative compatible with vacuum specification), and
- the cold mass temperature level (CM) at 2 K.

It is also assumed that specific cryogenic systems will be needed for insertion magnets and RF cavities. These insertions are not defined yet; consequently, in the following, only the continuous cryostats (CC) will be considered, i.e. arcs plus dispersion suppressors and associated current feed boxes.

HEAT INLEAKS

In first approximation the thermal performance of the HE-LHC cryostat is assumed to be similar to the one of the LHC cryomagnet. In addition, it is assumed that the LHC cryoline (QRL) is used with its present thermal performance [1]. The specific heat inleaks are given in Table 1.

Table 1: Specific heat inleaks on magnets and cryoline

Temperature level		LHC	HE-LHC
TS (50-75 K)	[W/m]	7.7	7.7
HI (4.6 K)	[W/m]	0.23	0.23
CM (2 K)	[W/m]	0.21	0.21

RESISTIVE HEATING IN SUPERCONDUCTING SPLICES

For HE-LHC, a main magnet current of 18 kA is assumed. The resistive heating in the magnet splices is proportional to the square of the magnet current, to the splice electrical resistance and to the number of splices. The corresponding heat load is deposited at the CM temperature level. As the HE-LHC hybrid coil design is based on 3 different cables, it is assumed that the number of splices increases by a factor 1.5 with respect to the LHC coil design based on 2 different cables. Table 2 gives the main parameters related to the resistive heating. The increase of the magnet current and of the number of splices, both by 50 %, translates into an increase of the resistive heating by a factor 3.4 with respect to the nominal LHC.

Table 2: Resistive heating in magnet splices

	LHC nominal	HE-LHC
Main magnet current [kA]	12	18
Splice resistance [nΩ]	0.5	0.5
Number of splice per arc [-]	2500	3750
Resistive heating on CM [W/m]	0.1	0.34

CURRENT LEAD COOLING

Concerning the cooling of the current leads (CL), it is assumed that HE-LHC is using the same type of HTS current lead as the LHC with the same cooling performance, i.e. a specific cooling rate per kA of 54 mg/s of helium between 20 and 300 K. In addition, as the optics of the HE-LHC is not yet fully defined the number of individually powered magnets is not known; consequently, it is assumed that the total current entering or exiting is proportional to the main magnet current. In addition, as for the LHC, it is assumed that high-load sectors enter two times more current than low-load sectors. Table 3 lists the main parameters for the current lead cooling.

Table 3: Current lead cooling

	LHC nom.	HE-LHC
Main magnet current [kA]	12	18
Total current in/out [kA]	2750	4130
Total current high load sector CC [kA]	460	690
Total current low load sector CC [kA]	230	345
Specific CL cooling flow [mg s^{-1} kA^{-1}]	54	54
High-load sector CL cooling flow [g/s]	25	37
Low-load sector CL cooling flow [g/s]	12	19

BEAM-INDUCED LOADS

The parameters impacting the beam-induced loads are the beam energy, the bunch population, the number of bunches, the bunch length and the beam-screen aperture. Table 4 gives the scaling laws to be applied for the different beam-induced loads. Table 5 lists the parameters and the beam-induced loads for the nominal LHC and the

HE-LHC. Compared with the nominal LHC, all beam-induced loads on the beam screens increase for the HE-LHC. The biggest change concerns the synchrotron-radiation load, which increases by a factor 17.

Table 4: Scaling laws of beam induced heat loads

Beam-induced load	Energy E	Bunch population N_{bunch}	Bunch number n_{bunch}	Bunch length σ_z [rms]	Beam-screen aperture b	Temp. level
Synchrotron radiation	E^4	N_{bunch}	n_{bunch}			BS
Image current		N_{bunch}^2	n_{bunch}	$\sigma_z^{-3/2}$	b^{-1}	BS
Photo-electron cloud		N_{bunch}^3	n_{bunch}		b^{-2}	BS
Beam gas scattering		N_{bunch}	n_{bunch}			CM

Table 5: Parameters and specific beam-induced loads

	LHC nom.	HE-LHC
Beam energy [TeV]	7	16.5
Bunch population [10^{11} p]	1.15	1.29
Bunch number [-]	2808	1404
Bunch length [cm]	7.55	6.55
Beam-screen aperture radius [cm]	2	1.3
Synchrotron radiation [W/m]	0.33	5.71
Image current [W/m]	0.36	0.44
Photo-electron cloud [W/m]	0.90	1.50
Beam gas scattering [W/m]	0.05	0.03

OPERATING THE BEAM SCREENS AT A HIGHER TEMPERATURE

In addition to the nominal operating temperature of the beam screens at 46-20 K (range BS1), other possible temperature operating ranges compatible with the beam vacuum specification are 40-60 K (range BS2) or 85-100 K (range BS3). Increasing the operating temperature of the beam screen will have the following consequences:

- As the electrical resistivity of the copper on the beam-screen surface increases with the temperature, the image-current load will also increase proportionally. Measurements at 20 K, 50 K and 92.5 K on LHC beam-screen samples give a copper resistivity increase by factors 5.5 and 22 (see Figure 1). Consequently, the image current heat-load will increase from 0.44 to 2.4 and 9.8 W/m. A coating with HTS (like Bi-2223 or Y-123) may improve this figure dramatically. However, today this is a speculation.
- The temperature difference between the beam screen and the cold bore will increase, i.e. the heat inleaks on the cold mass will increase as well. Measurements on String 2 [2] indicate a heat inleak increase on the cold-mass of 0.17 and 0.71 W/m (see Figure 2).
- The present design of the LHC beam screen cooling loop based on a unit length of 53 m and two 3.7-mm inner-diameter capillaries per aperture is locally limited to a heat extraction of 2.4 W/m per aperture, i.e. 4.8 W per meter of machine. Changing the operating conditions and the specific heat load has a direct impact on the cooling capillary diameter. Table 6 gives the operating conditions of the beam screen cooling loops and the corresponding required capillary diameter assuming the same cooling loop configuration as today. The operation of the beam screen at 20 bar and between 40 and 60 K minimizes the cooling capillary diameter.

Table 6: Beam screen cooling capillary diameter

	BS temperature range [K] BS1	BS2	BS3
Inlet temperature [K]	4.6	40	85
Inlet pressure [bar]	3.0	20	20
Outlet temperature [K]	20	60	100
Outlet pressure [bar]	1.3	18	18
Specific heat load [W/m]	7.65	9.45	16.3
Loop length [m]	50	50	50
Nb of capillary per aperture	2	2	2
Capillary inner diam. [mm]	4.4	3.8	6.0

HEAT LOAD SUMMARY

Table 7 resumes the specific cryogenic heat load for the different temperature levels. Compared with the nominal LHC, depending on the beam-screen operating temperature range, the heat loads on the beam-screen circuits increase by a factor 4 to 9, and those on the cold-mass circuits by a factor 1.6 to 3.6.

Concerning the heat loads on the cold-mass circuits, the present LHC cooling loop is locally limited to 0.9 W/m, i.e. it is not compatible with the HE-LHC specific heat load corresponding to the 85-100 K operating temperature range (BS3) of the beam screens.

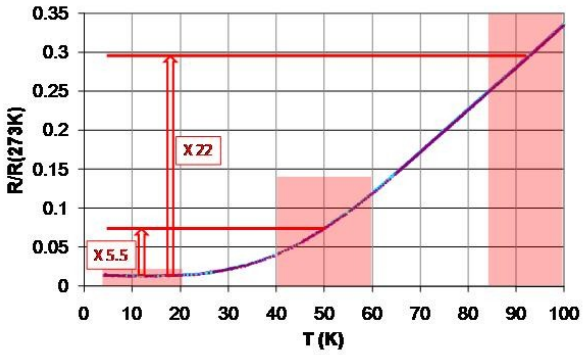

Figure 1: Copper resistivity

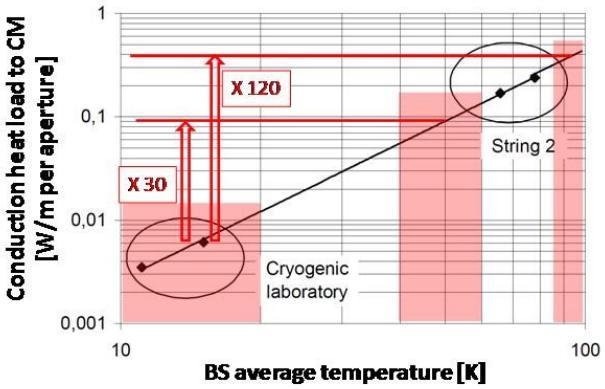

Figure 2: Conduction heat load to cold mass

Table 7: Cryogenic specific heat loads

Temperature level	Heat load source		LHC nominal	HE-LHC		
				BS1	BS2	BS3
TS	Heat inleaks	[W/m]	7.7		7.7	
	Total TS	**[W/m]**	**7.7**		**7.7**	
HI	Heat inleaks	[W/m]	0.23		0.23	
	Total HI	**[W/m]**	**0.23**		**0.23**	
BS	Heat inleaks	[W/m]	0	0	-0.17	-0.71
	Synchotron radiation	[W/m]	0.33	5.71	5.71	5.71
	Image current	[W/m]	0.36	0.44	2.40	9.81
	Photo-electron cloud	[W/m]	0.90	1.50	1.50	1.50
	Total BS	**[W/m]**	**1.82**	**7.65**	**9.45**	**16.3**
CM	Heat inleaks	[W/m]	0.21	0.21	0.38	0.92
	Resistive heating	[W/m]	0.10	0.34	0.34	0.34
	Beam-gas scattering	[W/m]	0.05	0.03	0.03	0.03
	Total CM	**[W/m]**	**0.36**	**0.58**	**0.74**	**1.29**

CONTINUOUS-CRYOSTAT COOLING CAPACITY

Assuming a continuous cryostat length of 2800 m and an overcapacity margin of 1.5, the required cooling capacity per continuous cryostat is given in Table 8 and is compared with the existing installed capacity of LHC sector cryogenic plants. Values in brackets correspond to the equivalent entropic capacity in kW at 4.5 K. Figure 3 shows the equivalent entropic capacity for the different temperature levels. Depending on the operating temperature range of the beam screen, the total equivalent entropic capacity of HE-LHC refrigerators varies from 31 to 19 kW at 4.5 K. Operating the beam screens between 4.6 and 20 K requires continuous-cryostat refrigerators about 1.7 times larger than the LHC sector refrigerators. Operating the beam screens between 40 and 60 K allows reducing the size of the continuous-cryostat refrigerators which becomes similar to the LHC sector refrigerators. Operating the beam screens between 85 and 100 K overloads the cold-mass temperature level. With a cold-mass operating temperature of 2 K, the optimum beam-screen temperature range is 40-60 K.

The electrical input power of the different scenarios, assuming a coefficient-of-performance of 250 W per W, is given in Table 9.

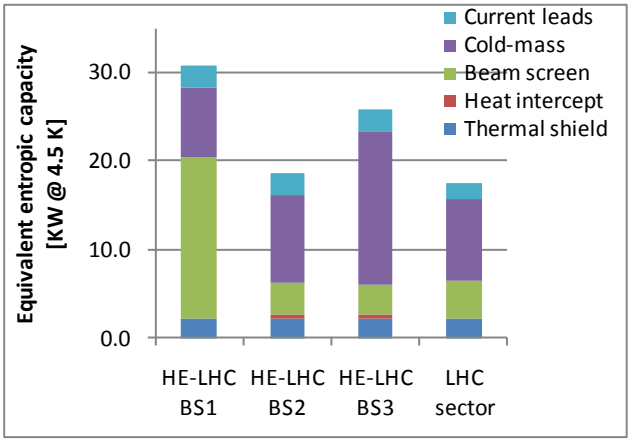

Figure 3: Equivalent entropic capacity

Table 8: Continuous cryostat cooling capacity per sector
(in brackets: equivalent entropic capacity in kW at 4.5 K)

Temp. level	HE-LHC continuous cryostat			LHC high load sector
	BS1	BS2	BS3	BS1
TS [kW]	33 (18.4)	32 (2.2)	1.0 (0.5)	33 (2.2)
HI [kW]		1.0 (0.5)	1.0 (0.5)	7.7 (4.3)
BS [kW]		40 (3.5)	69 (3.3)	
CM [kW]	2.4 (7.8)	3.1 (10)	5.4 (17.4)	2.7* (9.3)
CL [g/s]		56 (2.5)		41 (1.8)
Total	(30.8)	(18.6)	(25.8)	(17.6)

*: 2.4 kW at 1.8 K plus 0.3 kW at 4.5 K

Table 9: Electrical input power for continuous-cryostat refrigerators

Temp. level	HE-LHC CC refrigerator			LHC ref.
	BS1	BS2	BS3	
Input power/refrigerator [MW]	7.7	4.7	6.5	4.4
Number of refrigerators [-]	8	8	8	8
Total input power [MW]	62	37	52	35

CONCLUSION

In these present cryogenic studies, no contingency has been introduced in the numbers. A lot of assumptions have to be confirmed like the splice resistance and number, the main magnet current, the current-leads distribution and number, and the cryostat performance.

The optimization of the refrigeration cycle has still to be done. Transient heat loads (ramp/de-ramp, fast de-ramp, quench), have still to be considered in order to define the correct level of buffering. In addition, the LSS loads have still to be considered with probably new cryoplants for insertions accommodating experiments.

Depending on the cooling scenario, up to 9 temperature levels have to be distributed along the continuous cryostats to supply or recover the different cooling loops. A rationalization study has to be done for reducing the number of distribution headers like operating the beam screen and the thermal shield with the same temperature range and/or cooling the resistive part of HTS current lead with a helium flow at a higher temperature and pressure (e.g. 40 K, 20 bar).

At this preliminary study phase, it is definitely too early to state on the possible reuse of LHC cryogenics. Nevertheless, it should be recalled that, at the end of the LHC (2030), the LHC cryogenics will be 30 to 40 years old. Taking into account the 20-year operation initially specified, major and wide overhauling has to be considered for the equipments which could be reused for the HE-LHC project (cryogenic plants, QRL, distribution boxes…).

REFERENCES

[1] O. Bruning *et al*, LHC Design Report, Volume 1, CERN-2004-003, (2004)

[2] L. Tavian, Beam Screen Regenerative Heating : Cryogenic Impact and Feasibility, LHC Project Note 330, Geneva : CERN, (2003)

HE-LHC: REQUIREMENTS FROM BEAM VACUUM

J.M. Jimenez, CERN, Geneva, Switzerland

Abstract

First thoughts on the design of the beam vacuum system for the High Energy LHC (HE-LHC) are given with a particular focus on the impact of the synchrotron radiation. In the HE-LHC, the vacuum dynamic effects induced by the circulating beams are expected to be as compared to the LHC. These effects will be reviewed and first thoughts on how to avoid or mitigate their effects are discussed.

MACHINE PARAMETERS IMPACTING BEAM VACUUM

Even though the overall vacuum layout and integration issues could be very similar to the LHC [1], the parameter list of the HE-LHC [2] shows several changes, compared to the LHC, which can significantly affect the beam vacuum performances and stability [3].

The increase of the beam energy, of the bunch population, of the synchrotron radiation power and of the critical photon energy will influence the beam-induced effects taking place in vacuum systems which are linked both to the total intensity and to the bunched structure of the beams.

The decrease of the total number of circulating bunches, from 2808 to 1404 [2], will reduce the beam-induced effects in vacuum linked to the total beam intensity and will partly compensate the increase of the bunch population for the effects linked to the bunched structure of beams.

Finally, the increase of the beam potential resulting from the increase of the bunch population and emittance reduction, combined with the reduction of the magnet aperture will impact on the vacuum stability and electron cloud build up.

Desorption induced by primary beam losses

The sections at cryogenic temperature are the most critical due to the potentially large quantities of condensed gasses which can be released resulting from a local heat load. However, these sections are "protected" by the quench limit of the cryomagnets. Indeed, the cryomagnets quench level [4] i.e. the number of lost protons to create a transition to the normal state, correspond to a negligible pressure rise ($<<10^{-6}$ Pa). Primary beam losses will induce a local desorption of gasses but would never lead to a vacuum limitation.

Primary ionisation with circulating beams

The primary ionisation of the residual gas induced by the beams is linearly dependent on the ionisation cross section (about constant) and on the total intensity. As the ionisation cross-section is not expected to vary significantly between 7 and 16.5 TeV and taking into account the lower total intensity (60% of LHC), a similar effect as in the LHC is expected.

Ion induced instability

The ion induced instability is linearly dependent on the desorption yield (about constant), on the ionisation cross-section (also approximately constant), and on the total intensity (0.6 times smaller) and is inversely proportional to the effective pumping speed. The later become the dominant factor for the vacuum stability. To ensure the vacuum stability along the sections at cryogenic temperature, only the pumping speed available through the beam screen pumping slots is considered. Then, considering the new beampipe aperture, the transparency of the beam screen shall be increased to 6.2% (as compared to the 4.4 % of the LHC), which could imply impedance and HOM issues. This issue has still to be addressed.

Synchrotron radiation power

The synchrotron radiation power is proportional to the 4^{th} power of the energy and to the total beam intensity. An increase by a factor 17.3 is expected as compared to the LHC.

In the LHC, this heat load is intercepted by the beam screen. To keep such a design, an evaluation has to be made to ensure that the existing size of the cooling capillaries will be large enough to provide the cooling required. Any increase of the diameter of the capillary would lead to a further beam aperture reduction. An alternative could be to install photon absorbers in the cryomagnet interconnecting bellows (plug-in-modules), which would intercept the heat load outside the cryomagnets, in order to minimise the heat deposition onto the beam screens. The residual fraction of heat deposited on the beam screen would be determined by the length, aperture and bending angle of the dipole cryomagnets.

Linear photon flux

The photon flux per unit length depends linearly on the beam energy and intensity. This flux is 30% higher than in the nominal LHC. Similarly to the LHC, a sawtooth structure shall be used in the beam screen to reduce the photon reflection and the photo-electron yield.

Photon stimulated pressure rise

As compared to the LHC, the photon stimulated pressure rise is increased by a factor 7.4 since it grows with the 3^{rd} power of the beam energy and linearly with the beam intensity. This large increase is of concern for the vacuum system. Indeed, to ensure pressure stability,

the pumping should be increased by the same amount which would bring the equivalent transparency of the beam screen to 46%! As this transparency would probably not be compatible with impedance and HOM issues, the vacuum system will have to rely of the vacuum cleaning i.e. reduction of the desorption yield (η). Details studies shall be launched to estimate the duration of the vacuum cleaning and confirm that it stay compatible with the operation constraints.

Effects linked to the bunched structure of beams

The electron and ion cloud build-up are two avalanche phenomena which can take place in the beam pipe. Both are threshold effects i.e. only take place above a given bunch population. As compared to the LHC, the bunch population has been increased by 12%, 1.29×10^{11} p/bunch, well above the electron cloud threshold measured in the SPS i.e. 3.0×10^{10} p/bunch in a dipole field [5]. The beam potential has also been increased by 30% resulting from the smaller longitudinal and transverse emittances. Based on these new parameters, an electron cloud build up can be expected. However, the reduction of the number of bunches by a factor 2 and the resulting bunch spacing of 50 ns has shown its efficiency to reduce the electron cloud build up, e.g. a reduction by a factor 10, as measured in the SPS.

Two other parameters playing a major role in the electron build up are varying: the beam screen height is decreased from 36.8 to 26 mm and the magnetic field is increased by a factor 2.4. Changing the beam screen aperture could bring the system out of resonance conditions. Indeed, increasing the beam potential will increase the energy of the primaries and finally, the small Larmor radius (few micrometers for a 100 eV electron) can also change the SEY yield. Simulations have to be done to provide information on the electron cloud build-up i.e. threshold and saturation levels.

As the beam will ionise the residual gas and due to the slow motion of the ions and enhanced by the secondary ionisation effect by the trapped electrons from the cloud (if any), an ion-induced positive space charge can take place. This phenomenon opens the risk for feedback effects. However, the reduction of the beam pipe aperture will probably cancel this effect.

Feedback effects

In presence of an electron cloud, part of the electrons can be trapped by an ion space charge. These electrons will spiral along the magnetic field and contribute to an additional ionisation of the residual gas. This secondary ionisation effect can lead to ion instability. This effect still needs to be quantified.

Cold bore and beam screen operating temperature

To ensure a proper pumping of hydrogen, the dominant residual gas in the beam vacuum, an operating temperature for the cryomagnets below 2-3 K is recommended. At higher temperatures, the hydrogen released will condensed up to an equivalent of a monolayer and then, the equilibrium pressure (hydrogen partial pressure) will start increasing very fast with the temperature i.e. 10^{-9} Pa at 2 K and up to 10^{-4} Pa at 4.2 K [6]. Similarly to what was made in the LHC, a beam screen will be required to shield the condensed gasses on the cold bore from the beam induced effects (electrons, ions and photon-stimulated desorption). Above 2-3 K, the use of cryosorbers will be required to ensure the required hydrogen pumping speed and capacity. The option of an operating temperature of the beams screen between 85 and 100 K can also be studied.

A major obstacle to increase the operating temperature of the beam screen from 5-20 K to 85-100 K could be the unacceptable increase of the magneto-resistance of the beam screen. This issue shall be investigated.

REMEDIES TO VACUUM DYNAMIC EFFECTS

Synchrotron radiation

As made for the LHC, the use of a beam screen is required to intercept the synchrotron radiation induced heat load at a higher temperature. The use of photon absorbers will be considered, depending on magnet strength and length. At this stage of the discussion, the feasibility is not guaranteed. If considered, the cooling of these absorbers shall be decoupled from the cooling of the beam screens to preserve the cooling capacity of the beam screens. Similarly to what was done in the LHC, the photo-electron and photon reflection yields shall be reduced by using a sawtooth structure.

The photon and photo-electrons induced gas desorption will improve with time resulting from the vacuum cleaning effect (dose effect).

Ion induced instability

The design of the beam vacuum system shall be made to provide enough effective pumping speed considering beam pipe conductance. Considering the smaller aperture in the HE-LHC and the distributed induced gas desorption, the pumping provided by the pumping slots of the beam screen will dominate. The operating temperature of the cryomagnets is a key factor. As mentioned earlier, deeper calculations shall be made since the required transparency resulting from the preliminary estimations (46%) is certainly incompatible with impedance and HOM issues.

Electron cloud suppression or mitigations

The electron cloud is a fast avalanche and threshold phenomenon which behaviour depends on beam parameters. In existing machines, mitigation solutions are preferred since suppressing techniques cannot be easily retrofitted in an existing design.

For a new design, the suppressing techniques, e.g. techniques which prevent the electron avalanche to take place, shall be preferred. This will prevent any limitation for the future accelerator.

The suppressing techniques are often active solutions and the most commonly used are the clearing electrodes [7]. The use of clearing electrodes has many advantages since the electrodes capture the electrons right after their emission preventing any kind of avalanche effect. As compared to other solutions, this solution is not affected by venting to air and its efficiency is similar at ambient and cryogenic temperatures.

However their installation is complex since the clearing electrodes shall be in the vertical plane in the dipoles since electrons are confined along the dipole field lines. In the dipoles, the clearing electrodes shall be wide enough to cover the spacing of the vertical electron strips which spacing varies with bunch intensity.

An option for design could be to use the pumping port shields placed behind the pumping holes of the beam screens. Indeed, following the measurements made in the SPS, the LHC beam screens were equipped with shielding baffles placed between the beam screens and the cold bores and attached to the cooling capillaries. These baffles aim to intercept the electrons from the cloud, escaping from the beam screens through the pumping slots, to prevent the heat deposition onto the cold bore. Right from the design stage, the same configuration can be modified to convert the shielding baffles into clearing electrodes by insulating them from the cooling capillaries and polarising them to about 1 kV.

Coatings with a low secondary electron yield (SEY) are also mitigation solution to be considered. The coatings efficiencies depend on their ultimate SEY as compared with the needs of the accelerator.

Amorphous carbon coating is being considered in the SPS as LHC injector since it provides a low SEY (1.1) which is not affected by the venting to atmosphere. The behaviour of the amorphous carbon at cryogenic temperature will be investigated as an option for the sections operated at cryogenic temperatures. Another option is the NEG (TiZrV) coatings which also showed low SEY (1.1) after activation above 180°C. The need for a bake-out prevents its use in the sections at cryogenic temperature.

Scrubbing Runs

The scrubbing runs aim to reduce the desorption yields (η) and the SEY (δ) and to increase the bunch population threshold required to trigger an electron avalanche. This scrubbing effect is efficient only up to the bunch intensity used during the scrubbing periods, for a given filling pattern. Recent LHC studies with beams have confirmed the huge impact of the bunch spacing and length of bunch trains on the electron cloud build-up [8].

Measurements made in laboratories and observations on running accelerators have confirmed the efficiency of the scrubbing runs to decrease the electron cloud build-up. However, during these periods, the detectors cannot take any data during the scrubbing run since saturated by the background induced by the beam-gas scattering.

GAS LOAD ISSUES IN CRYOGENIC SECTIONS

Similarly to the LHC, the HE-LHC shall take into account thick gas coverage of the beam screens (BS) and the cold bores (CB) by atoms/molecules desorbed directly (beam losses) and indirectly (photons, electrons and ions). Indeed, this could lead to pressure oscillation and vacuum instabilities.

In practice, the expected coverage should not become a limiting factor since mitigation solutions exist. In case of thick gas coverage in the BS, it can be recycled by heating up to 80 K. The gas will be "flashed" towards the cold bore through the BS pumping holes. The conditions can be met during short technical stop (2-3 days) similarly to what is planned for the LHC.

In case of thick gas coverage in the CB, it can be recycled by warming-up to 80 K. The gas will be pumped away using mobile turbomolecular pumps. These conditions will be met in the LHC, once per year during the Christmas technical stop.

CLOSING REMARKS

Start-up scenario

An accelerator vacuum system cannot be designed for nominal performances as on day-one. Often, its design rely on vacuum cleaning (reduction of desorption yields η by photon, electron and ion bombardments) and on beam scrubbing (reduction of the secondary electron yields δ).

With bunched beams, two options are possible. The first option is to start the operation with the nominal number of bunches and progressively increase the intensity per bunch. This allows to benefit from the vacuum cleaning effects and therefore the effects linked to the bunched structure of beams (electron cloud and ion instability) are less limiting since stimulated desorption coefficients (η) would have decreased with time/dose before reaching bunch intensity thresholds for electron cloud. It is important to underline that the beam pipes with two circulating beams will behave differently.

The second option is to start the operation with the nominal bunch intensity and progressively increase the number of circulating bunches. This allows for higher luminosities with lower machine optimisation but all effects linked to the bunched structure of beams (electron cloud and ion instability) will be at their maximum. Using this scenario implies limitation for the operation since vacuum cleaning and beam scrubbing time will be required to improve the situation.

The LHC requires both a vacuum cleaning and scrubbing period but some constraints could slow down these improvements: background to the experiments, induced heat load to cryogenics and cryomagnet quench limits (beam-gas scattering) prevent operation with large electron cloud which should have lead to a faster vacuum cleaning and beam scrubbing.

Considering what was observed in other accelerator and in particular in the LHC, the HE-LHC shall go for more

conservative design: effects linked to the bunched structure of beams shall be suppressed at the design stage. This will help reducing the background to detectors and will help if the beam scrubbing of surfaces at cryogenic temperatures and cold/warm transitions is slower than initially considered. It will definitely save the operation in case the accumulation of the low energy electrons with high reflectivity (survivals) compensates the reduction of the secondary electron yield (SEY). Indeed, the beam scrubbing no longer help, photo-electrons production will dominate (design issue i.e. will not be significantly improving with time/dose).

Vacuum system design: preliminary considerations

The design of the HE-LHC beam vacuum shall be stable on day-one against ion-instability, reduce the number of photo-electrons and rely on vacuum cleaning (decrease of η_{ph}/η_{e-}) for gas desorption stimulated by synchrotron radiation and photo-electrons.

This design would imply the use of a beam screens but as compared to LHC, the following issues must be looked at:

- More pumping speed is required i.e. more pumping slots;
- Mechanical constraints: deformation with quench, impedance and HOMs;
- Cooling capillaries are required to cool down the beam screens
- Operating temperature of the beam screen between 85-100 K is being favored provided that the magnetoresistance of the beam screen stays compatible with impedance requirements;
- Cryosorbers are required in the cold bore side if the cryomagnets are operated above 3 K ;
- Clearing electrodes in dipoles behind the beam screens and attached to the cooling capillaries to suppress electron cloud, alternatively:
  - Proceed to a coating of quadrupoles and cold/warm transitions of standalone cryomagnets;
  - Use solenoids (3-5 mT) to mitigate electron cloud build up in vacuum instrumentation ports and interconnecting pieces which cannot be coated;
  - Long straight sections at ambient temperature should be baked and rely on NEG coatings, alternatively, install solenoids if the coating is not feasible.

These first thoughts on the design of the HE-LHC beam vacuum system need to be revisited once all pending issues have been correctly evaluated.

ACKNOWLEDGEMENTS

The author would like to thank O. Grobner and V. Baglin for their helpful discussions.

REFERENCES

[1] O. Brüning, et al., “The LHC Main Ring”, LHC Design Report, v.1, CERN (2004).

[2] R. Assmann, “First Thoughts on a Higher-Energy LHC”, CERN-ATS-2010-177 (2010).

[3] O. Gröbner, “Vacuum Issues for an LHC Upgrade”, 1st CARE-HHH-APD Workshop on Beam Dynamics in Future Hadron Colliders and Rapidly Cycling High-Intensity Synchrotrons, CERN (2004).

[4] J.-B. Jeanneret, “Quench levels and transient beam losses in LHC magnets”, LHC-Project-Report-44, CERN (1996).

[5] J. M. Jimenez, “Electron cloud with LHC-type beams in the SPS: A review of three years of measurements”, LHC-Project-Report-632, CERN (2003).

[6] C. Benvenuti, “Influence of thermal radiation on the vapor pressure of condensed hydrogen (and isotopes) between 2 and 4.5K”, J.Vac.Sci. 13(6), (1976), 1172-1182.

[7] D. Alessini, et al., “Design and Test of the Clearing Electrodes for e- cloud Mitigation in the e+ DAΦNE Ring”, EuCARD-CON-2010-043 (2010).

[8] F. Caspers, et al., “Comparison of Enamel and Stainless Steel Electron Cloud Clearing Electrodes Tested in the CERN Proton Synchrotron”, CERN-ATS-2009-129 (2009).

[8] J. M. Jimenez, et al., “Vacuum and Cryogenics observations for different bunch spacing”, Proc. of Chamonix 2011 LHC Performance Workshop, CERN (2011).

BEAM SCREEN ISSUES

E. Métral, CERN, Geneva, Switzerland

Abstract

In the High Energy LHC (HE-LHC), a beam energy of about 16.5 TeV is currently contemplated. The beam screen issues linked to the use of 20 T dipole magnets instead of 8.33 T are discussed, with a particular emphasis on two mechanisms, the magneto-resistance and the anomalous skin effect, assuming the nominal machine and beam parameters. The magneto-resistance effect always leads to an increase of the material resistivity (as the mean free path in the presence of a transverse magnetic field becomes smaller). As concerns the anomalous skin effect, the anomalous increase of surface resistance of metals at low temperatures and high frequencies is attributed to the long mean free path of the conduction electrons: when the skin depth becomes much smaller than the mean free path, only a fraction of the conduction electrons moving almost parallel to the metal surface is effective in carrying the current and the classical theory breaks down.

INTRODUCTION

In the LHC, about 90% (i.e. the beam screen) is maintained between 5 and 20 K, while the other 10% is at room temperature (with a 2 mm thick copper beam pipe). The main purpose of the beam screen is to shield the cold bore from the synchrotron radiation and it is made of stainless steel to resist to the mechanical stresses. A copper coating with a thickness of 75 μm is used to keep the resistivity as low as possible for the transverse resistive-wall coupled-bunch instability [1]. The latter is a low-frequency phenomenon, from a few kHz to a few MHz, where the Magneto-Resistance (MR) effect is important and must be correctly taken into account. The power loss is a more involved issue due, in addition, to the short bunch length, the Anomalous Skin Effect (ASE) and the surface roughness (both important at high frequencies). A much smaller copper thickness could have been chosen (of the order of 1 μm) if only this effect had to be taken into account. The drawback from copper coating is the eddy currents, which are mainly concentrated in the copper layer in the cases of magnet's quenches. Therefore, for the quench force consideration, which deforms the beam screen horizontally, the smaller the copper coating thickness the better.

It is worth mentioning that the other impedance issues carefully studied in the past were the pumping slots (needed for the vacuum) and the longitudinal weld. Furthermore, I will not discuss here (as it will be discussed elsewhere) the important issue of Synchrotron Radiation (SR), even if in the HE-LHC the power would be increased by ~ 30 (from ~ 3.8 kW for one beam to ~ 120 kW: the scaling goes with the fourth power of the energy) and the critical photon energy by ~ 13 (from ~ 43 eV to ~ 574 eV: the scaling goes with the magnetic field times the square of the energy), keeping all the other parameters constant.

In this paper, the current LHC beam screen is reviewed in Section 1. The MR effect is discussed in Section 2, recalling first what was done in the past, which was an approximation of the approximated Kohler's rule. The exact and approximate Kohler's rules are then discussed in some detail. Finally, Section 3 is devoted to the ASE, first reviewing what was done in the past, i.e. using the approximate formula, and then studying the exact formula from Reuter & Sondheimer.

CURRENT LHC BEAM SCREEN

Figure 1 shows a beam screen design as it was built and installed in the LHC. It is worth mentioning that in the dipoles, some baffles (i.e. shields of the pumping slots) were installed (see Fig. 1), to avoid a direct e^- path along the magnetic field lines to the cold bore (which would then add to the heat load). For the arc beam screens, the inner dimension between flats (i.e. between the two flat parts of the beam screen) is 36.8 mm and the inner dimension between radii (i.e. between the two circular parts of the beam screen) is 46.4 mm. The

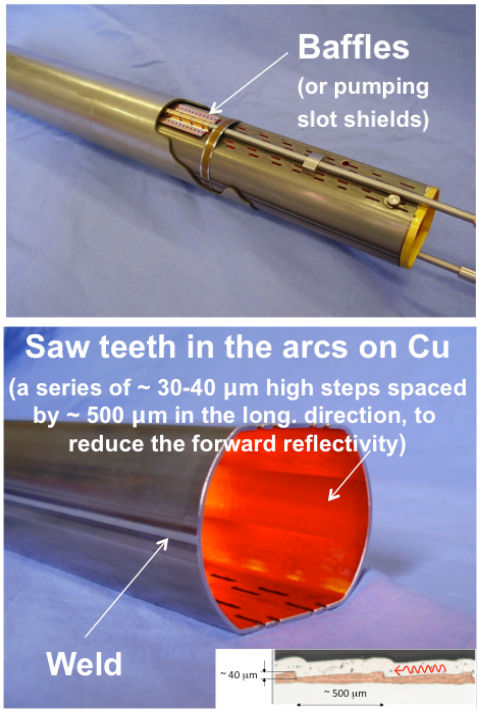

Figure 1: Beam screen as it was built and installed in the LHC (Courtesy of N. Kos).

stainless steel thickness is 1.0 mm and the copper coating thickness is 75 μm. For the LSS (Long Straight Section) beam screens, the inner dimension between flats varies between 37.6 mm and 61.0 mm, and the inner dimension between radii varies between 47.2 mm and 70.7 mm. The stainless steel thickness is 0.6 mm and the copper coating thickness is still 75 μm. The lengths of the slots needed for the vacuum pumping are 6, 7, 8, 9 or 10 mm, i.e. 8 mm on average. The width of the slots is 1.5 mm in the arcs and 1.0 mm in the LSS. Finally, the total surface covered by the holes is ~ 4.0% in the arcs, while it varies between ~ 1.8% and ~ 2.6% in the LSS, depending on the screen diameter.

The power loss from the induced currents in the beam screen (neglecting the holes) at 7 TeV/c is given by (the same numerical result is obtained with the more precise multi-layer impedance formula [2])

$$P_{loss/m}^{G,RW,1\,\mathrm{layer}} = \frac{1}{2\pi R}\,\Gamma\!\left(\frac{3}{4}\right)\frac{M}{b}\left(\frac{N_b\,e}{2\pi}\right)^2\sqrt{\frac{c\,\rho\,Z_0}{2}}\;\sigma_t^{-3/2} \quad (1)$$
$$\approx 85\ \mathrm{mW/m}\,,$$

where $R \approx 4243$ m is the average machine radius, $\Gamma(3/4) \approx 1.23$ the Euler gamma function, $M = 2808$ the number of bunches, $b = 18.4$ mm the beam screen half height, $N_b = 1.15\,10^{11}$ p/b the number of protons per bunch, e the elementary charge, c the speed of light, ρ the resistivity (i.e. $5.5\,10^{-10}$ Ωm for copper at 20 K), Z_0 the free space impedance (i.e. 377 Ω), and $\sigma_t = 0.25$ ns is the bunch length. Note that the power loss goes with the square of the bunch charge, which means that it is ~ 2 times higher for the ultimate intensity (1.7×10^{11} p/b) than for the nominal one (1.15×10^{11} p/b).

The power loss from the induced currents in the weld are given by

$$P_{loss/m}^{Weld} \approx P_{loss/m}^{G,RW,1\,\mathrm{layer}}\sqrt{\frac{\rho_{SS}^{20K}}{\rho_{Cu}^{20K}}}\;\frac{\Delta_l^{Weld}}{2\pi b} \approx 48\ \mathrm{mW/m}\,, \quad (2)$$

with

$$\frac{\Delta_l^{Weld}}{2\pi b} = \frac{2}{2\pi\,18.4} = \frac{1}{\pi\,18.4} \approx \frac{1}{60}\,, \quad (3)$$

where $\rho_{SS}^{20K} = 6\times10^{-7}$ Ωm . Therefore, even though the weld corresponds to only ~ 1/60 of the cross-section, the power loss due to the weld is not negligible at all and amounts to ~ 57% of the power loss without the weld.

If one compares the previous estimates with what was computed in the past for a single beam [3], we find that instead of the 85 mW/m a value of 110 mW/m (based on measurements of LHC dipole beam screen samples without magnetic field and subsequent extrapolation) is quoted (noting that the ASE, not yet taking into account here, gives an increase by ~ 11%). Note also that ~ 80 mW/m were obtained from simulations [4]. Concerning the weld, 10 mW/m were mentioned in Ref. [3] instead of the 48 mW/m computed in Eq. (2), while ~ 27 mW/m were found in Ref. [4]. Finally, ~ 1 mW/m is found for the most critical pumping holes in the arc beam screen (which is very close to the result of Ref. [5]), whereas 10 mW/m are mentioned in Ref. [3].

The transverse resistive-wall impedance in the classical regime, which is a good approximation in the present case, is given by

$$Z_\perp^{RW}(\omega) = (1+j)\,\frac{L\,Z_0}{\pi\,b^3}\sqrt{\frac{\rho}{2\,\mu_0\,\omega}}\,, \quad (4)$$

where j is the imaginary unit, L the longitudinal length of the structure, μ_0 the vacuum permeability and ω is the angular frequency. It can be seen that it is proportional to the square root of the resistivity and that it goes with the inverse of the pipe radius to the power of three. The transverse impedance should be weighted by the transverse betatron function at the location of the impedance to correctly model the beam dynamics. Using the exact dimensions of all the beam screens and the correct local transverse betatron functions, the transverse coupled-bunch instabilities were studied and the results for the horizontal plane are shown in Fig. 2. It should be reminded that - Im (ΔQ) / 10^{-4} = 1 corresponds to a rise time of ~ 1600 turns, i.e. ~ 140 ms, and that the transverse feedback should be able to damp down to ~ 20–40 turns [6]. It can be seen from Fig. 2 that the beam screen contributes very little to the real part of the tune shift (which is dominated by all the collimators), but contributes significantly (~ 50%) to the imaginary part.

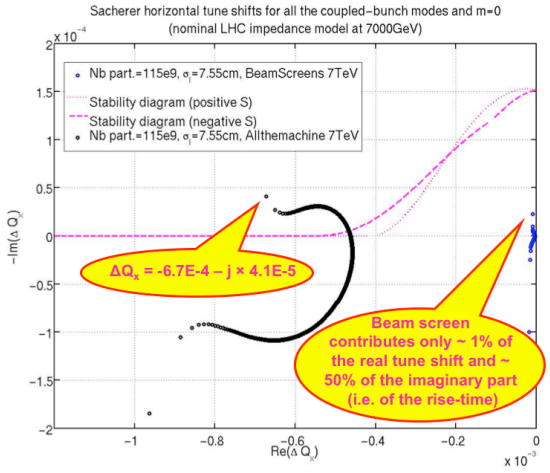

Figure 2: Horizontal tune shifts using Sacherer's formula [7] for all the coupled-bunch modes, for the head-tail mode 0 and for 0 chromaticity (using the LHC impedance model at 7 TeV/c). The two purple curves describe the stability diagrams with maximum otupoles' current [3]. Courtesy of N. Mounet.

MAGNETO-RESISTANCE (MR)

How were the values of the beam screen copper resistivity at low (i.e. injection) and high (i.e. top energy) magnetic field obtained? In Ref. [8], the following formula, referred to as "Kohler's law", was used

$$\frac{\rho(B,T)-\rho_0(T)}{\rho_0(T)}=\frac{\Delta\rho}{\rho_0}=10^{-2.69}\left(B\,RRR\right)^{1.055}, \qquad (5)$$

where B is the magnetic induction, T the temperature, ρ_0 the resistivity at temperature T but without magnetic field, and $RRR = R(273\,\mathrm{K})/R(T)$ is the Residual Resistance Ratio, which is a measure of purity of a material. Note that the resistance and resistivity are linked by the relation $R = \rho\, l / S$ (for long thin conductors), where l is the length and S the cross-sectional area, which means that $\Delta R / R_0 = \Delta\rho / \rho_0$.

As the resistivity decreases with temperature towards a minimum (determined by purity), the *RRR* is sometimes defined as the ratio of the DC resistivity at room temperature to its cold-DC lower limit (see Fig. 3) [9].

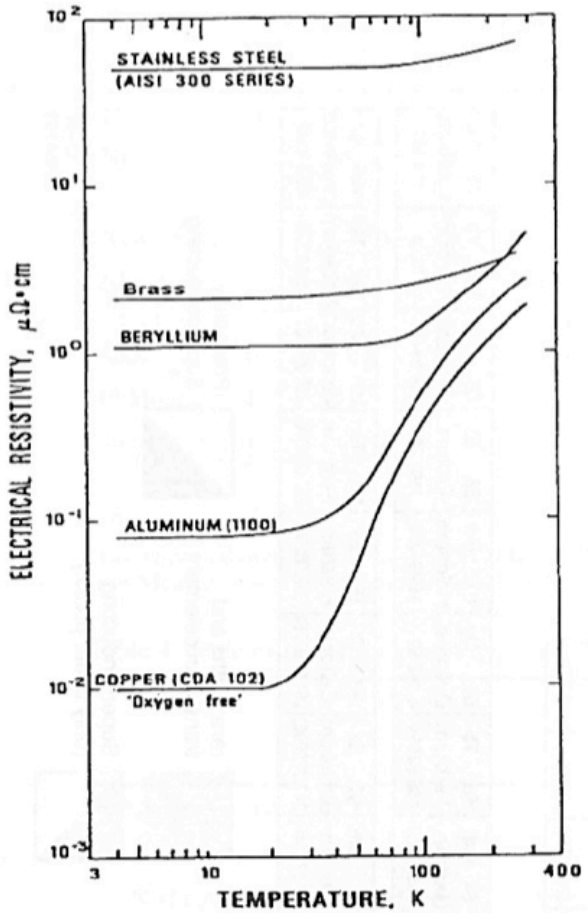

Figure 3: Resistivity of several metals vs temperature, in the absence of magnetic field.

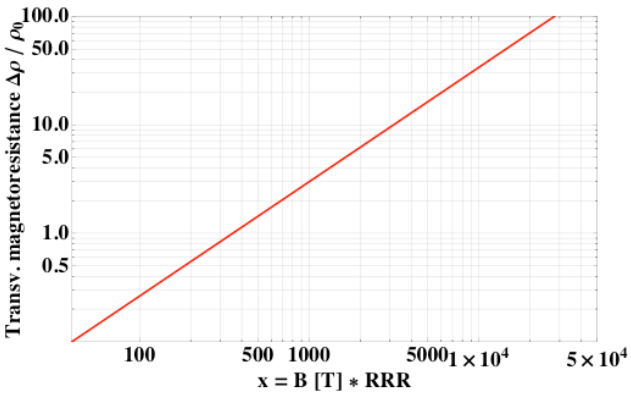

Figure 4: Plot of the approximate formula (of the approximate Kohler's rule) given by Eq. (5).

Assuming a *RRR* of 100 and a resistivity at 20 K of $1.55\,10^{-10}$ Ωm, yields a resistivity at 20 K and 0.535 T (i.e. for the injection energy) of $1.8\,10^{-10}$ Ωm and a resistivity at 20 K and 8.33 T of $5.5\,10^{-10}$ Ωm. Using the same formula as Eq. (5) yields a resistivity at 20 K and 20 T of $11.2\,10^{-10}$ Ωm. The plot of the approximate formula (of the approximate Kohler's rule) is given in Fig. 4. For 0.535 T, $x = 53.5$ (see Fig. 4) and $\Delta\rho/\rho_0 \approx 0.14$. For 8.33 T, $x = 833$ and $\Delta\rho/\rho_0 \approx 2.5$. For 20 T, $x = 2000$ and $\Delta\rho/\rho_0 \approx 6.2$.

It is worth mentioning that in general care must be exercised when applying Kohler's rule to the magneto-resistance of some conductors (including high Tc-superconductors), where the density of charge carriers might change with temperature [10]. In fact, Kohler's rule may take two forms, one exact and one approximate. If there is only one relaxation rate in the transport process of a certain conductor, the exact Kohler's rule writes

$$\frac{\Delta\rho}{\rho_0}=F\left(H\,\tau\right), \qquad (6)$$

which is generally a tensor, where $H = B/\mu_0$ is the magnetic field, τ the relaxation rate (or time) and F is a function given only by the intrinsic electronic structure and external geometry of the conductor. The link between the relaxation time and the DC resistivity under 0 magnetic field can be found by using Ohm's law for a wire carrying a current density. The equation of motion for one electron is

$$m\frac{d\vec{v}}{dt}=-e\,\vec{E}-\alpha\,\vec{v}, \qquad (7)$$

where m is the electron mass, $\vec{v}$ the velocity, t the time, $\vec{E}$ the electric field, and $\alpha = m/\tau$. In permanent (DC) regime, $d\vec{v}/dt = 0$ and $\vec{J} = -N\,e\,\vec{v} = \sigma_{DC}\,\vec{E}$ is the current density, where N is the density of carriers and

$$\rho_0 = \frac{1}{\sigma_{DC}} = \frac{m}{N\, e^2\, \tau}. \tag{8}$$

The exact Kohler's rule of Eq. (6) can then be re-written

$$\frac{\Delta\rho}{\rho_0} = F\left(\frac{H}{\rho_0}\,\frac{m}{N\, e^2}\right). \tag{9}$$

If the factor $m/(N\, e^2)$ does not change with temperature, then Kohler's rule can be simplified to

$$\frac{\Delta\rho}{\rho_0} = F\left(\frac{B}{\rho_0}\right). \tag{10}$$

Equation (10) is Kohler's rule in its approximate but often used form. Most of the problem comes from N, which could be very sensitive to the temperature in various conductors. Equation (10) can be rewritten

$$\frac{\Delta\rho}{\rho_0} = F\left(B\, RRR\right), \tag{11}$$

as

$$\rho_0 = \rho_0(T) \propto \frac{1}{RRR}. \tag{12}$$

Equation (11) is the form of Kohler's law used for instance in Ref. [9], where the corresponding plot is shown in Fig. 5.

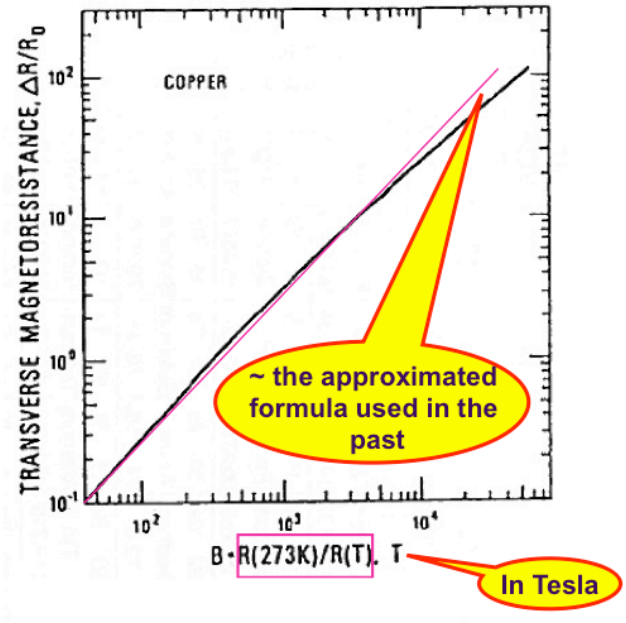

Figure 5: Kohler's plot for copper [9].

Experimental observations tell us that there is always an increase in resistance when the magnetic field is increased and that for small magnetic fields the resistance increase is proportional to the square of the magnetic field, whereas it becomes linear for very high magnetic fields. Note that Aluminum is an interesting material as concerns the magneto-resistance as it is one of the few materials which deviate from Kohler's rule [11] (a kind of saturation is observed; however, the secondary emission yield is very high, which prevents it from being used in machines where electron clouds could develop). But, why is there always an increase in resistance with increasing magnetic field? To answer this question it is useful to introduce two parameters, the mean free path of the electrons and the cyclotron radius. The mean free path $\lambda = \lambda(0)$ of a particle in the absence of magnetic field, is the average distance covered by a particle between successive impacts: $\lambda = \upsilon\,\tau$. This leads to

$$\lambda = \frac{m\,\upsilon}{e^2\, N\, \rho_0}. \tag{13}$$

As concerns the cyclotron radius, a particle, with a constant energy, describes a circle in equilibrium between the centripetal magnetic force and the centrifugal force, which leads to the cyclotron radius

$$r = \frac{m\,\upsilon}{e\, B}. \tag{14}$$

It can be seen from Eqs. (13) and (14), that

$$\frac{B}{\rho_0} \propto \frac{\lambda}{r}. \tag{15}$$

The case of a small transverse magnetic field is described in Fig. 6, where it can be seen that a smaller mean free path in the direction of motion is obtained, which means a larger resistivity (see Eq. (13)). Using the Taylor expansion of the sin function up to the second term, the mean free path can be approximated by

$$\lambda(H) \approx \lambda(0)\left\{1 - \frac{1}{6}\left[\frac{\lambda(0)}{r}\right]^2\right\}, \tag{16}$$

which leads to

$$\frac{\Delta\rho}{\rho_0} = -\frac{\Delta\lambda}{\lambda_0} \propto \left[\frac{\lambda(0)}{r}\right]^2 \propto \left[\frac{B}{\rho_0}\right]^2. \tag{17}$$

Equation (17) reveals indeed that for a small transverse magnetic field, the increase in resistivity due to the magneto-resistance is proportional to the square of the magnetic field.

Electrical measurements of beam screen wall samples in magnetic fields were performed in Ref. [13], which revealed that the trend line slopes of the voltage for all samples were always higher than the theoretical curves by

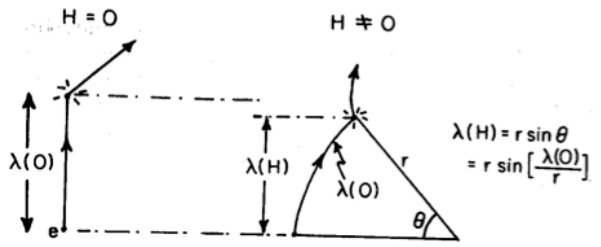

Figure 6: Reduction of the mean free path in the direction of motion in the presence of a transverse magnetic field. Courtesy of Jeff Fitzgerald [12].

~ 20% (see Fig. 7). These results confirmed the assumption of a heterogeneous *RRR* in the co-laminated copper layer: the copper close to the steel gets contaminated during the fabrication process such that the surface impedance is increased. The increase of the resistance has been compensated by increasing the thickness of the copper layer from 50 to 75 μm [3].

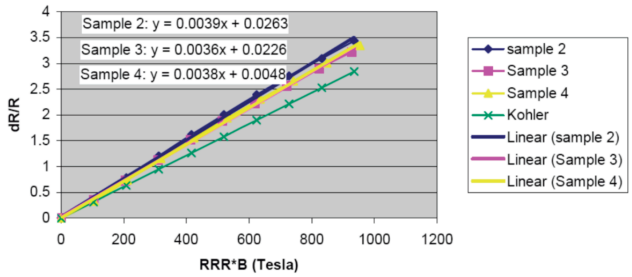

Figure 7: Electrical measurements of beam screen wall samples in magnetic fields compared to Kohler's formula. Courtesy of C. Rathjen [13].

ANOMALOUS SKIN EFFECT (ASE)

The ASE theory attributes the anomalous increase of surface resistance of metals at low temperatures and high frequencies to the long mean free path of the conduction electrons. When the skin depth becomes much smaller than the mean free path, only a fraction of the conduction electrons moving almost parallel to the metal surface is effective in carrying the current and the classical theory breaks down. Some measurements were performed in Ref. [14], which were in relatively good agreement with predictions.

In the Normal Skin Effect (NSE), the skin depth and surface resistance are given respectively by

$$\delta = \sqrt{\frac{2\,\rho}{\omega\,\mu_0}} \quad \text{and} \quad R_s^{\mathrm{NSE}} = \frac{\rho}{\delta} = \sqrt{\frac{\omega\,\mu_0\,\rho}{2}}\,. \tag{18}$$

In the ASE, and approximate formula for the surface resistance was used in the past [15], which is valid when $\alpha \geq 3$ and which is given by

$$R_s^{\mathrm{ASE}} = R_\infty \left(1 + 1.157\,\alpha^{-0.276}\right), \tag{19}$$

with

$$\alpha = \frac{3}{2}\left(\frac{\lambda}{\delta}\right)^2 = \frac{3\,\omega\,\mu_0}{4\,\rho^3}\left(\rho\,\lambda\right)^2, \tag{20}$$

$$R_\infty = \left[\frac{\sqrt{3}}{16\,\pi}\,\rho\,\lambda\left(\omega\,\mu_0\right)^2\right]^{1/3} = 1.123\times 10^{-3}\ \Omega\left(\frac{f}{\mathrm{GHz}}\right)^{2/3}. \tag{21}$$

The parameter R_∞ is independent of temperature and impurity, and $\rho\,\lambda = m\,\upsilon / (e^2\,N)$ is a characteristic of the metal, equal to $6.6\,10^{-16}\ \Omega\mathrm{m}^2$ for copper. The relative increase of the heating power (assuming that the ASE formula is valid over the full frequency range) is given by (with σ_z the rms bunch length in meters)

$$\frac{P_{ASE}}{P_{NSE}} = \frac{\int_{\omega=0}^{\omega=+\infty} d\omega\, R_s^{ASE}(\omega)\, e^{-\left(\frac{\omega\,\sigma_z}{c}\right)^2}}{\int_{\omega=0}^{\omega=+\infty} d\omega\, R_s^{NSE}(\omega)\, e^{-\left(\frac{\omega\,\sigma_z}{c}\right)^2}}\,. \tag{22}$$

Considering an rms bunch length $\sigma_z = 7.5\,\mathrm{cm}$ leads to an increase by ~ 46% at injection (using the resistivity $1.8\,10^{-10}\ \Omega\mathrm{m}$), an increase by ~ 11% at 8.33 T (using the resistivity $5.5\,10^{-10}\ \Omega\mathrm{m}$), and an increase by ~ 4% at 20 T (using the resistivity $11.2\,10^{-10}\ \Omega\mathrm{m}$). The plots of the

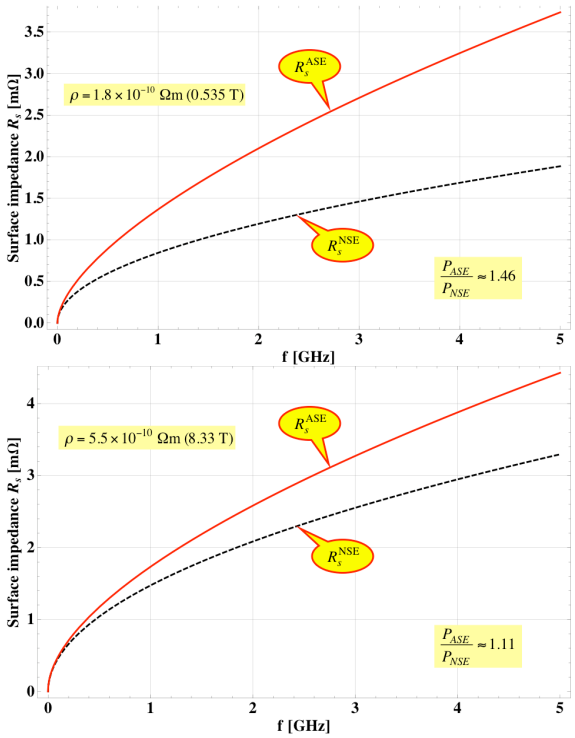

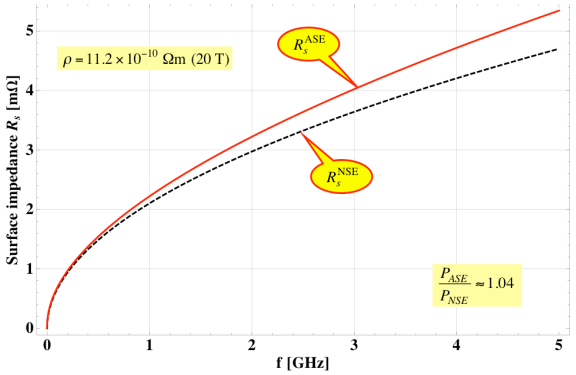

Figure 8: Surface impedance vs. frequency for both the NSE and ASE, assuming that they are valid over the full frequency range, for 0.535 T, 8.33 T and 20 T.

surface impedance in both the NSE and ASE are shown in Fig. 8.

Sergio Calatroni implemented the exact (full) formula from Ref. [16], for the specular reflection of the electrons (which is the usual approximation; the diffuse contribution is close to this result). It is compared to the approximate formula of Eq. (19) in Fig. 9, where it can be seen that the exact formula converges to the NSE result at high temperature and to the limit R_∞ at low temperature, whereas the approximate formula does not. Another interesting plot is shown in Fig. 10, where both the NSE and exact ASE formulae are plotted vs. *RRR* and magnetic field, for the particular frequency of 1 GHz. It is shown that for sufficiently high magnetic fields the result from NSE and ASE converge, and that in this case only the magneto-resistance needs to be taken into account as the ASE is small.

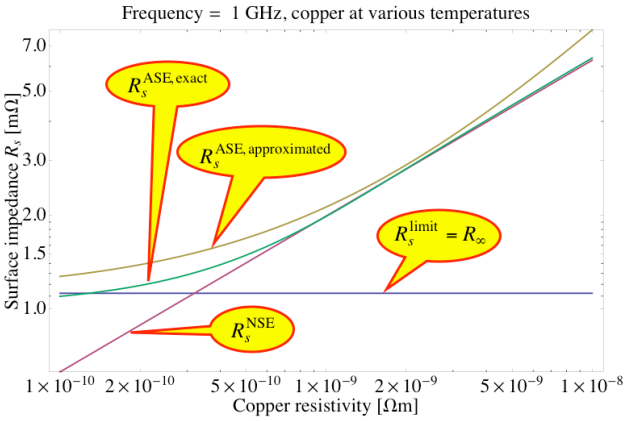

Figure 9: Surface impedance vs. copper resistivity (i.e. for different temperatures) and for the frequency of 1 GHz. The exact formula [16] is compared to the NSE and approximate ASE ones. This plot was made using the available *Mathematica* Notebook of Sergio Calatroni.

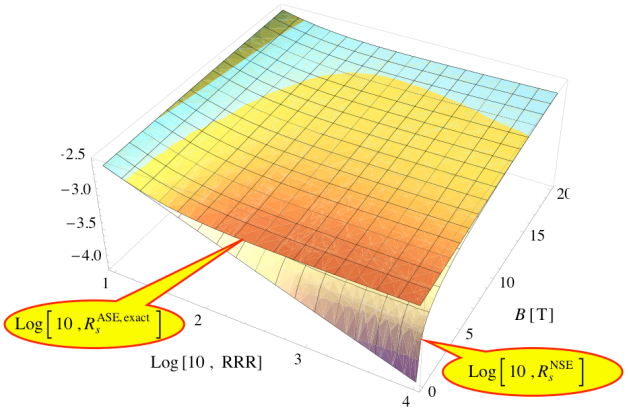

Figure 10: NSE and exact ASE formulae vs. *RRR* and magnetic field for the particular frequency of 1 GHz. This plot was made using the available *Mathematica* Notebook of Sergio Calatroni.

CONCLUSIONS AND OUTLOOK

The magneto-resistance is the dominant effect for the beam screen in the HE-LHC with 20 T dipole magnets and the anomalous skin effect can be neglected. The beam screen copper resistivity at top energy increases from ~ 5.5 10^{-10} Ωm (at 7 TeV/c) to ~ 11.2 10^{-10} Ωm (at 16.5 TeV/c), i.e. by a factor ~ 2.

As the longitudinal and transverse impedances scale with the square root of the resistivity, they are larger by ~ 40%, which should not be an issue for beam stability.

The total present power loss (from ohmic losses, pumping slots and the weld) is ~ 150 mW/m for one beam at 7 TeV/c. At 16.5 TeV/c, it increases only slightly to ~ 175 mW/m. Here again, no problem is expected.

In conclusion, no issues are anticipated for the beam screen if the beam energy is increased from 7 TeV/c to ~ 16.5 TeV/c. However, other impedance issues might arise with the collimators, whose gaps will be smaller and the transverse mode-coupling instability might be critical. It is worth reminding that at 7 TeV/c, the intensity threshold from the (single-bunch) transverse mode-coupling instability is estimated at (only) ~ 2 times the ultimate intensity. Furthermore, the threshold should even be smaller when taking into account the coupled-bunch effects [17], which are currently under study.

ACKNOWLEDGEMENTS

It is a pleasure for me to thank S. Calatroni for all the very interesting discussions we had on magneto-resistance and anomalous skin effects. I would like also to thank V. Baglin, F. Caspers and N. Kos for helpful information.

REFERENCES

[1] F. Ruggiero, Single-Beam Collective Effects in the LHC, Particle Accelerators, Vol. 50, pp. 83-104, 1995.

[2] N. Mounet, private communication, 2010.

[3] O. Brüning et al. (Editorial Board), LHC Design Report, Vol. I The LHC Main Ring, Chap. 5, CERN-2004-003, 4 June 2004.
[4] A. Mostacci, Beam-Wall Interaction in the LHC Liner, CERN-THESIS-2001-014, 2001.
[5] A. Mostacci, Beam-Wall Interaction in the LHC Liner: a Former PhD Student Experience, Francesco Ruggiero Memorial Symposium, CERN, 3 October 2007.
[6] W. Hofle, private communication, 2009.
[7] A.W. Chao, Physics of Collective Beam Instabilities in High Energy Accelerators, New York: Wiley, 371 p, 1993.
[8] F. Caspers et al., Surface Resistance Measurements and Estimate of the Beam-Induced Resistive Wall Heating of the LHC Dipole Beam Screen, LHC Project Report 307, 1999.
[9] A.W. Chao and M. Tigner (Editors), Handbook of Accelerator Physics and Engineering, 2nd Printing, p. 368.
[10] N. Luo and G.H. Miley, Kohler's Rule and Relaxation Rates in High-Tc Superconductors, Physica C 371 (2002) 259-269.
[11] L. Vos, Beam Vacuum Chamber Effects in the CERN Large Hadron Collider, CERN SPS/85-14 (DI-MST), 1985.
[12] Jeff Fitzgerald, Magnetoresistance, Physics 211A.
[13] A. Gerardin, Electrical Measurements of Beam Screen Wall Samples in Magnetic Fields, EST/SM-ME investigation report, EDMS N.329882.
[14] F. Caspers et al., Surface Resistance Measurements of LHC Dipole Beam Screen Samples, Proc. 7th EPAC, Vienna, Austria, 26-30 June 2000.
[15] W. Chou and F. Ruggiero, Anomalous Skin Effect and Resistive Wall Heating, LHC Project Note 2 (SL/AP), 1995.
[16] G.E.H. Reuter and E.H. Sondheimer, The Theory of the Anomalous Skin Effect in Metals, Proc. Royal Society (London), A195, 336 (1948).
[17] J.S. Berg and R.D. Ruth, Transverse Instabilities for Multiple Nonrigid Bunches in a Storage Ring, Physical Review E, Vol.52, N.3, September 1995.

SYNCHROTRON RADIATION DAMPING, INTRABEAM SCATTERING AND BEAM-BEAM SIMULATIONS FOR HE-LHC

A. Valishev, Fermilab, Batavia, IL 60510, U.S.A.

Abstract

The proposed High-Energy LHC project presents an unusual combination of strong synchrotron radiation (SR) damping and intrabeam scattering (IBS), which is not seen in present-day hadron colliders. The subject of investigation reported in this paper was the simulation of beam-beam effect for the HE-LHC parameters. Parameters of SR and IBS are calculated, and the luminosity evolution is simulated in the absence of beam-beam interaction. Then, a weak-strong numerical simulation is used to predict the effect of beam-beam interaction on particle losses and emittance evolution.

MACHINE AND BEAM PARAMETERS

Main parameters of HE-LHC relevant for our calculations are presented in Table 1.

Table 1: Machine and beam parameters

Parameter	Value
Beam energy	16.5 TeV
Number of bunches	1404
Number of interaction points	2
Bunch population	1.3×10^{11}
Initial normalized transverse emittance	3.75, 1.84 (x,y) μm
Initial momentum spread	0.9×10^{-4}
RF voltage	32 MV
Beta-function at IP	1.0, 0.43 (x,y) m
Full crossing angle	175 μrad

PARAMETERS OF SYNCHROTRON RADIATION

Calculation of synchrotron radiation integrals was based on current LHC optics V6.5. Main parameters of SR and equilibrium emittance were derived using the conventional formulae [1] (see Table 2):

$$U_0 = \frac{C_\gamma}{2\pi} E^4 I_2$$

$$\tau_{x,y} = \frac{ET_0}{U_0}, \tau_E = \frac{ET_0}{2\cdot U_0}$$

$$\frac{d\varepsilon_x}{dt} = -\frac{\varepsilon_x}{\tau_x} + \frac{55}{48\sqrt{3}}\frac{\hbar c}{T_0}\frac{r_0}{mc^2}\gamma^5 I_5$$

Table 2: Synchrotron radiation parameters

Parameter	Value
Synchrotron radiation integrals	I_2=0.002245 m^{-1}
	$I_3=7.99\times10^{-7}$ m^{-2}
	$I_5=2.11\times10^{-8}$ m^{-1}
Energy loss per turn	U_0=206.3 keV
SR power	67 kW
Emittance damping time	τ_x, τ_y=1.93 h
	τ_E=0.96 h
Normalized equilibrium emittance	0.01 μm
Equilibrium momentum spread	3.4×10^{-6}

Note that the equilibrium emittance and momentum spread due to synchrotron radiation are much smaller than the initial values, and the damping time is significantly shorter than the expected store duration (10 hours).

INTRA-BEAM SCATTERING AND LUMINOSITY EVOLUTION

Intrabeam scattering was treated in the smooth optics approximation by V.Lebedev [2] with the main parameters listed in Table 3.

$$\frac{d}{dt}\begin{pmatrix}\varepsilon_x\\ \varepsilon_y\\ \sigma_E^2\end{pmatrix} = \frac{Nr_0^2 cL_c}{4\sqrt{2}\beta^3\gamma^3\sigma_x\sigma_y\sigma_z\theta_\perp}\begin{pmatrix}\langle A_x\rangle_s\\ 0\\ 1\end{pmatrix}$$

Table 3: Parameters of IBS

Parameter	Value
Lattice parameters (LHC V6.5)	$\langle\beta_x\rangle$=104.8 m
	$\langle\beta_y\rangle$=109.4 m
	$\langle A_x\rangle$=2.29
Horizontal emittance growth time	82 h
Longitudinal emittance growth time	72 h

Evolution of the beam parameters and luminosity was then calculated via the numerical solution of the following system of equations:

*Fermilab is operated by Fermi Research Alliance, LLC under Contract No. DE-AC02-07CH11359 with the United States Department of Energy.

$$\frac{d\varepsilon_x}{dt} = -\frac{2\varepsilon_x}{\tau_{SRx}} + \frac{d\varepsilon_{xSR}}{dt} + \frac{d\varepsilon_{xIBS}}{dt} + \frac{d\varepsilon_{xBB}}{dt}$$

$$\frac{d\varepsilon_y}{dt} = -\frac{2\varepsilon_y}{\tau_{SRy}} + \frac{d\varepsilon_{ySR}}{dt} + \frac{d\varepsilon_{yIBS}}{dt} + \frac{d\varepsilon_{yBB}}{dt}$$

$$\frac{d\sigma_E^2}{dt} = -\frac{2\sigma_E^2}{\tau_{SRE}} + \frac{d\sigma_{SR}^2}{dt} + \frac{d\sigma_{IBS}^2}{dt} + \frac{d\sigma_{BB}^2}{dt}$$

$$\frac{dN}{dt} = -N_{IP}\frac{L}{N_b}\sigma_{tot}$$

Here L is the luminosity, N_b is the number of bunches, σ_{tot} is the p-p interaction cross-section, N_{IP} is the number of IPs, indices SR, IBS and BB label the emittance growth (or damping) rates for synchrotron radiation, intrabeam scattering, and scattering at IPs, respectively. These growth rates are calculated at every step of numerical integration for current beam parameters.

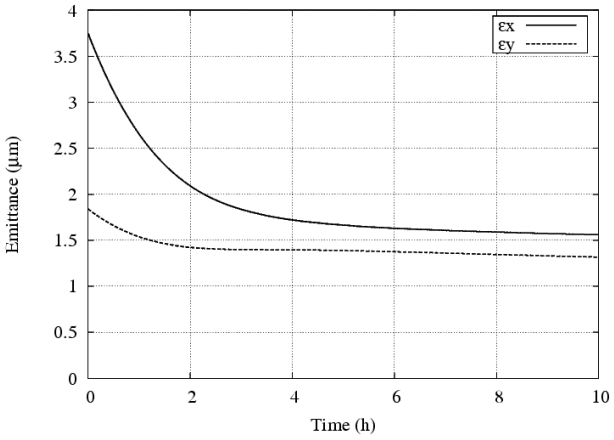

Figure 1: Evolution of transverse emittances.

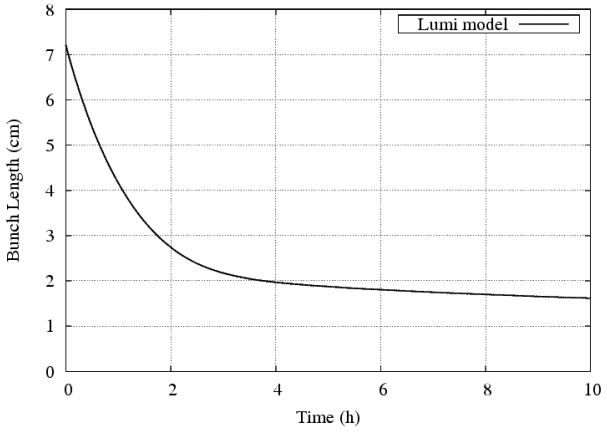

Figure 2: Evolution of bunch length.

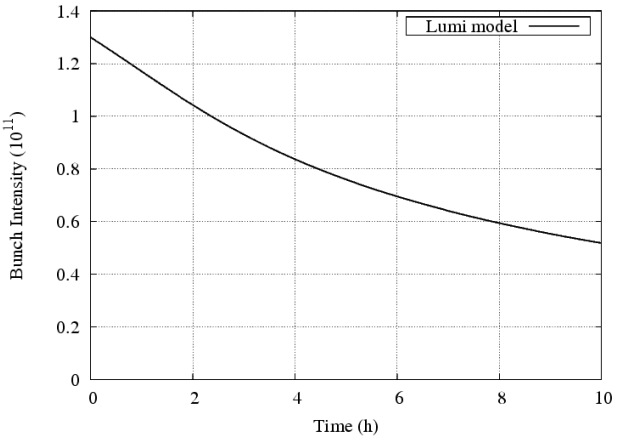

Figure 3: Evolution of bunch intensity.

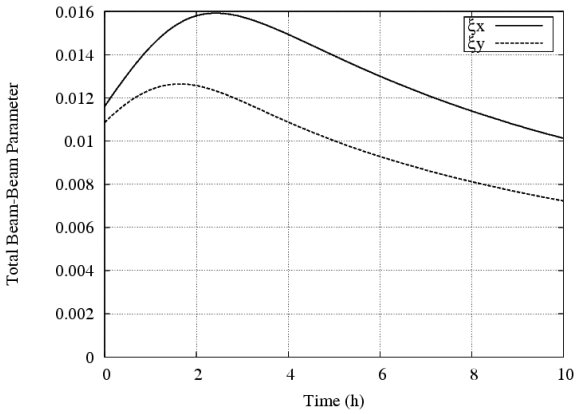

Figure 4: Beam-beam parameters vs. time.

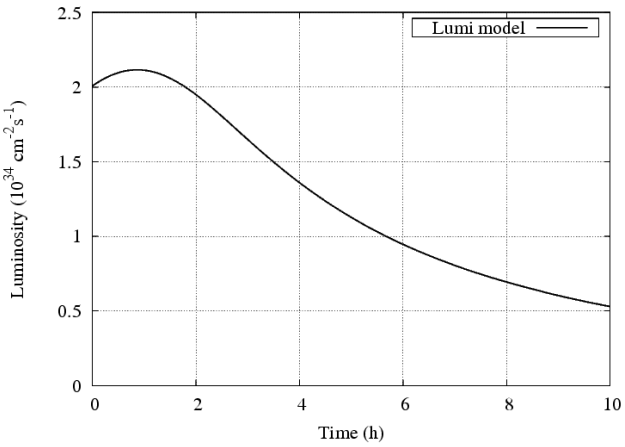

Figure 5: Evolution of luminosity. Luminosity integral over 10 h is 450 pb^{-1}.

Figures 1-5 present the calculated evolution of beam parameters over a period of 10 hours. An important feature of the beam dynamics is the reduction of transverse emittances due to synchrotron radiation by approximately a factor of two. Combined with the beam intensity decay caused by luminous particle losses, this results in the increase of the total beam-beam parameter by 50% (from the initial value of 0.01 to 0.016).

BEAM-BEAM SIMULATION

Numerical simulation was performed with the use of weak-strong tracking code Lifetrac. A bunch of 5,000 macro-particles with weighted Gaussian initial distribution was tracked for 5×10^7 turns (which corresponds to 1.2 h of beam time) in order to evaluate the importance of beam-beam effects. The machine optics was represented by linear 6D maps, no long-range collisions were considered. The synchrotron radiation damping, quantum excitation and intrabeam scattering were represented by kicks applied once per turn. The code does not include particle losses due to luminosity and diffusion caused by scattering at the IPs.

Figures 6-8 present the results of numerical simulation along with the curves obtained using the luminosity evolution model described in the previous section. Numerical simulation did not produce any particle losses. One can see that beam-beam interaction does not cause additional emittance growth.

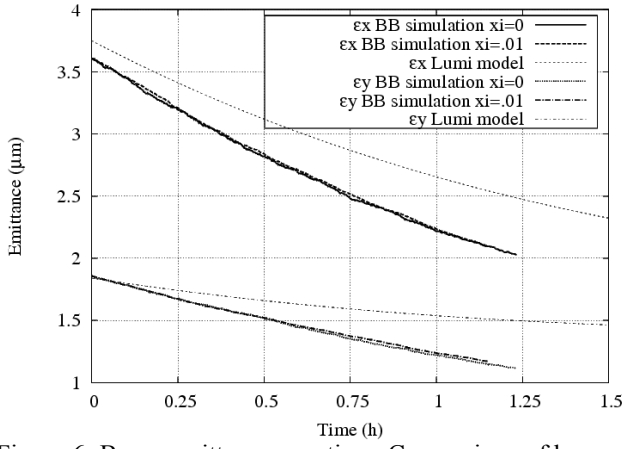

Figure 6: Beam emittances vs. time. Comparison of beam-beam simulation and luminosity model.

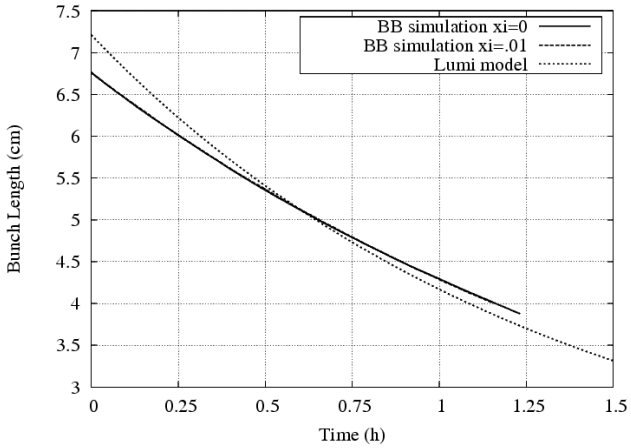

Figure 7: Comparison of bunch length from numerical beam-beam simulation and luminosity model.

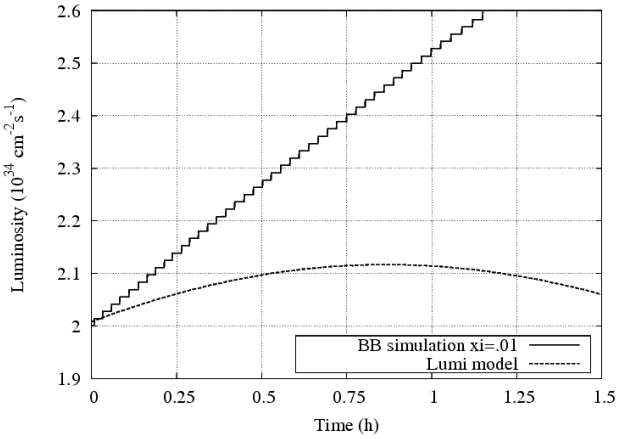

Figure 8: Luminosity vs. time. Beam-beam simulation and luminosity evolution model. Numerical curve is higher owing to the absence of the luminous beam decay in the model.

SUMMARY

Combination of parameters of the proposed High Energy LHC produces beam dynamics not observed at present hadron colliders. Synchrotron radiation causes emittance damping with the characteristic time of 2 hours. Intrabeam scattering, typically the dominant effect, is relatively weak with the initial emittance growth rate of 70 hours. As the beam emittance decreases, synchrotron radiation and intrabeam scattering come to equilibrium, a situation typical for low emittance electron damping rings. The resulting beam emittance is approximately half of the initial value. As the result, the beam-beam parameter experiences growth over the initial 2 hours of the store.

Numerical simulations with a weak-strong particle tracking code, which included major effects, predict that beam-beam effects would cause no particle losses. The evolution of beam emittance is not modified by beam-beam interaction. Modeling confirms that the luminosity integral of 450 pb^{-1} over 10 hours is achievable. The simulations employed a simplified accelerator model, in which no nonlinearities existed. Hence it is reasonable to expect extra losses due to machine nonlinearities.

REFERENCES

[1] A. Chao, M. Tigner, Handbook of Accelerator Physics and Engineering, World Scientific, 1999

[2] V. Lebedev, http://lhc-commissioning.web.cern.ch/lhc-commissioning/presentations/2010/VL_LHC_LuminosityEvolution.pdf

BEAM-BEAM STUDIES FOR THE HIGH-ENERGY LHC

K. Ohmi, KEK, Tsukuba, Japan; O. Dominguez, F. Zimmermann, CERN, Geneva, Switzerland

Abstract

LHC upgrades are being considered both towards higher luminosity (HL-LHC) and towards higher energy (HE-LHC). In this paper we report initial studies of the beam-beam effects in the HE-LHC [1]. The HE-LHC aims at beam energies of 16.5 TeV, where the transverse emittance decreases due to synchrotron radiation with a 2-hour damping time. As a result of this emittance, shrinkage the beam-beam parameter increases with time, during a physics store. The beam-beam limit in the HE-LHC is explored using computer simulations.

INTRODUCTION

At the High-Energy LHC, the proton beam energy is increased from the present LHC design energy of 7 TeV to an upgrade value of 16.5 TeV. The HE-LHC target luminosity is 2×10^{34} cm^{-2} s^{-1}. The parameters of the nominal and the High-Energy LHC are summarized in Table 1. The radiation damping time, which is 1 and 2 hours for the longitudinal and transverse plane, respectively, will be visible in operation.

The equilibrium horizontal emittance and energy spread that would arise from a balance of radiation damping and random quantum excitation (as in a typical electron storage ring) are very small, $\varepsilon_x \sim 5 \times 10^{-12}$ m and $\sigma_p \sim 1.1 \times 10^{-5}$, respectively. At the quantum equilibrium the diffusion rates per turn of the quantum radiation excitation are $\langle\Delta\varepsilon_x\rangle = 5.8 \times 10^{-20}$ m and $\langle\Delta\varepsilon_z\rangle = 4.2 \times 10^{-15}$ m, respectively, in the absence of any additional blowup. Assuming 20% emittance coupling, the vertical emittance and diffusion rate are $\varepsilon_y = 1 \times 10^{-12}$ m and $\langle\Delta\varepsilon_y\rangle = 1.2 \times 10^{-20}$ m respectively.

Table 1 Parameter list of nominal and high-energy LHC

	nominal	HE-LHC
Beam Energy (TeV)	7	16.5
Bunch population	1.15×10^{11}	1.29×10^{11}
Emittance *x*/*y* (m)	5.1×10^{-10}	$2.1/1.0 \times 10^{-10}$
Bunch length (m)	0.0755	0.065
Energy spread (10^{-4})	1.13	0.9
β^* *x*/*y* (m)	0.55/0.55	1/0.43
Damping time x&y/z (h)	25.8/12.9†	1.97/0.98†
Number of bunches	2808	1404
Luminosity (cm^{-2} s^{-1})	1.0×10^{34}	2.0×10^{34}

†Here the damping time refers to the emittance decrease, $\varepsilon_i = \varepsilon_{0,i} \exp(-t/\tau_i)$, not to amplitude. The amplitude damping times would be two times longer.

The quantum equilibrium is not reached, however, since intra-beam scattering (IBS) also causes a random excitation of the beam. The IBS diffusion rate depends on the phase space volume of the beam. The diffusion rate due to intra-beam scattering can be estimated using the nominal LHC optics and the MADX IBS module. The emittance growth rates found in this way are 64, 400 and 80 hours for the horizontal, vertical and longitudinal plane, respectively, at the initial design emittance. The diffusion rates per turn translate to $\langle\Delta\varepsilon_x\rangle = 6.6 \times 10^{-20}$ m, $\langle\Delta\varepsilon_y\rangle = 6.5 \times 10^{-21}$ m and $\langle\Delta\varepsilon_z\rangle = 2.3 \times 10^{-15}$ m. Therefore, initially the transverse rates are comparable to the radiation excitation. The diffusion rates of the intra-beam scattering strongly increase for smaller beam emittances. The equilibrium emittances reached due to the interplay of intra-beam diffusion and radiation damping are calculated as 8.6×10^{-11} m, 1.7×10^{-11} m and 1.4×10^{-6} m. At this IBS equilibrium, the diffusion rates per turn are 1.1×10^{-18} m, 4.2×10^{-20} m and 3.5×10^{-15} m. The beam-beam parameters for these emittances and with the initial bunch charge are 0.018 (*x*) and 0.025 (*y*). Keeping the longitudinal emittance constant, equal to 2.5 eVs, by means of an external excitation, the transverse equilibrium emittances become 5.1×10^{-11} m (*x*) and 1.0×10^{-11} m (*y*), resulting in the diffusion rates per turn of 6.2×10^{-19} m (*x*) and 2.5×10^{-20} m (*y*). Figure 1 shows the evolution of the emittance as a function of time. The beam-beam parameters for the final emittances are 0.026/IP (*x*) and 0.037/IP (*y*). In equilibrium with the radiation damping, the diffusion rate always equals $\langle\Delta\varepsilon_i\rangle = \varepsilon_i T_0/\tau_I$, or $\langle\Delta x^2\rangle^{1/2} = (T_0/\tau_x)^{1/2}\sigma_{x,eq} = 1.1 \times 10^{-4}\sigma_{x,eq}$.

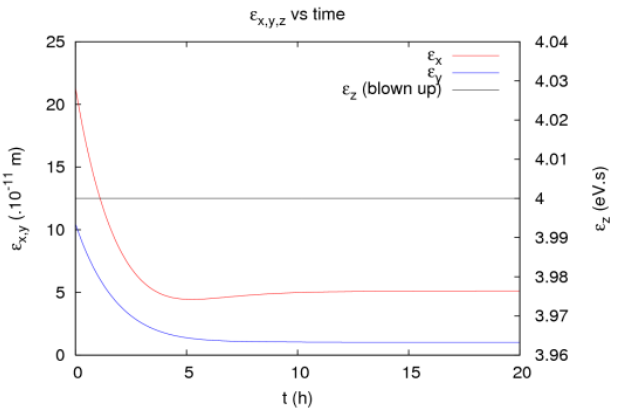

Figure 1: Horizontal and vertical emittances as functions of time. The radiation damping and the diffusion due to intra-beam scattering are taken into account, while proton burn off is not. It is assumed that the longitudinal emittance is continually blown up, so as to acquire a constant value of 4 eVs ($=4\pi\sigma_E\sigma_t$).

In this report, we do not take into account the proton loss due to the collision, partly since the bunch population

and the operation scheme are not yet fixed for HE-LHC. Instead the beam-beam limit related to the damping of the emittance is an interesting subject for us. In the beam-beam simulation, diffusion with a constant rate is taken into account in each plane. Our diffusion model does not represent the exact IBS diffusion. This approximation is justified if the emittances and diffusion rates do not vary enormously during the course of the simulation.

We discuss coherent and incoherent effects due to the beam-beam interaction by considering the high geometrical beam-beam parameters 0.026/IP (x) and 0.037/IP (y), and the aforementioned corresponding values for the IBS diffusion rates.

COHERENT EFFECT IN HE-LHC

In this section, we discuss coherent beam-beam effect using the strong-strong beam-beam simulation code BBSS. We consider a single interaction point. The collision is simulated by 2D model: i.e., the crossing angle is not taken into account. The actual diffusion rate is very small considering the typical statistics of the simulation using 1 million (0.1%) macro-particles and the resulting numerical noise. The simulations using the real radiation damping and the diffusion rate are hard for the computation time.

We study several model cases with faster damping times (and correspondingly increased diffusion rates) and then try to extrapolate the results to the real case. The damping times are assumed to be either 3.55 or 35.5 s, which is 2000 or 200 times faster than for the HE-LHC. The case with 20 time faster damping time has also been tried, but definite results could not be obtained within an acceptable calculation time.

Figure 2 shows the evolution of the luminosity and the beam size for the damping time of 3.55 s. The difference of the top and bottom two plots is the existence (top) or absence of diffusion (bottom). The diffusion rates of 6×10^{-17}(x) and 6×10^{-18} m (y) per turn are taken to be 200 times bigger than the actual IBS diffusion rates (together with the 2000 times faster damping rate leading to a ten times smaller equilibrium emittance), because the natural IBS diffusion rate is smaller than the noise induced by the limited number of macro-particles. The left plots of Fig. 2 display the luminosity per bunch and the beam size. The luminosity increases over the first 15-17 $\times 10^4$ turns, and then drops. At the same time the beam size shrinks up to the same number of turns and then increases. The beam-beam parameters calculated from the beam size, and the dipole amplitudes of the both beam are depicted in the right-hand plots. We can see that the luminosity drop is caused by a coherent dipole-mode beam-beam instability. The beam-beam parameter where the coherent instability arises is quite high, ξ=0.15. Already earlier, another weaker coherent instability is seen, after about 8×10^4 turns, in the top right picture. The beam-beam parameter is 0.03-0.04 at the occurrence of this weak coherent instability. Luminosity degradation is not visible here, and the weak instability disappears after 10^5 turns. The instability is also seen for the diffusion free case in the right bottom plot, though the amplitude is weaker than on the right top. The diffusion may enhance the coherent motion.

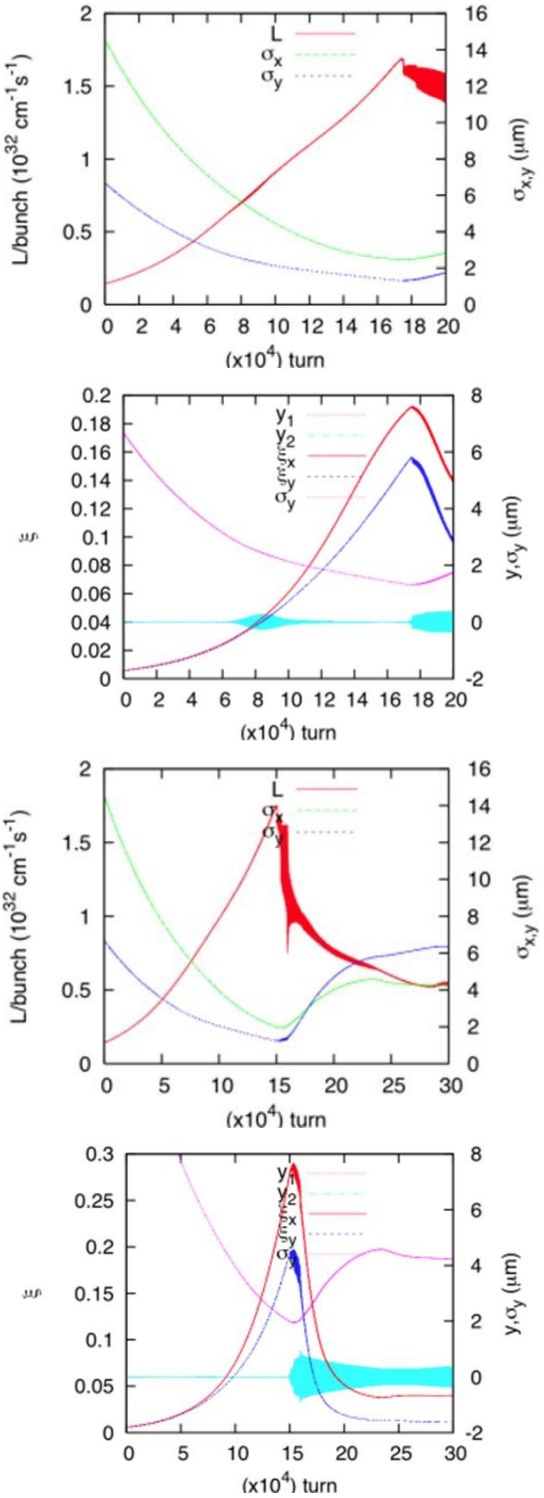

Figure 2: Evolution of the luminosity, beam size, beam-beam parameter and vertical dipole amplitudes. The difference between the top two and bottom two plots is existence (top) or absence of diffusion (bottom). The damping time is assumed to be 3.55 s (4,000 turns).

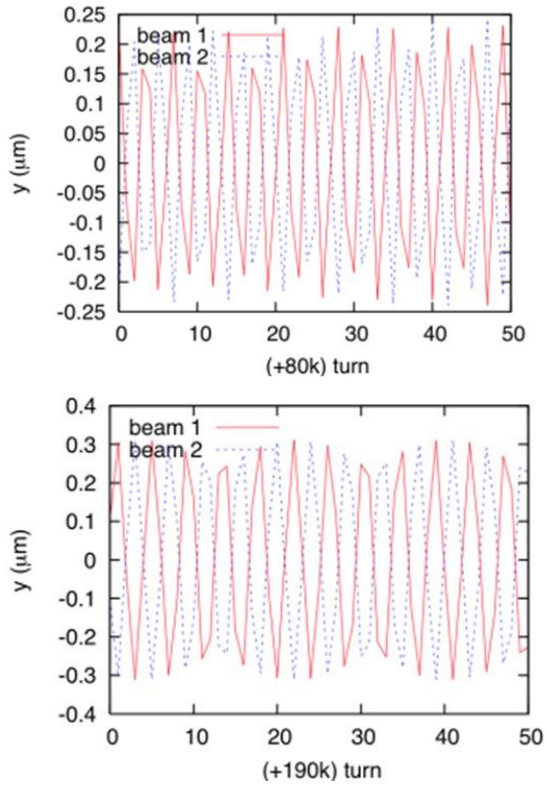

Figure 3: Coherent motion seen in Figure 1. The plots show the dipole amplitudes of the two colliding beams, in the presence of diffusion.

Figures 3 and 4 illustrate the coherent dipole amplitudes of the two colliding beams and Fourier spectrum of the motion for one beam, respectively. We clearly notice a π mode signal in both the beam oscillation and Fourier spectra.

Figure 5 shows the luminosity and beam size for the ten times slower damping time 35.5 s without diffusion. The results roughly scale by a factor ten in time compared with those obtained for the damping time of 3.55 s. The weak instability now occurs around 800,000 turns, though it is hard to see it in the figure. The strong coherent instability appears after about 1,800,000 turns. In view of the good scaling the results may be extrapolated to the case of the real damping time, in a straightforward manner. Actually, an incoherent emittance growth due to the beam-beam interaction dominates for the damping time, as is shown in next section. In addition, the emittance growth from IBS would also limit the beam size. Therefore such high beam-beam parameter is not realized in practice. A simulation with an "IBS" diffusion rate 20 times bigger than the actual one was also attempted, for the 35.5 s damping time. Here the incoherent emittance growth due to beam-beam and IBS dominated, i.e., the emittance did not shrink sufficiently to induce any coherent motion.

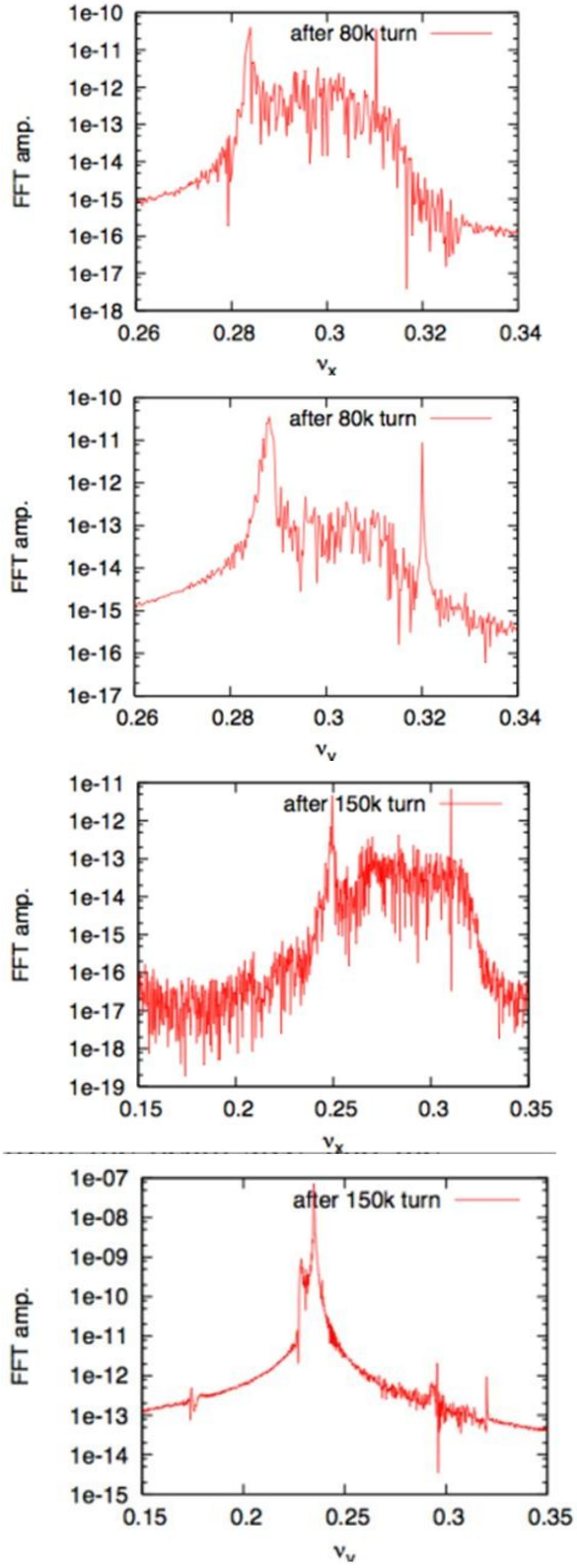

Figure 4: Fourier amplitude of the coherent motion for weak and strong instabilities seen after about 80000 and 180000 turns, respectively, in the presence of diffusion. Top and bottom plots display the horizontal and vertical signal, respectively.

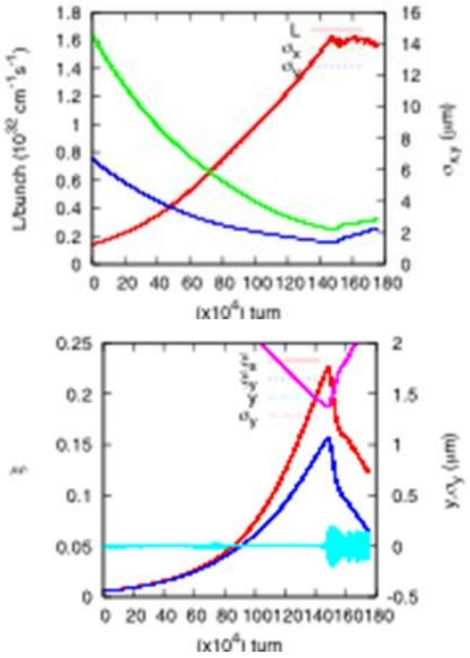

Figure 5: Evolution of the luminosity, beam size, beam-beam parameter and dipole amplitudes for the diffusion-free case. The damping time is assumed to be 35.5 s (40,000 turns).

INCOHERENT BLOWUP IN HE-LHC

Incoherent emittance growth for the HE-LHC is studied using a weak-strong simulation code (BBWS). Two interaction points are taken into account. A bunch is sliced into 5 pieces along the longitudinal direction. A crossing angle of 170 μrad is taken into account.

A full simulation with the realistic damping time is again too time consuming. Therefore, a weak-strong simulation is performed for various periods of time after starting the collision. We study how a high beam-beam parameter enhances the incoherent emittance growth, in the presence of radiation damping. Table 2 shows the emittance of each stage, in which the simulation is performed. Note that IBS limits the emittance and beam-beam parameters to (ε_x, ε_y)=(0.051, 0.011) nm and -(ξ_x, ξ_y)=(0.026, 0.037), which roughly corresponds the case of t=4-5 h. (The equilibrium emittance is realized by overshooting after 10 h in Fig. 1, because the true diffusion rate is a function of emittance.) In the simulation, a smaller emittance (i.e. smaller than the design value of Table 1) is introduced in order to investigate beam-beam emittance growth rate at higher beam-beam parameter.

Figure 6 shows the luminosity evolution at each stage of the beam storage listed in Table 2. The bunch population is kept equal to the initial value. The luminosity for the emittance after t=0, 1 and 2 hours (-ξ<0.013/IP) does not degrade at all. The luminosity degradation is visible for the emittance after t≥3 hours (-ξ>=0.021/IP). The degradation rate, which is defined as the inverse of luminosity exponential life-time in units of turns, is summarized in Fig. 7. The degradation rates corresponding to luminosity life-times of 1 hour and 1 day, respectively, are depicted in the figure. The beam-beam limit for 1day luminosity life is -ξ_y=0.013/IP. Since the damping time is 2 hours for HE-LHC, the limit is -ξ_y=0.02/IP.

Table 2: Expected time evolution of emittance and beam-beam parameter for HE-LHC at top energy due to radiation damping, without proton consumption

t (h)	ε_x (nm)	ε_y (nm)	ξ_x (/IP)	ξ_y (/IP)
0	0.21	0.1	0.0051	0.0052
1	0.13	0.062	0.0080	0.0084
2	0.076	0.037	0.012	0.013
3	0.046	0.022	0.017	0.021
4	0.027	0.014	0.023	0.031
5	0.016	0.0097	0.029	0.042

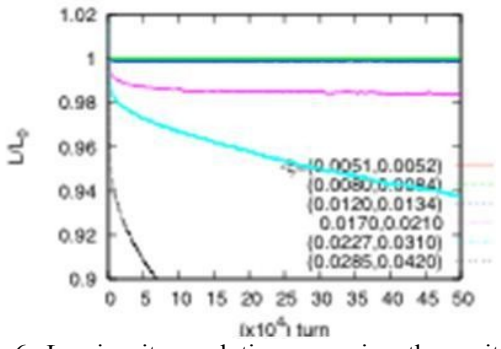

Figure 6: Luminosity evolution assuming the emittance expected after t=0-5 hours. The legend is corresponding beam-beam parameters to the emittance.

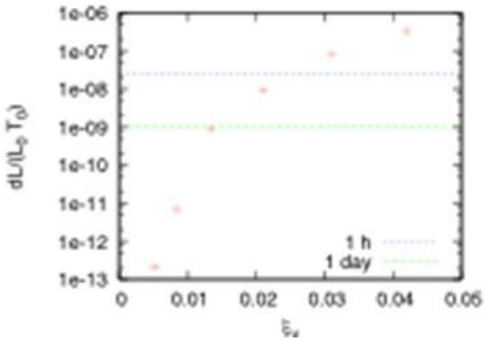

Figure 7: Luminosity degradation rate as function of the vertical beam-beam parameter.

A major source of the luminosity degradation is the crossing angle. Fig. 8 shows the luminosity degradation for collisions without crossing angle (left) and for 285 μrad crossing (right). This simulation was done for the nominal LHC. The luminosity lifetime without crossing angle is 10 times better than the one with the

nominal crossing angle. A similar behaviour has also been seen in simulations for KEKB [2].

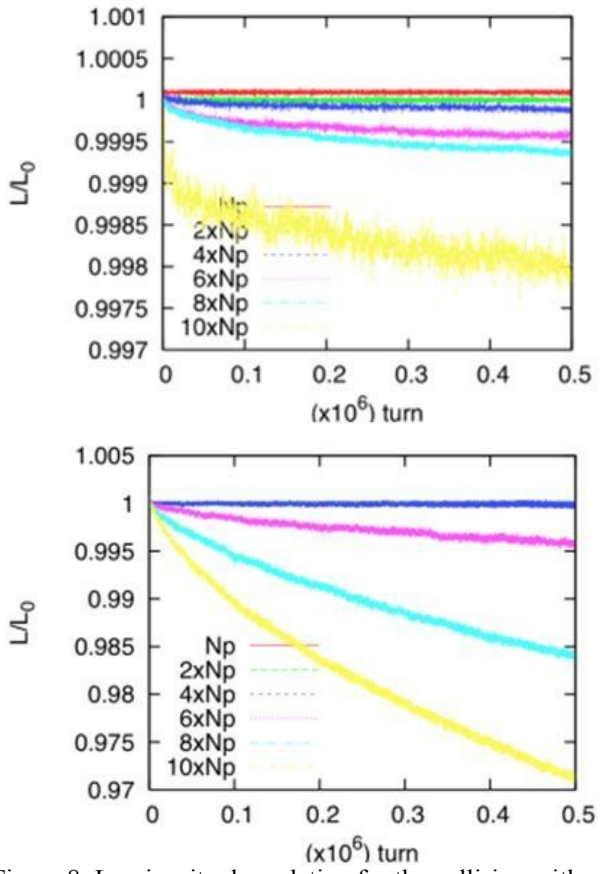

Figure 8: Luminosity degradation for the collision without crossing angle (top) and for 285 μrad crossing (bottom). This simulation was performed for the nominal LHC, with two collision points and alternating crossing.

EFFECT OF X-Y COUPLING AND DISPERSION FOR THE HE-LHC

In KEKB, the optimization of the linear *x-y* coupling and also of the chromatic coupling at the IP is indispensable to keep a high luminosity during the operation. Tuning of the parameters had continued for 24 hours every day.

The 6x6 revolution matrix, which contains 21 parameters, is parameterized by three sets of Twiss parameters $(\alpha, \beta, \nu)_{xyz}$, four *x-y* coupling parameters, and up to eight dispersion parameters, as follows,

$$M = H^{-} R^{-} M_2 R H$$

$$M = \begin{pmatrix} M_x & 0 & 0 \\ 0 & M_z & 0 \\ 0 & 0 & M_z \end{pmatrix}$$

$$M_i = \begin{pmatrix} \cos\mu + \alpha \sin\mu & \beta \sin\mu \\ -\gamma \sin\mu & \cos\mu - \alpha \sin\mu \end{pmatrix}$$

$$R = \begin{pmatrix} r_0 & 0 & r_4 & -r_2 & 0 & 0 \\ 0 & r_0 & -r_3 & r_1 & 0 & 0 \\ -r_1 & -r_2 & r_0 & 0 & 0 & 0 \\ -r_3 & -r_4 & 0 & r_0 & 0 & 0 \\ 0 & 0 & 0 & 0 & 1 & 0 \\ 0 & 0 & 0 & 0 & 0 & 1 \end{pmatrix}$$

$$H = \begin{pmatrix} 1 & 0 & 0 & 0 & 0 & -\eta \\ 0 & 1 & 0 & 0 & 0 & -\eta' \\ 0 & 0 & 1 & 0 & 0 & -\eta_{,} \\ 0 & 0 & 0 & 1 & 0 & -\eta_{,}' \\ \eta' & -\eta & \eta_{,}' & -\eta_{,} & 1 & 0 \\ 0 & 0 & 0 & 0 & 0 & 1 \end{pmatrix}$$

where four parameters related to $x=\zeta z$ have already been omitted, assuming that there is no transverse kick dependent on z, e.g. no crab cavity, and no cavity placed in a dispersive ($\eta \neq 0$) section. For KEKB the revolution matrix at the collision point determines the collision performance. The tuning performed in KEKB is just a luminosity optimization, performed by scanning r1-r4 and η_y, η_y' at the collision point.

We first discuss the effects of the *x-y* coupling on the coherent instability. Figure 9 shows the luminosity (beam-beam parameter) evolution for the case of damping time of 3.5sec. Three lines are given, corresponding to no-coupling, r1=0.01 and 0.05. The threshold for the coherent instability is higher the larger x-y coupling. Perhaps the x-y coupling suppresses the excitation of the coherent mode. However, the suppression is not drastic. The same simulations were done for the other coupling parameters r_2-r_4. The results were similar: the threshold beam-beam parameter is always higher for larger *x-y* coupling, but the gain is hardly significant.

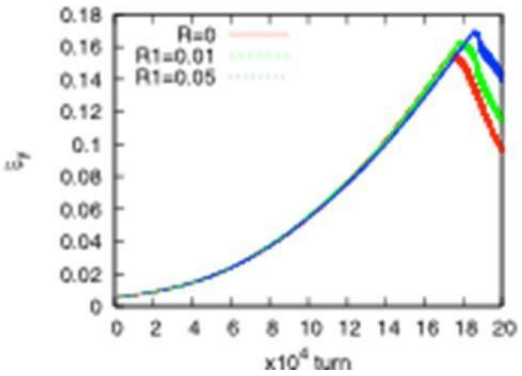

Figure 9: Evolution of beam-beam parameter with or without *x-y* coupling (varying the coupling parameter r_1).

Next we discuss the incoherent emittance growth in the presence of *x-y* coupling. Figure 10 shows the luminosity degradation with *x-y* coupling or vertical dispersion. The simulation is performed for a beam-beam parameter of $-\xi_y$=0.02/IP. The 5 plots illustrate the impact of changing r_1-r_4 and η_y, respectively. The sensitivity to any of these parameters is quite weak. For KEKB, the

tolerances were around r_1~0.003, r_2~0.001, r_3~r_4~0.1. The much reduced sensitivity for the LHC seems to be due to the difference of round (LHC) and flat beams (KEKB).

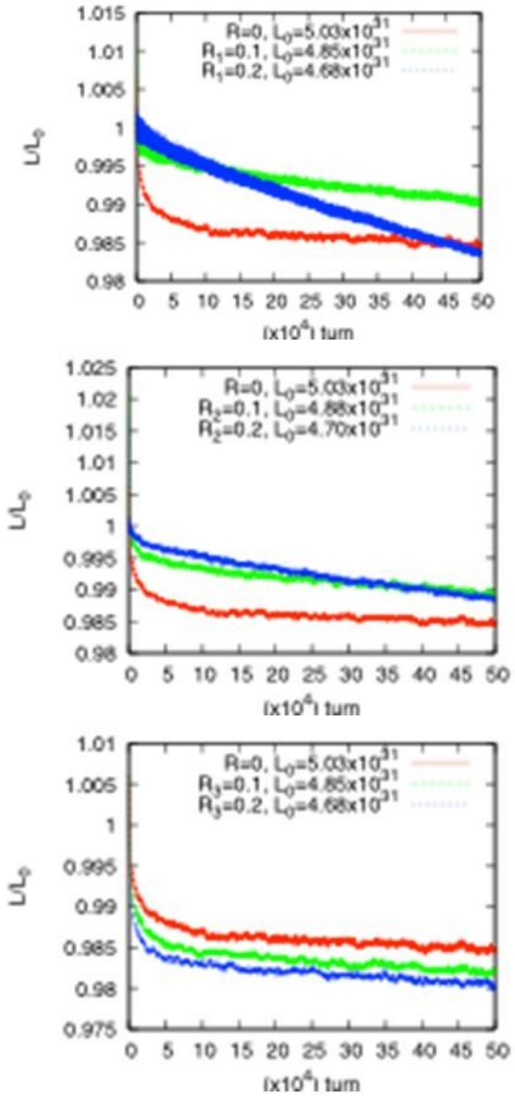

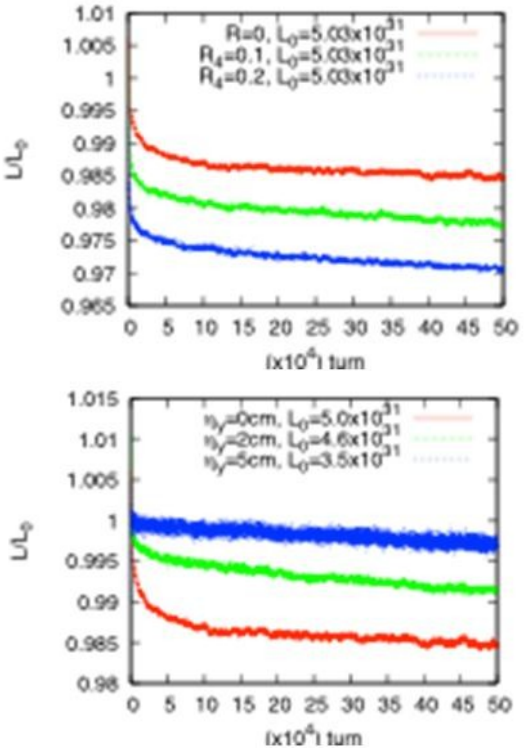

Figure 10: luminosity degradation in the presence of *x-y* coupling or vertical dispersion.

SUMMARY

Beam-beam effects in the High-Energy LHC have been studied. Both coherent and incoherent phenomena were discussed, using strong-strong and weak-strong simulations, respectively.

A coherent beam-beam instability is induced at high beam-beam parameter $-\xi>0.15$. The coherent instability is seen in simulations with unrealistically short damping time. For the true damping time, this type of instability is not realized due to the emittance growth caused by the incoherent beam-beam interaction or by IBS.

Incoherent emittance growth was evaluated for several beam-beam parameters. The beam-beam limit is found to be $-\xi=0.013$/IP without radiation ramping, and $-\xi=0.02$/IP for a radiation damping time of 2 hours. The incoherent emittance growth is mainly caused by the crossing angle. The emittance growth rate without crossing angle is about 10 times slower.

The sensitivity to *x-y* coupling and spurious vertical dispersion is quite weak compared with the flat-beam collision at the KEK B factory.

REFERENCES

[1] R. Assmann et al., "First Thoughts on a Higher-Energy LHC," CERN-ATS-2010-177 (2010).

[2] K. Ohmi et al., Phys. Rev. ST-AB 7, 104401 (2004).

PRELIMINARY CONSIDERATIONS ABOUT THE INJECTORS OF THE HE-LHC

R. Garoby, CERN, Geneva, Switzerland

Abstract

A hadron collider operating at an energy much larger than the LHC ("HE-LHC") would be a logical successor to the LHC itself, especially if its cost can be minimized by reusing a significant part of the CERN infrastructure like the existing tunnels and/or accelerators. The injector complex must however be extended to reach a beam energy of ~1.2 TeV and. in view of the time span of the HE-LHC project, the replacement of ageing accelerators can also be necessary. The main possible options are outlined together with their specificities.

INTRODUCTION

Beyond the need to satisfy the requirements of the HE-LHC, the options for the injector complex have to take into account the peculiarities of the existing accelerators and their other present or potential uses for physics. Moreover, choices have to result from an overall optimization of the whole HE-LHC project, taking into account the cost of dismantling and operation, as well as the opportunities offered by decommissioned installations like HERA, Tevatron and the LHC itself.

HE-LHC REQUIREMENTS

Preliminary considerations for a higher-energy LHC ("HE-LHC") [1] have lead to the figures listed in Table 1 for the beam characteristics at injection in the future collider.

Table 1: Beam characteristics in the HE-LHC

Injection energy	~1.2 TeV
Protons/bunch	1.3×10^{11}
Time interval between bunches	50 ns
Transverse emittances (H/V)	3.75 / 1.84
	or 2.59 / 2.59 μrad
Longitudinal emittance	< 4 eVs

The maximum energy of the SPS being of 450 GeV, a new accelerator is required in the injector chain to reach 1.2 TeV. All other requirements can be met by the CERN injector complex especially after its upgrade for the High Luminosity LHC ("HL-LHC") [2]. Considering however that the HE-LHC will start being operational in approximately 20 years, the present accelerators may represent a reliability concern if they have not been replaced.

PLANS FOR HL-LHC

Until the beginning of 2010, studies were taking place in view of building new accelerators to replace the PSB and PS, boosting performance and reliability of the first part of the injection chain, while simplifying the upgrade of the SPS by injecting at a much higher energy (50 instead of 26 GeV) [3, 4, 5]. This solution was however discarded after the 2010 LHC Performance Workshop in Chamonix, and the decision was taken to rather consolidate and upgrade the PSB and PS [6]. As a result, the SPS will keep operating with maximum injection energy of 26 GeV and the accelerators in the injector complex will date from 55 and 70 years when HE-LHC will start, except Linac4 which will be only ~14 years old.

OPTIONS FOR THE INJECTORS

Three main options are being considered for delivering beam at 1.2 TeV to the HE-LHC:

- New synchrotron using superconducting magnets in the SPS tunnel;
- New synchrotron using low field superconducting magnets in the LHC tunnel;
- LHC as a pre-accelerator.

New synchrotron in the SPS tunnel

Assuming the same filling factor than in the SPS, the maximum *B* field in the dipoles have to be of ~5.5 T. To provide the same proton flux at ejection (same filling time of the collider and same flux for fixed target physics), the *dB/dt* has to be of ~1.8 T/s. Such characteristics are close to the ones of the SIS300 dipoles for the FAIR project [7].

Injection in this new synchrotron has to be at ~100 GeV. If the 1.2 TeV accelerator can co-exist with the SPS in the existing tunnel, the possibility to use the SPS as injector could be considered. This is certainly difficult, but it cannot be rejected before some serious study. It is however more likely that a new machine will be preferable, either with a small footprint in the SPS tunnel, or in a new and shorter tunnel. The needs of this new accelerator will impact upon its injectors and significant work has to be invested for studying the options, especially if the requirements of other physics users have to be taken into account.

Another important consequence results from the need to rebuild the transfer lines TI8 and TI2 to the LHC (5.6 km in total). The possibility to use HERA or Tevatron magnets for that purpose is commented upon during this workshop [8, 9].

New synchrotron in the LHC tunnel

If acceleration above 450 GeV can be done by a machine located in the LHC tunnel, the transfer lines do not need to be modified and the SPS as well as the lower energy accelerators could in principle stay untouched. This solution requires however:

- The addition of a new dual beam synchrotron within the tight space left available by the collider;
- Finding a means to pass through or to by-pass the detectors.

This possibility has already been subject to a preliminary study [9] and it is addressed during this workshop [10]. The dipoles of the proposed new accelerator, called LER (Low Energy Ring) are based on the technology envisaged for the VLHC. In one option, two 1 km by-pass tunnels have to be built for the LER beam-pipe to avoid passing through the large detectors in IP1 and IP5. Beam transfer from LER to HE-LHC is tentatively located in IP7. In the second option, no by-passes are necessary because the LER beam is deflected to pass every turn through the centre of the detectors in IP1 and IP5. It relies on fast deflectors which would also solve the question of injection in the HE-LHC, although making it take place in a very fragile part of the machine, namely in the centre of the detectors.

LHC as a pre-accelerator for the HE-LHC

The cost of the magnets for the HE-LHC is likely to be very large, even compared to the cost of building a new and longer tunnel. An economical optimization will therefore be necessary, taking into account the variation of the magnets cost as a function of the maximum bending field and the cost of constructing a new and longer tunnel. It should be added in the analysis that, if the HE-LHC is located in a new tunnel, the LHC could remain in place and be used as injector, which would also remove the need and cost of its dismantling.

This option can only be considered after the R § D on the HE-LHC magnets will have sufficiently progressed

CONCLUSION

The HE-LHC raises two kinds of challenges for its injectors. The first one concerns beam energy, which has to be at ~1.2 TeV. It can be addressed with a new 1.2 TeV synchrotron either in the LHC tunnel or in the SPS tunnel. An alternative would be to use the LHC itself, if it is economically interesting to locate the HE-LHC in a new and longer tunnel. The second one results from the time period which covers ~2030-2050. This is likely to require the replacement of part or all of the existing synchrotrons e.g. to improve reliability, reduce the cost of maintenance (manpower and material) and decrease the environmental impact. The specifications of these new accelerators could also be influenced by the needs of other physics users (e.g. for neutrinos and/or nuclear physics).

In any case, as soon as the HE-LHC will become an attractive option for the future of particle physics, it would make great sense to start preparing the injector complex and let the HL-LHC and the other users benefit from new/ renovated accelerators.

REFERENCES

[1] R. Assmann, R. Bailey, O. Bruning, O. Dominguez, G.de Rijk, J.M. Jimenez, S. Myers, L. Rossi, L. Tavian, E. Todesco, F. Zimmermann, "First Thoughts on a Higher-Energy LHC", CERN-ATS-2010-177.

[2] F. Zimmermann, "Parameter Space Beyond 10^{34}", Proceedings of the Chamonix 2010 Workshop on LHC Performance, pp. 316-327, CERN-ATS-2010-026.

[3] R. Garoby, "Scenarios for Upgrading the LHC Injectors", LHC-LUMI-06 Proceedings, Valencia, Spain, 16 - 20 Oct 2006, CERN-2007-002, pp.107-110.

[4] R. Garoby, "Upgrade Issues for the CERN Accelerator Complex", CERN-LHC-Project-Report-1110.

[5] M. Benedikt, "What will LP-SPL and PS2 provide for the LHC?", pp.219-224, CERN-ATS-2010-026.

[6] P. Collier, V. Mertens, "Summary of Session 7: Future Upgrade Scenarios for the Injector Complex", pp. 20-23, CERN-ATS-2010-026.

[7] P. Fabbricatore, "Magnet Design Issues and Concepts for the New Injector",

[8] K.H. Mess, "Using LHC as Injector and Possible Uses of HERA Magnets/Coils", these Proceedings.

[9] Workshop on a Low Energy Ring in the LHC tunnel as Main Injector, CERN 11-12 October 2006, http://ler06.web.cern.ch/LER06/

[10] H. Piekarz, "Using Tevatron Magnets for HE-LHC or New Ring in LHC Tunnel", these Proceedings.

USING TEVATRON MAGNETS FOR HE-LHC OR NEW RING IN LHC TUNNEL*

Henryk Piekarz #, FNAL, Batavia, IL 60510, U.S.A

Abstract

Two injector accelerator options for HE-LHC of p^+ - p^+ collisions at 33 TeV cms energy are briefly outlined. One option is based on the Super-SPS (S-SPS) [1] accelerator in the SPS tunnel, and the other one is based on the LER (Low-Energy-Ring) [2] accelerator in the LHC tunnel. Expectations of performance of the main arc accelerator magnets considered for the construction of the S-SPS and of the LER accelerators are used to tentatively devise some selected properties of these accelerators as potential injectors to HE-LHC.

EXPECTED QUALITIES OF INJECTOR TO HE-LHC

Injector accelerator should transfer beam to a higher level accelerator with minimal beam losses. This is especially important for the HE-LHC where the scattered injected beam of energy in the TeV range can easily produce radiation levels not only causing quench but possibly damaging the magnets. In addition, the operations of the injector accelerator should be very robust minimizing in this way potentially lost time for the physics program with HE-LHC.

It is also important that the injector accelerator has the ability to pre-condition the injected beam in order to help optimize performance of the HE-LHC. One of the most important beam improvement options is a batch slip-stacking followed by bunch coalescing which may lead to as much as doubling the proton intensity in the bunch and as a result allow an increase of the HE-LHC luminosity by up to a factor of 4.

Finally, as the cost of HE-LHC accelerator construction and operations is expected to be very high the injector construction and operation cost should constitute only a fraction of the HE-LHC design.

S-SPS INJECTOR CONCEPT

The arrangement of the S-SPS accelerator as injector to the HE-LHC is shown in Fig. 1. The beam batches from the pre-injector chain are first injected into the SPS, accelerated to 150 GeV, and then transferred to the S-SPS. The S-SPS accelerator is built in the SPS tunnel, so it can fully contain the SPS batch. The S-SPS accelerates beam to 1 TeV [1], or 1.3 TeV [3], and then extracts it to TI2 and TI8 beam transfer lines connecting the S-SPS with the HE-LHC. This procedure is repeated 24 times to fill both HE-LHC rings. During beam stacking the S-SPS beam passes through the HE-LHC detector's beam pipe.

*This work has been authored by Fermi Research Alliance, ILC under Contract DE-AC02-07CHI1359,
#hpiekarz@fnal.gov

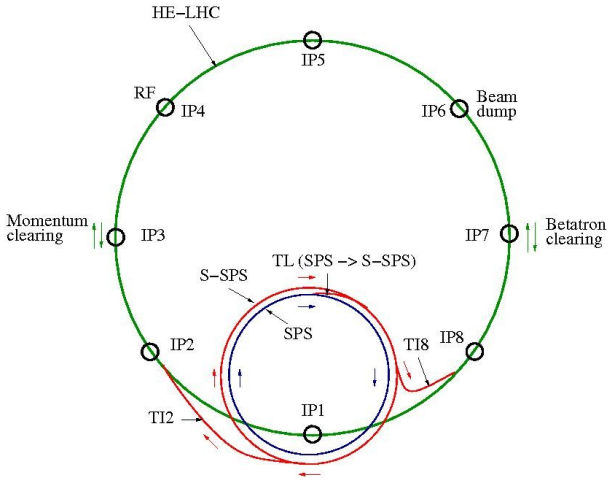

Fig. 1: S-SPS accelerator as injector to HE-LHC

The key element of the S-SPS injector proposal in [1] is that its cycle matched to the SPS eliminating the dead time incurred with the use of the S-SPS as a second stage accelerator. With the SPS beam energy set to 150 GeV its total cycle is 10.8 s. The S-SPS main arc magnet field has to be 4.5 T for 1 TeV beam and 5.9 T for 1.3 TeV one. In order to match the 10.8 s SPS cycle the ramping rate of the S-SPS magnets would have to be 1 T/s and 1.3 T/s for 1 TeV and 1.3 TeV beams, respectively. This would lead to the stacking time of 24 S-SPS beam batches in HE-LHC rings to be 4.4 minutes., as at present. As the S-SPS is also planned for the use in the fixed target experiments extending its cycle length beyond that of the SPS would cut into the benefit from the increased energy.

The increased beam energy of the S-SPS requires new construction of the TI2 and TI8 beam transfer lines to the HE-LHC using the superconducting magnets of 4 T and 5.2 T for 1 TeV and 1.3 TeV beams, respectively. The total new beam line construction for the S-SPS option is 12500 m, with 6900 m for the S-SPS ring and 5600 m for the TI2 and TI8 transfer lines.

LER INJECTOR CONCEPT

The LER injector is a dual beam synchrotron of 1.65 TeV energy per beam placed in the LHC tunnel. The beam batches from the SPS are stacked in two LER rings and circulate in the clock-wise and counter-clock directions. As the LER rings are of the same length as the HE-LHC the LER beam batches length matches exactly those of the HE-LHC. This allows correct and improve the future HE-LHC beam batch at the LER energy. Both LER beam batches are transferred to the HE-LHC rings simultaneously using a single injection mode assuring in

this way proper beam power balance in the HE-LHC two-bore magnets. The LER beam stacking time is 7.4 minutes as determined by the current SPS cycle with 24 injections (18.5 s × 24 = 444 s). The LER accelerator can work with the existing or the new pre-SPS injector chain. The SPS beam energy at the injection to the LER is 450 GeV. The LER accelerates beams to 1.65 TeV, or 10% of the HE-LHC top energy. There are two options for arranging the LER accelerator as an injector to the HE-LHC. The first option, shown in Fig. 2, allows the LER beams to bypass the detectors and the second one, shown in Fig. 3, requires the LER beams to pass through the detectors beam pipe.

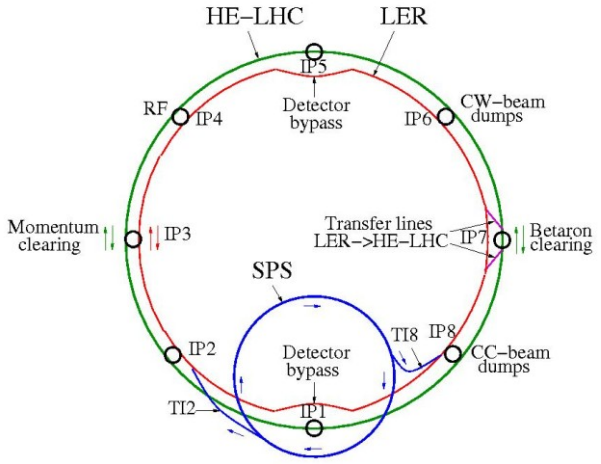

Fig. 2: LER injector Option 1 with LER beam bypassing detectors at IP1 and IP5intersection points

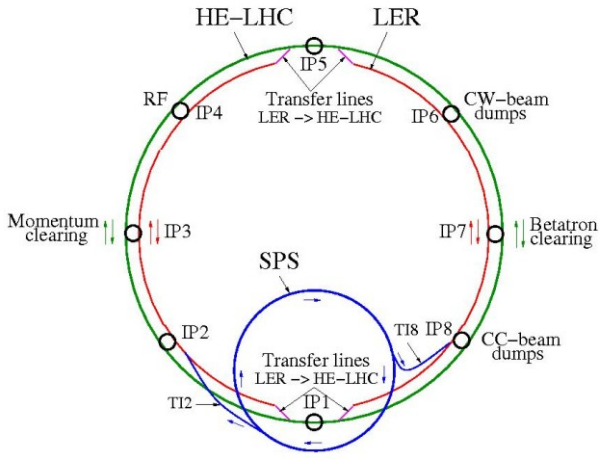

Fig. 3: LER injector Option 2 with LER beams passing the detector beam pipe at IP1 and IP5 intersection points

The advantage of the first option is that it fully secures safety of the HE-LHC during the SPS beam stacking operations in the LER. The disadvantage of this option is that construction of at least 2 x 1000 m of a new tunnel is required with the 8 T magnets used for these beam lines. For the Option 2, however, allowing the LER beams to pass through the IP1 and the IP5 intersections constitutes some risk for the detectors. For the LER Option 1 the two-beam transfer into the HE-LHC rings is enforced by two sets of kicker magnet strings located at IP7. For the LER Option 2 the two-beam transfer to the HE-LHC is enforced with total of four sets of fast switcher-magnet strings located on both sides of IP1 and IP5 intersections. The detector bypass lines in the LER Option 1 and the transfer lines in the LER Option 2 constitute an integral part of the LER synchrotron. The LER accelerator can share RF system with HE-LHC but it can also have its own installed in e.g. IP3 or IP7. For the LER Option 1 the RF system can also be placed in one of the detector bypass lines. In all cases a local expansion of the tunnel is required. The beam line construction for LER Option 1 is 26700 m long including 2000 m for the detector bypass lines and 200 m for kicker magnet strings. The total beam line construction for the LER Option 2 is 26300 m with 25904 m for the LER and 416 m for the 4 switcher magnet strings.

EXPECTED PROPERTIES OF S-SPS MAIN ARC MAGNET

There are three crucial elements of superconducting magnet performance: (1) stability of operations (quench prevention), (2) cryogenic power loss during fast-cycling operations, and (3) overall cryogenic and electrical power demand. It is assumed [1, 3] that the S-SPS injector will use the SIS300 type magnets of the FAIR accelerator [4]. The SIS300 magnetic design [5, 6, 7] calls for a 2.75 m long dipole of B_{max} = 6 T with a 50 mm gap and the dB/dt ramping rate of 1 T/s. At present the actual tests are available for 1 m long model SIS200 dipole of B_{max} = 4 T [8], and the power loss simulations for 2.6 m long SIS300 dipole of B_{max} = 6 T. We extrapolate data to match the simulations (Fig. 4), and use the points at 4.5 T and 6 T to estimate the SIS300 magnet power loss at 4.5 T and 6 T for the 1 TeV and 1.3 TeV S-SPS, respectively.

Assuming the SIS300 magnet trapezoid shape of the ramping cycle 4.5 s + 1.5 s + 4.5 s = 10.5 s for the S-SPS magnet at both 1 TeV and 1.3 TeV we estimate the power loss to be 10 W/m and 15 W/m for 4.5 T and 6 T magnets, respectively. Consequently, for the 6900 m long S-SPS magnet ring of 78% filling factor the projected cryogenic power loss is 54 kW and 80 kW for operations with 1 TeV and 1.3 TeV beams, respectively.

Stability of the S-SPS accelerator operation is dependent on, among other things, the temperature margin of the superconducting magnet cable. It was analyzed in [7] that the temperature margin for a 2.6 m long SIS300 magnet operating with field cycle B_{min} = 0.48 T, B_{max} = 6 T, dB/dt = 1 T/s, in a trapezoid time cycle 5.52-11-5.52-0 s would be no larger than 0.5 K with 40 g/s liquid helium flow. For the 6-m-long S-SPS magnet, the temperature margin will likely be even lower than 0.5 K due to the much diminished cooling efficiency in the longer cables. Consequently, one may expect the S-SPS magnet to be strongly prone to quenching and other instabilities.

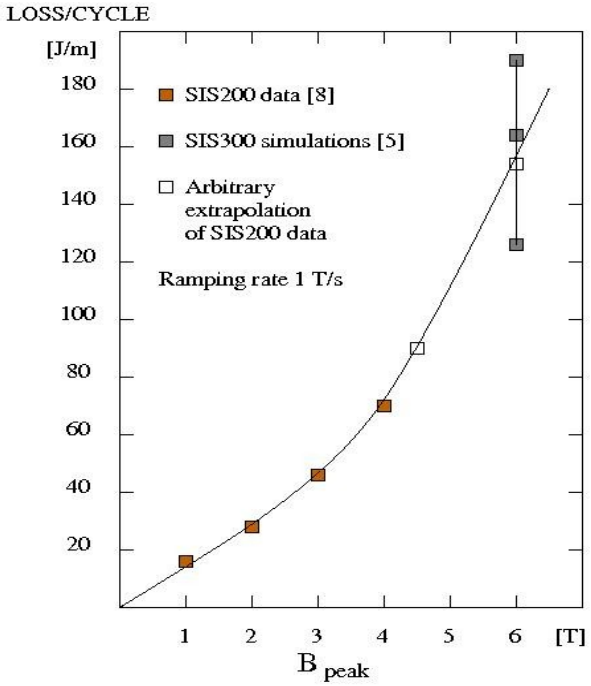

Fig. 4: SIS200 power loss data [8] for fields of 1-4 T at 1 T/s ramping rate, and extrapolation to simulations of SIS300 at 6 T

The 1 TeV S-SPS, but with ramping rate well below 1 T/s, may be a more practical solution for the large scale accelerator such as the S-SPS assuming that the lower ramping rate will indeed widen operational temperature margin. With the S-SPS as injector the stacking time in the HE-LHC rings ranges from 4.3 minutes for 1 TeV beam to 5.2 minutes for 1.3 TeV beam with the ramping rate of 1 T/s .

The electric power required for the cryogenic support (estimated using Carnot factor 70, Carnot efficiency factor 3.6 and the over-capacity factor 1.3) is 14 (17) MW for 1 (1.3) TeV S-SPS options. The ramping power of 230 kVA for the FAIR magnet scales-up to 375 (500) kVA for a 6 m long S-SPS magnet at B-fields of 4.5 T (6 T), respectively. The required ramping power for the S-SPS accelerator is then 6900 m × 0.78/6 m × 375 (500) kVA = 390 (518) MVA.

EXPECTED PROPERTIES OF LER MAIN ARC MAGNET

A sketch of the proposed LER main arc magnet design [2] is shown in Fig. 5. This design is a scaled-down (in field) version of the VLHC Stage 1 combined function dipole [9, 10, 11]. This is a super-ferric magnet powered with a single-turn superconducting cable made of NbTi strands cooled at 4.2 K. The drive conductor with its cryostat is in the center of the magnet yoke. The return conductor is inside the cryostat pipe which supports magnetic core and houses liquid helium distribution lines for the LER accelerator. The magnet position is set with 3 posts (2 in front and 1 in rear) independently adjustable in both vertical and horizontal directions. The length of the LER magnet is 14.3 m, the same as that of the HE-LHC. The LER magnetic core cross-section is 260 mm (vertical) by 230 mm (horizontal.). Two beam gaps separated by 150 mm allow for simultaneous circulation of two proton beams in the opposite directions. For the 1.65 TeV LER synchrotron the beam gaps are 30 mm (v) · 50 mm (h), B_{max} = 1.76 T, B_{inj} = 0.5 T and dB_y/dx = 6.5 T/m. The operating current is I_{peak} = 83 kA. As the entire main arc magnet string of the LER is energized using a single-turn conductor the ramping of the accelerator is performed with a single power supply. The proposed ramping time to the full field is 60 s requiring the ramping rate of 0.02 T/s.

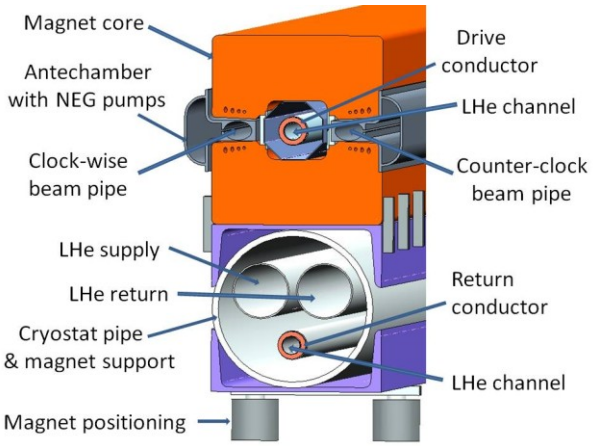

Fig. 5: LER main arc magnet position in the LHC tunnel

As in the VLHC-1, for every two dipoles there will be a set of corrector magnets consisting of horizontal and/or vertical dipole, quadrupole and sextupole magnets. The corrector magnets can be normal or superconducting. The availability of liquid helium distribution lines in HE-LHC tunnel suggests using superconducting correctors.

The stability of LER magnet cable is very high due to 2.5 K allowable temperature margin and very low static and dynamic cryogenic power losses. With 40 g/s liquid helium flow the static cryogenic heat load of the LER power cable is about 4.4 kW (scaled from the VLHC-1 design [9]). The estimated cryogenic heat load with 60 s ramping time is about 0.6 kW, leading in turn to 0.03 K temperature rise of the magnet power cable.

The total inductance of the LER accelerator ring sets the limit on the allowable cycling rates. The inductance of the LER ring (option 2, 26300 m) is about 120 mH and with 83 kA current ramping in a 60 s time period the voltage rise is 150 V. This requires the peak electrical power of 10 MVA. As the power cable can withstand much higher voltage, e.g. 1500 V, the ramping time could be shortened to e.g. 6 s with a supply of 100 MVA. The instantaneous cryogenic power loss of the LER would rise, however, to 45 kW causing the cable temperature to rise by about 2.3 K to 6.5 K, and thus approach the maximum allowable temperature of 6.9 K before

quenching. Consequently, we conclude that the 6 s ramping time is not practical for the 1.65 TeV LER.

The SPS beam stacking time in two LER rings is 24 × 18.4 s (SPS super-cycle) = 7.4 minutes, and the transfer time to the HE-LHC rings equals the LER batch length of ~ 90 μs (same as the HE-LHC batch length).

It is interesting to note that the LER of 1 TeV (B_{min} = 0.48 T, B_{max} = 1.07 T, dB/dt = 0.12 T/s) can operate with a cycle 4.5 s + 1.8 s + 4.5 s = 10.8 s thus matching the SPS cycle. The projected cryogenic power loss of ~ 8.5 kW will induce a power cable temperature rise of ~ 0.5 K. This operation reduces only slightly the allowable temperature margin from 2.5 K to 2 K. For the 1 TeV beam the LER magnet operating current is 50.5 kA and the voltage rise with 4.5 s ramping time is 670 V requiring the ramping power supply of 34 MVA. The described above LER operation can be used in the fixed target physics program, if desired.

In the LER Option 1 the accelerator sections bypassing the IP1 and IP5 intersections will use the LHC-style 8 T magnets. The power cable of these magnets will use the Nb_3Sn superconductor operating at 4.5 K. With allowable temperature margin of 10 K (T_C = 15 K at 8 T) it will be possible to apply 0.14 T/s ramping rate in order to reach the full field at 60 s time period. We estimate the cryogenic power loss for the 2000 m long magnet string to be about 12 kW increasing the total LER Option 1 cryogenic power to ~ 17 kW. The inductance of the 14.3 m long LHC magnet is estimated at 98.7 mH, the operating current is 11.4 kA and at the 60 s rise time there is a voltage drop of 19 V leading to about 220 kVA required ramping power. Assuming 95% magnet filling factor the two bypass beam lines will use a total of 132 magnets. The required ramping power for the bypass sections is then 29 MVA, and the total ramping power for the LER Option 1 is 39 MVA.

S-SPS TO HE-LHC TRANSFER LINE MAGNETS

At present the SPS to the LHC TI2 and TI8 transfer line magnets are normal conducting and operate at 1.81 T field with a beam gap of 25 mm × 70 mm. For the beam energy of 1 (1.3) TeV the dipole magnetic field has to increase to 4.0 (5.2) T. This can only be achieved with superconducting magnets. One possible candidate is the Tevatron magnet (dipole is shown in Fig. 6 and quad in Fig. 7) of B_{max} = 3.9 T and the radial aperture of 38 mm. As this magnet uses warm iron yoke far away from the coil the beam gap magnetic field is determined primarily by the superconductor, leading to a rather low level of higher-order multiples. Studies, however, would have to determine if such a design can be extended to higher fields. Another option is to use a cold-iron magnet, such as e.g. HERA's [12] 6 T field.

The Tevatron accelerator ring, whose circumference is comparable to the total length of TI2 and TI8 beam lines, requires 24 kW of cryogenic power at 4.2 K thus requiring about 7.9 MW of the electric power. One should expect the cryogenic power demand for the cold-iron magnets of the TI2 and TI8 beam lines to be much higher.

In summary, the S-SPS to HE-LHC beam transfer lines based on the superconducting magnets will add considerable construction and utilization costs to the HE-LHC injector chain.

The S-SPS beam would be extracted to the TI2 and TI8 lines using a combined system of kickers and septa similar to the ones used for the 450 GeV SPS beam. The kicker strength, however, will have to be considerably increased to accommodate the 1TeV or the 1.3 TeV S-SPS beams.

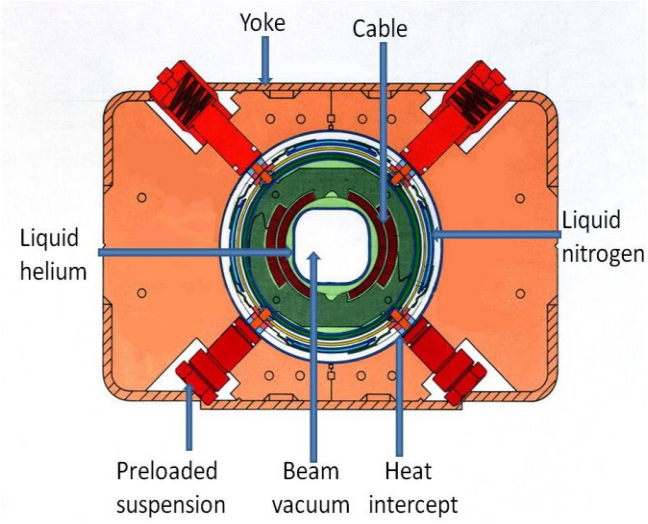

Fig. 6: Cross-section of Tevatron dipole with warm iron yoke; conductors and beam pipe are at liquid helium temperature

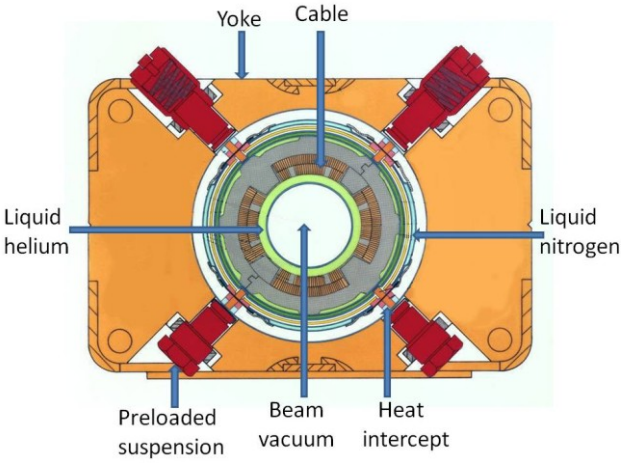

Fig. 7: Cross-section of Tevatron quadrupole with warm iron yoke; conductors and beam pipe are at liquid helium temperature

LER TO HE-LHC TRANSFER LINE MAGNETS

LER Injector Option 1

The simultaneous transfer of the LER beams to HE-LHC rings would take place at the IP7 area. A dual kicker

magnet string of non-superconducting technology similar to the MKD beam abort system for the LHC can be used [13]. Although the 1.65 TeV LER beam energy is much lower than the 7 TeV energy of the LHC beams the beam transfer is a very challenging undertaking as a very high quality of the injected beams to the HE-LHC rings has to be preserved [13].

LER Injector Option 2

The LER to HE-LHC beam transfer takes place in the short straight sections around the interaction points IP1 and IP5, as described in [2]. These sections are also part of the LER Option 2 synchrotron normal operations. A dual fast-switching (3 μs time) superconducting dipole string is the key element of this beam transfer system. The principle of a fast-switching dipole is presented in [2, 14]. The HE-LHC beams separation being enlarged to 300 mm facilitates the implementation of this design. The beam separation dipoles and quads in the IP1 and IP5 sections of HE-LHC are also taking part in the LER operations. In addition, four dual-bore 8 T Nb_3Sn superconducting magnets in each of the transfer lines constitute components of the LER accelerator. The estimated cryogenic power for these sections of the LER is 5 kW, and so the total LER Option 2 cryogenic power is 10 kW.

The inductance of 8 T magnets string used in the beam transfer sections of the LER Option 2 is estimated at 1.3 H thus requiring about 2.9 MVA ramping power supply for 60 s ramping time. The total required ramping power for the LER Option 2 is then about 13 MVA.

Table 1: HE-LHC beam properties at injection

Beam parameters	**450 GeV**	**1 TeV**	**1.65 TeV**
RMS bunch length [cm]	11.24	9.23	8.15
RMS energy spread	4.72×10^{-4}	2.58×10^{-4}	1.77×10^{-4}
Direct space charge tune shift	-1.54×10^{-3}	-3.8×10^{-4}	-1.58×10^{-4}
Laslett tune shift	-1.42×10^{-2}	-6.4×10^{-3}	-3.88×10^{-3}
Space charge transv. impedance [MΩ/m]	-j 6.71	-j 3.03	-j 1.83
Space charge longit. impedance [mΩ]	-j 6.04	-j 1.36	-j 0.528
Microwave thresh. intensity [N_p /bunch]	1.14×10^{13}	6.3×10^{12}	4.3×10^{12}
Landau damping thresh. intensity [Np /bunch]	2.5×10^{12}	9.5×10^{11}	5.1×10^{11}
TMCI thresh. intensity [N_p /bunch]	3.0×10^{12}	3.7×10^{12}	4.2×10^{12}

INJECTION ENERGY AND HE-LHC BEAM PARAMETERS

Best operation of the accelerator magnet is typically in the field range above some 10% of its top value. For the high-field type magnets the beam energy to magnetic field response is approximately linear suggesting that for the 16.5 TeV top energy the injected beam energy would be the best at 1.65 TeV, or higher. The LER accelerator can match this requirement. Beam injection energy affects beam dynamics of HE-LHC operations. The main issues are: dynamic aperture, persistent currents and snapback, instabilities, electron cloud, synchrotron radiation, and rest-gas scattering. A progression of the HE-LHC beam dynamics parameters with injection energy: 0.45 TeV, 1 TeV and 1.65 TeV is shown in Table 1 from [15]. The microwave instability threshold intensity and the Landau damping threshold intensity were found by assuming $(Z_L/n)_{eff} = 0.1\ \Omega$, and the TMCI threshold intensity is found assuming a transverse impedance $Z_T = 3.6$ MΩ/m.

The beam size decreases with the increased energy as $1/\gamma^{1/2}$ making the physical aperture larger in *rms* units of beam size. The persistent magnet currents are reduced at higher magnetic fields (hence higher injection energy) leading to much more stable magnetic cycle. The beam instabilities due to direct space charge and beam pipe image current, etc., decrease as $1/\gamma^2$, and the rise time for the electron cloud induced instabilities increases with γ thus reducing this effect. The synchrotron radiation power increases but critical energy at beam energies up to 1.65 TeV is well below the photo-electrons work function. The emittance growth rate due to elastic scattering falls with increasing energy as $1/\gamma$ being smaller at 1.65 TeV than at 1 TeV. In summary, higher injection energy of the LER will significantly improve the long-time circulating HE-LHC beam thus minimizing its losses, reducing setup time and thus increasing the integrated luminosity.

USING INJECTOR ACCELERATOR TO INCREASE HE-LHC LUMINOSITY

The batch slip-stacking followed by the coalescing of two bunches into a single bunch has been successfully applied at Fermilab [16]. This procedure doubles the bunch intensity, and as a result it increases instantaneous luminosity up to a factor of 4 (and so the integrated one as well). This procedure is enforced by the RF power, and for a given beam energy the higher the RF power the smaller are the beam losses. For the 450 GeV beam the particle loss is projected to be below the 5% level [2] with the RF power of 28 MV. Such an RF power (or higher) is now achievable with both normal and the superconducting RF systems. The batch slipping and bunch coalescing process would take about 11.3 s in the LER [2].

The batch slipping and bunch coalescing can also be performed in the S-SPS with the 150 GeV beams. The required RF power would be about 10 MV. This process, however, would have to be repeated 24 times for each S-

SPS batch. We estimate that the time to complete the batch slip-stacking and bunch coalescing for the SPS is about 2.9 s. The overall time for 24 batches of the S-SPS is then at least 70 s.

DETECTOR AND HE-LHC SAFETY

The S-SPS and the LER pilot beams will be used to test the readiness of HE-LHC, the same way the SPS and LHC operate at present. The readiness of the S-SPS and LER will be tested using the SPS pilot beams. The failure of the injector before the start-up of the beam stacking in HE-LHC rings will result in time loss for the HEP physics program. The failure of the injector during the stacking process may in addition damage accelerator components. Consequently, the robustness of injector operations is of a very great importance.

The required 24 stacking operations in order to fill the HE-LHC rings with S-SPS increases the potential for aborting the stacked beams if any of the subsequent beam transfers has failed. The failed beam transfers as well as the aborted beams carry risk of damaging detectors and accelerator components. This gives an advantage to the LER where a simultaneous, single transfer of both the clock-wise and counter-clock beams will take place.

The LER magnet cable is very robust with large liquid helium channel in direct contact with the superconductor. As a result this cable can accept an instantaneous heating due to beam loss or other source of temperature rise of up to 2.7 K. In the LER Option 1 the accelerator sections for the detector bypass will use magnets based on the Nb_3Sn superconductor thus likely exceeding the LER nominal operational temperature margin. In the LER Option 2 the transfer line magnets will also use Nb_3Sn superconductor cable and in addition the HTS superconductor cable of the fast-switching dipoles will be set to operate with a 20 K temperature margin. The main problem with Option 2 is the necessary application of a superconducting inductor which must inject a high current into the switcher magnet cable during the 3 μs long HE-LHC beam batch gap. The failure of the inductor will result in the beam loss. A set of collimators and beam dumps as described in [2] will have to be installed in the transfer lines sections to protect the accelerator components and detectors.

In the LER Option 2 the quads and separation dipoles at the interaction points are part of the LER accelerator during the beam stacking. As the energy of the LER beam at injection and transfer to HE-LHC is low compared to the top HE-LHC energy using these magnetic components in the LER operations should be considered very safe especially since the HE-LHC quads at the IP sections will use the Nb_3Sn superconducting cable.

ARRANGEMENT OF LER AND HE-LHC MAGNETS IN LHC TUNNEL

A possible arrangement of LER and HE-LHC magnets in the LHC tunnel is shown in Fig. 8. HE-LHC magnet size was scaled-up from the LHC magnet using the cold mass diameter of 800 mm with beam separation of 300 mm, as proposed in [17]. The vertical position of HE-LHC magnet is set to 1051 mm to facilitate creation of a maximum allowable space for the transportation of another HE-LHC magnet while the one is already in place. The supporting fixtures of HE-LHC magnet are the same as for the LHC except of their increased height. The space for passing the second HE-LHC magnet is rather limited but acceptable.

The LER magnet is placed at 2123 mm height, or 1072 mm above the HE-LHC one. In working-out its location we kept all tunnel fixtures (cable trays, etc.) unchanged. Each LER magnet is supported from two columns placed between the HE-LHC magnet cryostat flanges in a way that the brackets fastening the columns to the floor do not interfere with those supporting the HE-LHC magnet, as shown in Fig. 9. The top ends of the LER columns are fastened to the tunnel ceiling providing steadiness. With this arrangement of supports both LER and HE-LHC magnets can be independently placed or removed from their accelerator rings.

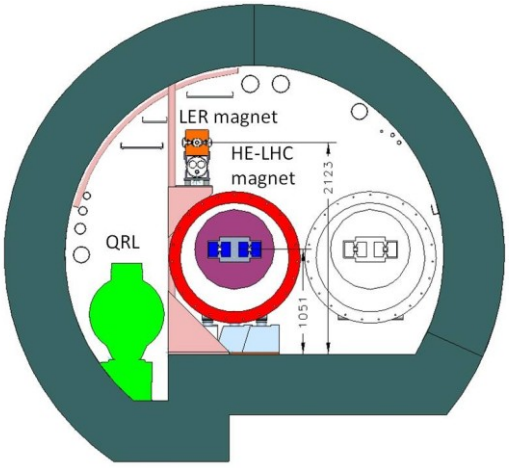

Fig. 8: Possible arrangement of LER and HE-LHC magnet rings in the LHC tunnel and position of a second HE-LHC magnet in transportation through the tunnel.

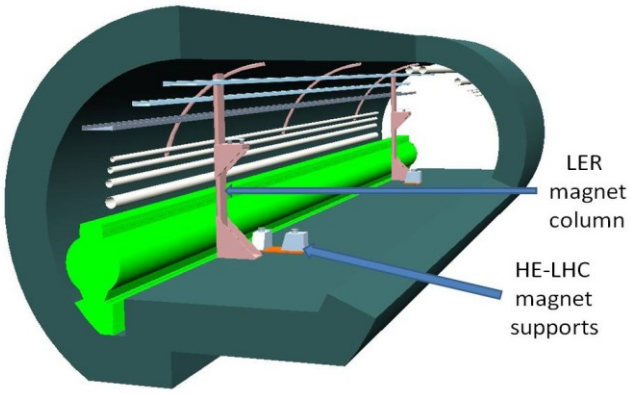

Fig. 9: Arrangement of LER magnet supporting columns relative to HE-LHC magnet supports

A perspective view of the HE-LHC and LER magnets in the LHC tunnel is shown in figure 10. The QRL cryogenic support system, all piping and cable trays are those used at present to support the LHC.

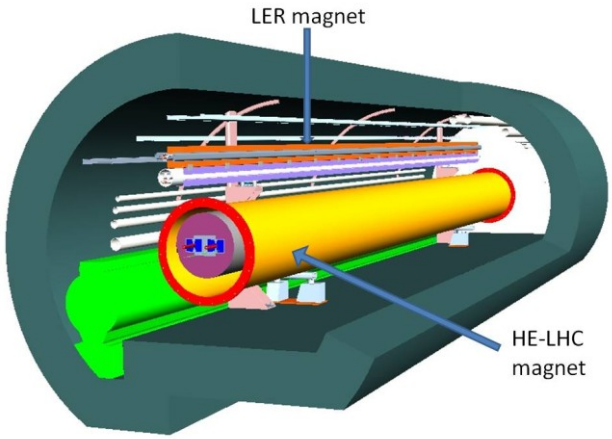

Fig. 10: Perspective view of LER and HE-LHC magnets in LHC tunnel

S-SPS AND LER SYNCHROTRONS COST ESTIMATE

The cost of development and construction of the 20 T magnets for the HE-LHC accelerator and the cost of their supporting cryogenic and power systems will be high. Therefore, it is important to lower as much as possible the injector cost in both the construction and the utilization phases, so they will constitute only a fraction of the total HE-LHC project. For evaluation of the accelerator cost we used the total cost of a synchrotron construction rather than that of the magnet strings alone which typically may constitute only a fraction of the total synchrotron cost.

For the S-SPS accelerator the SIS300 magnets of the FAIR project are being considered. Consequently, we use the FAIR projected cost [4, 18] to estimate the cost of the S-SPS accelerator. The FAIR synchrotrons cost is a sum of 82.1 M€ for SIS100, 96.0 M€ for SIS300 and 104.4 M€ for the Common Accelerator Systems (CAS). Assuming arbitrarily that 25% of CAS cost is due to the SIS300 synchrotron our projected cost of the SIS300 accelerator is (96.0 + ¼ 104) M€ = 122 M€. The total SIS300 magnet string length in the FAIR accelerator is 454 m, and so the cost per meter of the synchrotron magnet length is 122 M€/454 m = 0.269 M€/m. Using this scaling for the S-SPS magnet string length of 6210 m (6900 m × 0.78 filling factor) the projected cost is 1490 M€.

For the cost estimate of the LER we scaled-down from the VLHC Stage 1 accelerator [9]. This cost included all accelerator subsystems: main arc magnets, correctors, RF, electric power, refrigerators, cryogenic distribution lines, accelerator controls, vacuum system and installation of all subsystems in the tunnel. With the VLHC ring length of 233 km the scaling factor for the LER is 26.6/233 = 0.12. The major material cost was corrected for the price increase of the raw materials from 2001 to 2010 using the Camden Copper and GE Commercial Finance Future of Steel price evolutions. The projected in this way LER construction cost is 170 M€. The LER Option 1 cost includes two 1000 m long beam lines bypassing detectors at IP1 and IP5 interaction points. These beam lines will use magnets based on the Nb_3Sn conductor whose cost is about 4 times higher than NbTi [19]. Assuming that in the LHC-type magnet conductor constitutes 1/3 of the cost [19] we project the cost of the LER detector bypass beam lines scaling from the LHC accelerator cost (not just the magnets). The result is 170 k€/m of beam line, leading to about 326 M€ for 2000 m of the detector bypass lines. With added 50 M€ for the digging cost of a 2000 m tunnel the total cost of the LER Option 1 synchrotron is estimated at 546 M€.

TRANSFER LINES COST ESTIMATE

For the S-SPS the new TI2 and TI8 transfer lines cost is estimated by scaling-up the 220 M€ cost of the RHIC [20] 3834 m long superconducting synchrotron. Using this scaling the estimated cost of the TI2 and TI8 beam lines is 5600/3834 × 220 = 320 M€.

For the LER Option 1 two kicker-magnet strings such as the MKD in the LHC, but with the bending power for the 1.65 TeV beam, are required to transfer beams to the HE-LHC. We estimate the cost of two 50-m-long non-superconducting kicker-magnet strings at about 10 M€.

For the LER Option 2 four superconducting magnet strings of 100 m each are required. The first 80 m length of this string uses 8 T, two-bore Nb_3Sn magnets, and the remaining 20 m section uses 1.6 T HTS based fast-switching magnets. The total estimated cost of the 8 T magnets is 52 M€, and for all the fast-switching magnets we expect 48 M€, including R&D. The total estimated cost of the LER Option 2 beam transfer line sections to the HE-LHC is then 100 M€.

SUMMARY

We presented tentatively some properties of HE-LHC injectors based on the S-SPS or the LER synchrotrons. A summary of these properties is given in Table 2. The LER injector in either of its options is superior to the S-SPS. Both LER options offer much higher injection energy and as a result much improved quality of HE-LHC beam. In addition, they allow for up to a factor of 4 increase of the HE-LHC luminosity. The LER beam stacking time is longer by about 2 minutes relative to the HE-LHC beam stacking time with the S-SPS but this is relevant only for the LER Option 2 which uses the HE-LHC ring components at IP1 and IP5 interaction points. The beam stacking time into the HE-LHC rings with the LER Option 1 is equal to the LER beam batch length of about 90 μs.

The LER Option 1 is characterized by high safety for the detectors and high reliability of its operations due to wide temperature margins of all used superconducting magnets. In addition, the LER Option 1 is independent of

the HE-LHC operations, and the beam stacking in the LER rings (including bunch improvements) can be made while HE-LHC is still running the physics program. This makes the LER Option 1 injector possibly a dead-time free for the colliding beam physics.

The LER Option 2 does not require construction of new tunnels, and it will use rather short LER to HE-LHC beam transfer lines substantially minimizing the injector cost. This option, however, relies on using four strings of fast-switching magnets requiring a substantial R&D effort to make their operations secure for the detectors and for both accelerators as well.

The S-SPS synchrotron is based on the high-field, fast-cycling superconducting magnets which have not been proven yet to be applicable for a large scale synchrotron. As rather significant power losses are expected in the operations of these magnets the allowable temperature margin is very narrow suggesting a strong possibility of frequent quench occurrences and other instabilities. In view of the above the 1.3 TeV S-SPS is very unlikely to be practical. On the other hand the 1 TeV S-SPS, even if it turns out to be feasible, it will not provide satisfactory improvement in the quality of the HE-LHC beams at the injection, as indicated in Table 1.

The S-SPS could also be used to double the bunch intensity before injecting its beams to the HE-LHC. This procedure, however, would have to be performed 24 times to complete the beam stacking in the HE-LHC rings. Even a very small beam loss incurred during batch slip-stacking and bunch coalescing procedures would likely raise the S-SPS magnet cable temperature making all but certain the occurrence of a quench. Consequently, there would be a high probability of long down-times for HE-LHC physics program with the implementation of procedures aimed at bunch intensity increase with the S-SPS.

Although construction and utilization cost estimates presented above are crude we can say with a reasonable confidence that the use of the S-SPS as an injector will add considerably to the HE-LHC cost. On the other hand, the LER in either of its options is consistent with the low-cost expectation for the HE-LHC injector. In addition, the required cryogenic power for all LER injector magnets constitutes only a small fraction of that for the HE-LHC, and as they are located in the same tunnel, sharing the cryogenic support system with the HE-LHC one may be possible. This option would considerably further reduce the cost of the LER injector (this potential savings was not used in the above cost estimate).

As mentioned earlier the LER Option 1 allows for safe operation of 1 TeV beams with the cycling period matching that of the SPS at 150 GeV. This operation can be used e.g. to extract beams for production of secondary beams of the fixed target physics program. In such operation all beam stacking takes place only in the SPS and the LER serves simply as an energy booster, the same way as proposed for the S-SPS. The LER super-cycle will be twice longer than that of the SPS to allow injection of the SPS beam batches into two rings of the LER. The two LER beams will be simultaneously accelerated and then extracted onto the secondary beam production targets. A comparison of some selected properties of the S-SPS and LER synchrotrons operating with 1 TeV beams for the fixed target physics program are listed in Table 3.

Table 2: Estimated properties of S-SPS and LER injectors

Injector Properties	S-SPS	LER-1	LER-2
HE-LHC injection energy [TeV]	1 (1.3)	1.65	1.65
Number of injections	24	1	1
Doubling bunch intensity	No	Yes	Yes
HE-LHC filling time [min]	4.3 (5.2)	~ 0	7.4
Temperature margin [K]	0.5 (< 0.5)	2.5	2.5
Quench probability	High	Very low	Low
Operations complexity	High	Medium	Medium
Synchrotron cryogenic power @ 4.2 K [kW]	54 (80)	17	10
Transfer lines cryogenic power @ 4.2 K [kW]	30	0	0
Synchrotron ramping power [MVA]	390 (500)	39	13
Synchrotron cost estimate [M€]	1490	546	170
Transfer line cost estimate [M€]	320	10	100
Injector cost estimate [M€]	1810	556	270

Table 3: Estimated properties of S-SPS and LER Option-1 synchrotrons in application for fixed target physics program

Synchrotron properties	**S-SPS**	**LER-1**
Beam energy [TeV]	1	1
Number of beams	1	2
Operation super-cycle [s]	10.8	21.6
Temperature margin [K]	0.5	2
Cryogenic power @ 4.2 K	54	27
Ramping power [MVA]	390	178

In the proposed above fixed target LER operations the cryogenic and ramping powers are increased substantially

In the proposed above LER operations the cryogenic and ramping powers are increased substantially relative to the LER Option 1 operating as an injector to the HE-LHC. This increase is mostly due to Nb_3Sn, 8 T magnet strings used in the construction of the HE-LHC detector bypass lines. Nevertheless, the expected four times wider temperature margin, twice lower cryogenic and ramping powers, much simplified operation control system (single power supply with single quench detection and protection systems) and much lower construction and utilization costs are all in favor of selecting the LER synchrotron rather than the S-SPS one for the fixed target physics program.

CONCLUSIONS

We believe that the very narrow temperature margin, insufficiently high injection energy and very high cost of construction and utilization make the S-SPS synchrotron an unlikely candidate as injector to the HE-LHC. On the other hand, the 1.65 TeV LER Option 1 synchrotron with its wide temperature margin, optional doubling of the HE-LHC bunch intensity and moderate construction and utilization costs, should be considered as the primary candidate for the injector to the HE-LHC accelerator.

The LER Option 2 can be considered for the HE-LHC injector only after proving that the LER to HE-LHC beam transfer using fast-switching superconducting magnets is robust and safe for both the detectors and accelerators. We believe that the R&D effort to develop the fast-switching superconducting magnets is warranted as potential saving in the LER injector cost is high not only in the relative but more importantly in the absolute terms. In addition, this new superconducting magnet technology if successful will be very useful for other accelerator sub-systems e.g. kicker magnets, high-current dump switches, etc., as well as for the high-current superconducting cable industrial applications.

During the HE-LHC colliding beam period, the LER Option 1 accelerator can be safely used for the fixed target physics programs with the selection of the extracted beam energies from 0.45 TeV to 1 TeV, and up to 1.65 TeV, if the LER super-cycle is extended beyond the SPS one.

ACKNOWLEDGEMENTS

It is my pleasure to thank Jamie Blowers, Steve Hays and Tanaji Sen for reading the manuscript and several valuable discussions.

REFERENCES

[1] W. Scandale, "LHC upgrade based on high intensity, high luminosity, high energy injector chain" LHC-LUMI-05, 2005

[2] G. Ambrosio et al., *"LER-LHC Injector Workshop Summary", LUMI-06 Workshop"*, Valencia, 2006

[3] F. Zimmerman, *"LHC Beyond 2020",* KEK Seminar, 2010

[4] FAIR Baseline Technical Report – *Executive Summary*, ISBN 3-9811298-0-6, 50, 2006

[5] P. Scherbakov et al., *"Comparative analysis of wide aperture dipole designs for the SIS300 ring"*, Proc. RuPAC XIX, Dubna, 301-303, 2004

[6] I. Bogdanov et al., *"Study of the quench process in fast cycling dipole for the SIS300 ring"*, EPAC 2004, 1744-1746, Lucerne

[7] V. Zubko et al., *"Stability of fast-cycling dipole for the SIS300 ring"*, EPAC 2004,1756-1758, Lucerne

[8] M.N. Wilson et al., *"Measured and Calculated Losses in Model Dipole for GSI Heavy Ion Synchrotron"*, IEEE Trans. on Applied Superconductivity, 14, 306-309, 2004

[9] *VLHC Design Study*, Fermilab-TM-2149, 2001

[10] H. Piekarz et al.*"A Test of a 2 T Superconducting Transmission Line Magnet System"*, IEEE Trans. Appl. Superconductivity 16, 342-345, 2006

[11] G. Velev et al., *"Field Quality Measurements of a 2 T Transmission Line Magnet"*,IEEE Trans. Appl. Superconductivity, 16, 1840-1843, 2006

[12] K.-H. Mess, P. Schmüser and S. Wolf, *"Superconducting Accelerator Magnets"*, ISBN 981 02- 2790-6, 1996

[13] B. Goddard, *"LHC beam dump, injection system and other kickers"*, Workshop on HE- LHC, Malta, Oct. 14-16, 2010

[14] S. L. Hays, *"High-Current Superconducting Inductor"*, Private Communication, October, 2010

[15] T. Sen, *"Estimate of HE-LHC beam parameters at different injection energies"*, FERMILAB-TM-2478 –APC, 2010

[16] K. Seiya, et al, *"Multi-batch slip-stacking in the Main Injector at Fermilab",* PAC07, 742-743, 2007

[17] E. Todesco and L. Rossi, *"Conceptual Design of 20 T Dipoles for Higher Energy LHC",* Workshop on HE-LHC, Malta, Oct. 14-16, 2010

[18] C. Muehle, *"Fast-Pulsed Superconducting magnets"*, HB2006, Tsukuba, 324-328, 2006

[19] E. Todesco, *private communication*, 2010

[20] M. Harrison, S. Peggs and T. Roser, *"The RHIC Accelerator"*, Annu. Rev. Nucl. Part. Sci., 52:425-69, 2002

MAGNET DESIGN ISSUES & CONCEPTS FOR THE NEW INJECTOR

P. Fabbricatore, INFN Sezione di Genova, Italy

Abstract

Possible layouts of superconducting dipoles for the main injector of High Energy LHC (HE-LHC) are proposed on the basis of the experience matured with ongoing R&D activities at the Italian National Institute of Nuclear Physics (INFN), targeted at developing the technologies for high field fast cycled superconducting magnets for the SIS300 synchrotron of FAIR. Two different magnets are analysed: a) a 4 T dipole ramped up to 1.5 T/s, and b) a 6 T dipole to be operated at lower ramp rates.

INTRODUCTION

The Facility for Anti-proton and Ion Research (FAIR), under development at GSI, includes the synchrotron SIS300 [1]. The name of the accelerator is related to its 300 Tm magnetic rigidity, which is needed for bending high intensity proton beams (90 GeV) and heavy ions, e.g. U^{92+} up to 34 GeV/u. The dipole magnets have to be pulsed from the injection magnetic field of 1.0 T up to 4.5 T maximum field, at the rate of 1 T/s. The lattice includes two kinds of dipoles, only differing in length (3.9 m and 7.8 m) [2]. These magnets have the same geometrical cross-section with cos(θ) shaped coils, 100 mm bore and the particular characteristic to be geometrically curved, with a sagitta ranging from 28 mm for the short magnets to 112.9 mm for the long ones.

Since 2006, R&D activities are going on at the Italian National Institute of Nuclear Physics (INFN) aimed at developing the technologies for constructing these magnets. The activity is performed in the framework of a project called DISCORAP (*DIpoli SuperCOnduttori RApidamente Pulsati*), according to a specific INFN-FAIR Memorandum of Understanding signed by both institutions in December 2006.

Important steps of the DISCORAP project have been: a) the development of a low loss superconducting Rutherford cable [3], b) the construction of coil winding models for assessing the constructive feasibility of curved coils, c) the construction of a complete model magnet composed of a cold mass enclosed in its horizontal cryostat [4]. The last step is now close to be concluded.

The main parameters of the model magnet for SIS300 are shown in Table 1. The conductor involved in this magnet is similar to the cable used in the outer layer of the LHC main dipole. It is a 36-strand Rutherford cable optimized for low ac losses as discussed later. Some characteristics of strand and cable are reported in Table 2.

On the basis of this experience we try to give information and develop considerations aimed at addressing general and specific aspects of the dipole for the main injector of HE-LHC.

Hans Müller of GSI/FAIR is acknowledged for the fruitful discussions and for the revision of this paper

As starting point we assume that the protons are injected at 100 GeV and accelerated up to 1 TeV or, at maximum, to 1.5 TeV, hence involving a 4 T dipole ramped up from 0.4 T, and a 6 T dipole, respectively. For the field rates we considered values in the range of 1÷1.5 T/s.

There are two critical aspects concerning these dipoles. The first one is of mechanical nature, since the magnets have to support 10^7 magnetic cycles [5]. The second one is related to the need to limit the coil heating and reduce efficiently the heat dissipation [6]. The mechanical issues and the heat exchange problematic are related to the winding (lay-out, manufacture), the aspects of the heat dissipation are more related to the conductor design.

Table 1: Characteristics of the SIS300 model dipole under development at INFN

Parameter	**Value**
Magnetic Field (T)	4.5
Ramp rate (T/s)	1
Coil aperture (mm)	100
Magnetic length (mm)	3879
Maximum operating temperature (K)	4.7
Layers/Turns per quadrant	1/34 in 5 blocks (17,9,4,2,2)
Operating current (A)	8920

Table 2: Characteristics of the cable used in the SIS300 model dipole

Strand diameter (mm)	0.825
Filament twist pitch (mm)	5
Strand Ic @ 5 T, 4.22 K	>541
n-index @ 5 T, 4.22 K	>30
Stabilization matrix	Pure Cu and CuMn
Strand Number	36
Cable width (mm)	15
Cable thickness, thin edge (mm)	1.362
Cable thickness, thick edge (mm)	1.598
Transposition pitch (mm)	100

TEMPERATURE MARGIN

For any superconducting magnet the temperature margin is an important parameter. For a magnet operating

in ac mode, it is a key parameter because the heat load due to the ac losses causes an increase of the coil temperature, predictable only with some uncertainties and depending on parameters difficult to be fully controlled. For the SIS300 dipole we designed a temperature margin of 1 K, which is presently reduced to 0.75 K because the developed low loss conductor has a critical current 14% lower than specified. Furthermore we computed that the ac losses cause a (local) temperature increase of up to 0.25 K. The real margin is consequently reduced to 0.5 K.

The temperature margin is given by the difference between the current sharing temperature and the operating temperature. Let be $I_c(B,T)$ the function describing how the critical current of the conductor depends on the magnetic field and temperature [7], and $I(B)=\alpha B$ the magnet load line identifying the peak field in the winding. The current sharing temperature T_g is univocally indentified by the intersection of $I_c(B, T)$ with the load line at the operating current. The problem with this definition is that the functions involved can not be inverted for giving an analytical expression of T_g. Therefore we will use for the margin the definition given by M. Wilson [8]:

$$\Delta T = T_g - T_0 = \left[T_c(B) - T_0\right]\left[1 - \frac{I_0}{I_c(B,T_0)}\right], \quad (1)$$

which is valid for a linear dependence of the critical current on the temperature. In Eq. 1 I_0 is the operating current, T_0 the operating temperature and $T_c(B)$ the critical temperature as function of the magnetic field:

$$T_c(B) = T_{c0}\left[1 - \frac{B}{B_{c20}}\right]^{1/1.7}, \quad (2)$$

where T_{c0} is the critical temperature (9.2 K for NbTi) and B_{c20} is the critical field (14.5 T for NbTi).

From Eqs. 1 and 2 we can find a very simple expression relating the ratio of operating current critical current at fixed field and the temperature margin ΔT:

$$f = \frac{I_0}{I_c(B,T_0)} = 1 - \frac{\Delta T}{T_{c0}\left[1 - \frac{B}{B_{c20}}\right]^{1/1.7} - T_0}. \quad (3)$$

In Fig.1 this function is plotted vs. the magnetic field for two different values of the temperature margin (0.5 K and 1 K), allowing to make some interesting considerations about the margin in current we have to take. As nominal temperature we have assumed T_0=4.7 K coming from SIS300 parameters. The magnetic field in the abscissa is the peak field. For a dipole generating 4 T field (peak field of about 4.4÷4.5 T) we have to work at 64% of the critical current at fixed field for a margin of 1 K and at 82% for 0.5 K margin. A 6 T magnet (peak field presumably about 6.4 T) requires to be operated at 45% of the critical current for 1 K margin and 72% for 0.5 K margin. The critical issue here is the amount of superconducting material required. For a 6 T magnet operating with 1 K margin we have to check if a real winding can be fitted in.

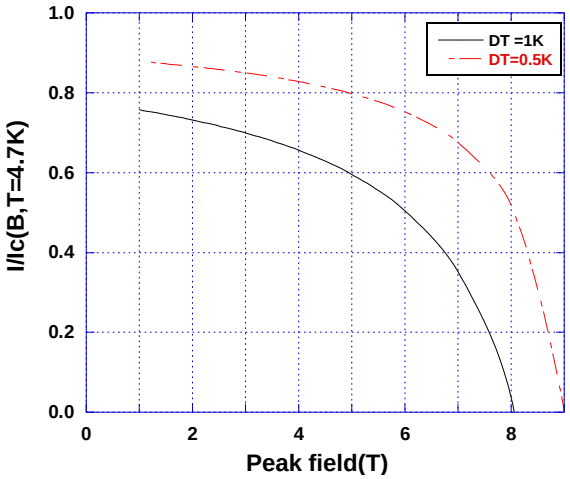

Figure 1: Operating to critical current ratio as function of the peak magnetic field for two different values of the temperature margin.

With this aim, let us try to evaluate the number of layers involved in a 4 T and 6 T dipole. For sake of simplicity we consider a sector coil [9] (just made of one sector) producing a dipole field B, which is directly proportional to the overall current density J_{ov} and the radial thickness of the sector w:

$$B = \frac{\mu_0}{\pi}\sqrt{3} J_{ov} w \quad , \quad (3)$$

considering that $B_{peak} = \gamma B$, we can find an expression for the sector thickness

$$w = \frac{\pi}{\mu_0 \sqrt{3}} \frac{B_{peak}}{\gamma \, f \, J_c(B_{peak}, T_0)\xi}. \quad (4)$$

For our calculations we use ξ (the fraction of superconductor in the winding)=0.283, γ (the ratio peak magnetic field to central field)=1.09 and $J_c(B, T = 4.7K)$ as calculated with a Bottura fit [7]. The results are shown in Fig.2. A dipole magnet producing a field of 4 T requires a coil radial thickness of 13÷14 mm for a temperature margin of 1 K. For the same margin a 6 T coil must have a thickness of more than 50 mm or 30 mm for 0.5 K margin. In term of layers made of practical Rutherford cables, a 4 T dipole magnet involves only one layer, whilst a 6 T dipole requires 2 layers and the temperature margin is closer to 0.5 K than 1 K.

PROPOSED MAGNETS

On the basis of the conclusions of the previous sections, the proposed option for 1 TeV maximum energy is a 4 T dipole composed of one layer. This magnet would be very similar to the SIS300 model under development at INFN. It is proposed to hold this lay-out except for the geometrical curvature. Consequently the characteristics for this option are the ones reported in Table 1 with the exclusion of the ramp rate (here 1.5 T/s) and the magnetic length.

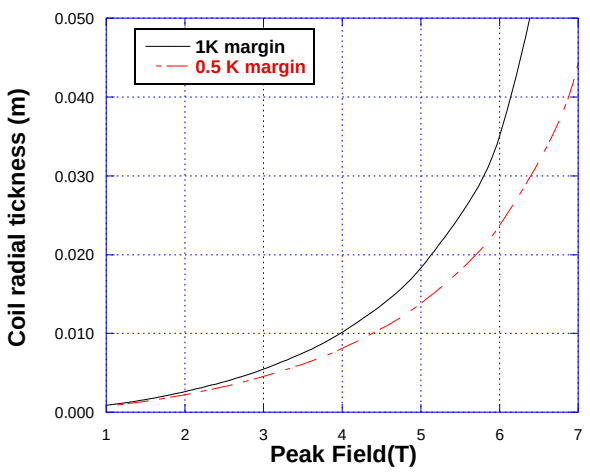

Figure 2: Coil radial thickness as function of the peak magnetic field for two different values of the temperature margin.

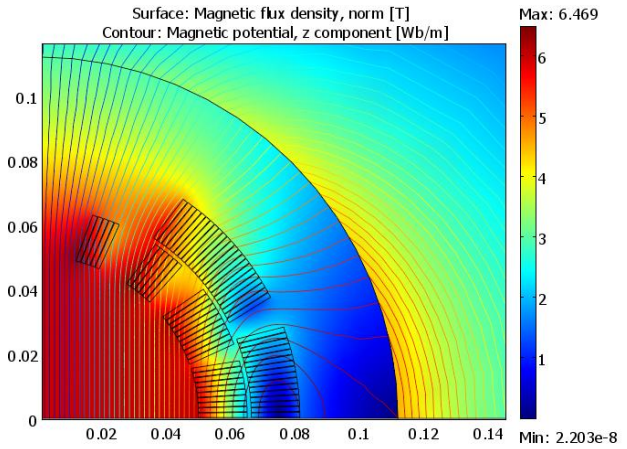

Figure 3: Layout of 6 T magnet (based on IHEP design) with the magnetic field distribution. The first quadrant is shown. The peak field is 6.42 T. The axes report dimensions in m.

For 1.5 TeV maximum energy we need a two layer coil. A very good candidate is the 6 T dipole developed at IHEP for SIS300 [10]. This design has been revisited and is proposed here with the characteristics shown in Table 3. The conductor is the same as for the 4 T option.

Table 3: Characteristics of the proposed 6 T option based on the 6 T SIS300 model dipole developed at IHEP

Parameter	**Value**
Magnetic Field (T)	6
Ramp rate (T/s)	1
Coil aperture (mm)	100
Maximum operating temperature (K)	4.7
Layers/Turns per quadrant	2/16 for first layer – 19 second
Operating current (A)	6720

In Fig. 3 a cross section of the first quadrant of the magnet is shown, with the magnetic field distribution at the operating current. Only the winding and the iron are included.

AC LOSSES

There are many sources of ac losses to be considered. They can be divided into three main categories: 1) ac losses in the conductor; 2) losses due to eddy currents in the mechanical structures; 3) losses in the iron yoke (magnetic, eddy and anomalous). Regarding the conductor, two main mechanisms are present: the hysteretic losses due to persistent currents in the filaments and the losses due to the intra-strand and inter-stand coupling currents.

The conductor and the magnet design of SIS300 were optimised for very low losses. The ac losses due to the persistent currents in the superconducting filaments were minimised using very fine filaments (2.5 μm geometrical diameter, 3.0 μm effective). The intra-strand coupling currents were minimised through both a small twist pitch (5 mm) and an optimised transverse electrical resistivity (0.44 nΩ). The inter-strand coupling currents were controlled through the contact resistance R_a between adjacent strands. Our design value of R_a is 200 μΩ. The contact resistance between opposite strands R_c is very high (mΩ range) because a 25 μm thick stainless steel sheet has been inserted inside the Rutherford cable; i.e. we are using a cored cable [11].

Presently four lengths of low loss conductor have been produced at Luvata Pori (FI) under INFN contract. The characteristics of this cable are acceptable but not completely fulfilling requirements. The filament effective diameter is 3.0 μm as expected but the measured inter-stand resistivity is lower (0.3 nΩ) and the inter-strand resistance R_a is higher than expected [12]. The average critical current of the extracted strand is 442 A (5 T, 4.22 K), or -14% compared to the design value. The critical current shows a large degradation of 6% after cabling and the n-index is 20. However, as stressed in [12], a new wire, with an improved design and an optimized manufacture cycle, is now under development at Luvata Pori.

The losses in the mechanical structure were reduced through the use of laminated collars: 3 mm thick austenitic plates electrically insulated. Steel laminations with a low value of the coercitive field (H_c= 40 A/m) were used for the yoke. The steel plates (1 mm thick) were electrically insulated and assembled using insulated bars.

Table 4 shows the different contributions to ac losses for the model of SIS300 magnet. The losses are given both in W/m and as percentage of the total power

dissipation in ramping condition. The energy dissipated during a cycle will depend on the peculiarities of the cycle (time for ramp-up, flat top, ramp down and flat at injection field). The values in Table 4 are design values. After cable production, we are expecting a reduction of hysteresis losses in filaments, an increase of intra-strand coupling losses and a decrease of inter-strand losses with respect to these values.

Table 4: Calculated ac losses in the magnet body (losses in coil ends not included) for the INFN model of short dipole for SIS300 when ramping from 1.5 to 4.5 at 1 T/s.

Loss source	**Loss (W/m)**	**Loss fraction (%)**
Hysteresis in sc filaments	2.31	30
Strand coupling	0.69	9
Interstrand coupling R_a R_c	0.46	6
Eddy currents in collars, yoke and coil protection sheets	0.46	6
Yoke magnetic	1.85	24
Beam pipe	1.08	14
Collar connection elements (keys, pins)	0.62	8
Yoke connection elements (clamps, bars)	0.23	3
Total	7.7	100

The same exercise done for the 4 T option is shown in Table 5. Computations were done for both 1 T/s and 1.5 T/s ramp rates. The information regarding the 6 T option is shown in Table 6.

Tables 5 and 6 report the ac losses for the two options on the basis of the present technology. In fact there are margins for further improvement requiring specific R&D activities. First of all it is necessary to improve the filament quality. The goal is an higher critical current density $J_c(5\ T, 4.22\ K)$=3000 A/mm^2, with filaments of effective diameter 2 μm. It is also important to better control the transverse resistivity through a manufacturing process limiting the filament deformation [12]. The strand twist pitch can be further reduced. The measurements done during the development demonstrated that a wire with diameter 0.825 mm could be twisted with a pitch as low as 4 mm, without a significant degradation of the critical current.

The use of electrical steel with lower coercitive field (30 A/m) can further decrease the contribution of the steel magnetization to the ac losses. Coil protection sheets made of insulating material can cut eddy currents in these components. There are also margins for decreasing the eddy currents in the other mechanical components. Table 7 reports the expected ac losses for the two proposed magnets after improving the conductor, the components and the design.

Table 5: Calculated ac losses in the magnet body (losses in coil ends not included) for the 4 T option when ramping from 0.4 to 4.0 T at different ramp rates.

Loss source	**Loss (W/m) and fraction 1 T/s**	**Loss (W/m) and fraction 1.5 T/s**
Hysteresis in sc filaments	3.11 (38%)	4.65 (30%)
Strand coupling	0.74 (9%)	1.70 (11%)
Interstrand coupling R_a R_c	0.50 (6%)	1.09 (7%)
Eddy currents in collars , yoke and coil protection sheets	0.50 (6%)	1.09 (7%)
Yoke magnetic	1.57 (19%)	2.63 (17%)
Beam pipe	0.92 (11%)	2.17 (14%)
Collar connection elements (keys, pins)	0.67 (8%)	1.55 (10%)
Yoke connection elements (clamps, bars)	0.25 (3%)	0.62 (4%)
Total	8.26	15.50

Table 6: Calculated ac losses in the magnet body (losses in coil ends not included) for the 6T option when ramping from 0.4 to 6.0 T at 1 T/s

Loss source	**Loss (W/m)**	**Loss fraction (%)**
Hysteresis in sc filaments	5.40	40
Strand coupling	1.22	9
Interstrand coupling R_a R_c	1.22	9
Eddy currents in collars , yoke and coil protection sheets	0.54	4
Yoke magnetic	3.10	23
Beam pipe	1.07	8
Collar connection elements (keys, pins)	0.68	5
Yoke connection elements (clamps, bars)	0.27	2
Total	13.5	100

The conductor ac losses in Tables 4÷7 were computed using Roxie™. The losses in the electrical steel were computed with FEMM [13]. Other computations were done with Comsol™. It is worth noting that the two options have very similar overall ac losses (about 11 W/m) and also the contributions to the losses are very similar. In all case there is a large contribution of persistent currents in the superconducting filaments (from 34% to 40%) and steel magnetization (from 20% to 25%)

Table 7: Calculated ac losses for 4 T dipole ramped at 1.5 T/s and 6 T ramped at 1 T/s (losses in coil ends not included).

Loss source	Loss (W/m) and fraction 4 T dipole 1.5 T/s	Loss (W/m) and fraction 6 T dipole 1 T/s
Hysteresis in sc filaments	3.91 (34%)	4.24 (40%)
Strand coupling	0.81 (7%)	1.17 (11%)
Interstrand coupling R_a R_c	0.92 (8%)	0.85 (8%)
Eddy currents in collars, yoke and coil protection sheets	0.11 (1%)	0.11 (1%)
Yoke magnetic	2.30 (20%)	2.65 (25%)
Beam pipe	2.18 (19%)	1.06 (10%)
Collar connection elements (keys, pins)	0.92 (8%)	0.32 (3%)
Yoke connection elements (clamps, bars)	0.35 (3%)	0.21 (2%)
Total	11.50	10.61

A COMPARISON BETWEEN THE TWO OPTIONS

Table 8 shows a comparison of characteristics and performances for the two proposed options. The parameters considered for the comparison are: 1) the injection field and the sextupole component of the field, 2) the maximum and the peak magnetic fields, 3) the temperature margin over the maximum operating temperature of 4.7 K; 4) the AC losses in the superconducting cable during ramp; 5) the AC losses in the structures during ramp: eddy currents and magnetization; 6) the weight; 7) the construction costs.

Table 8: Comparison between 4 T and 6 T options for He-LHC main injector

Parameter	4 T dipole 1.5 T/s	6 T dipole 1 T/s
Injection magnetic field [T] and b3	0.4 /-4.5	0.4 /-4.9
Maximum/ Peak magnetic field [T]	4/4.4	6/6.42
Temperature Margin (K) over 4.7K	1.66	0.65
AC losses in the superconducting cable during ramp [W/m]	5.6	6.3
AC losses in the structures during ramp(eddy currents and magnetization) [W/m]	5.9	4.3
Weight (t/m)	1.28	1.68
Construction costs in (k€/m)	60÷70	80÷90

Critical points for both magnets are the high values of the sextupole at the injection field. The 6 T option also works with a low temperature margin. Next year, the 6 T short dipole developed at IHEP, should be completely tested at GSI and the real limits would be clearer. The same considerations apply for the 4.5T model developed at INFN.

CONCLUSIONS

The R&D developments for SIS300 dipoles both at INFN and at IHEP in collaboration with GSI are setting the basis for giving the feasibility of superconducting magnets with fields of 4.5÷6 T ramped at 1 T/s or faster.

Advanced designs, construction techniques and first low loss conductors were developed.

For more conclusive considerations we have to wait for results of the testing of the model magnets at operating temperatures at GSI next year. In particular we are waiting for more information regarding the effects due to mechanical fatigue, which could be a major problem for fast cycled magnet.

On the basis of the present knowledge some extrapolations can be done for HE LHC injector magnets. A 4 T dipole ramped at 1.5 T/s has been analysed and compared with a 6 T dipole to be operated at 1 T/s ramp rate.

It appears that one can get ac losses as low as 11 W/m when ramping the magnets. For a further reduction of the ac losses major variations of the design are required. The 4 T option is less critical and less expensive as the 6 T one.

The field quality at injection energy could be an issue for both options.

REFERENCES

[1] W. F. Henning, "The GSI project: An international facility for ions and antiprotons",.Nuclear physics A, Nuclear ad hadronic physics 734 (2004) 654.

[2] G.Moritz, "Superconducting magnets, for the International accelerator facility for beams of ions and antiprotons at GSI" IEEE Trans Appl Supercond 13 (2003) 1329.

[3] G. Volpini, F. Alessandria, G. Bellomo, P. Fabbricatore, S. Farinon, U. Gambardella, M. Sorbi, "Low-loss NbTi Rutherford Cable for Application to the Development of SIS-300 Dipoles," IEEE Trans Appl Supercond 18 (2008) 997.

[4] P.Fabbricatore, F. Alessandria, G. Bellomo, S. Farinon, U. Gambardella, J.Kaugerts, R.Marabotto, G.Möritz, M. Sorbi, and G. Volpini, "Development of a curved fast ramped dipole for FAIR SIS300" IEEE Trans Appl Supercond 18 (2008) 232.

[5] S.Farinon, P.Fabbricatore, R.Musenich, F.Alessandria, G.Bellomo, M.Sorbi, G.Volpini, U.Gambardella, "A Model Dipole for FAIR SIS300: Design of the Mechanical Structure", IEEE Trans Appl Supercond 19 (2009) 1141.

[6] M. Sorbi, F. Alessandria, G. Bellomo, P. Fabbricatore, S. Farinon, U. Gambardella and G. Volpini, "Field Quality and Losses for the 4.5 T Superconducting Pulsed Dipole of SIS300" IEEE Trans Appl Supercond 18 (2008) 138.

[7] L.Bottura, "A practical fit for the critical surface of NbTi", IEEE Trans Appl Supercond 10 (2000) 1054.

[8] M.N.Wilson, "Superconducting Magnets", Oxford University Press, New edition (1987).

[9] L.Rossi and E.Todesco "Electromagnetic design of superconducting dipoles based on sector coils", Phys. Rev. ST Accel. Beams 10 (2007) 112401.

[10] S.Kozub, I.Bogdanov, V.Pokrovsky, A.Seletsky, P.Shcherbakov, L.Shirshov, V.Smirnov, V.Sytnik, L.Tkachenko, V. Zubko, E. Floch, G. Moritz, H.Mueller," SIS 300 Dipole Model", IEEE Trans Appl Supercond 20 (2010) 200.

[11] J. Kaugerts, G. Moritz, M. N. Wilson, A. Ghosh, A. den Ouden, I. Bogdanov, S. Kozub, P. Shcherbakov, L. Shirshov, L. Tkachenko, D. Richter, A. Verweij, G. Willering, P. Fabbricatore, and G. Volpini, "Cable Design for FAIR SIS 300", IEEE Trans Appl Supercond 17 (2007) 1477.

[12] G. Volpini, F. Alessandria, G. Bellomo, P. Fabbricatore, S. Farinon, U. Gambardella, M. Holm, B. Karlemo, R. Musenich, M. Sorbi, "Low loss NbTi superconducting Rutherford cable manufacture for the SIS300 INFN model dipole", contributed paper to ASC 2010, August 1-6, Washington D.C. (2010).

[13] Information about this code for "Finite Element Method Magnetics" can be foud at web site http://www.femm.info/wiki/HomePage

USING LHC AS INJECTOR AND POSSIBLE USES OF HERA MAGNETS/COILS

K. H. Meß, CERN, Geneva, Switzerland

Abstract

This workshop discusses the various aspects of a high energy version of the LHC in the LHC tunnel, the basic assumption being that the LHC will be decommissioned. The possibilities to recycle LHC and the already stopped HERA are discussed in this paper.

INTRODUCTION

It might seem too early to discuss the fate of the LHC magnets before they have reached their design performance and well before the LHC has produced sufficient luminosity to support or change our present concept of high energy physics. However, ideas, like the HE-LHC, need a long time to be accepted, planned, and eventually transformed into reality. Trying to contain the costs by studying the possibilities of recycling high investments of the past is an integral part of this process.

By the time of the HE-LHC the LHC will be decommissioned and the superconducting magnets of HERA [1] in Hamburg might also still be available and useful, if the DESY management decides so.

Table 1 shows a summary of the parameters, which are most important for a recycle. The LHC has, as of today, not reached its design performance, while HERA has been operated in the last years about 12% above design (values in brackets). In both cases the magnets are optimised for the specific purpose. The magnets are bent to maximise the aperture while minimising the coil diameter (as well as cost and stored energy). Evidently, the curvature is adapted to the respective bending radius ρ, given by the magnetic field B and beam energy E:

$$|B\,[T]| = \frac{\beta \cdot E\,[GeV]}{0.2998 \cdot \rho\,[m]}$$

Table 1: Some LHC and HERA parameters

Machine	LHC [2]	HERA [1]
Circumference	26.7 km	6.4 km
# of main bends	1232	422
Magnet length	14.3 m	8.9 m
Injection Field	0.535 T	0.227 T
Flat Top Field	8.33 T	4.649 (5.216) T
Current (inject.)	763 A	245 A
Current (top)	11850 A	5027 (5640) A
Inj.Energy	450 GeV	40 GeV
Top Energy	7 TeV	820 (920) GeV
Bending radius	2804 m	588 m
Inner coil Ø	56 mm	75 mm
Cold tube Ø	50 mm	55.3 mm
Sagitta	9.14 mm	14.4 mm
Nom. dI/dt	10 A/s	10 A/s
Tunnel Ø	3.76 m	5.20 m

LHC MAGNETS

The LHC magnets are designed for the LEP tunnel. Hence, for the useful range of the magnetic field, particle energy, and aperture, the magnets fit only into a tunnel of about 27 km circumference, i.e. the LEP tunnel.

Use of the LHC as injector

The injection energy of the HE-LHC is planned to be around 1.3 TeV. A somewhat higher energy would of course be beneficial, both in terms of persistent current effects and total filling time. The "old" LHC could evidently accelerate from 450 GeV to anything below 7 TeV and keep the two beams ready for injection, provided that the beams do not interfere with the HE-LHC, while it is still running at a much higher energy. The LHC could prepare the beams "in the shadow" and shorten the overall filling time of the HE-LHC, despite its low acceleration rate. This scenario does not require a new SPS and new injection lines operating above 1 TeV.

Space requirements for the LHC and HE-LHC

However, this forces the co-existence of the "old" and the "new" accelerator in a fair fraction of the tunnel and it needs new beam lines to bypass the experiments. The bypasses have to go through the galleries. To keep the two machines at the same length (which is essential for the use of the LHC as injector) the LHC has to be shifted towards the transport space everywhere else. Alternatively, the HE-LHC has to be shifted further to the outside, referred to the present layout. Neither of these options seems easily possible.

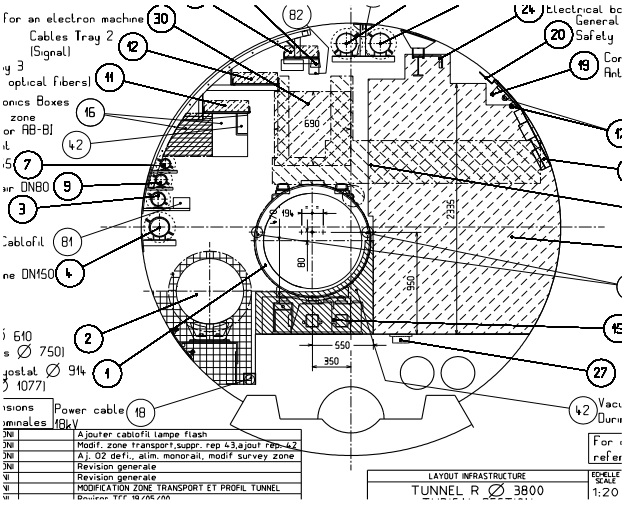

Figure 1. Sketch of the LHC tunnel

Fig 1 shows a sketch of the LEP tunnel with a LHC dipole. It presents the most benign case, without further obstructions in the way. It seems just possible to fit a much smaller electron accelerator of 50...60 GeV (LHeC) [3], [4]. The HE-LHC magnet is, however 230 mm wider than the LHC [5]. If the top energy of the LHC is decreased to, say, 2 TeV a large amount of flux steel can be taken away, thus saving space. The "slim" LHC and the HE-LHC could share the same cryostat. Such a combined machine might fit, but this proposal "works" only for the "easy" part of the machine.

Figure 2 and figure 3 show a more difficult case, where the trick, mentioned above, does not work: the area of the dump-ejection kickers and lines.

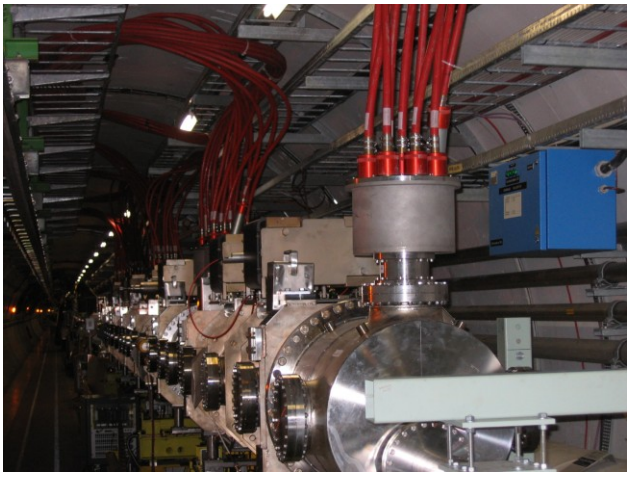

Figure 2. LHC dump kickers

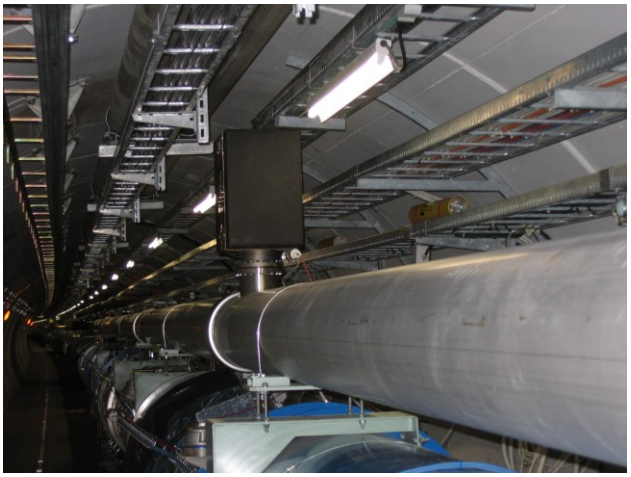

Figure 3. LHC dump line above the LHC

There is clearly no space to place a second set of kickers or dump lines as well as a wider HE-LHC, even under the assumption that kickers for 16 TeV can be produced fitting into the straight section longitudinally.

The RF section for the LHC would have to be moved to one of the new bypass sections, like it could be done for the LHeC. The cryogenics [6] for the HE-LHC, however, will be of the same size as the existing for the LHC. There is no space for it. The HE-LHC will need its own energy extraction system, which will consist of at least twice the number of switches and resistors as pointed out before [7]. There is no space for it. The HE-LHC will need its own set of collimators. The design is unknown [8]. However, the collimation system will not be smaller than the existing for the LHC. There is no space for it.

Conclusion

The HE-LHC and the LHC cannot fit into the LEP tunnel. The LHC magnets cannot be re-used in the context of the HE-LHC.

HERA MAGNETS

The case of the HERA magnets has been treated before [9]. This report summarises that work. Figure 4 shows a view of the HERA tunnel. The two accelerators are installed above of each other with the proton machine on the top. The dipoles [10] were produced partly in Italy (see figure) and partly in Germany. The quadrupoles were produced in France and mounted into their cryostat in Germany.

Figure 4. View of the HERA tunnel with the superconducting proton machine on top of the electron machine.

Use of the HERA magnets

The HERA magnets are designed as storage ring magnets. Hence, the acceleration rate is low (~1.6 GeV/s). The use as pre-accelerator in the SPS tunnel is not attractive, although the radius of curvature could be adapted to. The SPS tunnel is wide enough and additional aperture could be created by replacing the beam pipe. The present beam pipe diameter is determined by the corrector windings on the beam pipe [11].

The slow acceleration rate is of no concern, if the magnets are used for the injection lines TI2 and TI8. The question is: do the magnets fit there and can the cryogenic requirements be met?

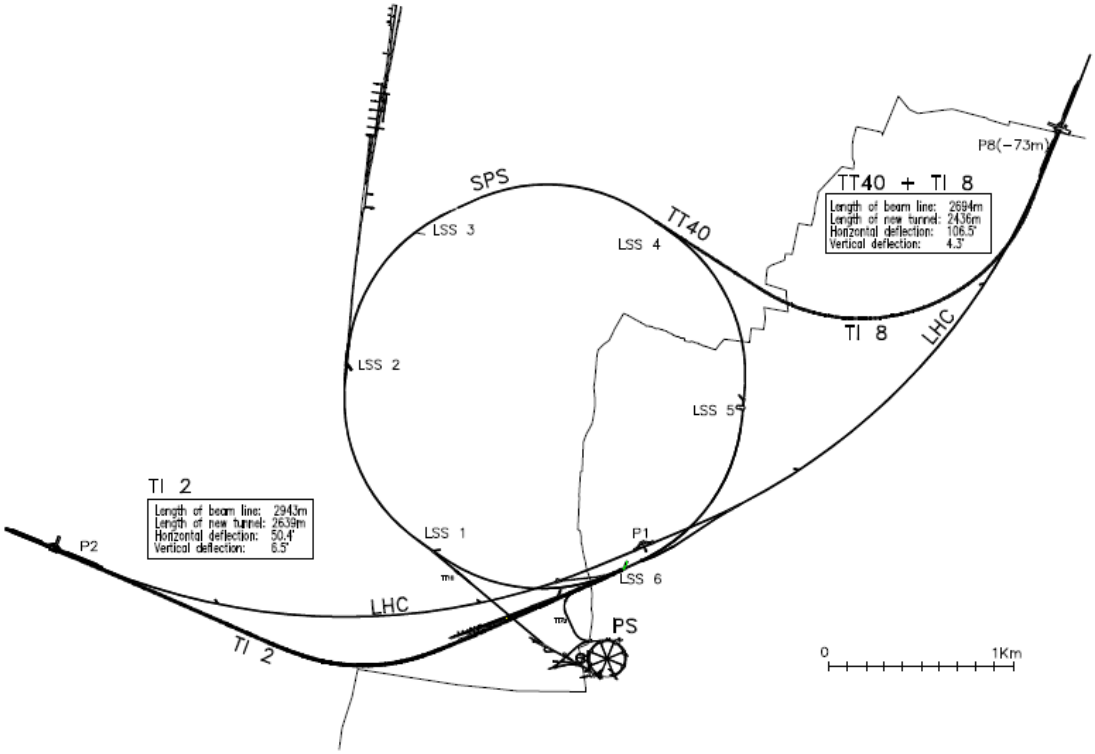

Figure 5. Layout of the injection lines TI2 and TI8

Injection line layout

The layouts of the TI8 and TI2 transfer lines are described in the LHC Project Note 128 [12] and in the LHC Design Report, Vol III [2]. TI2 has a length of about 2.9 km. It consists of one 48° horizontal bend and three vertical bends of 61, 42 and 9 mrad to avoid the underground valley below St. Genis. The steepest slope is 2.6%. TI8 is somewhat shorter (2.7 km) but steeper (3.77%). It consists of a horizontal bend of 103° in the descending part, preceded and followed by vertical bends of 38 and 35 mrad respectively.

The lines use a FODO structure with a half-cell length of 30.3 m and 4 dipoles per half-cell for the horizontal bending part. The vertical bends are made of a different type of bending magnets. The main features of the injection lines are shown in Figures 5 to 7, taken from the LHC project note 128. Note that the proton beam is bent counter-clockwise in TI8 and clockwise in TI2. Note further that in both cases the magnets are placed at the inner radius of the injection tunnel.

The HERA magnets

A HERA half-cell consists of one dipole on either side of the dipole-corrector and quadrupole assembly. The FODO cell has a length of 47.012 m. The dipoles contain beam-pipe corrector windings, as mentioned above. A dipole corrector and a beam position monitor are also integrated in the cryostat of the quadrupole. A few shorter quadrupoles and vertical dipoles exist to adjust the optics and to deflect the proton beam vertically. The key parameters of the various magnets can be found in Ref. [9].

In HERA the superconducting main magnets are connected in series. The current flows clockwise through the dipoles and counter-clockwise back through the quadrupoles. Hence the optical lattice is fixed. Adjustments to the tune are made by varying the relatively strong quadrupole correctors, wound around the beam pipe inside the dipoles. All dipoles are curved to follow the local bending radius of the beam of $r = 588$ m. The proton beam travels counter-clockwise in HERA. The magnets are placed on the outer side of the tunnel with the quench relief valves also pointing to the outside.

A HERA dipole deflects a 820 GeV beam by 2.9599 mrad at the nominal excitation with 5027 A (4.649 T).

The beam pipe is bent correspondingly. Note however that HERA has been operating for a number of years at 920 GeV with a field of 5.216 T. This was made possible by lowering the temperature of the coils.

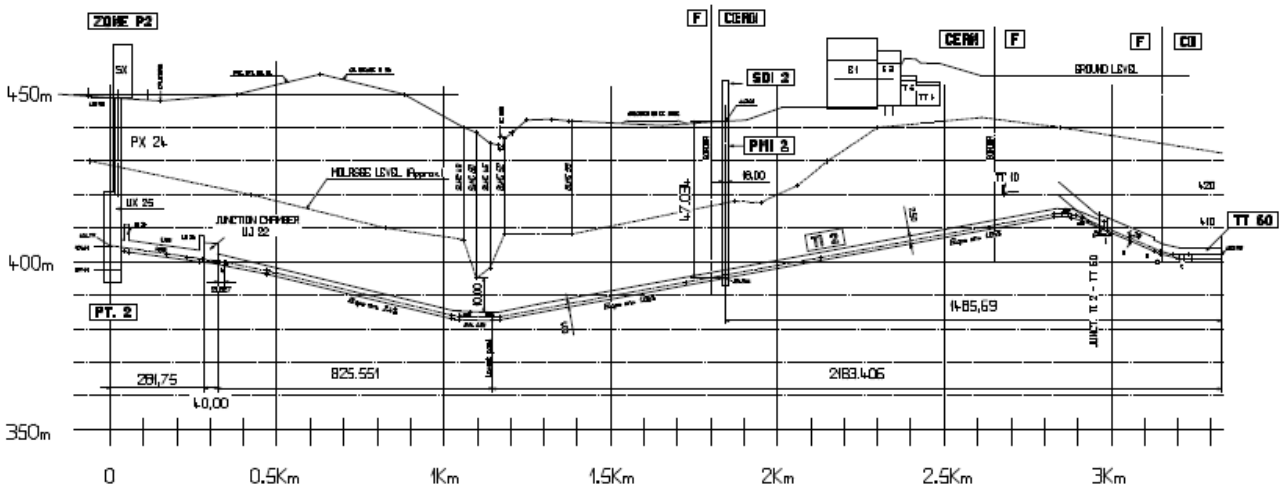

Figure 6. The vertical deflections in TI2

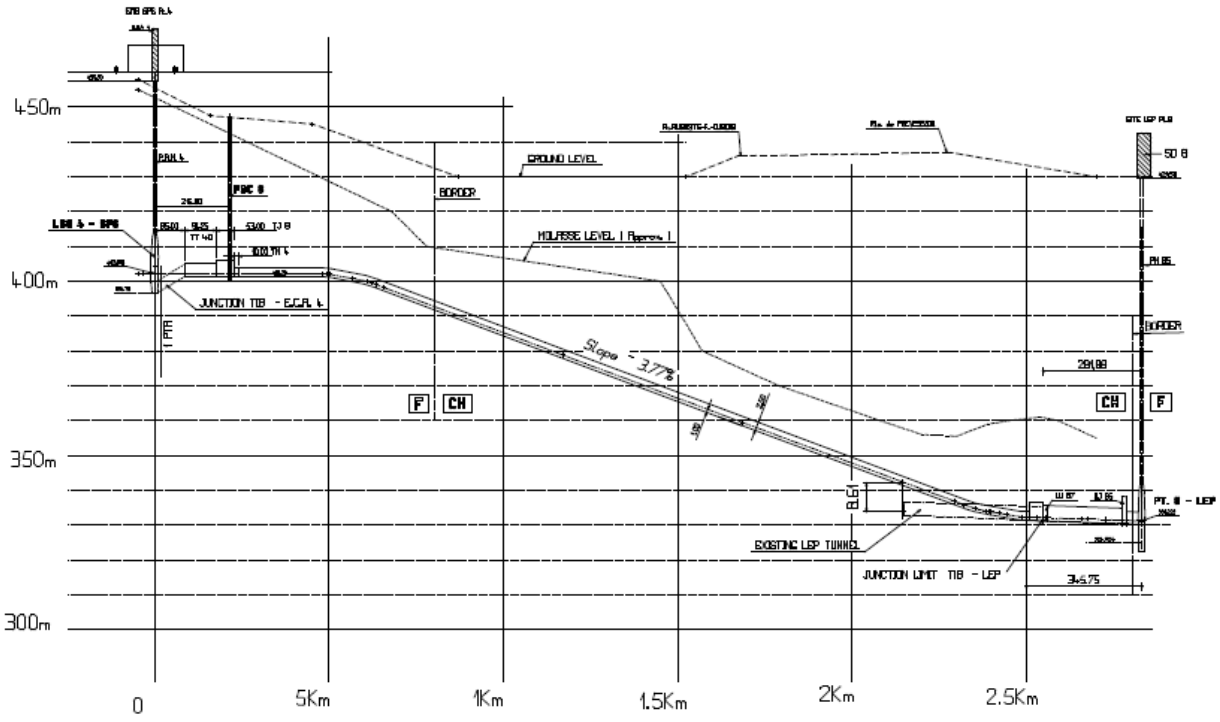

Figure 7. The vertical deflections in TI8

Space requirements and necessary changes

The HERA tunnel is much wider than TI2 and TI8. It will be difficult to accommodate HERA magnets in the LHC injection channels. The situation is particularly difficult in TI2, which is also used to transport LHC dipoles into the LHC tunnel.

Fig. 8 shows on the left this situation as it is now and a possible solution with the HERA magnets at the right.

Note that the beam is presently on the inner curvature of the tunnel in both cases. The HERA dipoles have their quench relief valves and the quench exhaust pipe at the outer curvature (i.e. in the transport space in this case), which would clearly obstruct the transport zone. Either the cryostats have to be modified or the beam line has to be moved to the outer curvature. The latter is not easy, because the position of PMI2 was chosen to lower LHC magnets into the space at the outer curvature of TI2. One could presumably install a transfer table at the lower end of the shaft, such that the TI2 magnets are in fact installed underneath the shaft at the outside curvature. Components for the LHC could then be lowered to the transfer table and moved sideways and lowered into TI2, to pass on the inner curvature. In this way one could avoid dismounting the vacuum pipe, which presently blocks the transport path. Fig. 8 does not show any cryogenic line. The number of cable trays, however, cannot be reduced drastically (it is likely to increase, because the quadrupoles need cables).

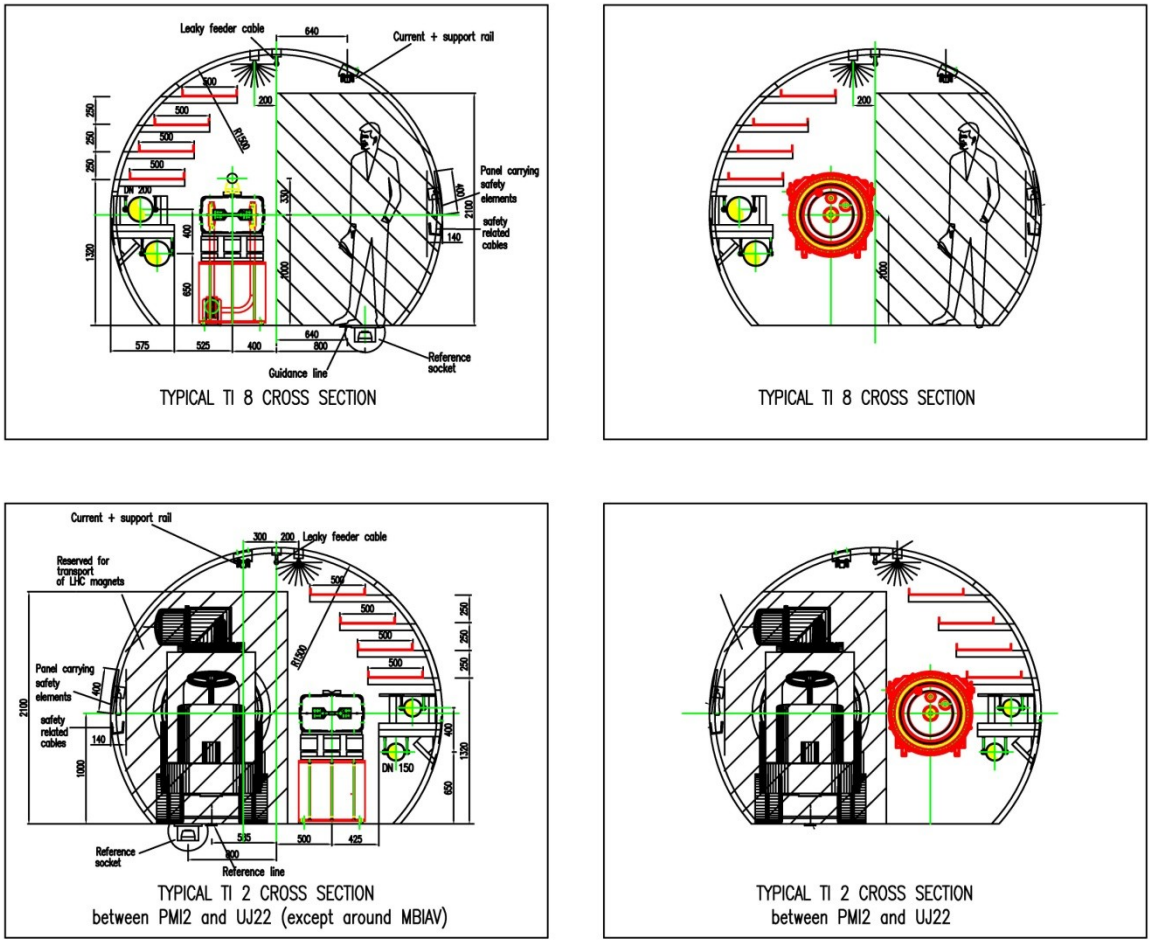

Figure 8. The TI2 and TI8 cross-sections in the present state (left) and with HERA dipoles (right)

It seems extremely difficult to fit the HERA magnets into TI2, as is illustrated by Fig. 9, now for the magnets on the outer curvature. The 500 mm quench relief pipe does not fit. The quench relief valves would need to be seriously reworked and still the cables would not find space. Even worse, as can be seen in Fig. 6, the deepest point of TI2 is underneath the creek Lion. According to the studies on cryogenics for the injection lines (see below), the single-phase helium will have to enter the string of magnets at the lowest point. However, the study does not take the actual configuration into account and will have to be repeated.

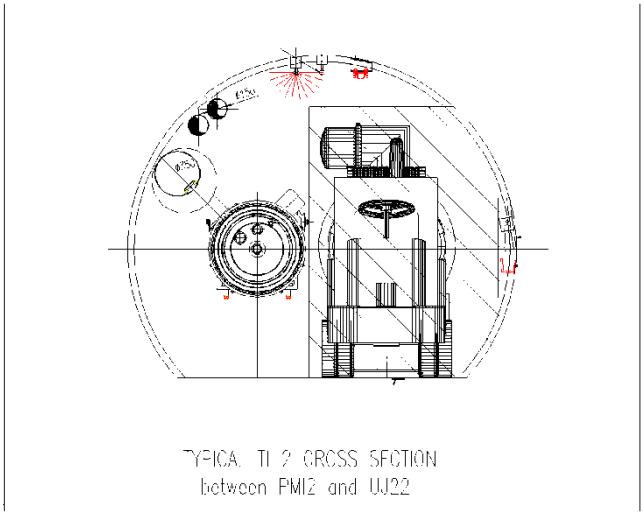

Figure 9. HERA dipoles in TI2 on the outer curvature in beam direction (two versions of the quench relief pipe)

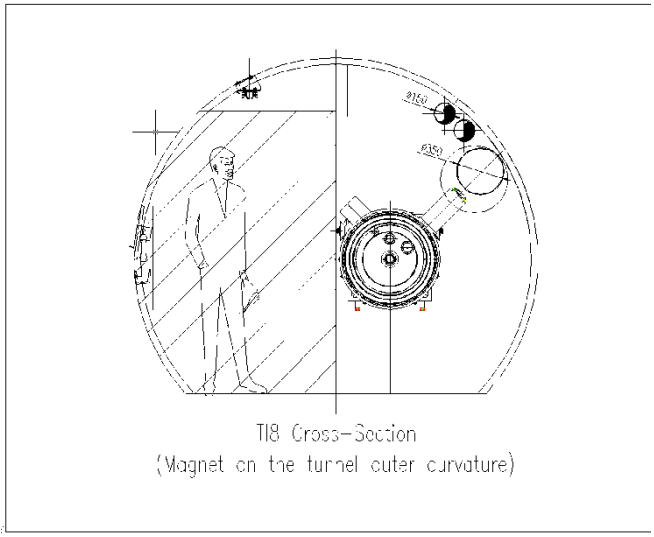

Figure 10. HERA dipoles in TI8 on the outer curvature in beam direction.

In TI2 the bending is clockwise. The HERA magnets would need to run with inverted polarity, which requires a change of the polarity of the protection diode. This can be achieved by removing the diode stacks, opening them, inverting the polarity, testing them under cryogenic conditions and reassembling. This is a tedious, but possible, operation. Alternatively, adapter pieces could be envisaged, which change the polarity inside the cryostat. This seems possible, because both magnet ends (end covers) will have to be opened in order to fulfil the conditions set by the cryogenics (see below).

Still, the cable ladders do not find space and water cooling will have to move also. While the cables are still needed, the water cooling could maybe be reduced. Presumably the beam line could be lowered somewhat, which seems possible at this stage. It is unclear, if and where the cryogenic re-coolers could be placed, unless they can be part of the connection cryostats or the magnets themselves.

The situation is slightly better in TI8. The bend is counter-clockwise, as in HERA. Hence the magnets can run with the original polarity. The magnets are however also here on the wrong side of the tunnel. Again they would have to be moved to the outer curvature to give space to the quench relief valves and quench pipe, which looks impossible, as can be seen in Fig. 10. Certainly the exhaust valves ("Kautzky valves") need to be reworked and the beam line has to be lowered.

Limits

It might be possible to rearrange the optics [11] to make optimal use of the properties of the HERA magnets and achieve higher energies. However the HERA magnets can also be mapped onto the existing structure. Because of the higher bending power of the HERA dipoles, compared to the normal conducting magnets, the present cell length of 60.6 m is sufficient to reach 900 GeV. The space between the dipoles will be filled with connection cryostats, containing the quadrupoles, the current leads and cryogenic feed-boxes. The limitation to 900 GeV is given by two constraints: the optics chosen as baseline and the bending radius of the magnets. Both constraints are somewhat flexible. The density of dipoles could be increased and hence the total bending power. However, in this case, the aperture would be reduced, due to the poorly matching sagitta of the beam pipe. This seems acceptable comparing the HERA aperture with the present beam line aperture. In conclusion, a 1 TeV beam line of sufficient aperture could presumably be made with a new optics design.

The proposed structure has, however, a very serious problem. In HERA the dipoles and quadrupoles are connected in series, containing only one bus-bar pair in the bypass. This is incompatible with the existing optics in TI2 and TI8 and the corrector quadrupoles inside the dipoles (2* 10.62 T integrated gradient) are insufficient to replace real lattice quadrupoles. They could, however be used for adjusting the optics.

Reference 9 lists all required dipoles and the aperture mismatches, all of which are very small. It also shows that the quadrupoles of HERA do not fit at all. New

quadrupoles would be needed. MQTL [2] type magnets would be sufficient, limiting the required current to below 600 A. The current could be distributed using the blocked cooling channel or by adding a "line N" type pipe on the outside of the cold mass.

Cryogenics

At present HERA is running under the following cryogenic conditions [13], [14]:

The magnets are cooled with supercritical helium with p> 2.5 bar, T=4.0 K (!). The supercritical helium is cooled by the counter flow of two-phase helium. The expansion is done at the lowest point of an octant, which is in the middle or at one end of an octant. There is a feed box containing the current leads and all the valves including a Joule Thomson valve. The two-phase flow is always directed uphill to avoid the capture of bubbles. To run at 920 GeV at HERA (as would also be required in the LHC injection lines) the temperature must be as low as T=4.0K. This is achieved by lowering the suction pressure of the screw compressors to 650 mbar. The pressure drop over the 620 m of one octant is about 100 mbar. The inclination of the HERA tunnel (max 10 mrad) is so small that the resulting pressure drop due to gravity can be neglected. The stationary mass flow is 35 g/s. A study has to be made of how to achieve similar conditions in the steep LHC transfer line tunnels.

In 1993 N. Delruelle et al. [15] studied a possible cryogenic system for the injection lines. At that time the ideas about the injection lines had not yet converged to the present design. Hence not all conclusions in this study can be applied to the present case. However, the slopes were planned to be even higher. The authors assume HERA or UNK like magnets of only 5.7 m length at 4.5 K. The preferred solution foresees single phase helium with re-coolers. The helium is fed in at the bottom of the arc (of which 3 were planned at that time) and proceeds through the magnets at a rate of 60 g/s. The liquid is re-cooled at the end of each cell by a heat exchanger in a bath of boiling helium. The gas is returned through the magnets using the holes in the iron laminations of the magnets, which in the case of the HERA magnets is either used for the heat exchanger or blocked (lower orifice). Thermally insulated pipes have to be inserted, to prevent heat propagation between the cells. Note that HERA quadrupoles do not have these heat exchanger holes, a further reason, why they cannot be used here. In addition a 500 mm quench relief line is needed.

Alternatively a two-phase cooling scheme with phase separators at the end of the cells has been considered. This scheme offers many advantages. However the authors request further tests before the solution can be seriously pursued, because "its feasibility is still doubtful".

The study does not include the very special actual geometry of TI2 with its up-hill and down-hill slopes. The narrow tunnel will not be able to accommodate a refrigerator. A study has to be made on the basis of the actual geometries, whether and how stable conditions can be achieved at 4.0 K.

Protection issues

The HERA dipoles come with a quench protection system [16], which is based on magnetic amplifiers. To operate this system requires special know-how, which is difficult to find even now. It has to be replaced in due time. Likewise, the capacitors in the heater power supplies will not operate any more after 40 years. In short, the electronics needs to be replaced.

The magnets are protected against the energy of the other magnets in the string by cold diodes. The diodes and the heat sinks are constructed to survive a decay time of 20 s from 6 kA. As the maximum voltage during the extraction has to be limited to below ±530 V, leading to an extraction resistance of less than 175 mΩ, the maximum inductance per protection block is limited to 3.3 H or 55 magnets of 60 mH each. This is close to the 56 or two times 57 magnets needed in the long arcs, but a bit too low. The resistors in HERA are simple bifilar stainless steel pipes, which could be reused adding some electrical protection. The switches are laterally of the size of the magnets and should fit. The same holds for the electronics.

A number of dipoles will need its own power converter. In these cases the diode might prevent a fast discharge.

The quench protection and energy extraction for the quadrupoles depend on the choice of the quadrupole system. Forty quadrupoles of the MQTL type connected in series have an inductance of 5 H. Bypass resistors, as implemented in the LHC for this magnet type, will be necessary. The resulting time lag is not important for the application as injection line magnets.

Conclusions

The special geometry of the TI2 and TI8 transfer lines poses serious problems for upgrading them into the 1 TeV range. The HERA dipoles, with the required cryogenic pipe and cable trays, will not fit in, unless heavily reworked. A major rework of the magnets is also necessary to accommodate to the different cryogenic conditions (and the opposite field direction in TI2). The magnets will have to be taken out of their cryostat, the end-covers will have to be removed, the heat-exchanger pipes will have to be replaced and new connections will be necessary. Eventually only the collared coils with their flux iron can be reused. In any case, the end covers need to be closed again, after rerouting the pipe for the exhaust valve. Finally, new cryostats will have to be constructed.

The HERA quadrupoles can in all probability not be used, unless the optics is completely changed and the cryostats, the cold bus-bars and the internal helium pipes are redesigned. As a result around 180 new quadrupoles will have to be made.

The cryogenics has to be extraordinary slim in order to fit into the tunnel. The steep slope puts additional constraints. In particular TI2 with positive and negative

slopes presents problems. This should be addressed in a separate study again.

SUMMARY

In summary, the LHC and HE-LHC together do not fit in the LEP tunnel. The curvature of the LHC dipoles prevents any other use (except very special cases and in small quantities).

HERA dipoles could be used for a 900 GeV, probably 1TeV, beam line in TI2 and TI8. This requires however important changes of the cooling scheme and consequently of the cryostats. The quadrupoles cannot be used.

In view of these difficulties the use of combined function magnets [17] might have more advantages.

The cooling scheme has to be designed yet and may be very space consuming. This applies, of course, for any kind of superconducting injection lines.

REFERENCES

[1] HERA, A proposal for a large electron-proton colliding beam facility at DESY, DESY, HERA 81-10.
[2] LHC Design Report, CERN 2004-003.
[3] K. H. Meß, LHC-LHeC Interference, LHeC design meeting, Tuesday 02 February 2010, http://indico.cern.ch/conferenceDisplay.py?confId=83244
[4] LHeC CDR, to be published.
[5] E. Todesco, this workshop.
[6] D. Delikaris, this workshop.
[7] K.H. Meß, Machine Protection, 1st CARE-HHH-APD Workshop on Beam Dynamics in Future Hadron Colliders and Rapid Cycling High-Intensity Synchrotrons, CERN, Geneva, Switzerland, 8 - 11 Nov 2004, pp. 15-17.
[8] R. Assmann, this workshop.
[9] K.H. Meß, D. Smekens, CERN, A Possible Upgrade of the LHC Injection Lines to 900 GeV using HERA Dipoles , CARE-Note-2006-012-HHH
[10] K. Balewski et al., Cold yoke dipole magnets for HERA, 1987, Presented at: Applied Superconductivity Conference, Baltimore, MD, USA, 28 Sep - 3 Oct 1986, pp. 1233-1235.
[11] C. Daum et al,, Superconducting Correction Magnets for the HERA Proton Storage Ring, IEEE Transactions on Magnetics, Vol. 24, No 2, March 1988, p 1377.
[12]A. Hilaire et al, The Magnet System of the LHC Injection Transfer Lines TI2 and TI8, August 2000, LHC Project Note 128.
[13] H Lierl, (DESY), private communication
[14] G. Horlitz et al., Computer Calculation on Steady-State Operation and Different Modes of Cool Down and Warm Up of the HERA Superconducting Proton Ring, Advances in Cryogenic Engineering, Vol 31, 1985, p 723.
[15] N. Delruelle et al., Design criteria of the Cryogenic system for the CERN LHC injection lines, CERN-AT-93-24-CR; LHC-NOTE-240.
[16] K. H. Meß, Quench Protection at HERA, PAC Washington 1987, Washington 1987, IEEE Particle Accelerator Conference, p 1474.
[17] T. Ogistu et al, IEEE Transactions on Applied Superconductivity, Vol. 15, No. 2, June 2005, p 1175.

INTENSITY ISSUES AND MACHINE PROTECTION OF THE HE-LHC

R. Assmann, CERN, Geneva, Switzerland

Abstract

The HE-LHC study investigates the possibilities for upgrading the beam energy of the Large Hadron Collider CERN from 7 TeV to 16.5 TeV. This paper presents a preliminary investigation of intensity issues and machine protection for the HE-LHC.

INTRODUCTION

The HE-LHC design parameters [1] that are most relevant for collimation and machine protection are summarized in Table 1. It is seen that the total stored energy E_{stored} is 33% higher and the energy density ρ_e is increased 5-fold in each beam. The extrapolation of the HE-LHC is compared in Fig. 1 and Fig. 2 to various accelerators and designs, including the parameters achieved in the LHC during the 2010 run.

The advance in energy density is driven by the decrease in the geometric transverse emittance $\varepsilon_{x,y}$ from 0.5 nm to 0.15 nm. It is noted that the increases of stored energy and energy density are even more pronounced for a single bunch, which must be considered for many machine protection studies.

Table 1: Collimation and protection relevant parameters compared between the nominal LHC and HE-LHC (round beam scenario).

Parameter	Nominal	HE-LHC
E	7 TeV	16.5 TeV
γ	7,461	17,587
$\varepsilon_{x,y}$	0.5 nm	0.15 nm
E_{stored} (total)	362 MJ	482 MJ
ρ_e (tot)	2.9 GJ/mm^2	15.4 GJ/mm^2
E_{stored} (1bunch)	128 kJ	242 kJ
ρ_e (1bunch)	1.0 MJ/mm^2	7.7 MJ/mm^2

COLLIMATION EFFICIENCY

The LHC has a sophisticated collimation system [2] that intercepts unavoidable beam losses and safely absorbs them before the associated heat can be deposited in any downstream superconducting magnet. The stored beam energy of 362 – 482 MJ is to be compared to quench limits of around 5 – 20 mJ/cm^3 in magnets. The collimation system must intercept and absorb stray particles with ultra-high efficiency. The LHC collimation system is located in two dedicated cleaning insertions of the LHC, the betatron collimation system in IR7 and the momentum collimation system in IR3.

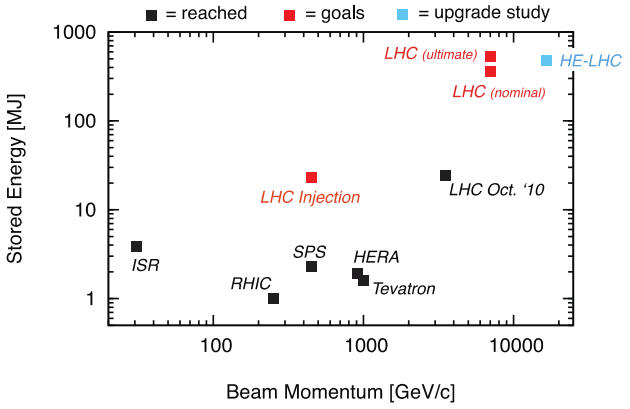

Figure 1: Stored energy per beam versus beam momentum for various accelerators. Filled black squares indicate achieved values, red squares show design values and the blue square represents the HE-LHC design.

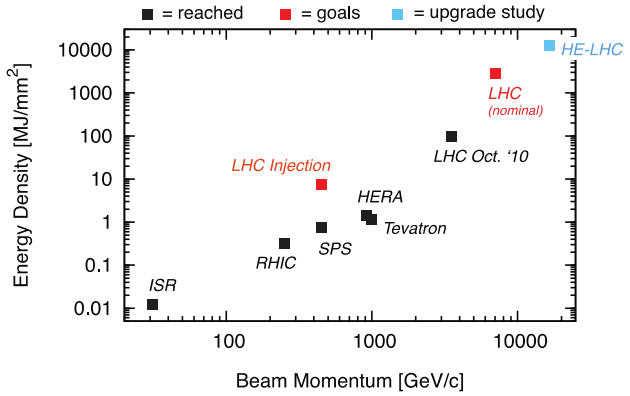

Figure 2: Energy density versus beam momentum. See explanations for Fig. 1.

The LHC collimation system has been designed for optimal performance at 7 TeV along various paths [3]:

- Proper choice of 138 collimator locations for the two beams. 108 collimators have been installed for the first years of LHC operation ("phase 1").
- The use of a 4-stage collimation hierarchy, extending the classical two-stage cleaning design.
- The use of 4 different jaw materials (graphite, fiber-reinforced carbon, copper, tungsten), carefully balancing robustness versus efficiency requirements.
- The use of 2 different lengths of jaws (0.6 m and 1.0 m flat top plus tapering).
- The use of 4 different orientations for optimal coverage in the horizontal (x), vertical (y) and skew planes.

Various nuclear physics processes that depend strongly on beam energy govern the interaction of particles in the

collimator jaws. The collimation system therefore behaves differently at higher beam energies.

Definition of cleaning inefficiency

The cleaning inefficiency describes the leakage from the collimation system into critical machine elements, for example all superconducting magnets. We define a local cleaning inefficiency as the maximum leakage to one meter of critical superconducting magnets [4]:

$$\tilde{\eta}_{ineff} = \max_i \left(\frac{\Delta N_i / L_i}{N_{impact}} \right) \quad (1)$$

Here, ΔN_i is the number of lost protons in the superconducting magnet number i of length L_i N_{impact} gives the number of protons that impact on the primary collimators.

Cleaning inefficiency versus beam energy

Simulations have shown that the efficiency of the LHC collimation system will be limited by losses in the dispersion-suppressors of the LHC for beams with TeV energies. The energy dependence of the simulated local cleaning inefficiency [5] is shown in Fig. 3 with two possible settings for collimators ("tight" and "intermediate").

It is seen that the LHC cleaning inefficiency gets worse with increased beam energy in the range from 1 TeV to 7 TeV. This is due to reduced multiple Coulomb scattering angles at higher beam energies and an increased probability of single-diffractive scattering.

Single diffractive scattering generates off-energy protons that cannot be intercepted by collimators in the straight sections of the cleaning insertions (lack of dispersive dipole kicks). These off-momentum protons are then lost in the dispersion suppressors downstream of the cleaning insertions. The higher is the beam energy, the higher is the fraction of single-diffractively scattered protons and the higher is the leakage (or inefficiency).

The LHC collimation simulations have been fully confirmed by measured losses downstream of the LHC betatron collimation insertion, as shown in Fig. 4. The proton losses are intercepted, as designed, at the primary collimators. From there onwards, losses are reduced with additional collimators by about four orders of magnitude. Single diffractive protons are lost in two characteristic, superconducting dipoles, as easily seen.

The existing simulation data in the range from 1 TeV to 7 TeV can be fitted as a function of beam energy E, here expressed in units of TeV:

$$\frac{\tilde{\eta}_{ineff}}{10^{-4}} = 0.0276 \frac{1}{m} + 0.0231 \frac{1}{m} E + 0.0051 \frac{1}{m} E^2 \quad (2)$$

This relationship is valid for so-called "tight" collimator settings, referring to nominal settings with primary collimators at 6 σ, secondary collimators at 7 σ, tertiary collimators at 8.4 σ and absorbing collimators at 10 σ.

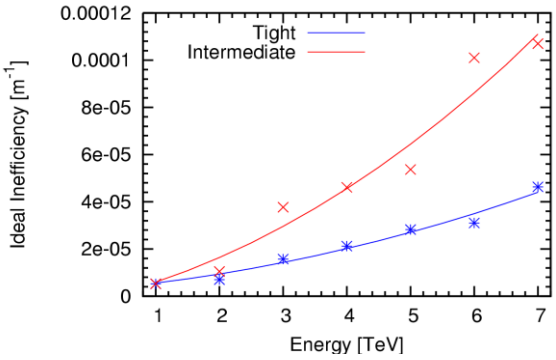

Figure 3: Simulated cleaning inefficiency of the LHC multi-stage collimation system. The two curves show two different settings of collimators. The lines show a fit to the data (see text). The data is from [5].

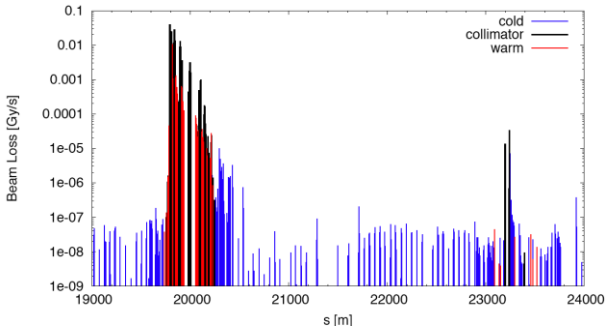

Figure 4: Measurement of proton losses in the betatron cleaning insertion IR7 and through the downstream arc into IR8, performed at 3.5 TeV beam energy. Black bars indicate losses at collimators, red bars at warm machine elements (not critical) and blue bars at superconducting magnets (critical). The beam runs in direction of s.

Simplified scaling law

A simplified scaling law can be derived for the probability P of single-diffractive losses versus beam energy. This scaling takes into account the following ingredients:

- The multi-TeV protons traverse an increased integrated length of jaw material. As the multiple Coulomb scattering angle scales with $1/E_1$ more material must be traversed to accumulate enough kick θ_{min} for reaching the aperture of secondary collimators.
- The required kick θ_{min} scales with $1/\sqrt{E_1}$.
- The cross section for single-diffractive scattering scales with ln $(0.3\ E_1)$.

Compared to some initial state 0 (with P_0 and E_0) the impact of single-diffractive scattering scales as follows:

$$\frac{P_1}{P_0} = \frac{E_1 \ln (300 E_1)}{E_0 \ln (300 E_0)} \quad (3)$$

Here, energies are to given in units of TeV. This simplified scaling law is compared in Fig. 5 to the fit from the simulation data. It is seen, that single diffractive scattering can indeed explain the loss of efficiency.

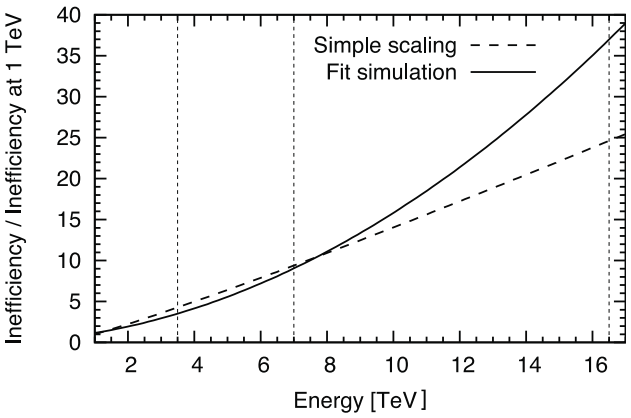

Figure 5: Extrapolation of cleaning inefficiency versus beam energy, comparing a fit of simulation data in the range from 1 TeV to 7 TeV and a simplified scaling law.

According to the two different models it is predicted that the cleaning inefficiency at 16.5 TeV will be increased by a factor between 2.6 and 3.9. This increase in inefficiency (leakage) must be compensated by system improvements in order to avoid collimation-induced intensity limitations. The already foreseen additional collimators in the dispersion suppressors will alleviate this limitation. Detailed studies are required for conclusions of collimation intensity reach at 16.5 TeV beam energy.

MACHINE ROBUSTNESS

The energy density in the beams and in a single bunch will increase significantly for the 16.5 TeV LHC. The LHC collimators and protection devices have been designed for nominal and ultimate intensities. We assume that all these elements are robust for ultimate bunch intensity and nominal emittance at 7 TeV beam energy. Then we can establish the following brightness limit:

$$\frac{N_p}{\varepsilon} \leq 3.4 \times 10^{20}\, m^{-1} \qquad (4)$$

The present parameters of the HE-LHC study violate this robustness limit by about a factor 2.6. A further study on increased emittance, damage limits or more robust collimator materials is required.

It is interesting that the luminosity reach at the robustness limit is:

$$L \leq \frac{10^{40}(cm\,s)^{-1}}{\gamma\beta^*}\frac{E_{stored}}{500\,MJ} \qquad (5)$$

It is an easy function of the stored energy, of β^* and of γ. The geometric correction factor F from the crossing angle is neglected here.

ISSUES DUE TO SMALLER GAPS

The primary collimation is set to 5.7 σ in the LHC. Here, we assume that the same normalized setting is required at 16.5 TeV. Due to the adiabatic emittance scaling the absolute half gap of the primary collimators then reduces from about 1.1 mm to 0.6 mm. Transverse resistive wall impedance scales with the third power of the inverse half gap. Consequently, the collimator-induced impedance at 16.5 TeV can be up to a factor 6 larger than at 7 TeV.

An increase of the limiting super-conducting apertures allows relaxing the required normalized setting of the primary collimators. If impedance becomes a limit then it might be required to replace the triplet and other IR magnets with larger aperture hardware.

HINTS ON MACHINE PROTECTION

The issues for robustness of passive protection collimators have been covered already. There will be additional issues for a few injection and dump protection elements. A detailed analysis by experts is required.

Other possible issues include systematic effects in safety-critical instrumentation, dynamic range limitations in beam loss monitors, interlock thresholds, surveillance levels, etc. A dedicated study by the machine protection experts must address the full picture.

HINTS ON CLEANING INSERTIONS

The cleaning insertions of the LHC were carefully designed for collimation with the following goals:

1. Establishment of a three stage cleaning per insertion with coverage in horizontal, vertical, skew and momentum phase space.
2. Protection of magnets and accelerator components against excessive heating and radiation damage.
3. Proper radiation control and possibilities for remote handling.

It has to be realized that the available space is already very limited with 7 TeV magnets. The phase advance is at the limit of requirements and cannot be reduced. The optics must be kept similar to the 7 TeV solution. Therefore there is no possibility to decrease the lattice strength, to remove quadrupoles or to increase the beta functions.

The redesign of the cleaning insertions of the LHC for 16.5 TeV is a major challenge.

CONCLUSION

The parameters of the HE-LHC impose new challenges for operating beams with high intensity:

- A factor between 3 – 6 is lost in collimation efficiency. Improvements must be implemented to compensate this loss. Ongoing collimation upgrades might, however, be sufficient to cope with this.
- The HE-LHC parameters are a factor of about 3 beyond the present robustness limit. Either the emittance is increased or new and more robust materials and technologies should be developed.
- The normalized aperture at 16.5 TeV should be increased by about 50% to avoid operation with small collimator gaps. Such gaps can be operationally unstable and can increase the LHC impedance 6-fold.

Alternatively, new collimator technologies are required.

- Machine protection requires further attention and studies. Presently no show-stoppers are expected.
- The re-design of the LHC cleaning insertions for 16.5 TeV is a major challenge and must be addressed early on in the design process.

REFERENCES

[1] F. Zimmermann. These proceedings.

[2] R. Assmann et al, "The final collimation system for the LHC". EPAC06. LHC-Project-Report-919.

[3] R. Assmann, "Collimation for the LHC High intensity beams". Proc. 46th ICFA Advanced Beam Dynamics Workshop on High-Intensity and High-Brightness Hadron Beams (HB2010). Sep. 27 – Oct 1 2010, Morschach, Switzerland.

[4] R. Assmann, "Collimators and Cleaning, Could this Limit the LHC Performance?". CERN-AB-2003-008 ADM (2003).

[5] C. Bracco, "Commissioning Scenarios and Tests for the LHC Collimation System". CERN-THESIS-2009-031 EuCARD-DIS-2009-004. Lausanne: École Polytechnique Fédérale de Lausanne, 2009.

INJECTION AND DUMP CONSIDERATIONS FOR A 16.5 TEV HE-LHC

B. Goddard, M. Barnes, W. Bartmann, J. Borburgh, C. Bracco, L. Ducimetière, V. Kain, M. Meddahi, V. Mertens, V. Senaj, J. Uythoven, CERN, Geneva, Switzerland

Abstract

Injection and beam dumping is considered for a 16.5 TeV hadron accelerator in the current LHC tunnel, with an injection energy in the range 1 – 1.3 TeV. The present systems are described and the possible upgrade scenarios investigated for higher beam rigidity. In addition to the required equipment performance, the machine protection related aspects are explored. The expected constraints on the machine layout are also given. The technological challenges for the different equipment subsystems are detailed, and areas where R&D is necessary are highlighted.

ASSUMED PARAMETERS

The most important parameters assumed for injection and extraction from HE-LHC are listed in Table 1, with the values for LHC (ultimate bunch intensity) also included. The resulting total energy per transfer (injection or extraction) and beam sizes are also included.

Table 1. Assumptions of target parameters for HE-LHC.

		LHC		HE-LHC	
		Inject	Extract	Inject	Extract
Bunch I	p+	1.7e11	1.7e11	1.3e11	1.3e11
p·c	TeV	0.45	7	1.3	16.5
Rigidity	Tm	1503	23337	4337	55004
Nb/transfer		288	2808	144	1404
E/transfer	MJ	3.5	535	3.9	482
ε_{xyn}	μm	3	3	2	2
$\beta_{x/y}$ (septum)	m	100	100	100	100
β_{xy} (dump)	m	4500	4500	4500	4500
σ_{xy} (septum)	mm	0.79	0.20	0.38	0.11
σ_{xy} (dump)	mm	5.30	1.34	2.55	0.72
Injection gap	μs	1.00	1.00	1.00	1.00
Dump gap	μs	3.00	3.00	3.00	3.00

INJECTION AT 1.3 TEV

Present injection system

The present fast injection systems in P2 (Beam 1) and P8 (Beam 2) use DC powered laminated steel Lambertson septum magnets and ferrite yoke transmission line pulsed extraction kicker magnets. The kickers use thyratron switches and have ceramic vacuum chambers which support screening elements to reduce the beam coupling impedance.

The injection systems also comprise beam instrumentation and dedicated passive protection devices to intercept beam in case of an injection kicker failure. Overviews and details of the systems and components can be found in [1,2].

The injection systems for Beam 1 and Beam 2 are located to the left of P2 and right of P8, respectively, and are integrated into the matching sections of the low-β insertions for the ALICE and LHCb experiments. This cohabitation imposes some optics constraints and also has proven to introduce operational complications with the background and beam losses at injection.

Assumptions

It is assumed that the existing transfer line tunnels from the SPS will be used, with superconducting magnets for the 1.3 TeV beam transfer, and also that the insertions in P2 and P8 will continue to house the physics experiments and low-β insertions, although the insertion layout and optics may change.

Injection kicker considerations

A major issue with 1.3 TeV injection is the strength of the injection kicker. The system will require a similar deflection to the present 0.8 mrad (this maybe be reduced by 10-15% by changes in the optics and increasing the kicker-septum drift, but probably no more). The present system is already very pushed in terms of performance, and is considered to be at the technological limit with the 60 kV switches, cables, pulsed HV insulation in vacuum and beam screens. There is no extra space in the present layout, and clearly any solution which modifies the layout is complicated by the requirement to combine the injections and experiments in the same insertions. The possible options are considered. In both cases it is assumed that the horizontal magnet gap can be reduced from 52 to 42 mm.

The first option is to increase the installed kicker length from 16.9 m to around 34 – 40 m. This would imply 40 – 46 m spacing between adjacent quadrupoles, compared to the present 22 m, and a completely new insertion layout and optics.

The second option is to double the present 1 μs rise time to around 2 μs, e.g. with the kickers in short circuit mode or with lower impedance. The installed length could then be kept to around the present length of 17 m. The ferrite saturation might be an issue with a peak field in the ferrite of about 0.26 T. This would reduce the number of bunches per injection by about 20, or about 10% of the total number of bunches. To partially compensate for this reduction, it would be rather simple to increase the Pulse Forming Network (PFN) and kick pulse length from 8 to up to 16 μs (also for the SPS extraction kickers), although this might pose other limitations in the SPS with a much higher total intensity.

The system parameters for these two options are compared with the present system in Table 2.

Table 2. Parameters for 1.3 TeV injection kicker system options. Critical values are shown in red.

Parameter	Unit	LHC nominal	More magnets	Longer rise time
H gap	mm	54	42	42
Rise time	μs	1.00	1.00	**2.20**
Angle	mrad	0.8	0.8	0.8
∫B.dl	Tm	1.2	3.5	3.5
Gap field	T	0.08	0.11	0.24
Peak field	T	0.09	0.12	**0.26**
dI/dT	kA/μs	5.40	5.39	5.51
Imax	kA	5.4	12.1	12.1
Lmag	m	14.6	**32.9**	14.6
Filling		0.864	0.864	0.864
Ltotal	m	16.9	**38.0**	16.9
#magnets		4	**9**	4

Other aspects which would need detailed consideration for a new design would include impedance, beam screens, magnet core heating and electron cloud.

Injection septum considerations

The injection septum design is very similar to the dump septum (see later). If stronger units cannot be designed then more magnets and hence more space will be needed. The present 22 m installed length would need to increase to about 43 – 55 m. With the 22 m drift needed to clear the upstream cryostat, this imposes 50 – 60 m drift between the quadrupoles surrounding the septum.

Injection protection considerations

As for the dump protection, the injection protection device design increases in difficulty for 1.3 TeV. The protection in the transfer lines and the protection against the kicker failures would need redesign, for the 4 MJ and 1.3 TeV energy. The kicker protection devices would increase in length from 4 to maybe 6 – 8 m.

DUMPING THE 16.5 TEV BEAM

Present LHC beam dump

The present LHC beam dump uses a sequence of extract → dilute → absorb to abort the ~500 MJ beam, in a 'loss-free' way. The system comprises laminated steel pulsed extraction kicker magnets, DC powered laminated steel Lambertson septum magnets, laminated steel pulsed dilution kicker magnets and a 7.7 m long, 0.7 m Ø C cylinder forming the beam dump block, surrounded by steel and concrete shielding. Both extraction and dilution kickers use the same solid state Fast High Current Thyristor switch technology. The dump kickers have ceramic vacuum chambers with a few μm of Ti coating for reducing the beam coupling impedance.

Beam instrumentation and dedicated passive protection devices to intercept beam in case of a kicker error complete the dump system. More details on the system and components can be found in [3,4].

The total length of the beamline from extraction kicker to dump block is about 975 m. The dump block is separated from the vacuum of the beamline and the LHC by a 15 mm thick carbon composite (CC) entrance window, which for vacuum tightness has a 0.2 mm thick steel backing foil. The dump systems for Beam 1 and Beam 2 are located symmetrically about P6 of the LHC, and use the full straight section, with a special optics to provide the long drift distance needed between kicker and septum, and from the septum to the next machine quadrupole to allow the beam to be extracted past the cryostat. For the layout, there are only two stand alone matching quadrupoles each side of the IP (Q4 and Q5) which are not in the continuous cryostat. A schematic layout of the elements in P6 is shown in Figure 1.

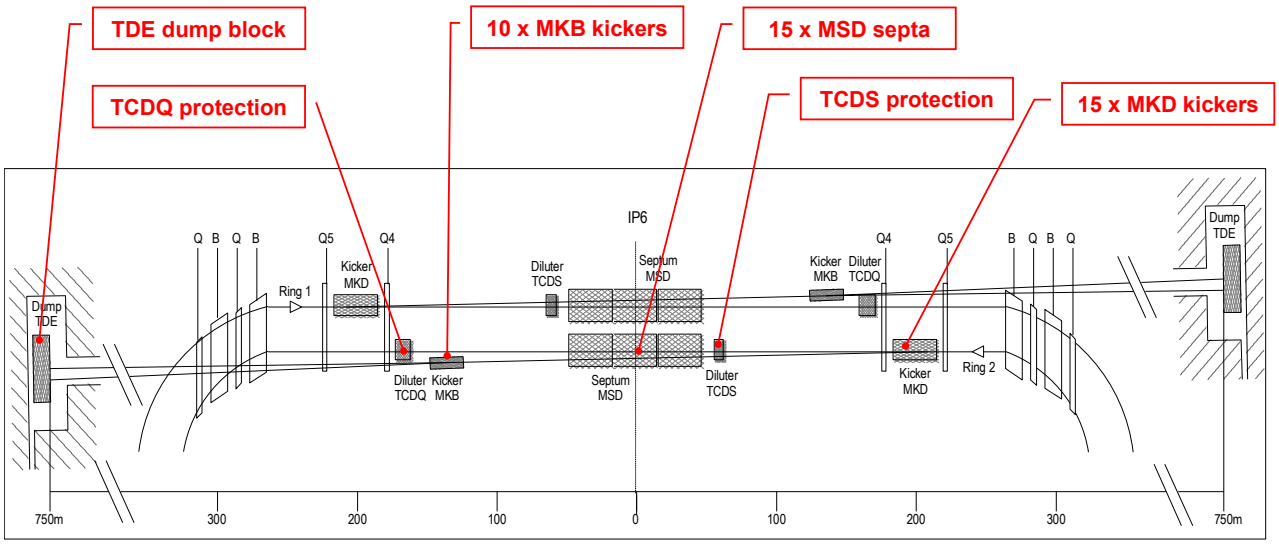

Figure 1. Schematic layout of dump elements in P6.

Assumptions

It is assumed that the existing tunnel and caverns are reused, Figure 2, which implies the same (similar) extraction trajectories in horizontal and vertical, and therefore similar kicker and septum angles. A maximum ~300 mm dilution sweep radius is permitted, otherwise extra civil engineering would be needed to enlarge the TJ62 and TJ68 junction caverns with the LHC. The insertion layout and optics could change if required.

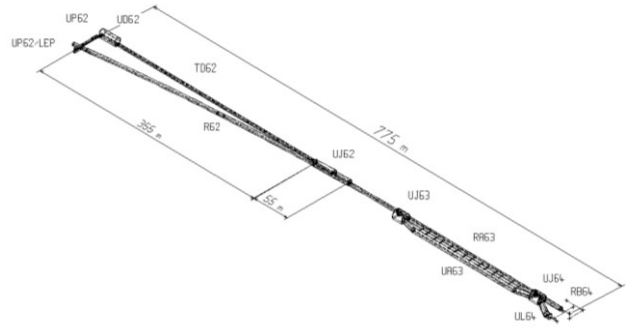

Figure 2. Underground layout for the left side of P6, showing the dump tunnel and UD62 cavern for Beam 2.

Extraction kicker with 3 μs rise time

An option for the extraction kicker system would be to keep 3 μs rise time and similar magnets. The required ∫B.dl could then be obtained by increasing the number of magnets, or increasing the current per magnet. These are compared to the present situation in Table 3.

A total of 35 magnets would be required if the parameters per magnet are unchanged – this would imply an installed length of 64.4 m, which is not compatible with retaining a similar optics; the distance between Q4 and Q5 would have to be much larger.

Table 3. Parameters for 3 μs rise time beam dump extraction kicker system. Critical values are shown in red.

Parameter	Unit	LHC Nominal	More magnets	Higher current
V gap	mm	72	72	72
Rise time	μs	3.00	3.00	3.00
Angle	mrad	0.27	0.27	0.27
∫B.dl	Tm	6.3	14.9	14.9
Gap field	T	0.30	0.30	0.71
Peak field	T	0.41	0.41	0.95
dI/dT	kA/μs	6.17	6.23	**14.53**
Imax	kA	18.5	18.7	**43.6**
Vmax	kV	30.0	30.0	**70.7**
Lmag	m	21.0	49.0	21.0
Filling		0.761	0.761	0.761
Ltotal	m	27.6	**64.4**	27.6
# magnets		15	**35**	15

For higher current per magnet with a similar magnetic length to present, the peak current would increase to 43.6 kA and the peak field to 0.95 T, which may be about feasible. However, the dI/dt increases to 14.5 kA/μs, which requires that the system voltage increases enormously, from 30 kV to over 70 kV. This is simply not possible with the air insulated generators and switches which form the core of the system. A change to an oil insulated system would introduce many complications with footprint, maintenance and complexity and also safety issues with large quantities of oil underground. The maximum oil-insulated system voltage of around 60 kV would still not be enough to fit the system in a similar length to the present system. In addition a current feedthrough for 44 kA would be very challenging.

Extraction kicker with longer rise time

The second option for the kicker system would be to use longer rise time and a different magnet design. The vertical gap could be reduced to take advantage of the smaller beam size at 1-1.3 TeV injection energy. In a first assumption it is assumed that the clear vertical vacuum chamber aperture can be reduced from 62 to 42 mm, which is a factor √(450/1000). This may be slightly optimistic for 1 TeV as the allocation for orbit, mechanical and alignment tolerances are fixed quantities. The ceramic chamber and associated tolerances require another 10 mm opening, so the final vertical gap between the poles would be reduced from the present 72 mm to 52 mm. Limiting the dI/dt to the present value (which may be slightly pessimistic), the parameters obtained are shown in Table 4.

Table 4. Parameters for beam dump extraction kicker system with smaller gap and longer rise time. Critical values are shown in red.

Parameter		LHC Nominal	Smaller gap
V gap	mm	72	**52**
Rise time	μs	3.00	**5.10**
Angle	mrad	0.27	0.27
∫B.dl	Tm	6.3	14.9
Gap field	T	0.30	0.71
Peak field	T	0.41	0.95
dI/dT	kA/μs	6.17	6.17
Imax	kA	18.5	**31.5**
Vmax	kV	30.0	30.0
Lmag	m	21.0	21.0
Filling		0.761	0.761
Ltotal	m	27.6	27.6
# magnets		15	15

In this configuration the extraction requires a 5.1 μs abort gap which reduces the number of bunches in the machine by about 42 at 50 ns spacing, or about 3%. The maximum current would be almost 32 kA, which would require R&D on high current switches and high current feedthroughs, but should be feasible. This system would still be air insulated and would operate at 30 kV.

Beam dump block considerations

For the beam dump block, a full study would be needed to analyse the extra dilution required from the MKB kicker system for a 16.5 TeV beam. In the absence of such a study, some simple scaling considerations can be made.

The peak p+ density will be a factor ~2.4 times higher, for similar beta functions at the dump block. The shower maximum will be further into the dump block, and the transverse shower extent at the shower maximum is assumed to be independent of the transverse beam size, which may be slightly optimistic. The total energy impacting the dump is about 500 MJ, similar to the LHC ultimate beam. The sweep length should therefore be similar to the present value of 100 cm. The present block is 7.7 m long and composed of carbon with different densities of 1.73 and 1.1 g cm^{-3}. A longer block with lower densities is likely to be required, or at least a different grading of the existing carbon densities. The longitudinal space exists in the present 25 m UD caverns.

Dilution kicker upgrade options

Assuming a 100 cm long sweep length at 16.5 TeV would require 2.3 times the present ∫B.dl. However, the iron of the magnet cores of the MKB dilution kickers are already near saturation, with 1.52 T peak, so it is not possible to increase the field per magnet. The apertures are determined (to first order) by the required sweep length and failure cases, and not the beam size, such that it is not possible to greatly reduce the magnet gaps. The magnets are already under vacuum with no chamber, which means nothing can be gained here in the gap size (some small optimisation could be possible with 2 families per plane with different openings).

Again two options, Table 5, are possible to increase the dilution kicker ∫B.dl – the first is to increase the number of installed magnets, keeping the switch voltage at 30 kV. 22 magnets would be needed compared to the present 10, requiring the installed space to increase from 23 to 50 m. This might be possible from an integration point of view, as the machine is not very crowded in this vicinity. The present 10 magnets are installed on the extracted beam line in the long drift space between the extraction septa and Q4, Figure 3. Space for generators in the adjacent galleries might be more problematic.

The second option would be to increase the frequency of the sweep from 14 to 28 kHz, reducing the strength and using 18 magnets in total. The system voltage could be kept at 30 kV and a sweep length of 100 cm achieved. The total installed length would then be 41 m. Damping of the diluter kicker currents is needed to achieve a spiral, which means the sweep will cross at one point on the dump block; possible waveforms and resulting sweep are shown in Figures 4 and 5. The temperature profile and dynamic mechanical stresses in the dump block would need to be evaluated.

As the magnet core is not saturated, this second solution would also have the advantage that developments in switch and insulation technology could allow an increase of the switch voltage beyond 30 kV, with a concomitant reduction in the number of magnets required. For instance, being able to increase the system voltage to 40 kV would result in a peak field of 1.3 T and a reduction to about 14 magnets.

Table 5. Parameters for dump dilution kicker system for more magnets of the present type, and for a system with higher frequency.

Parameter	Unit	LHC	More magnets	Higher frequency
F	kHz	14.0	14.0	28.0
Angle	mrad	0.27	0.27	0.135
∫B.dl	Tm	6.3	14.9	7.4
Field	T	1.13	1.21	0.74
Peak field	T	1.52	1.63	0.99
Voltage	kV	22.30	23.89	29.20
Current	kA	25.0	26.8	16.4
Lmag H+V	m	11.2	**24.6**	**20.2**
Filling		0.49	0.49	0.49
Ltotal	m	22.9	**50.3**	41.1
#magnets		10	22	**18**

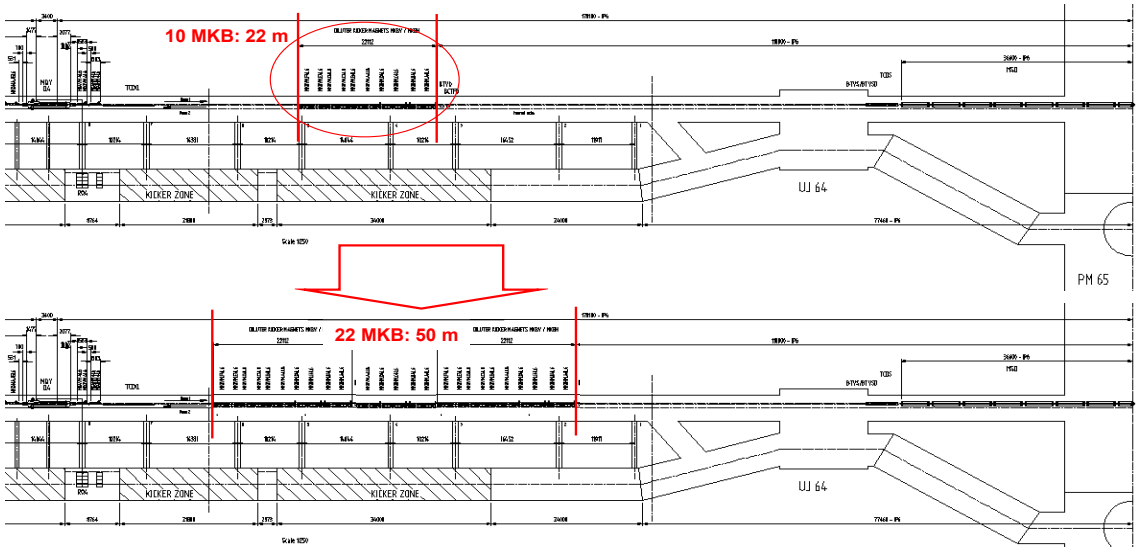

Figure 3. Present layout R6 with 10 dilution kickers (uper) and with 22 kickers (lower).

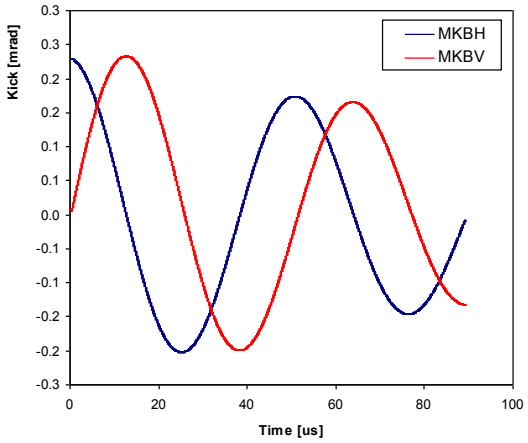

Figure 4. Possible waveforms for higher frequency sweep.

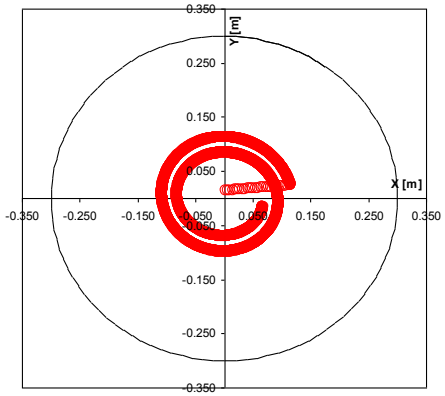

Figure 5. Sweep form on the dump block with 100 cm length and 28 kHz frequency. The sweep crosses itself, which will give locally a higher temperature in the dump.

Dilution with a quadrupole in the beamline

An option to supplement the dilution kickers would be to install a quadrupole or a quadrupole doublet in the beamline. If located upstream of the dilution kickers this could provide a larger beta function at the dump block. If downstream a doublet might also give a kick enhancement in both planes, increasing the effective kick strength.

The present beta values are 4-5 km at the dump. Betas of 12 km would increase the sigmas at 16.5 TeV to the present values, although this might not help the peak energy deposition if the transverse size at the shower maximum does not depend strongly on the beam size. To obtain this beta would require a 6 m quadrupole with gradient of about 150 T/m and 100 mm full aperture. The resulting line optics are shown in Figure 6.

One issue could be the trajectory offsets introduced from LHC orbit changes – with this arrangement a 4 mm orbit offset would give an additional kick of 45 μrad, producing 30 mm offset at the dump, assumed to be 650 m from the quadrupole. This should be possible to accommodate in the present 600 mm diameter dump line.

Integration of such a quadrupole is likely to be difficult upstream of the dilution kicker magnets.

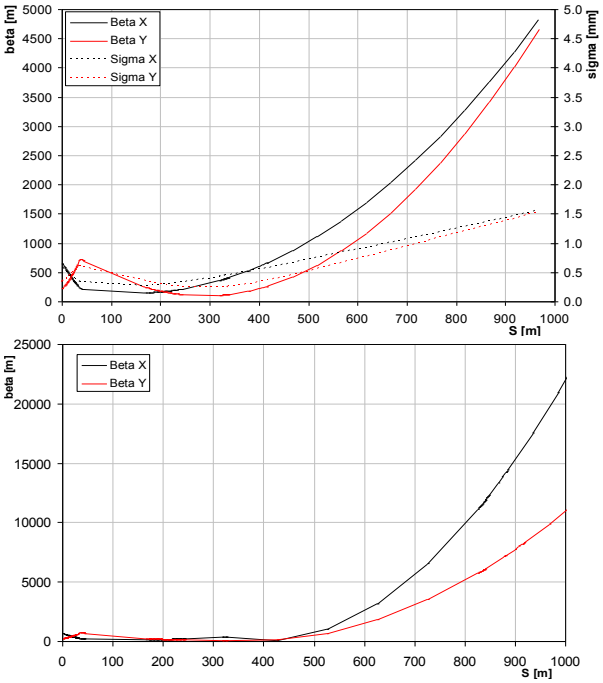

Figure 6. Present dump line optics (upper) and possible optics with 6 m long, 150 T/m dilution quadrupole (lower).

Extraction septum considerations

Extraction of the beam is made vertically, above the continuous cryostat. The present design uses Lambertson septa with three different septum thicknesses. For an upgrade only types B and type C would be used, as the thinnest septum is not needed behind the dedicated protection device. The field could also possibly be increased to the maximum possible value. The total number of magnets needed would then increase from 15 to 28, Table 6, and the total installed length from 73 m to 136 m. This would be difficult (although maybe not impossible) to integrate in the layout, as the drift between extraction kicker and septum entrance would be reduced by 30 m, which could in turn mean that more kick strength is required.

Alternatives are limited. Beamloss at extraction is inevitable, and so it may not be possible to build a superconducting septum. A superferric septum seems superficially interesting, to reach fields of around 2 T; however, as with all septa, saturation of the iron in the septum will strongly affect the field quality for the circulating beam, and operation above the present peak of 1.2 T may not be feasible. More studies would be needed on the septum to investigate possible alternative concepts, including ideas such as a massless superconducting septum [5].

Table 6. Extension of present extraction septum system for 16.5 TeV by increasing number of magnets.

	Unit	LHC	HE-LHC
Angle	mrad	2.4	2.4
∫B.dl	Tm	56.0	132.0
Nominal field	T	0.84	1.06
Lmag	m	66.7	**124.8**
Filling factor		0.916	0.916
Ltotal	m	72.8	**136.2**
#magnets		15	**28**

Dump protection devices

Failure cases of the extraction system include asynchronous beam dumps and high beam population in the abort gap. Protection of the septum, of the first machine quadrupole Q4 and of the collimation system from the 7 TeV beam imposes the use of long (6 m) low density (C) absorbers to intercept undiluted bunches.

The absorbers have to be low density to avoid material damage; for 16.5 TeV the densities will need to be reduced and the total length of material increased to dilute the energy density. Very long objects will be needed. A dilution factor of about 10^7 is needed, which imposes 16 λr of C, which gives about 6 m of 1.8 g cm^{-3} at 7 TeV. For 16.5 TeV, with smaller spot size and more energy deposited a density as low as 0.6 – 0.8 g cm^{-3} may be needed to avoid damage, which would give an absorber 14-16 m long. For the fixed absorber in front of the septum this would reduce the aperture available and increase slightly the kick angle needed; for the mobile absorber in front of Q4 the challenge would be mechanical, as the absorber jaw needs to move in as the energy is ramped. Some optimisation with graded density may be possible to get more λr to reduce the length somewhat.

If the asynchronous dump events remain very rare (fewer than one per year, for example), an alternative would be to build sacrificial absorbers which would be damaged by a full intensity dump, and which would be easily replaceable in the event of damage. Such an option would allow shorter devices to be built, but would require R&D into failure modes and tests in a facility such as HiRadMat to check the calculations and prototypes.

OTHER KICKER SYSTEMS

The tune kickers are not a concern for 16.5 TeV operation. They are weak devices without strong constraints on rise time, and are presently single magnets with multiple functions (several generators). It would be simple to add more kicker modules and to separate the functions, and there are no serious space constraints.

CONCLUSIONS

Injection into HE-LHC at 1.3 TeV will need a completely new injection region layout. A longer kicker rise time of 2.2 μs with a longer pulse is feasible, as is a 1 μs rise time with 8 – 9 magnets and 40 m spacing between the adjacent quadrupoles. The number of septa would need to be doubled if stronger units could not be developed (which seems difficult), and this would require 60 m spacing between the quadrupoles. The injection protection devices also need more space. New layout and optics designs need to be investigated, which clearly have to respect the constraints coming from the experiments in injection regions.

A dump system for 16.5 TeV looks to be feasible in a similar layout to the present system. A 5 μs kicker rise time is possible with the present total system length, whereas maintaining 3 μs would require a doubling of the installed length and a major change to the insertion layout and optics. Increasing the extraction septum ∫B.dl requires an increase in septum length by a factor 1.9. This seems possible if the integration issues can be addressed. The best way of increasing the dilution sweep length seems to be by doubling the system frequency to 28 kHz. More dilution or the addition of a superconducting dilution quadrupole (or doublet) also could prove viable alternatives. The upgrade of the dump block would be rather straightforward, whereas changes to the protection devices would need much more study and development.

Potential or required areas of R&D

These first considerations of injection and dump systems for HE-LHC give an idea of the possible R&D directions which would be required, or which could significantly reduce other constraints on layout, optics etc.
Areas which need studies, simulations or equipment R&D (and of course the accompanying resources) are:

- Injection layout and optics;
- Dump layout and optics;
- Kicker beam screens and impedance;
- HV insulation under vacuum above 60 kV;
- Low inductance HV cables above 60 kV;
- High saturation (0.3 T) low-loss ferrites;
- High current (>40 kA) pulsed feedthroughs;
- High voltage, high current, fast solid state switches;
- Higher frequency damped generator design;
- Protection devices (low density, high strength, sacrificial designs);
- Dilution with SC quadrupoles and kickers;
- High field, beam loss resistant septa (possibly with SC or SF design).

REFERENCES

[1] O. Brüning et al., "LHC Design Report Volume 1", ISBN 92-9083-244-0, Geneva 2004, Chapter 16.
[2] A. Hilaire, V. Mertens, E. Weisse, "Beam Transfer to and Injection into LHC", Proc EPAC'98, p.2117-211.
[3] O. Brüning et al., "LHC Design Report Volume 1", ISBN 92-9083-244-0, Geneva 2004, Chapter 17.
[4] B. Goddard, "Injection and beam dump", Proc. Chamonix 2009, pp.219-225.
[5] S. Fartoukh, "A semi-analytical method to generate an arbitrary 2D magnetic field and determine the associated current distribution", LHC Project Report 1012, 2007.

RADIATION PROTECTION ISSUES AFTER 20 YEARS OF LHC OPERATION

D. Forkel-Wirth, M. Magistris, S. Roesler, C. Theis, L. Ulrici, H. Vincke and Hz. Vincke,
CERN DGS-RP, Geneva, Switzerland

Abstract

Since November 2009, the LHC commissioning progresses very well, both with proton and lead beams. It will continue in 2011 and nominal LHC operation is expected to be attained in 2013. In parallel, plans for various LHC upgrades are under discussion, suggesting a High-Luminosity (HL) upgrade first and a High-Energy (HE) upgrade in a later state. Whereas the upgrade in luminosity would require the modification of only some few key accelerator components like the inner triplets, the upgrade in beam energy from 7 TeV to 16.5 TeV would require the exchange of all dipoles and of numerous other accelerator components.

The paper gives an overview of the radiation protection issues related to the dismantling of LHC components prior to the installation of the HE-LHC components, i.e. after about 20 years of LHC operation. Two main topics will be discussed: (i) the exposure of workers to ionizing radiation during the dismantling of dipoles, inner triplets or collimators and experiments and (ii) the production, conditioning, interim storage and final disposal of radioactive waste.

EXPOSURE OF WORKERS TO IONIZING RADIATION

Dismantling of accelerator components from hadron accelerators implies the exposure of workers to ionizing radiation. The ionizing radiation (β,γ) is caused by the radioactive decay of spallation induced radionuclides produced inside the components and their surroundings during beam operation. The level of induced radioactivity is a function of the chemical composition of the component, of the beam particle type and energy, of the beam losses (accelerator) and of luminosity (experiment detectors).

Prior to any dismantling work, a risk analysis has to be performed. Usually, ambient dose equivalent rates and levels of induced activity are measured after the beam stop and fed into the overall job and dose planning for dose optimization. However, the risk analysis for the dismantling of LHC components in 20 years time can only be based on the results of Monte Carlo simulations. Indeed, the comparison with and the extrapolation from measurements are not yet possible, as the activation and the radiation levels in the LHC are still very low.

Most of the FLUKA calculations for the LHC were performed assuming 180 days of operation at nominal beam conditions. The extrapolation up to 20 years of LHC operation requires additional inputs, such as the radiation protection relevant LHC parameters (beam energy, beam intensity, luminosity) for 20 years of LHC operation (see Table 1) determining the build-up of long lived isotopes (e.g. ^{60}Co, ^{22}Na), as well as their contribution to the ambient dose equivalent rate. For this purpose a generic study was performed: the activation of a simplified magnet (iron or steel cylinder) was simulated to estimate the contribution of the long-lived radionuclides to the ambient dose equivalent rate assuming 180 days, 5 years and 20 years of LHC operation. The 5 (20) years of LHC beam operation were approximated by assuming 5 (20) times one year of 180-day irradiation and 185-day shut-down. The simulation took into account the chemical composition of the material used for LHC components. As an example, the composition of steel for the LHC dipoles is listed in Table 2.

Figure 1 gives the FLUKA results per proton at 7 TeV, for the three different irradiation times and followed by 4-month cooling time.

Table 1: LHC parameters relevant for the calculation of induced radioactivity at the various stages of LHC operation

LHC Phase	**Energy (TeV)**	**Beam Intensity (pr. per beam)**	**Peak Luminosity (cm^{-2} s^{-1})**	**Year**
Commission.	3.5	$5.1\cdot10^{13}$	$2\cdot10^{32}$	2010
Commission.	3.5	$1.5\cdot10^{14}$	$1\cdot10^{33}$	2011
Nominal	7	$3.2\cdot10^{14}$	$1\cdot10^{34}$	2013
Ultimate	7	$4.7\cdot10^{14}$	$2.3\cdot10^{34}$	2017
HL-LHC	7	$4.7\cdot10^{14}$	$5\cdot10^{34}$	2021
HE-LHC	16.5	$2.5\cdot10^{14}$	$2\cdot10^{34}$	>2030

Table 2: Chemical composition of steel used for the LHC dipoles

Steel composition					
Elem.	Wt-%	Elem.	Wt-%	Elem.	Wt-%
Fe	63.09	S	0.00	Mo	0.09
Cr	17.79	Cu	0.09	C	0.10
Ni	6.50	O	0.00	W	0.01
Mn	11.43	Ti	0.01	P	0.02
Si	0.38	V	0.07	Nb	0.01
N	0.31	Co	0.11		

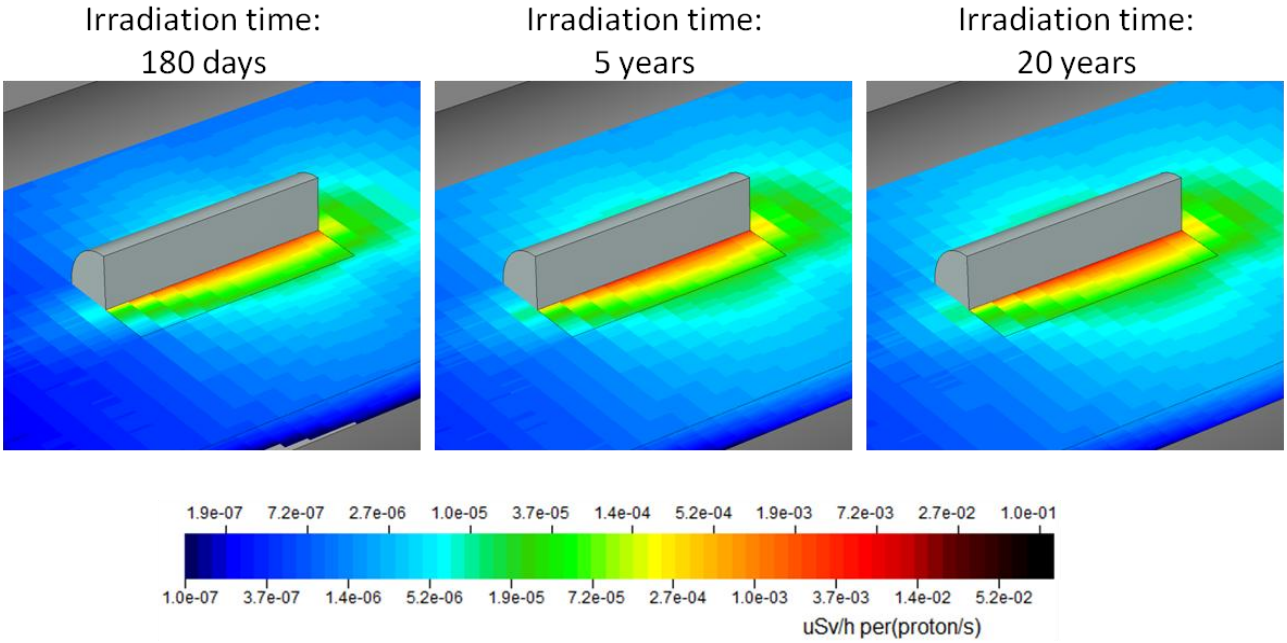

Figure 1: Results of generic calculations of ambient dose equivalent rates (per proton) after irradiation of a simplified magnet (steel cylinder) at 7 TeV and 4-month cooling. Three different irradiation times are considered: 180 days, 5 years and 20 years of LHC operation.

The graphic in Fig. 2 compares the ambient dose equivalent rates found along the magnet for the three scenarios. The results indicate an increase of the ambient dose equivalent rate by a factor of about 1.7 between 1 year and 5 years of operation and about a factor 2 between 1 year of operation and 20 years of operation.

To allow the extrapolation from presently available results of FLUKA calculations, it was assumed that the LHC technical installation will not be modified and the beam loss pattern will not change over the next 20 years. Under these assumptions, the ambient dose equivalent rates depend on beam energy ($E^{0.8}$), luminosity (experiments, inner triplet), beam intensity (arcs, collimators) and total number of protons.

Three examples will be given for extrapolated ambient dose equivalent rates:

- **LHC ARCs**: the ambient dose equivalent rates were calculated for nominal operation, assuming 180 days of operation, a beam gas interaction rate of 2.4×10^4 protons/m/s (both beams) at 7 TeV and which corresponds to a H_2-equivalent beam gas density of 4.5×10^{14} m^{-3}. Under these assumptions, the ambient dose equivalent rates inside the arc magnets and close to the beam line will reach 20 μSv/h after 1-month cooling, about 300 to 400 nSv/h at the surface of the cryostate and about 200 nSv/h in the aisle. After 20 years of LHC operation, in particular after operation of LHC as HL-LHC, the expected ambient dose equivalent rates are estimated to be about a factor of 3 higher.
- **Inner triplet**: the ambient dose equivalent rate at the surface of the cryostat will be in the order of 600 μSv/h after 5 years of operation under nominal conditions and 4-month cooling. After 10 years of HL-LHC, the ambient dose equivalent rate at the surface of the cryostate will reach about 1 mSv/h after 4-month cooling. Inside the magnets the dose rates will be higher and of a different order of magnitude.
- **Collimator Region**: After one year of operation at the nominal beam intensities the ambient dose equivalent rate in the aisle will reach some 10 to 100 μSv/h, and close to the collimator it will be 100 μSv/h to 1 mSv/h after 4-month cooling. After 20 years of LHC operation and the same cooling time, the dose rates are estimated to be about a factor of 3 higher and reach up to 3 mSv/h close to the collimator.

The removal of dipoles will imply destructive work, like for example cutting the beam pipes and splices. This work entails a risk of contamination. Adequate techniques will have to be developed already for the splice-repair campaign, which is foreseen for 2012. The dose to the workers has also to be optimized for the transport of components: passing the collimators in Point 3 and Point 7 may result in non-negligible doses to the transport team.

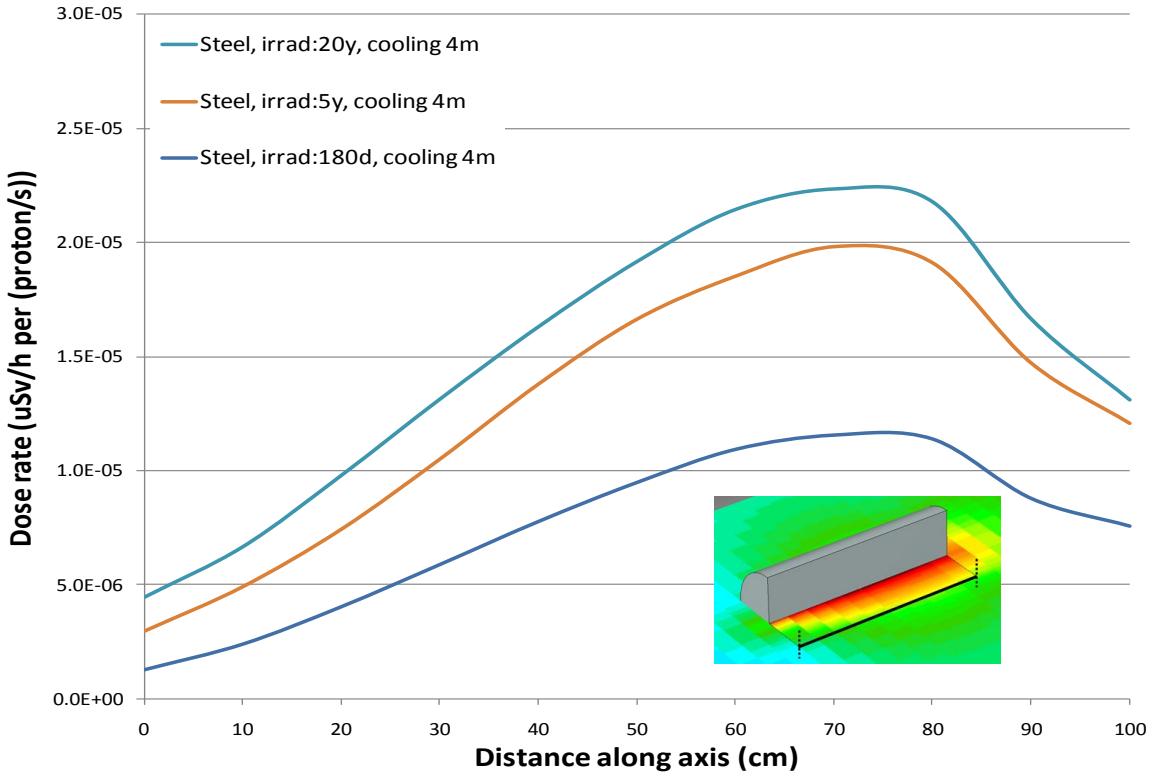

Figure 2: Results of calculations of ambient dose equivalent rates along an irradiated steel cylinder for irradiation times of 180 days, 5 years and 20 years.

The removal of the Inner triplet will imply destructive work on material with a relatively high level of radioactivity. Experience will be gained from the first triplet exchange in a few years from now. As mentioned above, the dose rates outside the magnets at Point 1 and Point 5 will be about 600 μSv/h after 4-month cooling and may reach much higher radiation levels inside the magnets. These values require a major optimization of the new generation of inner triplets with respect to design, installation, removal and transport. Material choice, flange connections and handling means need to be optimized.

The removal of collimators and warm magnets will lead to risk of workers' exposure to ambient dose equivalent rates in the order of some few 100 μSv/h up to mSv/h – even after four months of cooling. The dismantling of collimators was thoroughly studied and optimized and the development of a remote handling tool is well in progress. The dismantling of warm magnets and passive absorbers needs to be prepared and optimized – which is a priority for the next years of LHC operation. The installation of additional equipment to the already existing, radioactive material in Point 3 and Point 7 seems extremely difficult.

RADIOACTIVE WASTE

The production of radioactive waste after 10 years of nominal operation of LHC was already estimated some years ago in the framework of the LHC waste study. After 20 years of operation, the waste production might turn out to be higher then the estimated one, because of increased intensities and luminosities and/or due to changes in the European legislation. CERN's present interim storage for radioactive waste, in the ISR tunnel, is not adapted to store LHC dipoles, also because of the lack of adequate means of transport. Therefore, a "light" storage solution for dipoles need to be studied. The dipoles might fulfill the acceptance criteria for low level waste in France and thus be eliminated towards the final repository Centre de stockage des déchets de très faible activité (CSTFA) in Aube. Radioactive waste others than dipoles will be temporarily stored at CERN - in shielded areas equipped with proper handling means - until elimination pathways are determined. It has to be taken into account that waste disposal regulation and techniques are likely to evolve over the next 20 years.

CONCLUSIONS

Experience in removing components (dipoles, triplet, collimators) will already be gained in the next few years. The design of new components like the next generation of inner triplets needs to be optimized before being installed.

The radioactive waste production, storage and disposal should be addressed today – as even small amounts of radioactive waste from LHC risk to pose problems in view of handling, storage and elimination. The upgrade of the LHC to HE-LHC will increase the amount of radioactive waste. Options of recycling of components and material should be assessed, with a view to reduce the production of radioactive waste.

SUMMARY OF SESSION 1: INTRODUCTION AND OVERVIEW

J. P. Koutchouk, R. Bailey, CERN, Geneva, Switzerland

PROGRAM OF SESSION 1

This workshop being the first discussion opportunity for this very ambitious LHC energy upgrade (HE-LHC), session 1 was dedicated to setting the scene and browsing through the most significant challenges:

- The physics case, by James Wells/Cambridge University, UK.
- Motivation, status and strategy for HE-LHC studies, by Steve Myers/CERN
- Beam parameters, optics and beam dynamic issues, Frank Zimmermann/CERN
- Magnet concepts and cost evaluation, Ezio Todesco/CERN
- Relevant studies for VLHC/SSC, Uli Wienands/SLAC
- Detector plans and constraints for HE-LHC, Marzio Nessi/ATLAS

This summary attempts at underlining the salient aspects, summarizing discussions and drawing provisional conclusions.

THE PHYSICS CASE

James Wells

The salient points

The added value of HE-LHC would be to extend the discovery range; precision physics is best served by the luminosity upgrade. This extension of discovery range is illustrated in this presentation by the "Naturalness" problem: in the SM, the expression of the Higgs mass, expanded versus the Planck mass, exhibits a quadratic divergence. Three approaches allow resolving this issue:

- Technicolor theories, now less likely with LEP and Fermilab results showing signs of a low Higgs mass. HE-LHC would significantly extend the discovery reach for these theories.
- Extra-dimensions, where the mass scale can be reduced and convergence restored. Higher energy pays huge dividends to observe the KK graviton.
- Supersymmetry: the extended capability to detect supersymmetric particles may be one of the principle motivations for HE-LHC.

The discussion

- HE-LHC versus CLIC/ILC?: their respective capabilities depend in detail on the processes of interest. HE-LHC is good for discovery of strongly interacting particles, CLIC/ILC for weakly interacting.
- Could running longer the LHC at its nominal energy give a similar reach extension? No.
- Is a major investment yielding only a factor of two in energy justified? Yes, because energy gains explore new territory, e.g., by approaching or exceeding the gravity energy scale.
- Can the LHC results expected in the years to come change this analysis? Yes.

Tentative conclusions

The strength of the HE-LHC is to enhance significantly the detection of new physics at the energy frontier. Its precise impact on the ideas discussed -- technicolor-like theories, supersymmetry, and extra dimensions -- will need to be reassessed in a few years, based on the LHC results.

MOTIVATION, STATUS AND STRATEGY FOR HE-LHC

Steve Myers

The salient points

Beyond the goal of operating the LHC at its nominal parameters, CERN is engaged in a number of projects or studies to prepare the future: luminosity upgrade of the LHC (HL-LHC) for installation around 2020, technical design report for a linear collider scheduled for 2016-2020, the subject of this workshop i.e. the HE-LHC study, R&D on high-power proton linacs, as well as a conceptual design study of an electron-proton option for the LHC.

The discussion

- What is the timescale for the HE-LHC study? 1 to 2 years.
- ILC versus CLIC? CERN option is to treat all LC studies together. LHC results will make the case for one or the other.
- When will the users enter the HE-LHC study? An open HE-LHC workshop will be organized as soon as the major possible showstoppers are eliminated.

Tentative conclusions

This workshop kicks off the HE-LHC studies, open to global collaborations. All workshop participants are thanked for their interest and contributions.

BEAM PARAMETERS, OPTICS AND BEAM DYNAMIC ISSUES

Frank Zimmermann

The salient points

The major parameters for the users are: 33 TeV cm energy, 50 ns bunch spacing, with 25 ns spacing kept as

an option, a luminosity of 2 10^{34} $cm^{-2}s^{-1}$, yielding a multiplicity of 76. The basic accelerator parameters suffer mild changes: similar optics, same bunch charge, emittance reduced by a factor of 2, injection at 1 TeV, beam half-aperture of 13mm. The significant difference is the radiated light that reaches 2.8 W/m and produces a much reduced damping time of 1 hour. Emitances will need to be kept constant by heating. Damping is favourable for beam dynamics, reducing the adverse effect of the beam-beam interactions. A larger beam-beam limit can be anticipated and values up to 0.03 (three times nominal) are being considered.

The discussion

- It would be valuable to foresee increasing the injection energy to 3 TeV, to maximize aperture
- A 40 mm bore was originally considered an acceptable challenge for the SSC. A compromise must be found between small aperture and high field quality.
- Is it safe to assume an emittance two times lower than nominal to define the magnet aperture?
- Isn't the assumed beam-beam limit optimistic? In fact, the performance does not depend much on it.

Tentative conclusions

From the machine design and beam dynamics point of view, HE-LHC does not appear at first view especially challenging. The synchrotron radiation damping and a weaker long-range beam-beam effect are both favourable.

MAGNET CONCEPTS AND COST EVALUATION

Ezio Todesco

The salient points

A preliminary investigation of a 20 T magnet, with 20% margin, shows that a composite coil of Nb-Ti (8T), Nb_3Sn (+7T) and Bi2212 (+5T), where Nb_3Sn is graded, provides the required field when cooled at 1.9K. The field quality is not really an issue, given the large coil size/aperture ratio. The strains are below the degradation limit of 200 MPa. Operational currents of about 400 A/mm^2 allow "compact" coils. The magnet design is a two-in-one structure with a beam separation enlarged to 300 mm to avoid crosstalk. A number of significant challenges have to be addressed, e.g. HTS with suitable current density, complexity of a hybrid coil and its protection, etc. A realistic estimate of the cost of 1200 dipoles is about 5.5 B$, i.e., 5 times the LHC dipole cost.

The discussion

- Are stray fields acceptable? Yes.
- What is the impact of the higher voltage to ground? To be studied.
- Bi is an issue under radiation: Polonium is produced and the consequences must be evaluated.
- What is the timeline for a 20 T magnet? A time line can be defined for a 15 T Nb_3Sn magnet, not for this hybrid concept that is pure R&D now.
- Can the 20% margin be reduced? Not at this stage.
- What would be the consequence of being the major HTS customer on the market? Good question.
- Given the extremely high cost of HTS (50% of the cost), a new longer tunnel for a HE-LHC built of Nb_3Sn magnets (without HTS) could become the economical solution, in addition to being more flexible.

Tentative conclusions

The initial study of a 20 T magnet shows that the mechanical stresses and the field quality should not be major issues. However, serious issues like hybrid coils, and protection, must be studied to establish the feasibility. There is confidence that the construction of a 15 T Nb_3Sn magnet for the HE-LHC time line can be made. The HTS coils needed to reach 20 T open a range of technical and cost issues.

RELEVANT STUDIES FOR VLHC/SSC

Uli Wienands

The salient points

There is a trade-off between magnet aperture and injection energy. For the SSC, aperture between 40 and 50 mm were considered, with injection varying between 1 and 2 TeV. Neuffer's non-linear mid-cell correction scheme was considered essential for 1 TeV injection even with 50-mm dipoles. The synchrotron radiation of HE-LHC is similar to that of VLHC. However, discrete photon stops as considered for VLHC are most likely not applicable, given the different geometries. The SSC diffusion model may be useful in estimating the gas loads. The SR damping may indeed increase the beam-beam limit, but perhaps not so much. Flat beams were investigated, with a simpler doublet instead of the triplet final focus. Other studies have not been conducted much beyond that of the LHC.

The discussion

Why 80K foreseen for the beam screen of SLHC? It came from a balance between cooling efficiency and heat load.

Tentative conclusions

The cost optimization must include both the magnet aperture and the injector requirements. A number of references are given on reports touching common issues between HE-LHC and VLHC. A very relevant one is that on the flat beam option.

DETECTOR PLANS AND CONSTRAINTS FOR HE-LHC

Marzio Nessi

The salient points

A higher energy LHC will buy much more, because rare physics cross-sections, in particular if large mass objects are involved, will be boosted. Of course, with the experience gained after years of running at an upgraded luminosity, it is likely that users will require a combined energy and luminosity upgrade. By the time of HE-LHC, the detectors will be obsolete and highly irradiated. Major RP issues will have to be faced, from 2016. Related show-stoppers may not be excluded in ATLAS. The option of a new detector, in addition to ATLAS and CMS could be a way out, letting the present LHC detectors cool down. In fact, the question of the HE-LHC will be best addressed in summer 2011.

The discussion

- Would ATLAS and CMS change their magnetic configurations? No

Tentative conclusions

It is important to associate the user community to the HE-LHC study from 2011.

SUMMARY OF SESSION 2: MAGNETS FOR THE HE-LHC

L. Rossi, E. Todesco, CERN, Geneva, Switzerland

Abstract

This second session of the workshop is devoted to the status of high field magnets research in the world. Overview of the main programs for accelerators magnets based on Nb_3Sn and Nb_3Al conductors are given. The statues of high temperature superconductors, which are an essential ingredient to bring the field from 15 to 20 T, are also addressed.

SESSION OVERVIEW

The session consisted of seven talks:

- LHC accelerator R&D program (LARP) by G. Sabbi: this is the Department of Energy program active since 2004, whose main aim is to develop large aperture (90 mm to 120 mm) Nb_3Sn quadrupoles for the LHC interaction regions with peak fields of the order of 12-15 T.
- 'Core' program of LBL, by S. Caspi, giving an overview of the program in Berkeley, mainly focused on high field Nb_3Sn dipoles (13-16 T) with 40 mm aperture and accelerator field quality.
- 'Core' program of FNAL, by A. Zlobin, giving an overview on the high field Nb_3Sn magnets program in Fermilab, focused on dipoles in the range of 11-12 T.
- European program in high field magnets, by G. De Rijk; the European Union, has launched a research program to first develop a Nb_3Sn conductor (CARE-NED) and then to master the technology through the construction of a challenging large aperture (100 mm) magnet in the range of 13-15 T (EUCARD-HFM, Fresca2 test station).
- Development program in KEK on Nb_3Al, given by T. Nakamoto; Japan is pushing for the development of this material since many years. At his stage, the main challenges are at the level of the conductor development.
- Status report on the magnets based on High Temperature Superconductors (HTS), by J. Schwartz.
- An overview on the construction of magnets based on HTS in BNL, by R. Gupta.
- An overview of the path towards 20 T magnets, by P. McIntyre, University of Texas, who first proposed such a magnet for an LHC tripler.

Nb_3Sn

Is Nb_3Sn an eternal promise of higher fields for the accelerator community, which will never be fulfilled? Or will it be really able to bring the operational field from the 8 T Nb-Ti limit to 12 T, and possibly up to 15 T? Already at the end of to 80's, the fathers of the LHC were considering the option of main dipoles in Nb_3Sn at 4.2 K, as an alternative to the Nb-Ti technology at 1.9 K. The CERN-Elin Nb_3Sn prototype successfully went close to 10 T, and the final choice on Nb-Ti has been dictated by manufacturing feasibility, experience with the technology, and price considerations. Since then, in a few years the record of Nb_3Sn magnets was brought to 11 T (MSUT, University of Twente, 1995), and above 13 T (D20, Berkeley, 1997). These successive records went hand in hand with an impressive progress in the cable performance: the current density of Nb_3Sn (at 12 T and 4.2 K) increased by more than a factor two, jumping from 1200 A/mm^2 to almost 3000 A/mm^2 during the first decade of the century. FNAL launched at the end of the 90's a program to build 11 T magnets for the VLHC based on Nb_3Sn technology, fully satisfying accelerator requirements. Indeed, the program was blocked for a few years on what has been understood later as a conductor instability, limiting the magnet performances at 60% of the short sample field. The last three magnets of these type (HFDA05-07) managed to reach about 80% of the short sample after some training, reaching the 10 T barrier for an accelerator dipole.

Thanks to the massive DOE investment in LARP, in the past decade the Nb_3Sn technology has been proved for quadrupoles in the range of 10 T operational peak field with the TQ models. The program has also showed that (i) several models are needed to master all the details relative to the manufacturing; (ii) the LARP Nb_3Sn conductor has shown to be able to withstand stresses up to 200 MPa with moderate degradation; (iii) a collarless bladder & shell structure where the stress is mainly imposed during the cool down is extremely efficient; (iv) a collar structure seems less forgiving on errors and tolerances, but can anyway provide equivalent results as the TQE models proved; (v) the performance at 1.9 K is still affected by instability issues, and the additional 10% given by lowering temperature from 4.2 K to 1.9 K is not at hand; (vi) training appears longer than in Nb-Ti magnets but in many cases the 80% operational level can be reached very rapidly or without quenches; (vii) the scaling from 1 m to 3.4 m long magnet can be mastered successfully (LQ model). On the other hand, the technology still shown to be fragile and sensitive to many issues that are not totally mastered: the first results of HQ, the 120 mm aperture quadrupole, gives a magnet well above 70% of the short sample, but limited at less than 80%, and affected by electrical problems: this after many years of development of short models in the LARP framework.

Novel layouts as the block coil have been explored for Nb_3Sn dipoles by LBL (HD2 model). Also in this case, the results are mixed: the magnet is above 70% of the short sample field but is blocked at around 80% by quenches in the transition to the coil heads. A design,

which would charm everybody by its beautiful simplicity (squared block coils, no copper wedges), shows to have more hidden issues than the cosθ.

Summarizing, the Nb_3Sn technology, which was proved to bring the operational field from above 8 T to up to 12-13 T in the 90's, has been extensively studied in the past decade, showing several problems and hidden issues, but also significant advancements. Today it is very close to maturity, but still a few steps are needed before installation in an accelerator.

Nb_3Al

Nb_3Al is an interesting material since it allows to go beyond 10 T and, contrary to Nb_3Sn, has a limited degradation with strain. Whereas it has been abandoned in US, Japan has decided to pursue this technological development, with important investments on the conductor. At the level of 15 T, Nb_3Al can provide about 800-1000 A/mm^2, i.e., 50-70% of Nb_3Sn. At the same time, wire manufacturing has not yet been mastered, and R&D is still ongoing to finalize the strand lay-out. In parallel with cable development, KEK is planning to build short racetracks to test the cable in its field and master the issues related to coil fabrication. Compared to Nb_3Sn, there is still an evident gap, both in terms of development and of resources. In the next years it will be possible to judge if this promising material can become a reality for accelerator magnets.

HTS

The ultimate limit of Nb3Sn is probably an operational field of 15 T, i.e., 18 T short sample field with a 20% margin. To get the last five T needed to reach 20 T, one has to use HTS, which can tolerate very high magnetic fields, i.e., well above 30 T.

In solenoids, HTS have been successfully used to reach field of the order of 25-30 T (six demonstrators for 25 T, and two for 30 T). Solenoids have much easier geometry with respect to accelerator magnets, and coils are self supporting under the electromagnetic forces.

REBCO (YBCO) has a very large current density in the superconductor, but needs a very large dilution (1-2%), greatly reducing the engineering current density, i.e., the current density over the whole cable. Moreover, it is manufactured only in tapes which are good for small solenoids but not for large accelerator magnets. Finally, the material is highly anisotropic and in a dipole or quadrupole one cannot minimize the perpendicular field as in solenoids. It is also limited to the react-and-wind technique. Bi-2212 can be cabled and has a large filling factor (30%), but it has a lower current density. It can be used with the wind-and-react technique, and due to chemical reasons it is more challenging than for the Nb_3Sn. Today is the natural choice for accelerator magnets, starting from small racetracks which are the first step to prove the technology.

Quench detection is an additional challenge, since the velocity of propagation of the quench is slower than for Nb_3Sn or Nb-Ti case, thus inducing higher spot temperature before than the quench can be detected. Optical fibers are being studied to solve this issue.

HTS programs for accelerator magnet are active in BNL (talk by R. Gupta), LBL, FNAL, and Eucard (high field insert in Fresca2).

HYBRID COILS

A 20 T magnet would need an hybrid coil to minimize the cost: even in the time scale of 20 years it is difficult to imagine that the prices of Nb_3Sn and HTS could converge to the Nb-Ti price. The construction of an hybrid magnet poses additional challenges since each material needs a different heat treatment, and has different mechanical properties. A very limited experience is present in the field, which could be one of the most difficult issues of the project.

DISCUSSION

- G. L. Sabbi points out that the presence of very few producers in Nb_3Sn strands is an intrinsic fragility of the project: in US all the strands is made by OST, and after many efforts another producer is reaching the specifications in Europe. One should avoid to be dependent on a few manufacturers, also in view of the large production load that will be induced by ITER, which could exhaust the production capabilities.
- L. Rossi points out that the magnet has to be designed for 20 T. The 80% limit means that, from a purely electromagnetic point of view, the magnet should reach 25 T at short sample. Indeed, all the other aspects of the magnet (mechanical structure, protection, …) should be designed to withstand 20 T, and not 25 T.
- J.-P. Koutchouk asks about if instabilities at 1.9 K could limit the performance. This is possible, even though the loadline of the magnet is very flat (high field and low current density) so probably the problem should be less relevant.
- E. Todesco asks about the time needed to get an existing strand from a producer: 15 months in average.
- L. Rossi asks about the training retention in the Nb3Sn LARP quadrupoles: in general there is a good memory.
- A. Yamamoto points out that a block structure as it has been used for HD2 requires more conductor, and that the flared end are not straightforward. On the other hand, the cos 2θ LARP quadrupoles rarely showed problems with ends. S. Caspi replies that the experience of HD3 will be crucial to validate this challenging design.
- R. Gupta asked about the absence of wedges in the Fresca2 design: G. De Rijk answered that the required field quality is about 0.1%, and therefore there is no need of copper wedges.

- L. Bottura pointed out that the aspect related to radiation on insulation are very critical and underestimated: there are no facilities, and it is a complex study to which more resources should be allocated. The use of the HighRadMat facility at CERN, as suggested by S. Myers, would be difficult since one needs cryogenics. F. Bordry asks about how this problem is solved for ITER: the spectrum is pretty different the the facilities have been now dismantled. After a wide discussion, there is a general consensus on the need of well specifying doses and spectra, and to find/build a facility to perform the necessary tests.
- The necessity of a cored cables is questioned by E. Todesco, who points out that the strong effects on field quality visible at 70 A/s (ramp rate of Tevatron) disappear at 10 A/s. L. Rossi and L. Bottura point out that a core could be needed to avoid quenching during a fast discharge.
- G. De Rijk remarks that FNAL and LARP data show a longer training in Nb_3Sn dipoles than in quadrupoles.
- L. Rossi points out that the main challenge for REBCO conductors is to manufacture a round wire. J. Schwartz answers that many tentative are ongoing. Justin also points out that the application should drive the research on the conductor: up to now HTS research has not been driven by accelerator magnets applications.
- The HTS needed to add the last 5 T opens a wide debate. G. Sabbi points out that today it would be short-sighted to limit the magnet at 15 T and to exclude HTS. E. Prebys observes that the 20 years span from today to 2030 is not so wide: 10 years ago Nb_3Sn was in a much better state than what is HTS today, and nevertheless Nb_3Sn accelerator magnets are still not at hand. J. P. Koutchouk points out that the cost looks today as one the main issues, the HTS part to reach 20 T having approximately the same cost as what is needed to go to 15 T.
- E. Todesco asks to R. Gupta the field level achieved in the HTS racetracks: around 2 T.
- L. Bottura comments on the talk by S. Gourlay on future directions in the high field magnets: for the HTS, the strong requirements are a cable with high current density and small filament size, with round wire. For Nb3Sn, one should manufacture a magnet with all features needed to be installed in a machine.
- R. Garoby observes that one should also consider the option of an accelerator with a longer tunnel and a smaller field. K. H. Mess points out that the practical issues related to a very large size (above 50 km) should not be neglected.

CONCLUSION

One can draw three main conclusions: (i) there is no apparent showstopper for a dipole in a with a 16-20 T operational field; (ii) 20T should be kept as ultimate limit for the design, with a 20% margin, and (iii) high temperature superconductors are necessary to go beyond 15 T: the feasibility of a HTS coil pushing the field from 15 to 20 T should be addressed in the next 5 years.

SUMMARY OF SESSION 3: SYNCHROTRON RADIATION AND BEAM DYNAMICS

V. Shiltsev (Fermilab) and E. Métral (CERN)

Abstract

Below we summarize presentations, discussions and general conclusions of the Workshop session on beam dynamics issues. Major subjects include effects due to Synchrotron Radiation (SR), cryogenic loads, electron cloud, impedances, Intra-Beam Scattering (IBS) and beam-beam interactions.

INTRODUCTION

The charge to the workshop is to "… take a first look at a Higher-Energy LHC (HE-LHC) with about 16.5 TeV beam energy and 20-T dipole magnets", therefore, in the morning session on Friday October 15, we have concentrated our efforts onto understanding and evaluating the potential issues with beam dynamics in HE-LHC and identification of the topics for future, more technical studies.

There were seven presentations on the subject: 'Heat load and cryogenics' by Dimitri Delikaris (CERN) [1]; 'Requirements from the vacuum system' by Jose Miguel Jimenez (CERN) [2]; 'Beam screen issues' by Elias Metral (CERN) [3]; 'IBS and cooling at RHIC and HE-LHC active emittance control' by Wolfram Fischer (BNL) [4]; 'Modeling IBS and cooling' by Oliver Boine-Frankheim (GSI) [5]; 'SR damping, IBS, and beam-beam simulations' by Alexander Valishev (FNAL, presented by V. Shiltsev) [6]; 'SR and beam-beam simulation' by Kazuhito Ohmi (KEK) [7].

CRYOGENICS, VACUUM LOAD AND BEAM SCREEN

The HE-LHC will be the first hadron machine dominated by Synchrotron Radiation (SR). Compared to design LHC parameters, it will see 17-fold increase of the SR power from 0.33 to 5.7 W/m. The analysis performed in Ref. [1] shows that the total heat load on the beam screen (SR + image current heating + rest) will be about 10 W/m and suggests that the optimal temperature of the beam screen is in the range 40-60 K (vs. 4.5-20 K now). The optimal temperature of the magnet cold mass is 2 K as it allows some ~ 2 T higher peak dipole filed (and thus, more than 10% higher energy) and also greatly helps to assure field stability in the magnet. Equivalent total HE-LHC cryo capacity is about what LHC has now, but how much of that could be refurbished in ~2030 (after > 20 years of operation) is now clear yet.

It was noted in Ref. [2] that the resistivity of the 40-60 K beam screen is ~5.5 higher than in the LHC, and in addition, higher dipole magnetic field will cause an additional factor of ~2 increase due to the magneto-resistance effect in the higher (20 T) field [3].

It was also found that anomalous skin effect will be negligible [3]. In total, the resistive wall (RW) impedance of the beam screen which scales as $\rho^{1/2}$ will be a factor 3.3 higher than in the LHC but probably that is not of great concern (from the point of view of the beam instabilities) because the beam energy will be higher by a factor of 2.4 at "flat top" or 2-3 at the injection (if a higher energy injector will be built). The discussions in the group ended up in an overall conclusion that instabilities should not be a major issue in the HE-LHC but further considerations will be needed. Among various ideas to reduce instabilities we discussed a possibility of a superconductive HTS coating – which was found to be not appropriate as that will keep the magnetic flux frozen and forbid ramping of the machine – and use of Al screen to reduce impedance and magneto-resistance – that option is not too advantageous either because of higher e-cloud yield.

What was found of significant practical concern is the beam-induced pressure rise in HE-LHC (see Ref. [2]). The flux and energy of the SR photons radiated inside the beam screen will be significantly higher than those in the LHC that will lead to about 74 (!)-fold increase in the beam-induced pressure rise. So far, no single solution of the problem was found, so a number of measures were offered to keep the problem under control: a) Increase pumping speed with larger area of slots in the beam screen (now ~ 4%, can possibly be doubled); b) Use TiN or amorphous-C coating in cold sectors to control electron cloud formation; c) Consider use of clearing electrodes (say, + 500V strip all along the beam pipe) or solenoids; d) NEG coating in warm sectors (where it is possible to bake the pipe to activate the coating); e) One can also count on the vacuum cleaning by SR and e- bombardment and beam scrubbing (by losses) – that will take time, and may force to start operation with a low number of protons per bunch. The overall conclusion on the issue was that at the moment, the vacuum does not look as the HE-LHC showstopper, but that is something definitely to be concerned of, and a more detail study of the issue will be required, based on the LHC experience.

SYNCHROTRON RADIATION DAMPING EFFECTS, INTRA-BEAM SCATTERING AND BEAM-BEAM EFFECTS

Contrary to other high energy hadron colliders, in the HE-LHC the SR emittance damping times - of about 1 hour (longitudinal) and 2 hours (transverse) – will be much shorter than the IBS growth times (> 50h), thus, the SR will dominate the luminosity dynamics unless beam-

beam or other effects will be stronger. During the presentations [4-7] and in the following discussions it has been shown that the SR damping/fluctuations and their effects on the beam dynamics are well understood [4,6,7]; the IBS theory, and proven models and simulation codes are available [4,5]; the initial HE-LHC luminosity integral estimates of ~ 0.8 fb^{-1}/day are correct and confirmed by others [4,6,7]. The understanding of the beam-beam effects is somewhat poorer and the predictive power of modern beam-beam modeling tools is limited. The design beam-beam parameter in the HE-LHC is not outstandingly high compared to other machines and the LHC start up conditions (see Fig.1).

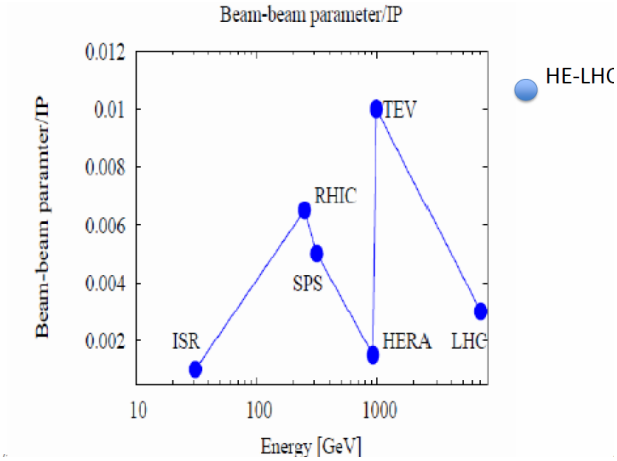

Figure 1: Beam-beam parameter in the hadron colliders, from Ref. [8].

It was noted that experience from the LHC operation will be quite important to make predictions for the HE-LHC. It will tell which kind of bean dynamics phenomena sets the most stringent limits on the luminosity performance: a) Instabilities; b) Head-on or/and long range beam-beam effects; c) Intolerable beam losses; d) Emittance blowups; e) Beam luminosity/lifetime; f) Collimation system (in)efficiency; g) External noises, drifts; h) Some other effects or combination of the above mentioned effects. (At the current stage of 1% of the design luminosity – it seems to be too early to draw conclusions and make strong recommendations for the HE-LHC on the basis of the LHC performance).

It was brought up in the discussions that on one hand, in the HE-LHC: the luminosity burn up and the SR damping will dominate the luminosity evolution and daily integral; the IBS does not matter to a ~ 1% level; the beam-beam effects do not matter ~ 10% level; while on the other hand, there are several interesting questions to answer: a) Does the SR damping/cooling help to increase beam-beam limit?; b) If "yes", then by how much? Can one count on the parameter $\xi > 0.01$/IP)?; c) Can even faster beam cooling help further? E.g. the so called optical stochastic cooling [9] or coherent electron cooling [10] can give extra < 1 hour of the emittance cooling decrement reduction; d) Is some kind of beam heating (controlled emittance blow up) needed to stay at the beam-beam limit or the beam-beam induced emittance blow up can stabilize itself (e.g. in Tevatron b-b emittance blowup is much faster than 1 hour)? [11]; e) How effective might be various compensation schemes: e.g. electron lenses [12], current carrying wires [13], "crab waist" collision scheme with flat beams [14]?; f) How serious are the concerns of coherent beam-beam instabilities, and in particular, multi-bunch beam-beam phenomena?

Although at present, synchrotron radiation, IBS and beam-beam effects do not seem to pose major concerns, the questions raised above are better be carefully studied.

REFERENCES

[1] D. Delikaris, "Heat load and cryogenics", these proceedings.
[2] J.M. Jimenez, "Requirements from the vacuum system", these proceedings.
[3] E. Métral, "Beam screen issues", these proceedings.
[4] W. Fischer, "IBS and cooling at RHIC and HE-LHC active emittance control", these proceedings.
[5] O. Boine-Frankenheim, "Modeling IBS and cooling", these proceedings.
[6] A. Valishev, "SR damping, IBS, and beam-beam simulations" these proceedings.
[7] K. Ohmi, "SR and beam-beam simulations", these proceedings.
[8] T. Sen, ICFA BD Newsletter, N.52 (2010).
[9] A. Mikhailichenko and M. Zolotorev, Phys. Rev. Lett. **71**, 4146 (1993); M. Babzien, *et a.l,* Phys. Rev. ST Accel. Beams **7**, 012801 (2004).
[10] V. Litvinenko, Ya. Derbenev, Phys. Rev. Lett. **102**, 114801 (2009).
[11] V. Shiltsev, *et al.,* Phys. Rev. ST Accel. Beams **8**, 101001 (2005).
[12] V. Shiltsev, *et al.*, Phys. Rev. Lett. **99**, 244801 (2007).
[13] J.P. Koutchouk, LHC Project Note 223, 2000 & PAC2001.
[14] M. Zobov *et al.,* Phys. Rev. Lett. **104**, 174801 (2010).

SUMMARY OF SESSION 4: HE-LHC INJECTORS AND INFRASTRUCTURE

E. Prebys, FNAL, Batavia, IL 60510, U.S.A.

Abstract

This note summarizes the fourth session of the HE-LHC workshop: HE-LHC Injectors and Infrastructure. This session was primarily concerned with the preparation and injection of the beam into the HE-LHC, but also included the issue of collimation with higher energy beams, as well as radiation issues which would arise after 20 years of normal LHC running.

Table 1: List of speakers and topics

Speaker	Topic
Roland Garoby	Optimal injector cascade for HE-LHC and possible implementations
Henryk Piekarz	Using Tevatron magnets for HE-LHC or new ring in LHC tunnel
Peter Spiller	FAIR magnets and design concepts of interest to HE-LHC
Karl Hubert Mess	Using LHC as injector and possible uses of HERA magnets/coils
Ralph Assmann	Intensity limits and machine protection
Brennan Goddard	Beam transfer and beam dump issues*
Doris Forkel-Wirth	Radioprotection issues after 20 years of LHC operation

* The speaker was unable to attend the workshop and this talk was canceled; however, the slides and the paper were ultimately published in the appropriate slot at the workshop website and are summarized in the appropriate section below.

SESSION OVERVIEW

The session on injectors and infrastructure was the fourth and last of the workshop before the summaries. The list of speakers and topics is shown in Table 1.

While this note attempts to summarize the key issues and discussion from the session, readers are encouraged to refer to the individual talks and proceedings for details.

Table 2: HE-LHC Injector Specifications

Parameter	Nominal LHC	HL-LHC	HE-LHC
Injection Energy (GeV)	450	450	>1000
Bunch Spacing (ns)	25 ns	25 ns	50 ns
Bunch Size (10^{11} p)	1.2	1.8	~1.4
Normalized Transverse Emittance (μm)	3.75	>2	3.75(H), 1.84(V), 2.59 (H&V)
Longitudinal Emittance (eVs)	1	1	?(<4)

Table 2 shows the injection parameters of the HE-LHC compared to the nominal and high luminosity LHC configurations. Most parameters are comparable or even relaxed compared to the 7 TeV LHC, and the "only" challenge is the injection energy, which will have to exceed 1 TeV[1].

Most consideration was given to solutions involving an additional new accelerator to take beam from the existing SPS and accelerate it to the HE-LHC injection energy. Most of the discussion focused on options for this accelerator:

- Super-SPS (S-SPS): a rapid cycling superconducting synchrotron which would share the tunnel with the SPS. This accelerator would have to match the ramp frequency and rate of the SPS for LHC loading.
- Low Energy Ring (LER): a synchrotron which would share the tunnel with the LHC. The SPS would inject the entire load of protons into the LER, which would accelerate them to the injection energy of the LHC and transfer them all at once. It is assumed this ring would have a single aperture and would therefore have to be bi-polar, cycling separately for each beam direction.

There were some brief discussions of other alternatives, which will be summarized shortly.

Other topics which were presented and discussed included beam transfer, injection, extraction, and dumping. In addition, collimation and machine protection

were considered, as were the radiological issues after 20 years of LHC operation.

SUPER-SPS (S-SPS)

This scenario is illustrated in Figure 1. A new accelerator would be built in the SPS tunnel. This would accelerate the beam from 150 GeV to 1.0 or 1.3 TeV, depending on the injection energy which is ultimately chosen for the HE-LHC. The required maximum field strength would be 4 T or 5.2 T, respectively. Beams would be transferred to the HE-LHC using the existing TI2 and TI8 tunnels, but of course new beam lines would have to be built to accommodate the increased energy.

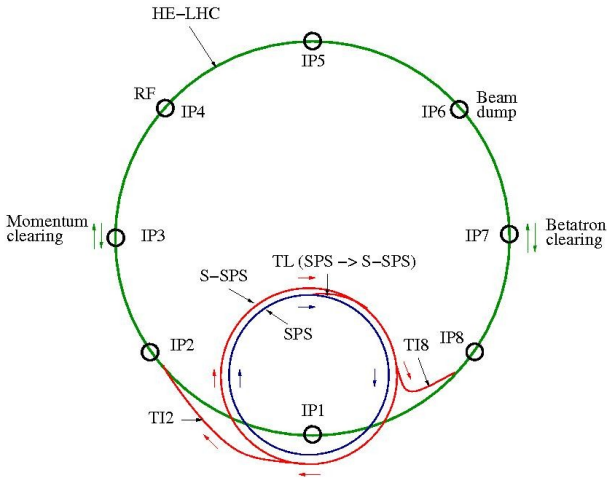

Fig. 1 Arrangement of S-SPS accelerator as an injector to the HE-LHC

The S-SPS would accelerate beam directly from the SPS and would therefore require 24 cycles to fill the LHC. In order to preserve the current fill time of 4.4 minutes, the individual transfers would have to occur in 10.8 s cycles, requiring a ramp rate of 1.3 T/s for the highest energy injections case [2].

Such high ramp rates are extremely challenging for superconducting magnet design. The most relevant recent work has been done in conjunction with the new Facility for Antiproton and Ion Research (FAIR) being built in Darmstadt, Germany [3].

FAIR is pursuing two relevant superconducting magnet R&D projects:

- SIS100: $B\rho$= 100 Tm, B_{max} = 1.9T, dB/dt=4 T/s
- SIS300: $B\rho$= 300 Tm, B_{max} = 4.5T, dB/dt=1 T/s

The latter is of particular interest, although, even in the most optimistic scenarios, the heat load on the cryogenic system from such magnets remains a significant concern.

LOW ENERGY RING (LER)

The second class of solutions to the injector problem involve a secondary accelerator in the LHC tunnel. One idea would be to use the existing LHC itself as an injector for the HE-LHC[4]; however, a cursory analysis of the tunnel layout shows that there is insufficient space for a second, higher energy ring. The only possible solution would be to re-cryostat the cold masses of the current LHC together with the magnets of the new LHC. This idea was not analyzed in any depth.

It is considered more promising to design a new, single aperture LER to share the tunnel with the HE-LHC. Figure 2 shows one proposal, based on R&D which was done for the Very Large Hadron Collider (VLHC), which was proposed in the US[2].

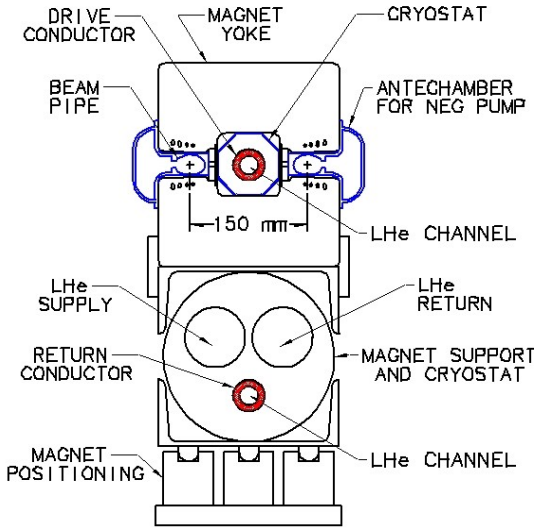

Fig. 2 Sketch of the proposed LER main arc magnet. The return conductor is inside the cryostat pipe which supports the magnet and houses liquid helium distribution lines for the LER.

A scaled down version for the HE-LHC would have B_{max}=1.76 T and a maximum ramp rate of dB/dt=6.5 T/min, although a slower ramp rate would likely be used to reduce the power load.

Of course, an LER sharing the tunnel with the HE-LHC would require a method of bypassing the interaction regions. This could be done by either designing bypass beam lines around the regions, or by switching the LER beam into the HE-LHC in those areas.

ALTERNATE PROPOSALS

New tunnels

The scenarios discussed above assume that we are limited to using existing tunnels for the new injector. It was suggested that we consider building a completely new tunnel. However, this immediately raised the question of whether it would be better to build a newer, larger tunnel for the HE-LHC itself, which would obviate the need for exotic magnets. At that point, it was decided that the discussion of new tunnels was beyond the scope of this workshop.

Completely new injector complex

It was pointed out that by the time that an HE-LHC could conceivably be built, parts of the existing injector complex would be extremely old. In light of this, perhaps it would make sense to consider a completely new injector chain, inspired by Fermilab's Project X. Straw man parameters for such a complex are shown in Table 3.

Table 3: Proposed new injector complex

Accelerator	Tunnel	Energy range	Max ramp rate
SC Linac	new	0-8 GeV	---
S-PS	PS	8-100 GeV	3 T/s
S-SPS	SPS	100 – 1200 GeV	2 T/s

BEAM TRANSFER AND DUMP ISSUES

It is assumed that the existing TI2 and TI8 will be used for transfers from the SPS tunnel to the LHC tunnel. If the beam is coming from a higher energy S-SPS, then the transfer line magnets would have to be replaced. Options for reusing magnets from existing accelerators were considered. The minimum curvature radius of these transfer lines is the same as the SPS, so the same field would be required as the S-SPS. Tevatron magnets might be sufficient for a 1 TeV injection energy, but not if the energy is higher [2]. HERA magnets have the required field, but would need significant retrofitting to fit in the tunnel and to handle the fact that the polarity is reversed relative to HERA. Also, TI2 has a large vertical slope, which would present problems for any superconducting magnets not specifically designed for it [4].

The injection, extraction and dump systems present significant challenges at increased energy; however, they do not appear to be *a priori* insurmountable [6] †.

The dump system consists of extraction kickers, septum, dilution sweep magnets, and the physical dump itself, none of which are adequate at 16.5 TeV. In addition, there are passive elements which protect the accelerator in the event of kicker misfires or beam in the abort gap, and these would also be destroyed at the increased energy.

Increasing either the length or the field of the existing extraction kickers does not appear feasible. However, one can design new kickers with smaller apertures thanks to the smaller maximum beam size that comes with the increased injection energy. These appear to present a reasonable option.

The extraction appears just feasible by using an increased number of existing B and C type septa, running at the maximum field. The total required length would increase from 73 to 136 m, and the resulting integration issues would have to be carefully studied.

† The speaker, Brennan Goddard, was unable to attend the workshop. This discussion summarizes the transparencies which he subsequently submitted.

Although the total stored energy of the beam does not increase, the energy density does, requiring an increased amplitude and/or frequency of the dilution kickers. These appear to be feasible, although more study is needed. It might be possible to amplify the effect of these kickers with quadrupoles in the dump line, but integration might be an issue.

The dump itself would have to be redesigned, likely made longer with a lower density material. However, there is room to accommodate this.

The passive protection devices in the extraction area are inadequate for the increased energy and energy density, and it's not clear that a robust solution exists to replace them. In a worst case scenario, "sacrificial" absorbers could be implemented, which would be replaced after (hopefully rare) exposure to high intensity beams.

The injection system is somewhat more challenging. This is because the existing injection kickers use all the available space, assuming that the HE-LHC magnet layout is similar to the current layout. Again, taking advantage of the fact that a smaller aperture can be used with the higher energy beams, new, higher field kickers should be feasible.

INTENSITY LIMITS AND MACHINE PROTECTION

Although the total stored energy of the HE-LHC will be roughly the same as the HL-LHC, the increased beam energy and energy density will have significant implications for the collimation system [5].

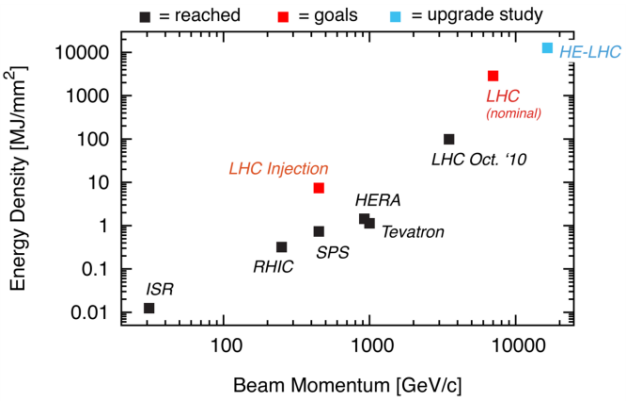

Figure 3: Energy Density of various machines, including the LHC and HE-LHC.

Figure 3 shows the energy density of various machines. As can be seen, the LHC has already exceeded all previous records in this area, but the nominal LHC will be more than an order of magnitude higher and the HE-LHC would be roughly two orders of magnitude.

Collimation inefficiency is a complex function of energy, but it is approximately proportional to the fraction of protons which undergo single diffractive (SD) scattering in the primary collimators compared to those which experience only multiple Coulomb scattering (MCS). This fraction scatters in a controlled way into

secondary and tertiary collimators, while the former produce off energy protons that are lost in an uncontrolled way.

Based on this model, the collimation inefficiency will be a factor of two to three worse at 16.5 TeV than at 7 TeV. This will have a strong impact, but it is believed a solution can be found.

The other effect of the higher energy density will be the robustness of the collimators in the event of catastrophic beam loss. At the nominal brightness, the HE-LHC exceeds the currently implemented limits for collimator survival. It is possible that these limits are overly conservative, and that further simulation and tests in the HiRadMat facility might allow the limits to be raised, but this is not guaranteed. Another solution would be to decrease the brightness, but this would lead to a decrease in luminosity. It is hoped that the problem can be solved through research to find a new, more robust, absorber material.

The reduced physical beam size at higher energy will necessitate smaller collimator gaps to achieve the desired cleaning efficiency and protection of the triplet aperture. This will have implications for beam control, and will also dramatically increase the impedance of the collimation system. Detailed calculations and simulations will be required to determine the impact of these effects.

RADIOLOGICAL ISSUES

In the current plan, the HE-LHC would be built after that ~3000 fb^{-1} have been collected at the LHC and HL-LHC. Thus, radiological considerations are very important. Thought must be given to both the handling of activated components and their eventual storage and/or disposal [7].

The most radioactive areas will be the inner triplets and collimators. After 10 years of operation at HL-LHC luminosities, these could generate exposures to those working nearby of more than 1 mSv/h, respectively, after a four-month cool down. Preparation must be made for ALARA procedures, and quite likely some degree of automation will need to be employed.

Objects with this level of activation will be very difficult to dispose of and will likely need to be stored at the laboratory indefinitely.

The majority of the accelerator components will have a much lower level of activation. After four months of cooling, the dipoles will produce less than 1 μSv/h at the surfaces and less than 10 μSv/h near the interconnect areas. With care, worker exposure can be kept to a minimum.

The dipoles could potentially be disposed of at an offsite location, such as the CSTFA facility in Aube, which currently charges about 1000 Euros/m^3 for long term storage of low level waste. It is important to remember, however, that rules for handling of radioactive waste may well change in the next 20 years.

SUMMARY

While there are no obvious show stoppers for the injectors and other infrastructure required for the HE-LHC, there are significant engineering challenges. There are pros and cons to both the S-SPS and LER options for intermediate acceleration, and careful consideration must be given to injection and extraction form the HE-LHC itself.

At least at this point, it looks like little use can be made of magnets from existing machines, or indeed from the existing LHC itself. Collimation, machine protection, and radiological issues appear manageable, but certainly should not be neglected.

REFERENCES

[1] R. Garoby, “Optimal injector cascade for HE-LHC and possible implementations”, presented in the fourth session of this workshop.

[2] H. Piekarz, “Using Tevatron magnets for HE-LHC or new ring in LHC tunnel”, presented in the fourth session of this workshop.

[3] P. Spiller, “FAIR magnets and design concepts of interest to HE-LHC”, presented in the fourth session of this workshop.

[4] K.-H. Mess, “Using LHC as injector and possible uses of HERA magnets/coils”, presented in the fourth session of this workshop.

[5] R. Assmann, “Intensity limits and machine protection”, presented in the fourth session of this workshop.B.

[6] Goddard, “LHC Beam Dump, Injection System, and Other Kickers”, submitted to the fourth session of this workshop.

[7] D. Forkel-Wirth, “Radioprotection Issues after 20 Years of LHC Operation”, presented in the fourth session of this workshop.